

UNIVERSITY OF BELGRADE
FACULTY OF CIVIL ENGINEERING

Miloš M. Jočković

**ISOGOMETRIC APPROACH IN DYNAMIC
ANALYSIS OF SPATIAL CURVED BEAMS**

Doctoral Dissertation

Belgrade, 2021

UNIVERZITET U BEOGRADU

GRAĐEVINSKI FAKULTET

Miloš M. Jočković

**IZOGEOMETRIJSKI PRISTUP U
DINAMIČKOJ ANALIZI PROSTORNIH
KRIVOLINIJSKIH GREDNIH NOSAČA**

doktorska disertacija

Beograd, 2021

Advisors:

Assoc. Prof. Dr. Marija Nefovska - Danilović
University of Belgrade, Faculty of Civil Engineering

Prof. Dr.-Ing. Matthias Baitsch
Hochschule Bochum, Bochum University of Applied Science

Committee:

Assoc. Prof. Dr. Marija Nefovska - Danilović
University of Belgrade, Faculty of Civil Engineering

Prof. Dr.-Ing. Matthias Baitsch
Hochschule Bochum, Bochum University of Applied Science

Prof. Dr. Rastislav Mandić (Retd.)
University of Belgrade, Faculty of Civil Engineering

Assoc. Prof. Dr. Aleksandar Borković
University of Banja Luka, Faculty of Architecture, Civil Engineering and Geodesy

Assist. Prof. Dr. Miroslav Marjanović
University of Belgrade, Faculty of Civil Engineering

Defense date: _____

Acknowledgments

First of all I want to express my deep gratitude to my co - advisor Prof. Marija Nefovska - Danilović for her scientific advice, patient understanding, selfless support, encouragement, and careful review of reports, papers, and this thesis. I would also like to thank Prof. Matthias Baitsch for his willingness to be a co - advisor of my work and for having me welcomed several times during my research stays at Hochschule Bochum. I would like to express a very deep gratitude to deceased Prof. Gligor Radenković for his selfless support, continuous encouragement during the development of the thesis, and valuable discussions.

Much gratitude also goes to all those people who provided me with advice and suggestions that were fundamental for the successful completion of PhD studies: Prof. Mira Petronijević, Dr. Anina Šarkić Glumac, Prof. Stanko Brčić and Prof. Rastislav Mandić.

Thanks to my colleagues from the Department of engineering mechanics and theory of structures, especially to Dr. Miroslav Marjanović, Dr. Marko Radišić, Emilija Damnjanović, Dr. Marko Marinković, Dr. Nevenka Kolarević, Marija Milojević, Dragan Kovačević, Kristina Konstantinović - Vranešević. I express my deep gratitude to all of them for covering my duties during my research stays in Germany, and for making our joint work so enjoyable.

I want to thank my family for their support throughout my PhD and more generally my education and life. My parents and my sister Dragana have always pushed me do more and to achieve my best. I am grateful to my wife Milena for having faith in me, her understanding during difficult periods and her love. Thank you for being always by my side!

Financial Support

The work on this thesis was supported by the Government of the Republic of Serbia Ministry of Education, Science and Technological Development, under the Project **TR-36046** (project leader Prof. Dr. Mira Petronijević).

The financial support has been also provided through the **SEEFORM** (South Eastern European Graduate School for Master and Ph.D. Formation in Engineering) project financed by German Academic Exchange Service - **DAAD** (project leader Prof. Dr. Rüdiger Höffer). The author was granted a DAAD scholarship that gave him the opportunity to spend six months in frame of three years at the Hochschule Bochum, Bochum University of Applied Science under management of Prof. Dr.-Ing. Matthias Baitsch.

Isogeometric approach in dynamic analysis of spatial curved beams

Abstract:

Accurate numerical modeling of curved beams is of significant importance in different engineering fields. Several challenges can be present during the curved beam formulation, primarily due to the issues regarding the beam geometry, discretization and beam theory assumptions.

In this dissertation, the isogeometric approach is applied in the dynamic analysis of spatial curved beams. A novel beam element was formulated using the Bernoulli - Euler hypothesis and the fundamental relations of the differential geometry, as well as the Cauchy continuum beam model. The geometry of the beam, as well as the displacement, velocity and acceleration fields, were defined using the Non-Uniform Rational B-Spline (NURBS) basis functions, which present the basis concept of the isogeometric approach. Complex geometry of the curved beams can be modeled accurately using NURBS - based isogeometric approach. Formulation of the spatial beam is conducted for the linear case, while the geometrically nonlinear formulation is conducted only for the plane curved beam using an explicit integration procedure. Free and forced vibration analyses of the curved beams are studied. In the latter, the influence of the moving mass on the curved beams is analyzed. The presented approach had shown that, in comparison to the classical finite element method (FEM), a less number of degrees of freedom are required in order to obtain accurate results. Consequently, fewer computational resources are needed to reach the appropriate level of accuracy for the curved beams. This makes the presented approach competitive with the conventional FEM, especially in the analysis of the flexible spatial engineering structures with complex geometry.

Keywords: Isogeometric analysis, Bernoulli - Euler beam, Free and transient analysis, Geometrically nonlinear formulation

Scientific field: Civil Engineering

Scientific subfield: Engineering Mechanics and Theory of Structures

Izogeometrijski pristup u dinamičkoj analizi prostornih krivolinijskih grednih nosača

Sažetak:

Tačno numeričko modeliranje krivolinijskih gredna nosača je od izuzetnog značaja u mnogim inženjerskim oblastima. Geometrija krivolinijskog grednog nosača, diskretizacija grede kao i potrebne pretpostavke grede, predstavljaju poteškoće prilikom formulacije krivolinijskog grednog elementa.

U ovom radu je primenjen izogeometrijski pristup u dinamičkoj analizi prostornih krivolinijskih grednih nosača. Novi gredni element je definisan primenom Bernuli - Ojlerove pretpostavke, kao i osnovnih relacija diferencijalne geometrije i mehanike kontinuuma Košijeve grede. Geometrija grede, kao i polje pomeranja, brzine i ubrzanja su definisani primenom NURBS baznih funkcija, što predstavlja fundamentalnu osobinu isogeometrijskog pristupa. Složena geometrija krivolinijskog grednog nosača može se tačno modelirati primenom izogeometrijskog pristupa zasnovanog na NURBS baznim funkcijama. Formulacija prostornog krivolinijskog grednog nosača je izvedena u uslovima linearne teorije, dok je geometrijski nelinearna teorija primenjena samo na ravanskom krivolinijskom grednom nosaču, primenom eksplicitne metode integracije. Izvšena je analiza slobodnih i prinudnih vibracija. Analiza prinudnih vibracija je fokusirana na uticaj pokretnog opterećenja na krivolinijski gredni nosač. Primenom date formulacije dobijeni su rezultati zadovoljavajuće tačnosti sa manje stepeni slobode u poredjenju sa klasičnom metodom konačnih elemenata. U skladu sa tim, u cilju dobijanja rezultata zadovoljavajuće tačnosti krivolinijskog grednog nosača nepohodna je primena manje resursa. Ovo čini prikazani pristup konkurentnijim klasičnoj metodi konačnih elemenata u analizi fleksibilnih inženjerskih konstrukcija sa složenom geometrijom.

Ključne riječi: Izogeometrijska analiza, Bernuli - Ojlerova greda, Slobodne i prinudne vibracije, Geometrijski nelinearna formulacija

Naučna oblast: Građevinarstvo

Uža naučna oblast: Tehnička mehanika i teorija konstrukcija

Contents

Acknowledgments	i
Financial Support	iii
1 Introduction	1
2 Review of previous research	5
3 NURBS	9
3.1 B-Spline functions	9
3.2 NURBS functions	10
3.3 Refinements	11
4 Differential geometry	15
4.1 NURBS parameterization	16
5 Linear dynamic formulation of spatial Bernoulli - Euler beam	19
5.1 Deformed configuration of the beam	20
5.2 Displacement field	21
5.3 Velocity field	24
5.4 Acceleration field	25
5.5 Kinematic relations	26
5.6 Constitutive relations	28
5.7 Strong formulation	29

5.8	Weak formulation	29
5.9	Governing equation of motion of the Bernoulli-Euler beam	30
5.10	Free vibration analysis	33
5.11	Transient analysis	33
5.12	Moving load and moving mass model	34
5.13	Boundary conditions	35
6	Geometrically nonlinear dynamic formulation of the plane Bernoulli - Euler beam	37
6.1	Deformed configuration of beam	38
6.2	Displacement field	39
6.3	Velocity field	41
6.4	Acceleration field	41
6.5	Kinematic relations	42
6.6	Constitutive relations	43
6.7	Weak formulation	44
6.8	Transient analysis	45
7	Object-Oriented Computer Program	47
8	Numerical examples	51
8.1	Free vibration analysis	51
8.1.1	Validation study	51
8.1.2	Convergence study	54
8.1.3	Influence of boundary conditions	57
8.2	Linear dynamic analysis of a curved spatial beam	58
8.2.1	Moving load problem	58
8.2.2	Moving mass problem	67
8.3	Nonlinear dynamic analysis of curved plane beam	73
8.3.1	Harmonic load	74

8.3.2	Moving load problem	79
8.3.3	Moving mass problem	83
9	Conclusions and recommendations for future work	103
	Biography	111

List of Figures

1.1	<i>Tiger and Turtle – Magic Mountain</i> , Duisburg (Germany), built 2011, base 44 x 37 m, height 21 m	1
1.2	<i>Horizont Observatorium</i> , Herten (Germany), built 2008, arches radius approximately 45 m	2
3.1	(a) Shape variations of the plane arbitrary shaped curve with the corresponding control polygon, (b) B-Spline functions of polynomial degree $p = 3$, constructed over the knot vector $[0\ 0\ 0\ 0\ 1\ 2\ 3\ 3\ 3\ 3]$	11
3.2	(a) Control polygons of the plane curve with constant shape for three cases of H - refinement (a - initial shape, b - 1st refinement, c - 2nd refinement), (b) the B-Spline functions of polynomial degree $p = 3$ constructed using the different knot vectors	12
3.3	(a) Control polygons of the plane curve for two cases of P - refinement (a - initial shape, b - 1st refinement), (b) the B-Spline functions of polynomial degree $p = 3$ constructed using different knot vectors	13
4.1	Spatial beam element with an arbitrary shape obtained using NURBS parameterization [48]	17
5.1	Deformed and undeformed configuration of the beam's centerline with the corresponding control polygon and the displacement vectors for the centerline and the first control point	20
5.2	Schematic representation of the central difference method	34
6.1	Arbitrary curved plane beam	37
7.1	Simplified UML class diagram of the dynamic analysis of the isogeometric Bernoulli - Euler beam	48
8.1	(a) conical helix geometry; (b) interpolation points of the conical helix; (c) NURBS based parameterization control points of the conical helix	51

8.2	First three mode shapes of the conical helix obtained using: (a) presented isogeometric approach, (b) FEM based software Abaqus	53
8.3	An arbitrary curve $\mathbf{C}(\xi)$ with corresponding control points \mathbf{P}_i	54
8.4	Convergence of the first ten natural frequencies computed using the H - refinement for isogeometric beam element	55
8.5	Convergence of the first ten natural frequencies computed using the P - refinement for isogeometric beam element	56
8.6	Finite element models of the spatial beam	57
8.7	First five mode shapes of the spatial beam obtained using: (a) presented isogeometric approach, (b) FEM based software Abaqus	59
8.8	Geometry of the beam subjected to the moving load	60
8.9	In-plane displacement (u) of the beam's midpoint obtained using the P - refinement procedure	60
8.10	Out-of-plane displacement (w) of the beam's midpoint obtained using the P - refinement procedure	61
8.11	In-plane displacement (u) of the beam's midpoint obtained using the H - refinement procedure	62
8.12	Out-of-plane displacement (w) of the beam's midpoint obtained using the H - refinement procedure	63
8.13	In-plane displacement (u) of the beam's midpoint obtained using the K - refinement procedure	63
8.14	Out-of-plane displacement (w) of the beam's midpoint obtained using the K - refinement procedure	64
8.15	Simply supported curved spatial beam subjected to moving mass	64
8.16	Normalized u displacement with respect to the moving load magnitude variation	65
8.17	Normalized v displacement with respect to the moving load magnitude variation	65
8.18	Normalized w displacement with respect to the moving load magnitude variation	66
8.19	u displacement with respect to the moving load velocity	66
8.20	v displacement with respect to the moving load velocity	67
8.21	w displacement with respect to the moving load velocity	68
8.22	In-plane (u) and out-of-plane (w) beam's midpoint displacement obtained using moving mass model (<i>mass</i>) and moving load model (<i>load</i>)	68
8.23	Normalized u displacement with respect to the moving mass magnitude variation	69

8.24	Normalized v displacement with respect to the moving mass magnitude variation	70
8.25	Normalized w displacement with respect to the moving mass magnitude variation	70
8.26	u displacement with respect to the moving mass velocity	71
8.27	v displacement with respect to the moving mass velocity	71
8.28	w displacement with respect to the moving mass velocity	72
8.29	Displacements of the beam at the position of the moving mass of velocity $V = 1$ m/s obtained from moving load and moving mass model	72
8.30	Displacements of the beam at the position of the moving mass of velocity $V = 10$ m/s obtained from moving load and moving mass model	73
8.31	Displacements of the beam at the position of the moving mass of velocity $V = 30$ m/s obtained from moving load and moving mass model	73
8.32	Displacements of the beam at the position of the moving mass of velocity $V = 50$ m/s obtained from moving load and moving mass model	74
8.33	Circular arch subjected to the time varying load	75
8.34	Convergence of the horizontal displacement of the beam free end obtained using the P - refinement isogeometric procedure	75
8.35	Convergence of the vertical displacement of the beam free end obtained using the P - refinement isogeometric procedure	76
8.36	Convergence of the horizontal displacement of the beam free end obtained using the H - refinement isogeometric procedure	76
8.37	Convergence of the vertical displacement of the beam free end obtained using the H - refinement isogeometric procedure	77
8.38	Convergence of the horizontal displacement of the beam free end obtained using the K - refinement isogeometric procedure - Part 1	77
8.39	Convergence of the horizontal displacement of the beam free end obtained using the K - refinement isogeometric procedure - Part 2	78
8.40	Convergence of the vertical displacement of the beam free end obtained using the K - refinement isogeometric procedure - Part 1	78
8.41	Convergence of the vertical displacement of the beam free end obtained using the K - refinement isogeometric procedure - Part 2	79
8.42	Normalized tip horizontal displacement with the variable amplitude of the load .	80
8.43	Normalized tip vertical displacement with the variable amplitude of the load . .	80
8.44	Circular arch subjected to moving load	81

8.45	Convergence of the horizontal displacement of the beam's midpoint obtained using P - refinement	81
8.46	Convergence of the vertical displacement of the beam's midpoint obtained using P - refinement	82
8.47	Convergence of the horizontal displacement of the beam's midpoint obtained using H - refinement	83
8.48	Convergence of the horizontal displacement of the beam's midpoint obtained using H - refinement	84
8.49	Convergence of the horizontal and vertical displacement of the beam's midpoint obtained using K - refinement, part 1	86
8.50	Convergence of the horizontal and vertical displacement of the beam's midpoint obtained using K - refinement, part 2	87
8.51	Convergence of the horizontal and vertical displacement of the beam's midpoint obtained using K - refinement, part 3	88
8.52	Convergence of the horizontal and vertical displacement of the beam's midpoint obtained using K - refinement, part 4	89
8.53	Convergence of the horizontal and vertical displacement of the beam's midpoint obtained using K - refinement, part 5	90
8.54	Convergence of the horizontal and vertical displacement of the beam's midpoint obtained using K - refinement, part 6	91
8.55	Convergence of the horizontal and vertical displacement of the beam's midpoint obtained using K - refinement, part 7	92
8.56	Convergence of the horizontal and vertical displacement of the beam's midpoint obtained using K - refinement, part 8	93
8.57	Convergence of the horizontal and vertical displacement of the beam's midpoint obtained using K - refinement, part 9	94
8.58	Convergence of the horizontal and vertical displacement of the beam's midpoint obtained using K - refinement, part 10	95
8.59	Convergence of the horizontal and vertical displacement of the beam's midpoint obtained using K - refinement, part 11	96
8.60	Convergence of the horizontal and vertical displacement of the beam's midpoint obtained using K - refinement, part 12	97
8.61	Normalized horizontal displacement of the beam's midpoint for different moving load magnitude	98
8.62	Normalized vertical displacement of the beam's midpoint for different moving load magnitude	98

8.63	Horizontal displacement of the beam's midpoint for different moving load velocities	99
8.64	Vertical displacement of the beam's midpoint for different moving load velocities	99
8.65	Load velocity horizontal projection for two cases of load magnitude, $F = 1kN$ and $F = 200kN$	100
8.66	Moving load/mass study - horizontal displacement	100
8.67	Moving load/mass study - vertical displacement	101

List of Tables

8.1	First ten natural frequencies [Hz] obtained using the present study (IGA) compared with the literature results (Yildirim) and the results from the Abaqus (Abaqus) presented with the relative error [%] between corresponding frequencies ($\Delta_{X-Y} = \frac{X-Y}{X} * 100$)	52
8.2	Convergence of the first ten natural frequencies of the presented approach with variable numbers of DOFs obtained applying H - refinement procedure	55
8.3	Convergence of the first ten natural frequencies of the presented study using the P - refinement procedure	56
8.4	Convergence of the first ten natural frequencies obtained using FEM - based software Abaqus	58
8.5	Influence of boundary conditions on the spatial curved beam	58
8.6	In-plane (Ω_u) and out-of-plane (Ω_w) natural frequencies [rad/s] obtained using isogeometric approach, FEM software Abaqus and the results from the literature	61
8.7	Number of degrees of freedom (DOF), time step (Δt), number of required time steps (n_t) and number of integration points (n_{int}) for the converged models obtained using P -, H - and K - refinement procedures	85

1 Introduction

Beams are the most commonly used structural elements in numerous engineering fields, Figures 1.1 and 1.2. Consequently, its accurate formulation and efficient application are of essential importance. Behaviour of beam elements is defined using a mathematical model of a beam. This model is developed using the principles of physics and corresponding beam assumptions. Solutions of engineering problems described with the mathematical model of a beam are usually obtained applying the numerical procedures, of which the finite element method (FEM) is the most widely used nowadays. The FEM is based on a physical discretization in which the structural domain is divided into smaller domains, referred to as finite elements, forming a mesh with the corresponding number of degrees of freedom (DOFs). If the solution of the engineering problem obtained using FEM is not accurate, the number of DOFs should be increased, which can be conducted by the mesh's refinement. It is important to note that the FEM is implemented in most software packages for structural engineers.



Figure 1.1: *Tiger and Turtle – Magic Mountain*, Duisburg (Germany), built 2011, base 44 x 37 m, height 21 m

Due to the aesthetic and functional requirements in the design process, curved spatial beam elements cannot be avoided. Geometrical model of the curved spatial beam represents the spatial curve, which can be obtained using computer-aided design (CAD) software packages. To accurately describe the free-form curves, and the curves of conic sections like circle, ellipse, parabola and hyperbola, CAD software packages utilize the NURBS basis functions.



Figure 1.2: *Horizont Observatorium*, Herten (Germany), built 2008, arches radius approximately 45 m

CAD and FEM software packages have been developed independently. Therefore the direct relation has not been established yet [1], which represents one of the main disadvantages in nowadays design process. During the mesh refinement procedure, the initial geometry model defined using CAD software packages is used to obtain finite element mesh. This procedure is repeated until the solution to the engineering problem converges. Consequently, the design process has the potential to become costly and time-consuming. In order to overcome this disadvantage, the isogeometric approach has been formulated, in which a direct relationship between the geometry and the numerical model of the structure is established. The NURBS functions as basis functions of the numerical model's solution space in the isogeometric approach have enabled the direct relation. In accordance with the aforementioned, when the geometry model of the structure is defined, all properties of the geometry model are taken as a starting point of the numerical model. If the geometry model of the structure is accurately presented using NURBS basis functions, errors due to geometric approximation are eliminated. If necessary, the accuracy in the isogeometric analysis can be increased applying the refinement procedures. However, the refinement is conducted only in the numerical model and does not influence the structure's geometry. Three refinement procedures are distinctive in the isogeometric approach, H -, P -, and K - refinements. First two have their counterpart in the FEM, while the third, where basis function degree and continuity can be arbitrary, is only unique for the isogeometric approach.

The choice of the beam mathematical model (beam theory), which defines the behaviour of the beam element, depends on numerous factors such as the accuracy of the required results and the beam's dimension amongst others. In general, the beam theories are based on the assumption that the cross-section of the undeformed configuration, modeled as a rigid body, is perpendicular to the beam's centerline. One of the commonly used theories is the Timoshenko beam theory, which takes into account axial, shear and bending effects. Consequently, the beam's kinematic is defined using the displacements of the beam's centerline, torsional rotation and the rotation about the principal axes. However, when used for slender beams, the locking effect occurs. To overcome this effect, the Bernoulli-Euler beam theory can be formulated, in which the rigid cross-section remains perpendicular to the beam's centerline during the deformation process. Due to this hypothesis, the shear deformation term vanishes at the beam's centerline. Therefore the rotations about the principal axes are coupled with the beam's centerline displacements.

In the case of the plane beam formulation only displacements of the beam's centerline can be used as a DOFs, forming rotation - free element, while in the case of the spatial beam formulation displacements of the beam's centerline and the torsional rotation can be used as a DOFs. Consequently, the number of DOFs can be decreased compared to the Timoshenko beam theory. Another advantage of the Bernoulli - Euler beam theory can be found in the case of plane beams, where only beam's centerline displacements are DOFs, forming rotation-free beam formulation. The advantage is beneficial for the geometrically nonlinear analysis.

During their lifetime, beam-like structures are often subjected to dynamic load. Therefore, dynamic formulation of beam elements is necessary for accurate prediction of their free vibration properties and dynamic response due to dynamic load, which can vary both in time and space. Moving dynamic load is induced by the mass moving along the element. This dynamic load is usually modeled as moving force with constant magnitude and direction, while the inertial term of the moving mass is neglected. However, in some cases, the effect of the inertial term of the moving mass can significantly affect the response of structure and thus cannot be neglected. Inertial part of the moving load is caused by an effect of the moving mass acceleration on its trajectory and is dependent on the moving mass velocity and trajectory curvature.

If the structure's configuration is significantly changed from the initial state during the deformation process, the application of linear analysis is no longer valid, and the non-linearity has to be introduced. In the linear formulation, the displacement and rotation vectors can be used as a DOFs, while for the case of nonlinear formulation, the rotation represents a tensor quantity.

This thesis presents the application of the isogeometric approach in the dynamic analysis of the Bernoulli-Euler beam subjected to spatially varying dynamic loads. The linear dynamic formulation of the spatial beam and the geometrically nonlinear dynamic formulation of the plane beam have been derived. Basic properties of the differential geometry and the continuum mechanics have been used during the derivation process of the beam governing equation of motion.

After the Introduction section, Chapter 2 elaborates the literature overview and the previous research in this field. The geometry representation of the curves using NURBS basis function and its properties have been shown in Chapter 3. At the end of this chapter, a brief review of the refinement procedure has been presented as an essential parameterization property. In Chapter 4, the basic properties of the differential geometry related to the curves are presented, and the relation with the NURBS parameterized curves is established. In addition, the ξ_λ parameterization of the curves, proposed by Radenković [2], is introduced to simplify the derivation procedure. A linear dynamic formulation of the spatial Bernoulli-Euler beam element is derived in Chapter 5, for the free vibration and transient analysis. In the transient analysis moving mass problem is studied using two models: moving load and moving mass. The theoretical considerations of the geometrically nonlinear dynamic formulation of the plane curved Bernoulli-Euler beam have been shown in Chapter 6. The main contributions of this thesis have been shown in Chapters 5 and 6. All formulated beam models and presented procedures have been implemented in the original Matlab code, Chapter 7, which is used for the numerical verifications and parametric studies presented in Chapter 8. Finally, the conclusions of the presented work and future research recommendations in this field are given in Chapter 9.

2 Review of previous research

Nowadays, in order to solve wide range of problems in structural engineering, isogeometric analysis (IGA) can be applied. Concept and the term were first introduced by Hughes and his co-workers in their paper [3] where motivation, the basic idea, advantages and performances of the structural analysis approach were presented. In addition, available refinement procedures of the approach were given, denoted as H -, P - and K - refinement. Detail explanation of the refinement procedures for the isogeometric approach in structural analysis and their advantages and comparison to the FEM refinement procedures were given in [4], while [5] gave the error estimates for the NURBS approximation in terms of the refinements. The performance of the isogeometric approach was compared with the performance of the classical FEM in [6] using different refinement procedures for the simple dynamic problems in the structural analysis. In addition, the structural vibration analysis of simple beam problems, shell and solid elements was given in [7]. A brief review of the isogeometric analysis and its formulation in wide range of engineering problems was presented in [1], which can be observed as an isogeometric handbook.

Given the main idea of IGA - representation of the geometry and solution space of the numerical model using the same basis functions, most of the research in this field was based on the NURBS basis functions, used for their capability to accurately describe various geometric shapes. Details of the NURBS functions, their construction, properties and advantages can be found in [8], [9]. During the derivation of the Bernoulli-Euler beam element, integration has to be conducted in order to define some quantities. Since the NURBS basis functions are rational functions, it is important to define a numerical integration procedure. Due to the increased continuity between the elements, the NURBS - based isogeometric analysis has an advantage related to the numerical integration. In comparison to the classical Gauss quadrature, fewer integration points are necessary to obtain accurate results, as shown in [10].

Beam elements are solid bodies in which one dimension is significantly larger than the other two. Therefore during the derivation process, the simplifications are introduced using proper assumptions. Depending on the assumptions, the various beam theories are formulated, briefly shown in the paper [11]. In this paper, the four engineering beam theories are given, Bernoulli-Euler, Rayleigh, shear and Timoshenko theory, which are classified by their assumptions. As a conclusion of this paper, the Bernoulli-Euler theory, as a classical beam theory, can be used for slender beams, while the application of the Timoshenko theory is a well suited for the non-slender beams.

Most of the studies in the field of the isogeometric beam formulation were focused on the Timoshenko beam theory. The shear locking effect was detected as the main problem in these papers. Beirão da Veiga showed [12] that the shear locking effect of the Timoshenko beam can be avoided applying the isogeometric collocation approach with the mixed formulation, which

is numerically validated for the straight beam. Auricchio et al. [13] used these procedures to overcome the shear effects for the spatial curved Timoshenko beam. The reduced integration and projection method were proposed by Bouclier et al. in [14] as an alternative procedure for the locking effects solution of the Timoshenko beam. Besides the Timoshenko isogeometric beam, the third-order shear deformation beam was formulated using the isogeometric approach by Li and his co-workers [15].

The first work on the Bernoulli-Euler isogeometric beam was published by Hughes and his co-workers in paper [3], where the potential of the isogeometric approach in the analysis of straight plane beam was demonstrated. However, the full potential of the isogeometric approach can be exploited for the case of the curved beams. One of the first papers on curved spatial Bernoulli-Euler beam was given by Greco and Cuomo [16], where only linear static formulation was presented. In this paper, the configuration of the deformed spatial curved beam was given by two operators, one that translates beams' centerline triads and the other that imposes cross-section torsional rotation. In addition, Greco and Cuomo analyzed the Bernoulli-Euler spatial curved beam continuity and suggested the solution of the G1 continuity in the parametric domain [17]. Using the isogeometric concept, Raknes et al. [18] developed the spatial cable model of the non-shear beam element, in which the torsional rotation term was neglected, forming a rotation-free model. In this model, only the beam's centerline displacements were employed as DOFs. Borković et al. presented the rotation-free isogeometric formulation of the plane Bernoulli-Euler beam element for static [19] and dynamic [20] analysis. The spatial curved Bernoulli-Euler beam element for linear static analysis was published by Radenković et al. [21], where torsional rotation, as a DOF, was introduced. The convergence properties of the free vibration analysis of the straight plane Bernoulli-Euler beams were improved by Wang et al. in [22] using higher-order mass matrices.

If the load applied to the structure induces large displacements, the application of the linear analysis is not valid. In such cases, geometrically nonlinear analysis should be performed. The geometrically nonlinear formulation assumes small deformation but finite strain, which requires finite displacements and rotations [23]. Most of the research in the field of geometrically nonlinear formulation are conducted for the straight beam using FEM. Bathe and Bolourchi [24] derived the two - node spatial beam elements for the geometrically nonlinear static analysis using total Lagrangian and update Lagrangian FEM formulation and showed that the latter is computationally more efficient formulation. This article represents a particular case of a general geometrically nonlinear procedure, which Bathe presented in book [25]. Belytschko [26] gave the review of the implicit and explicit geometrically nonlinear formulations with their advantages and restrictions in the structural analysis. Lo [27] presented finite element formulation of the Timoshenko spatial beam element defined using finite strain and large rotation, which was applied only for the static analysis. Hsiao and Yang [28] formulated the geometric nonlinear co-rotational finite element of a curved planar Bernoulli-Euler beam for dynamic analysis. Although the rotations in this work were taken to be large, the deflections of the beam element measured in the element coordinates were small. Therefore, the beam dominantly behaved as a rigid body. Chan [29] presented the procedure for large deflection deformations of the spatial Bernoulli-Euler beam defined in the geometrically nonlinear finite element formulation applied for the stability analysis with the post-buckling behaviour and the dynamic analysis. The finite element formulation of the thin-walled composite beams within the large deformation and small strain was published by Saravia [30]. He reviewed the main inconsistencies of the geometrically nonlinear formulations present in most research papers. Aforementioned inconsistencies arose from the inadequate representation of the rotation tensor as a vector quantity and application of the inadequate strain-stress relations in the geometrically

nonlinear formulation. Three kinematic representations of large rotations for the highly flexible spatial curved beams undergoing arbitrarily large elastic deformation was analyzed by Pai [31]. Based on the parametrization of the spatial curved beam element given by Greco and Cuomo [16], Bauer et al. [32] gave the geometrically nonlinear static formulation of the spatial Bernoulli-Euler curved beam using isogeometric approach.

Dynamic response of the mass moving along the structure has drawn attention to numerous researchers for a century and a half. Most of the research in this field was related to the analysis of mass moving along straight beam using linear FEM-based analysis.. One of the earliest investigations in this field was carried out by Stokes in 1849 [33], where an inertial term of moving mass on the plane straight Bernoulli-Euler beam was neglected, forming moving load model. Also, in this paper, the inertial term of the beam was not taken into account, which was included by Jeffcott in 1929 [34]. He analyzed basic cases of the straight plane Bernoulli-Euler beams subjected to the moving load. Skeer and Hribar [35] and Stanišić and Harding [36] presented more practical numerical-analytical solutions of the moving load problem, which can be only applied to simply supported straight plane beam. Akin and Mofid developed the analytical-numerical solution of the moving mass problem on the Bernoulli-Euler plane straight beam with different types of boundary conditions [37], introducing the inertial part of the moving mass resulted from beam's vibrations. It was shown that the difference between the results of the moving load and moving mass model could be significant for the case of higher velocity of the moving mass. Genin et al. [38] formulated plane curved simply supported Bernoulli-Euler beam subjected to the moving mass, which induced out-of-plane vibrations, while Yang et al. [39] extended it to the in-plane vibrations. Both papers are limited to the linear theory and curved beams with constant curvature. Lin and Lee in [40] analyzed the influence of the boundary conditions and the moving mass velocity on the plane arch beam in the linear case. In this paper, the moving mass had been formulated using two models: moving load and moving mass model, and the difference between the formulations had been demonstrated. Sheng and Wang [41] presented the geometrically nonlinear formulation of the moving mass problem on the straight simply supported plane Bernoulli-Euler beam. The dynamic analysis of the geometrically nonlinear three-dimensional beam subjected to the moving mass was published by Zupan and Zupan [42]. In their work, two subsystems were analyzed, one is the beam defined using the geometrically nonlinear formulation, while the moving mass was formulated as a point mass. Li and Ren [43] gave analytical study on linear dynamic responses of a horizontally curved beam with constant curvature subjected to three-directional moving loads. The isogeometric approach in the moving mass problem formulation was applied by Van Do et al. in [44] for the plane straight Bernoulli-Euler beam.

3 NURBS

In this chapter, the geometry representation of the curves parameterized using NURBS basis functions is discussed. Main properties, as well as the advantages of the given parameterization, are presented. At the end of the chapter, the refinement procedures of the NURBS parameterized curves are explained, and their effect on the shape of the curves is shown.

Geometry description of the physical structure represents the critical step in the structural analysis. Beam, as three-dimensional structure, can be described as a spatial curve due to the beam assumptions. This curve is denoted as a beam's centerline. Besides the explicit and implicit definition of the curve, the parametric description is the most useful for the geometric representation of the curve [9]. One of the parametric description advantages can be found in the straightforward boundary condition application for the beam-like structures.

Computed-aided design (CAD) software packages, nowadays widely used for geometry description of the structures, are based on the parametric representation. Utilization of NURBS functions in these software packages gives the possibility to accurately represent the curves with free form and conical section shapes. In order to comprehend NURBS functions, it is essential to formulate their constructive functions, B-Spline functions.

3.1 B-Spline functions

The B-Spline functions are constructed in the parameter domain using a knot vector. The knot vector ξ is a set of non-decreasing real numbers (the knots, ξ_i) which represent coordinates of the parametric space ξ . The interval between two adjacent knots is denoted as a knot span. If the values of the adjacent knots are equal, the knot span is empty. The non-empty knot spans subdivide the domain into elements.

The B-Spline functions are piecewise polynomial functions constructed using Cox de Boor algorithm [8]. In the case of zero degree of polynomial ($p = 0$), the i -th B-Spline function is:

$$N_{i,0} = \begin{cases} 1, & \text{if } \xi \in [\xi_i, \xi_{i+1}[\\ 0, & \text{otherwise} \end{cases} \quad (3.1)$$

while for higher polynomial degree case, $p > 0$:

$$N_{i,p} = \begin{cases} \frac{\xi - \xi_i}{\xi_{i+p} - \xi_i} N_{i,p-1}(\xi) + \frac{\xi_{i+p+1} - \xi}{\xi_{i+p+1} - \xi_{i+1}} N_{i+1,p-1}(\xi), & \text{if } \xi \in [\xi_i, \xi_{i+p+1}[\\ 0, & \text{otherwise} \end{cases} \quad (3.2)$$

Since the i -th B-Spline function is defined over multiple adjacent knot spans, it is crucial to determine the continuity of the B-Spline function between the elements in the parametric domain. The continuity is determined by the number of the B-Spline polynomial degree and the number of the repeated knots $k - C^{p-k}$. The non-negativity and the partition of unity of the B-Spline functions are additional important properties, used in the following formulations. Some of the B-Spline properties are directly related to the knot vector properties. The knot vector is denoted as an open vector if the number of repeated knots at the beginning and the end of the parametric domain is equal to the B-Spline polynomial degree. The B-Spline functions constructed over the open knot vector have an interpolatory property at the beginning and the end of the domain.

Due to the recursive formulation of the B-Spline function, the derivative is easily obtained:

$$\frac{d}{d\xi} N_{i,p}(\xi) = \frac{p}{\xi_{i+p} - \xi_i} N_{i,p-1}(\xi) - \frac{p}{\xi_{i+p+1} - \xi_{i+1}} N_{i+1,p-1}(\xi) \quad (3.3)$$

An arbitrary curve in Euclidean space $\mathbf{C}(\xi)$ can be constructed as a linear combination of the B-Spline functions:

$$\mathbf{C}(\xi) = \sum_{i=0}^n N_{i,p}(\xi) \mathbf{P}_i \quad (3.4)$$

where \mathbf{P}_i represents the i -th control point, which discretizes curve in the Euclidean space, while n is the number of the control points (basis functions). It is important to define control polygon, which is constructed by the linear interpolation of the adjacent control points.

Depending on the B-Spline polynomial degree and the knots' multiplicity, the B-Spline basis functions are non-zero functions on the exact number of the knot spans. Consequently, the i -th control point only locally influence the shape of the curve, where the i -th B-Spline basis function has a non-zero value in the parametric domain. In Figure 3.1 various curve shapes are presented with corresponding control polygons. As can be noticed, control point \mathbf{P}_0 has an influence only on the part of the curve defined over the first knot span, where corresponding B-Spline basis function has non-zero values. The rest of the curve has not changed its shape during the change of the first control point position. Aforementioned represents an additional advantage of the presented procedure for parameterization of the curves with an arbitrary shape. Another essential property of the parametrized curve is its continuity, which is directly coupled to the parametric continuity of the B-Spline basis functions.

Derivative of the curve is obtained from the derivative of the B-Spline basis function:

$$\frac{d}{d\xi} \mathbf{C}(\xi) = \sum_{i=0}^n \frac{dN_{i,p}(\xi)}{d\xi} \mathbf{P}_i \quad (3.5)$$

In addition, the B-Spline basis function degree p , the number of control points ($n_{cp} = n + 1$) and the number of the terms in the knot vector (m) are coupled by the relation:

$$m = n_{cp} + p + 1 \quad (3.6)$$

3.2 NURBS functions

The B-Spline basis functions are capable only to represent the polynomial curves accurately. This limitation can be overcome with Non-Uniform Rational B-Spline (NURBS) functions for

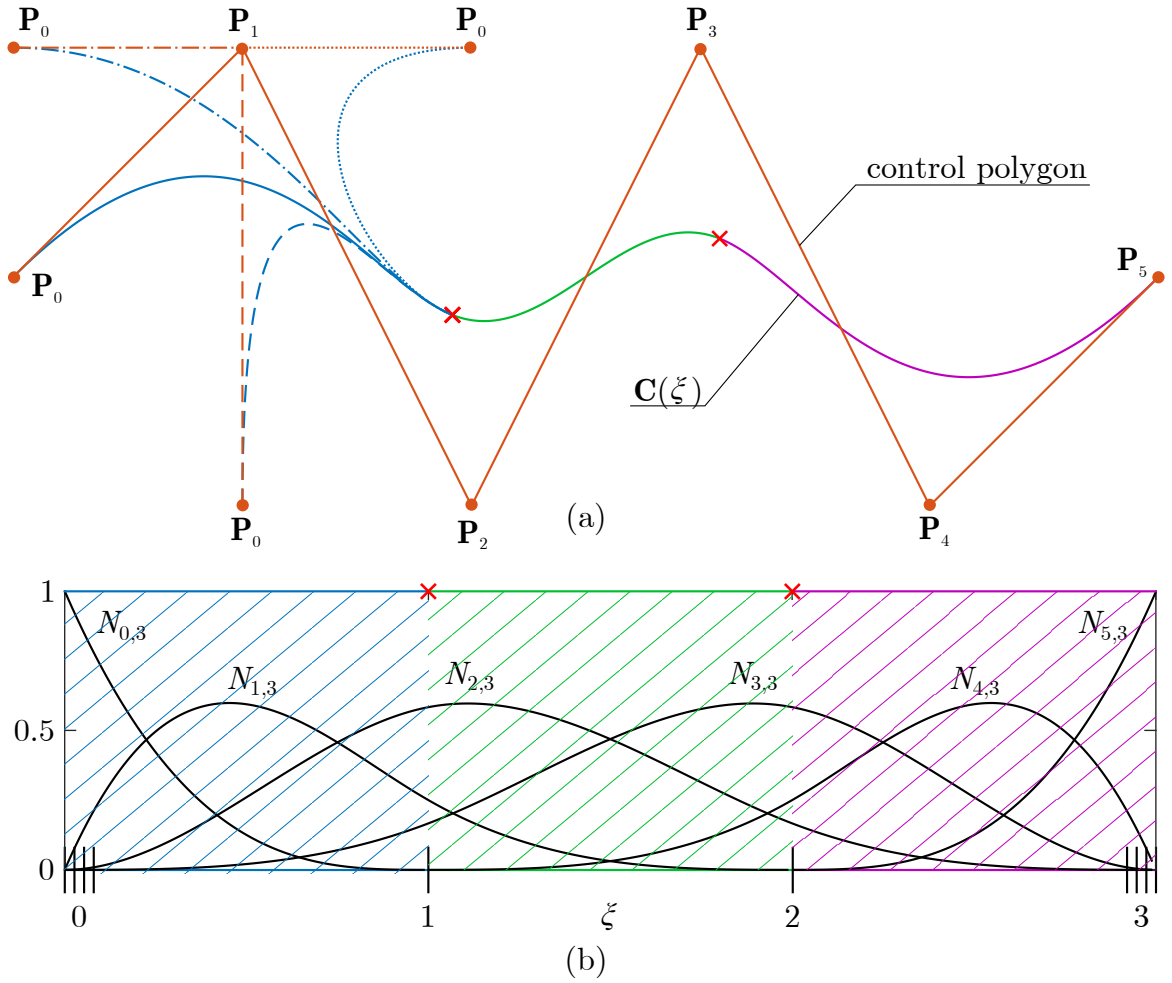


Figure 3.1: (a) Shape variations of the plane arbitrary shaped curve with the corresponding control polygon, (b) B-Spline functions of polynomial degree $p = 3$, constructed over the knot vector $[0, 0, 0, 0, 1, 2, 3, 3, 3, 3]$

curves like circle, ellipse, parabola and hyperbola. As a rational functions, NURBS are derived from the B-Spline functions:

$$R_{i,p}(\xi) = \frac{\sum_{i=0}^n \frac{N_{i,p}(\xi) w_i}{\sum_{j=0}^n N_{j,p}(\xi) w_j}}{\quad} \quad (3.7)$$

where w_i represents the weight of the corresponding control point. Weights can be interpreted as heights of the control points in the higher dimensional space.

NURBS basis functions have inherited the properties of the B-Spline basis functions such as the partition of the unity, the local influence of the control points, and non-negativity. B-Spline basis functions can be obtained directly from NURBS basis functions if the weights have equal values for all control points. An arbitrary curve in Euclidean space constructed using NURBS basis functions is obtained using Equation 3.4 by replacing $N_{i,p}$ by $R_{i,p}$.

3.3 Refinements

In some cases, the local influence of the control point has to be reduced without changing the shape of the curve. This can be achieved applying the refinement procedures given for the

B-Spline and NURBS functions denoted as H -, P - and K - refinement procedures [45]. The H - refinement represents the knot insertion procedure conducted by inserting the additional knot at a non-empty knot span. Consequently, the number of elements and the control points increases by one without changing the curve shape.

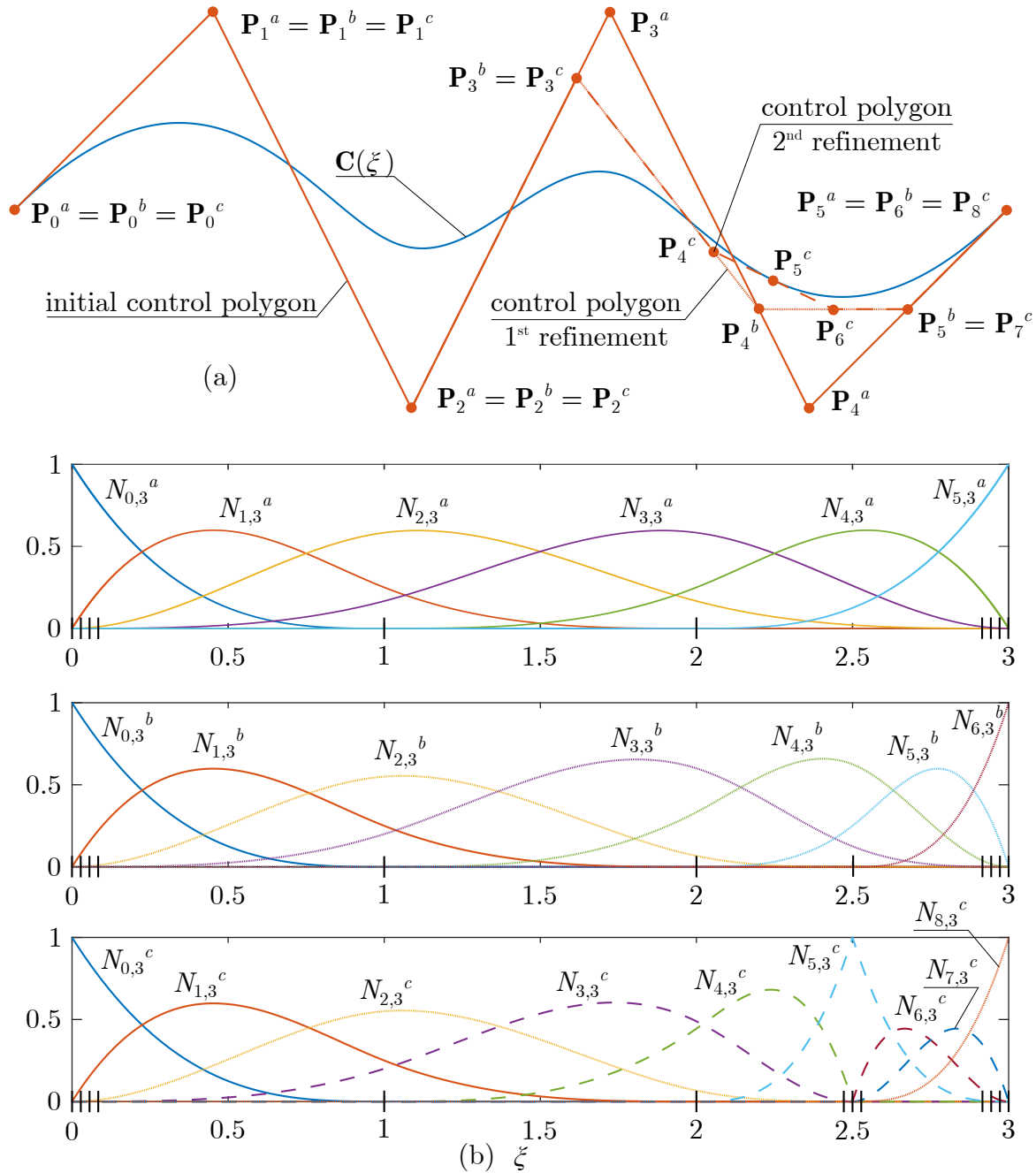


Figure 3.2: (a) Control polygons of the plane curve with constant shape for three cases of H - refinement (a - initial shape, b - 1st refinement, c - 2nd refinement), (b) the B-Spline functions of polynomial degree $p = 3$ constructed using the different knot vectors

In Figure 3.2, the arbitrary plane curve is defined using the B-Spline basis functions of the polynomial degree $p = 3$, constructed over the knot vector $\xi = [0, 0, 0, 0, 1, 2, 3, 3, 3]$. By inserting additional knot at the parametric coordinate 2.5, the number of basis functions and the number of control points have been increased by one. In addition, the control polygon has changed its shape, while some of the basis functions have been modified. At the end of the presented H - refinement example, the knot has been additionally inserted twice at the parametric coordinate 2.5. Consequently, the knot multiplicity has been equal to the polynomial

order of the basis functions. In this particular case, the non-boundary control point (\mathbf{P}_5^c) has become an interpolatory point.

The P - refinement denotes refinement procedure of the basis functions order elevation. Applying the P - refinement, the geometry and the parameterization of the curve are intact, while the degree of the basis function is elevated by preserving the parametric continuity, which is achieved by the knot insertion at the initially defined knots.

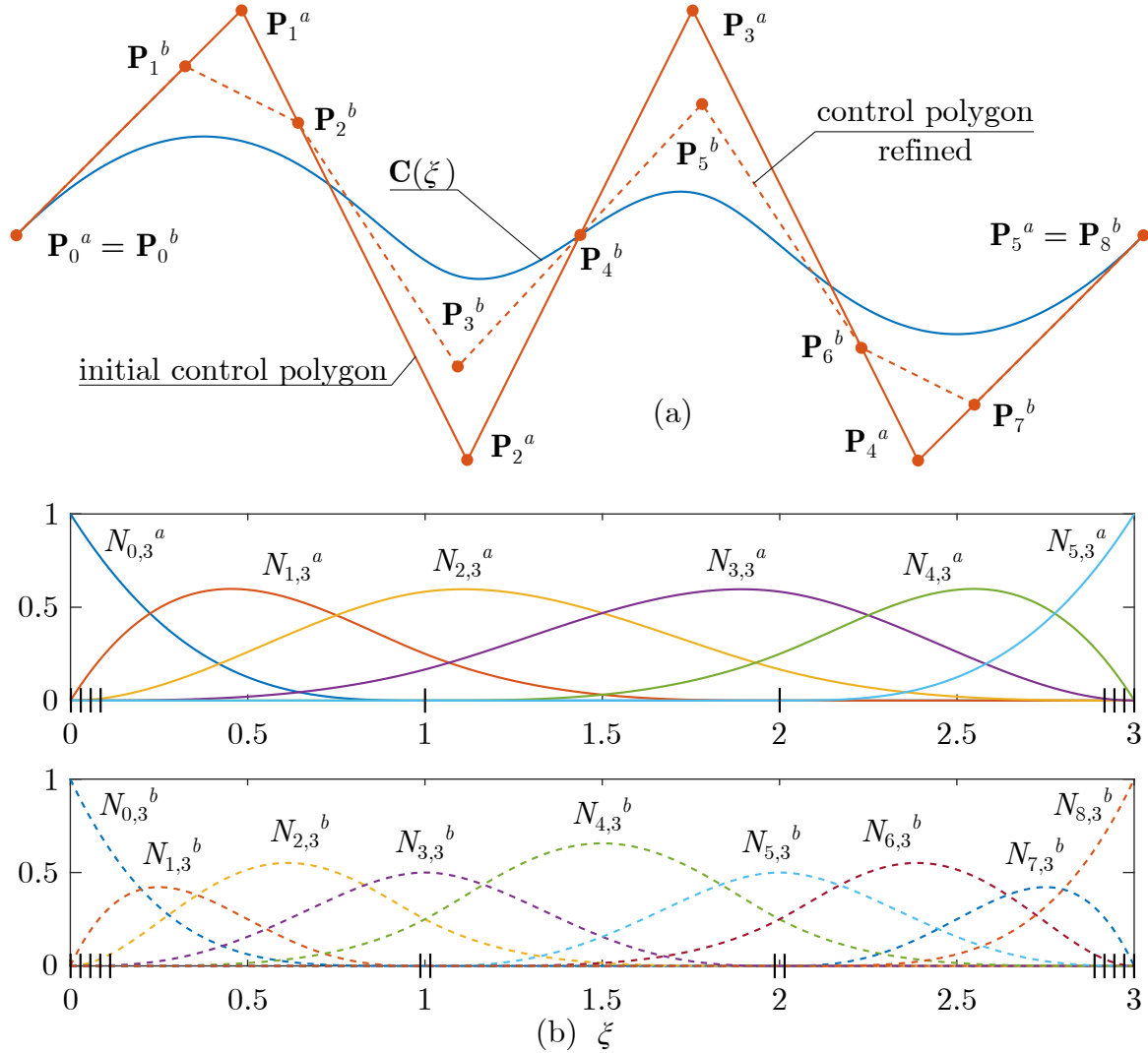


Figure 3.3: (a) Control polygons of the plane curve for two cases of P - refinement (a - initial shape, b - 1st refinement), (b) the B-Spline functions of polynomial degree $p = 3$ constructed using different knot vectors

In Figure 3.3, the plane curve has been constructed using the control points (\mathbf{P}_i^a) and the corresponding B-Spline basis functions ($N_{i,3}^a$). The P - refinement is conducted in order to elevate the polynomial degree by one, while the parametric continuity is unchanged. Consequently, the additional knots have been repeated. As can be noticed from the figure, the shape of the curve and the number of elements is unchanged.

Additional refinement procedure unique for the isogeometric concept is the K - refinement, representing the combination of the above refinement procedures. The order of activity in the K - refinement is crucial, where knot insertion is conducted after the order elevation is done [4]. It is important to emphasize that the activity order is not commutative, and the reversed procedure will not provide the required results.

4 Differential geometry

In this chapter, the differential geometry is applied in order to define a 3D deformable beam with respect to the beam's centerline. In general, beam's centerline is a spatial curve which can be parametrized using NURBS parametrization. Introduction of the ξ_λ frame of reference [2] has preserved the orthogonality of an arbitrary beam point basis vectors, which is convenient for the Bernoulli-Euler beam formulation.

As a deformable body, the spatial beam can be derived directly from the three-dimensional continuum applying appropriate beam assumptions, by reducing three-dimensional space to one-dimensional one. As one dimension of the beam is significantly larger than the other two, all kinematic and stress quantities of the beam can be given as a function of this dimension, denoted as the beam's centerline. Aforementioned represents the axis, which in general has an arbitrary shape in Euclidean three-dimensional space, forming the curved beam. All formulations and analyses of the curved beam will be conducted using a curvilinear coordinate system attached to the beam's centerline.

The beam's centerline is defined by the position vector \mathbf{r} . First basis vector of the curvilinear beam's system is a tangent unit vector [46] derived using differential geometry:

$$\mathbf{t} = \frac{d\mathbf{r}}{ds} = \mathbf{r}' \quad (4.1)$$

where s is the arc-length parameter. In order to complete the three-dimensional Euclidean space of the curvilinear system, additional two basis vectors are required, the normal \mathbf{n} and binormal \mathbf{b} vectors:

$$\mathbf{n} = \frac{1}{K} \frac{d\mathbf{t}}{ds} = \frac{\mathbf{K}}{K} \quad (4.2)$$

$$\mathbf{b} = \mathbf{t} \times \mathbf{n} \quad (4.3)$$

In Equation 4.2, term \mathbf{K} is the curvature vector with modulus K . Using this formulation, normal and binormal vectors are also unit vectors. Consequently, the curvilinear beam's system in arc-length parameterization is orthonormal, i.e. its metric tensor is a unit tensor. Due to the orthogonality of the basis vectors and the assumption of the rigid beam cross-section perpendicular to the beam's centerline, normal and binormal vectors are located in the beam cross-section plane. The presented curvilinear system given in arc-length parameterization forms the Frenet - Serret frame of reference with well-known relations [47]:

$$\begin{bmatrix} \mathbf{t}' \\ \mathbf{n}' \\ \mathbf{b}' \end{bmatrix} = \begin{bmatrix} 0 & K & 0 \\ -K & 0 & \tau \\ 0 & -\tau & 0 \end{bmatrix} \begin{bmatrix} \mathbf{t} \\ \mathbf{n} \\ \mathbf{b} \end{bmatrix} \quad (4.4)$$

where τ is the torsion of the beam's centerline.

4.1 NURBS parameterization

NURBS parameterization presents an efficient approach to parameterize the curve with an arbitrary shape. Using this parameterization, the basis vectors are defined as:

$$\mathbf{g}_1 = \frac{d\mathbf{r}}{d\xi} = \frac{d\mathbf{r}}{ds} \frac{ds}{d\xi} = \mathbf{t}\sqrt{g_{11}} \quad (4.5)$$

$$\mathbf{G}_2 = \mathbf{n} = \frac{1}{K} \frac{d\xi}{ds} \frac{d}{d\xi} \left(\frac{\mathbf{g}_1}{|\mathbf{g}_1|} \right) \quad (4.6)$$

$$\mathbf{G}_3 = \mathbf{b} = \frac{\mathbf{g}_1 \times \mathbf{n}}{|\mathbf{g}_1 \times \mathbf{n}|} \quad (4.7)$$

In Equation 4.5, the term g_{11} is the component of the NURBS parametrized centerline metric tensor, which is in general different from 1. Consequently, the tangent vector \mathbf{g}_1 is not a unit vector. However, it is collinear to the tangent vector of the arc-length parameterization, \mathbf{t} . Using NURBS parameterization of the beam's centerline, its metric tensor is:

$$\mathbf{g}_{ij} = \begin{bmatrix} g_{11} & 0 & 0 \\ 0 & 1 & 0 \\ 0 & 0 & 1 \end{bmatrix} \quad (4.8)$$

such that $\det(\mathbf{g}_{ij}) = g_{11} = g$. In addition, the derivative of the basis vectors with respect to the NURBS parameter is:

$$\begin{bmatrix} \mathbf{g}_{1,1} \\ \mathbf{G}_{2,1} \\ \mathbf{G}_{3,1} \end{bmatrix} = \begin{bmatrix} \Gamma_{11}^1 & gK & 0 \\ -gK & 0 & \sqrt{g}\tau \\ 0 & -\sqrt{g}\tau & 0 \end{bmatrix} \begin{bmatrix} \mathbf{g}_1 \\ \mathbf{G}_2 \\ \mathbf{G}_3 \end{bmatrix} \quad (4.9)$$

where $(\cdot)_{,1}$ denotes the derivative with respect to the NURBS parameter ξ , while $\Gamma_{11}^1 = \frac{1}{2} \frac{g_{,1}}{g}$ represents the Christoffel symbol of the second kind. Generally, beam formulation is defined with respect to the beam's principal axes, which do not coincide with vectors \mathbf{G}_2 and \mathbf{G}_3 . Consequently, new basis vectors in the direction to the principal axes, denoted as \mathbf{g}_2 and \mathbf{g}_3 , are introduced:

$$\begin{bmatrix} \mathbf{g}_2 \\ \mathbf{g}_3 \end{bmatrix} = \begin{bmatrix} \cos \beta & \sin \beta \\ -\sin \beta & \cos \beta \end{bmatrix} \begin{bmatrix} \mathbf{G}_2 \\ \mathbf{G}_3 \end{bmatrix} \quad (4.10)$$

where β represents the angle between the beam cross-section principal axes and the basis vectors \mathbf{G}_2 and \mathbf{G}_3 . Vectors \mathbf{g}_1 , \mathbf{g}_2 and \mathbf{g}_3 form the moving frame of reference of the beam's centerline in the principal axes direction in NURBS parameterization i.e. NURBS moving frame of reference, Figure 4.1.

Applying Equation 4.10, the metric tensor is unchanged, while the derivatives of the basis vectors with respect to the parameter ξ are:

$$\begin{bmatrix} \mathbf{g}_{1,1} \\ \mathbf{g}_{2,1} \\ \mathbf{g}_{3,1} \end{bmatrix} = \begin{bmatrix} \Gamma_{11}^1 & \bar{K}_3 & \bar{K}_2 \\ -K_3 & 0 & K_1 \\ K_2 & -K_1 & 0 \end{bmatrix} \begin{bmatrix} \mathbf{g}_1 \\ \mathbf{g}_2 \\ \mathbf{g}_3 \end{bmatrix} \quad (4.11)$$

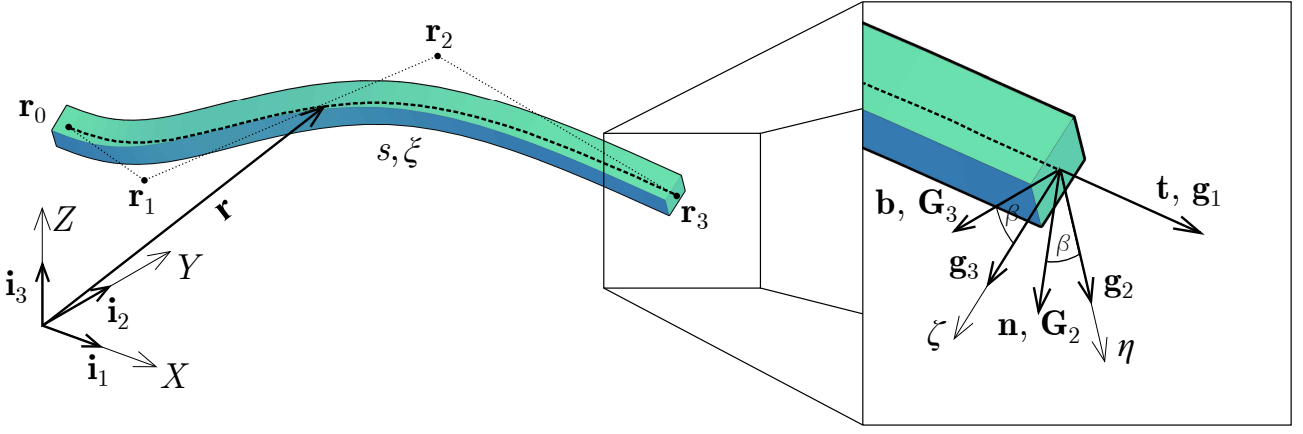


Figure 4.1: Spatial beam element with an arbitrary shape obtained using NURBS parameterization [48]

where $K_1 = \sqrt{g}\tau$, $K_2 = K \sin \beta$, $K_3 = K \cos \beta$, $\bar{K}_i = gK_i$, ($i = 2, 3$).

The contravariant basis vectors of the NURBS moving frame of reference are easily obtained using its metric tensor:

$$\mathbf{g}^{ij} = \begin{bmatrix} 1/g & 0 & 0 \\ 0 & 1 & 0 \\ 0 & 0 & 1 \end{bmatrix} \quad (4.12)$$

Using NURBS moving frame of reference, an arbitrary point of the beam can be defined using the position vector:

$$\hat{\mathbf{r}} = \mathbf{r} + \eta \mathbf{g}_2 + \zeta \mathbf{g}_3 \quad (4.13)$$

where η and ζ are coordinates of the principal axes. The tangent vector of an arbitrary point is given as:

$$\hat{\mathbf{g}}_1 = \frac{d\hat{\mathbf{r}}}{d\xi} = \mathbf{g}_{1,1} + \eta \mathbf{g}_{2,1} + \zeta \mathbf{g}_{3,1} = g_0 \mathbf{g}_1 + \eta K_1 \mathbf{g}_2 + \zeta K_1 \mathbf{g}_3 \quad (4.14)$$

where $g_0 = 1 - \eta K_3 + \zeta K_2$, while the vectors \mathbf{g}_2 and \mathbf{g}_3 are translated from the beam's centerline to the arbitrary point due to the rigid beam cross-section. Metric tensor of an arbitrary point is given as:

$$\hat{\mathbf{g}}_{ij} = \begin{bmatrix} \hat{g}_{11} & -\zeta K_1 & \eta K_1 \\ -\zeta K_1 & 1 & 0 \\ \eta K_1 & 0 & 1 \end{bmatrix}, \quad \hat{g}_{11} = g_0^2 g_{11} + (\zeta^2 + \eta^2) K_1^2 \quad (4.15)$$

The basis vector $\hat{\mathbf{g}}_1$ is not perpendicular to the basis vectors \mathbf{g}_2 and \mathbf{g}_3 , which can be concluded from the nonzero off-diagonal components of the metric tensor. In order to maintain the same basis vectors for the centerline and an arbitrary point, a new parametrization has to be performed introducing the ξ_λ frame of reference [2]. As mentioned before, basis vectors \mathbf{g}_2 and \mathbf{g}_3 are the same for every beam cross-section point due to the rigid cross-section assumption in the beam theory. However, the tangent vector in the ξ_λ frame of reference has to be the same as the tangent vector of the centerline:

$$\mathbf{g}_\lambda = \frac{\partial \hat{\mathbf{r}}}{\partial \xi_\lambda} = \frac{\partial \zeta}{\partial \xi_\lambda} \hat{\mathbf{g}}_1 + \frac{\partial \eta}{\partial \xi_\lambda} \mathbf{g}_2 + \frac{\partial \zeta}{\partial \xi_\lambda} \mathbf{g}_3 = \mathbf{g}_1 \quad (4.16)$$

In order to satisfy this condition, the relation between two parametrizations is given as:

$$\frac{\partial \xi}{\partial \xi_\lambda} = \frac{1}{g_0}, \quad \frac{\partial \eta}{\partial \xi_\lambda} = \zeta K_1 \frac{\partial \xi}{\partial \xi_\lambda}, \quad \frac{\partial \zeta}{\partial \xi_\lambda} = -\eta K_1 \frac{\partial \xi}{\partial \xi_\lambda} \quad (4.17)$$

In the ξ_λ frame of reference, the metric tensor of an arbitrary point is the same as the metric tensor of the NURBS moving frame of reference of the beam's centerline, Equation 4.8.

Employing the procedure for the geometric representation of the spatial curves using NURBS basis functions, the position vector of the beam's centerline is:

$$\mathbf{r} = \sum_{i=0}^N R_i(\xi) \mathbf{r}_i = \sum_{i=0}^N R_i(\xi) r_i^m \mathbf{i}_m = x^m \mathbf{i}_m \quad (4.18)$$

where $R_i(\xi)$ is the i -th NURBS basis function, \mathbf{r}_i is the i -th control point, r_i^m is the m -th Cartesian component of the vector \mathbf{r}_i , while x^m is the m -th Cartesian component of the position vector with corresponding basis vectors of the Cartesian coordinate system, Figure 4.1.

Using Equations 4.5 - 4.7 and Equation 4.10, the basis vectors of the beam's centerline can be obtained using NURBS parameterization. The basis vectors in the Cartesian coordinate system are:

$$\mathbf{g}_i = x_i^m \mathbf{i}_m \quad i = 1, 2, 3 \quad (4.19)$$

with corresponding Cartesian components:

$$x_1^m = x_{,1}^m \quad (4.20)$$

$$x_2^m = \frac{1}{\sqrt{gK}} \left(x_{,11}^m - \Gamma_{11}^1 x_{,1}^m \right) \cos \beta + \frac{1}{\sqrt{gK}} x_{k,1} x_{l,11} e^{klm} \sin \beta \quad (4.21)$$

$$x_3^m = \frac{1}{\sqrt{gK}} x_{k,1} x_{l,11} e^{klm} \cos \beta - \frac{1}{\sqrt{gK}} \left(x_{,11}^m - \Gamma_{11}^1 x_{,1}^m \right) \sin \beta \quad (4.22)$$

In previous relations $x_{,11}^m$ represents the second derivative with respect to the parameter ξ , while e^{klm} is the permutation symbol.

5 Linear dynamic formulation of spatial Bernoulli - Euler beam

In this chapter, the linear formulation of the spatial curved Bernoulli-Euler beam element using the isogeometric approach is presented. Displacement, velocity and acceleration fields are derived accounting for the infinitesimal displacements and rotations. Only linear parts are taken into account in the kinematic and constitutive relations. Governing equations of motion of the Bernoulli-Euler beam for the free vibration and forced vibration analysis are derived. Latter are solved applying explicit direct integration scheme using central difference method. Some of the presented theoretical considerations are published by the author in [48].

Beam theories are based on the assumption that beam cross-section can be modeled as a rigid body. The motion of the rigid body is the composition of a reference point translation and a rotation about the reference point. In beam formulation, the centroid of beam cross-section is chosen for the reference point. The sum of all cross-section centroids forms the beam's centerline, where all beam quantities required for the beam formulation are defined.

In linear formulation, where both geometrical and material linearities are assumed, displacements and rotations are infinitesimal vector quantities, therefore can be used as degrees of freedom. It is essential to point out that the beam formulation will be presented in the convective coordinate system. Using this system, coordinates of the material and spatial coordinate system are the same, i.e. the label of the material point in the material coordinate system will be preserved in the spatial coordinate system. Consequently, the basis vectors of the NURBS moving frame will change during the deformation process.

The assumption of beam rigid cross-section causes additional simplifications. During the deformation process some of the strain components in the convective coordinate system vanish, i.e:

$$\varepsilon_{22} = 0, \quad \varepsilon_{33} = 0, \quad \varepsilon_{23} = 0 \quad (5.1)$$

In addition, Bernoulli-Euler beam theory introduces additional assumption that the rigid cross-section remains perpendicular to the beam's centerline during the deformations. Consequently, the strain tensor components in the convective coordinate system at the beam's centerline are:

$$\varepsilon_{12} = 0, \quad \varepsilon_{13} = 0 \quad (5.2)$$

5.1 Deformed configuration of the beam

Due to external impact on the spatial beam, an initial undeformed configuration defined using position vector \mathbf{r} will have a new deformed configuration \mathbf{r}^* given as:

$$\mathbf{r}^* = \mathbf{r} + \mathbf{u} \quad (5.3)$$

where \mathbf{u} represents the displacement vector of the beam's centerline, Figure 5.1.

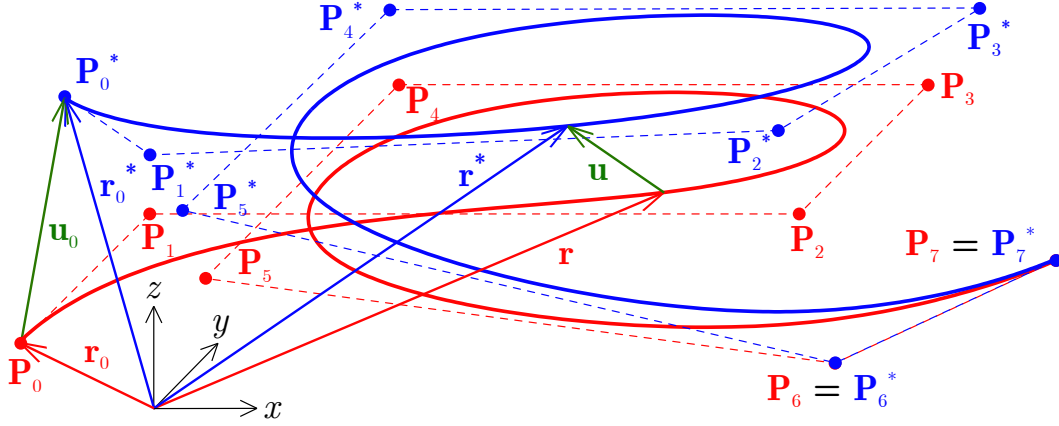


Figure 5.1: Deformed and undeformed configuration of the beam's centerline with the corresponding control polygon and the displacement vectors for the centerline and the first control point

Using NURBS parametrization described in Section 4.1 the displacement vector can be represented as:

$$\mathbf{u}(\xi) = \sum_{i=0}^n R_{i,p}(\xi) \mathbf{u}_i \quad (5.4)$$

where \mathbf{u}_i is the displacement vector for the i -th control point. It is important to emphasize that the displacement vector and the beam's centerline geometry are presented using the same NURBS parameterization. This concept is the fundamental property of the isogeometric approach in structural analysis. In addition, the displacement vector can be represented as:

$$\mathbf{u} = u_\alpha \mathbf{i}_\alpha = \tilde{u}^m \mathbf{g}_m = \tilde{u}_n \mathbf{g}^n \quad (5.5)$$

where u_α is the α -th Cartesian component of the centerline displacement vector, while \tilde{u}^m and \tilde{u}_n are the m -th contravariant and n -th covariant components of the centerline displacement in the NURBS moving frame of reference.

The position vector of an arbitrary point of deformed beam in convective coordinates is:

$$\hat{\mathbf{r}}^* = \mathbf{r}^* + \eta \mathbf{g}_2^* + \zeta \mathbf{g}_3^* \quad (5.6)$$

which shows that the deformed beam configuration imposes new basis vectors of the beam's centerline. Using the convective coordinate system, basis vectors of the NURBS moving frame for deformed configuration are:

$$\mathbf{g}_i^* = (\delta_t^m + \tilde{u}^m|_t) \mathbf{g}_m \quad (5.7)$$

where $\tilde{u}^m|_t$ presents the m -th component of the t -th covariant derivative.

In addition, basis vectors of the deformed configuration can be expressed as:

$$\mathbf{g}_m^* = \mathbf{g}_m + \mathbf{u}_m \quad (5.8)$$

where \mathbf{u}_m represents the displacement vector of the m - th basis vector.

Use of the convective coordinate system provides an additional formulation of the deformed basis vectors:

$$\mathbf{g}_m^* = \mathbf{F} \cdot \mathbf{g}_m \quad (5.9)$$

In the previous relation, \mathbf{F} represents the deformation gradient, which becomes the rotation tensor \mathbf{R}_g for the second and third base vector due to the beam assumption. Rotation about the reference point in the linear formulation is defined as:

$$\mathbf{R}_g = \mathbf{I} + \mathbf{\Phi} \quad (5.10)$$

where \mathbf{I} is the unit tensor, while $\mathbf{\Phi}$ is a skew-symmetric tensor, which represents the tensor of infinitesimal rotation. By definition, the skew - symmetric tensor can be written as:

$$\mathbf{\Phi} \cdot \mathbf{g}_j = \boldsymbol{\phi} \times \mathbf{g}_j, \quad j = 2, 3 \quad (5.11)$$

where $\boldsymbol{\phi}$ is the axial (dual) vector of the skew - symmetric tensor. Vector $\boldsymbol{\phi}$ represents the vector of infinitesimal rotation, which can be defined in NURBS moving frame of reference as:

$$\boldsymbol{\phi} = \phi^i \mathbf{g}_i, \quad \phi^i = \frac{1}{2\sqrt{g}} \tilde{u}_{jk} e^{kji} \quad (5.12)$$

5.2 Displacement field

Displacement of an arbitrary point of beam can be defined as:

$$\hat{\mathbf{u}} = \hat{\mathbf{r}}^* - \hat{\mathbf{r}} \quad (5.13)$$

Using Equations 4.13, 5.6 and 5.8 displacement field is expressed as:

$$\hat{\mathbf{u}} = \mathbf{u} + \eta \mathbf{u}_2 + \zeta \mathbf{u}_3 \quad (5.14)$$

Equation 5.14 can be expressed in matrix form as:

$$\hat{\mathbf{u}} = \underbrace{\begin{bmatrix} 1 & \eta & \zeta \end{bmatrix}}_{\mathbf{C}} \underbrace{\begin{bmatrix} \mathbf{u} \\ \mathbf{u}_2 \\ \mathbf{u}_3 \end{bmatrix}}_{\mathbf{u}_c} \quad (5.15)$$

The first component of the displacement field \mathbf{u} represents the displacement of the beam's centerline defined by Equation 5.5 as:

$$\mathbf{u} = \underbrace{\begin{bmatrix} \mathbf{i}_1 & \mathbf{i}_2 & \mathbf{i}_3 \end{bmatrix}}_{\mathbf{i}} \begin{bmatrix} u_1 \\ u_2 \\ u_3 \end{bmatrix} \quad (5.16)$$

Other components of the displacement field are defined applying Equations 5.7 and 5.8 and relation $\tilde{u}^m|_t = \tilde{u}_{j|t}g^{jm}$:

$$\mathbf{u}_2 = \frac{\tilde{u}_{1|2}}{g}\mathbf{g}_1 + \tilde{u}_{2|2}\mathbf{g}_2 + \tilde{u}_{3|2}\mathbf{g}_3 \quad (5.17)$$

$$\mathbf{u}_3 = \frac{\tilde{u}_{1|3}}{g}\mathbf{g}_1 + \tilde{u}_{2|3}\mathbf{g}_2 + \tilde{u}_{3|3}\mathbf{g}_3 \quad (5.18)$$

Applying the beam rigid cross-section assumption, as well as the Bernoulli-Euler assumption, derivatives of the displacement components in the NURBS moving frame are:

$$\tilde{u}_{2|2} = 0, \quad \tilde{u}_{3|3} = 0, \quad \tilde{u}_{1|2} = -\tilde{u}_{2|1}, \quad \tilde{u}_{1|3} = -\tilde{u}_{3|1}, \quad \tilde{u}_{2|3} = -\tilde{u}_{3|2} \quad (5.19)$$

Consequently, the terms \mathbf{u}_2 and \mathbf{u}_3 are:

$$\mathbf{u}_2 = -\frac{\tilde{u}_{2|1}}{g}\mathbf{g}_1 + \tilde{u}_{3|2}\mathbf{g}_3 \quad (5.20)$$

$$\mathbf{u}_3 = -\frac{\tilde{u}_{3|1}}{g}\mathbf{g}_1 - \tilde{u}_{3|2}\mathbf{g}_2 \quad (5.21)$$

The relation between the derivatives of the displacement components given in the NURBS moving frame and in the Cartesian coordinate system is:

$$\tilde{u}_{i|j} = \mathbf{u}_{,j} \cdot \mathbf{g}_i = u_{m,j}x_i^m \quad (5.22)$$

If the previous relation is applied for the component $\tilde{u}_{3|2}$, the derivative of the beam's centerline displacement with respect to the coordinate ζ , denoted as $(\cdot)_{,3}$, appears:

$$\tilde{u}_{3|2} = \mathbf{u}_{,3} \cdot \mathbf{g}_2 \quad (5.23)$$

In the conventional beam formulation, only the derivative of the beam's centerline displacement with respect to the ξ coordinate exists. However, $\tilde{u}_{3|2}$ appears in the first component of the vector of infinitesimal rotation, given in Equation 5.12, when the beam assumption is applied:

$$\phi^1 = \frac{1}{\sqrt{g}}\tilde{u}_{3|2} \quad (5.24)$$

Consequently, the term $\tilde{u}_{3|2}$ represents the physical component of the rotation in direction to the axis \mathbf{g}_1 , i.e. the torsional rotation of the beam cross-section, which will be denoted as φ in the following. The torsional rotation represents the additional degree of freedom for the Bernoulli-Euler beam besides the beam's centerline translation.

By substituting Equations 5.22 and 5.24 into Equations 5.20 and 5.21, displacement vectors \mathbf{u}_2 and \mathbf{u}_3 are:

$$\mathbf{u}_2 = \underbrace{\begin{bmatrix} -\frac{x_2^1}{g}\mathbf{g}_1 & -\frac{x_2^2}{g}\mathbf{g}_1 & -\frac{x_2^3}{g}\mathbf{g}_1 & \mathbf{g}_3 \end{bmatrix}}_{\mathbf{A}_u} \begin{bmatrix} u_{1,1} \\ u_{2,1} \\ u_{3,1} \\ \varphi \end{bmatrix} \quad (5.25)$$

$$\mathbf{A}_u^T = \underbrace{\begin{bmatrix} -\frac{x_2^1}{x_1^1}x_1^1 & -\frac{x_2^1}{x_1^1}x_2^1 & -\frac{x_2^1}{x_1^1}x_3^1 \\ g_2 & g_2 & g_2 \\ \frac{x_2^2}{x_1^1}x_1^1 & \frac{x_2^2}{x_1^1}x_2^1 & \frac{x_2^2}{x_1^1}x_3^1 \\ g_3 & g_3 & g_3 \\ \frac{x_2^3}{x_1^1}x_1^1 & \frac{x_2^3}{x_1^1}x_2^1 & \frac{x_2^3}{x_1^1}x_3^1 \\ -\frac{x_2^1}{x_1^1}x_1^1 & -\frac{x_2^1}{x_1^1}x_2^1 & -\frac{x_2^1}{x_1^1}x_3^1 \\ g & g & g \\ x_3^1 & x_3^2 & x_3^3 \end{bmatrix}}_{\mathbf{B}_u} \underbrace{\begin{bmatrix} \mathbf{i}_1 \\ \mathbf{i}_2 \\ \mathbf{i}_3 \end{bmatrix}}_{\mathbf{i}^T} \quad (5.26)$$

$$\mathbf{u}_3 = \underbrace{\begin{bmatrix} -\frac{x_3^1}{g}\mathbf{g}_1 & -\frac{x_3^2}{g}\mathbf{g}_1 & -\frac{x_3^3}{g}\mathbf{g}_1 & -\mathbf{g}_2 \end{bmatrix}}_{\mathbf{C}_u} \begin{bmatrix} u_{1,1} \\ u_{2,1} \\ u_{3,1} \\ \varphi \end{bmatrix} \quad (5.27)$$

$$\mathbf{C}_u^T = \underbrace{\begin{bmatrix} -\frac{x_3^1}{x_1^1}x_1^1 & -\frac{x_3^1}{x_1^1}x_2^1 & -\frac{x_3^1}{x_1^1}x_3^1 \\ g_2 & g_2 & g_2 \\ \frac{x_3^2}{x_1^1}x_1^1 & \frac{x_3^2}{x_1^1}x_2^1 & \frac{x_3^2}{x_1^1}x_3^1 \\ g_3 & g_3 & g_3 \\ \frac{x_3^3}{x_1^1}x_1^1 & \frac{x_3^3}{x_1^1}x_2^1 & \frac{x_3^3}{x_1^1}x_3^1 \\ -\frac{x_3^1}{x_1^1}x_1^1 & -\frac{x_3^1}{x_1^1}x_2^1 & -\frac{x_3^1}{x_1^1}x_3^1 \\ g & g & g \\ -x_2^1 & -x_2^2 & -x_2^3 \end{bmatrix}}_{\mathbf{D}_u} \underbrace{\begin{bmatrix} \mathbf{i}_1 \\ \mathbf{i}_2 \\ \mathbf{i}_3 \end{bmatrix}}_{\mathbf{i}^T} \quad (5.28)$$

Finally, components of the displacement field can be represented in the matrix form as:

$$\mathbf{u}_c = \underbrace{\begin{bmatrix} \mathbf{i} & 0 & 0 \\ 0 & \mathbf{i} & 0 \\ 0 & 0 & \mathbf{i} \end{bmatrix}}_{\mathbf{G}_u} \underbrace{\begin{bmatrix} \mathbf{I} & 0 \\ 0 & \mathbf{B}_u^T \\ 0 & \mathbf{D}_u^T \end{bmatrix}}_{\mathbf{u}_{cc}} \begin{bmatrix} u_1 \\ u_2 \\ u_3 \\ u_{1,1} \\ u_{2,1} \\ u_{3,1} \\ \varphi \end{bmatrix}, \quad \mathbf{I} = \begin{bmatrix} 1 & 0 & 0 \\ 0 & 1 & 0 \\ 0 & 0 & 1 \end{bmatrix} \quad (5.29)$$

Components of the vector \mathbf{u}_{cc} represent the Cartesian components of the beam's centerline displacement and its derivatives with respect to the parameter ξ and the torsional rotation. These components can be parametrized using the NURBS parametrization as:

$$\mathbf{u}_{cc} = \sum_{i=0}^N \mathbf{R}_i \mathbf{q}^i = \mathbf{R} \mathbf{q} \quad (5.30)$$

where

$$\mathbf{R}^T = \begin{bmatrix} \mathbf{R}_0 \\ \mathbf{R}_1 \\ \vdots \\ \mathbf{R}_i \\ \vdots \\ \mathbf{R}_N \end{bmatrix}, \quad \mathbf{R}_i = \begin{bmatrix} R_i(\xi) & 0 & 0 & 0 \\ 0 & R_i(\xi) & 0 & 0 \\ 0 & 0 & R_i(\xi) & 0 \\ R_{i,1}(\xi) & 0 & 0 & 0 \\ 0 & R_{i,1}(\xi) & 0 & 0 \\ 0 & 0 & R_{i,1}(\xi) & 0 \\ 0 & 0 & 0 & R_i(\xi) \end{bmatrix} \quad (5.31)$$

$$\mathbf{q}^T = [\mathbf{q}^0 \quad \mathbf{q}^1 \quad \dots \quad \mathbf{q}^i \quad \dots \quad \mathbf{q}^N], \quad \mathbf{q}^i = \begin{bmatrix} u_1^i \\ u_2^i \\ u_3^i \\ \varphi^i \end{bmatrix} \quad (5.32)$$

Finally, the displacement field can be represented as:

$$\hat{\mathbf{u}} = \mathbf{C}\mathbf{G}_u\mathbf{R}\mathbf{q} \quad (5.33)$$

5.3 Velocity field

The velocity field represents the derivative of the position vector with respect to time and can be derived directly from the displacement field as its material derivative:

$$\hat{\mathbf{v}} = \frac{D}{Dt}(\hat{\mathbf{u}}) = \dot{\hat{\mathbf{u}}} = \dot{\mathbf{u}} + \eta\dot{\mathbf{u}}_2 + \zeta\dot{\mathbf{u}}_3 \quad (5.34)$$

Using Equation 5.8 velocity field can be written as:

$$\hat{\mathbf{v}} = \mathbf{v} + \eta\dot{\mathbf{g}}_2^* + \zeta\dot{\mathbf{g}}_3^* = \mathbf{v} + \eta\mathbf{v}_2 + \zeta\mathbf{v}_3 \quad (5.35)$$

Equation 5.35 can be written in the matrix form as:

$$\hat{\mathbf{v}} = \underbrace{\begin{bmatrix} 1 & \eta & \zeta \end{bmatrix}}_{\mathbf{C}} \underbrace{\begin{bmatrix} \mathbf{v} \\ \mathbf{v}_2 \\ \mathbf{v}_3 \end{bmatrix}}_{\mathbf{v}_c} \quad (5.36)$$

The first term in Equation 5.35 represents the velocity of the beam's centerline and is obtained directly from Equation 5.16 as:

$$\mathbf{v} = \underbrace{\begin{bmatrix} \mathbf{i}_1 & \mathbf{i}_2 & \mathbf{i}_3 \end{bmatrix}}_{\mathbf{i}} \begin{bmatrix} \dot{u}_1 \\ \dot{u}_2 \\ \dot{u}_3 \end{bmatrix} \quad (5.37)$$

Other terms are obtained from Equation 5.9:

$$\mathbf{v}_2 = \dot{\mathbf{g}}_2^* = \dot{\mathbf{R}}_g \cdot \mathbf{g}_2 = \dot{\Phi} \cdot \mathbf{g}_2 \quad (5.38)$$

$$\mathbf{v}_3 = \dot{\mathbf{g}}_3^* = \dot{\mathbf{R}}_g \cdot \mathbf{g}_3 = \dot{\Phi} \cdot \mathbf{g}_3 \quad (5.39)$$

The skew-symmetric tensor Φ can be represented using the axial (dual) vector ϕ , thus the previous relations can be represented as:

$$\mathbf{v}_2 = \dot{\phi} \times \mathbf{g}_2 \quad (5.40)$$

$$\mathbf{v}_3 = \dot{\phi} \times \mathbf{g}_3 \quad (5.41)$$

where the components of the vector $\dot{\phi}$ in terms of the NURBS moving frame are:

$$\dot{\phi}^k = \frac{1}{2\sqrt{g}} e^{klm} \dot{u}_{l|m} \quad (5.42)$$

In the previous relation, the term $\dot{u}_{l|m}$ represents the derivative of the velocity components given in the NURBS moving frame of reference.

Using Equations 5.22 and 5.42, the velocity field is obtained as:

$$\hat{\mathbf{v}} = \mathbf{C}\mathbf{G}_u\mathbf{R}\dot{\mathbf{q}}, \quad \dot{\mathbf{q}}^T = [\dot{\mathbf{q}}^0 \quad \dot{\mathbf{q}}^1 \quad \dots \quad \dot{\mathbf{q}}^i \quad \dots \quad \dot{\mathbf{q}}^N], \quad \dot{\mathbf{q}}^i = \begin{bmatrix} \dot{u}_1^i \\ \dot{u}_2^i \\ \dot{u}_3^i \\ \dot{\varphi}^i \end{bmatrix} \quad (5.43)$$

where the components of the vector $\dot{\mathbf{q}}^i$ are the velocity components in the Cartesian coordinate system and torsional rotational velocity of the i -th control point.

5.4 Acceleration field

Acceleration field of the beam is obtained as a time derivative of the velocity field:

$$\hat{\mathbf{a}} = \frac{D}{Dt}(\hat{\mathbf{v}}) = \dot{\hat{\mathbf{v}}} = \dot{\mathbf{v}} + \eta\dot{\mathbf{v}}_2 + \zeta\dot{\mathbf{v}}_3 = \mathbf{a} + \eta\mathbf{a}_2 + \zeta\mathbf{a}_3 \quad (5.44)$$

Equation 5.44 can be written in the matrix form as:

$$\hat{\mathbf{a}} = \underbrace{\begin{bmatrix} 1 & \eta & \zeta \end{bmatrix}}_{\mathbf{C}} \underbrace{\begin{bmatrix} \mathbf{a} \\ \mathbf{a}_2 \\ \mathbf{a}_3 \end{bmatrix}}_{\mathbf{a}_c} \quad (5.45)$$

Acceleration of the beam's centerline is given as:

$$\mathbf{a} = \underbrace{\begin{bmatrix} \mathbf{i}_1 & \mathbf{i}_2 & \mathbf{i}_3 \end{bmatrix}}_{\mathbf{I}} \begin{bmatrix} \ddot{u}_1 \\ \ddot{u}_2 \\ \ddot{u}_3 \end{bmatrix} \quad (5.46)$$

while:

$$\mathbf{a}_2 = \ddot{\boldsymbol{\phi}} \times \mathbf{g}_2 \quad (5.47)$$

$$\mathbf{a}_3 = \ddot{\boldsymbol{\phi}} \times \mathbf{g}_3 \quad (5.48)$$

Components of the vector $\ddot{\boldsymbol{\phi}}$ are:

$$\ddot{\phi}^k = \frac{1}{2\sqrt{g}} e^{klm} \ddot{u}_{l|m} \quad (5.49)$$

where $\ddot{u}_{l|m}$ are the derivatives of the acceleration components given in the NURBS moving frame of reference.

Using Equations 5.22 and 5.49 the acceleration field is obtained as:

$$\hat{\mathbf{a}} = \mathbf{C}\mathbf{G}_u\mathbf{R}\ddot{\mathbf{q}}, \quad \ddot{\mathbf{q}}^T = [\ddot{\mathbf{q}}^0 \quad \ddot{\mathbf{q}}^1 \quad \cdots \quad \ddot{\mathbf{q}}^i \quad \cdots \quad \ddot{\mathbf{q}}^N], \quad \ddot{\mathbf{q}}^i = \begin{bmatrix} \ddot{u}_1^i \\ \ddot{u}_2^i \\ \ddot{u}_3^i \\ \ddot{\varphi}^i \end{bmatrix} \quad (5.50)$$

where components of the vector $\ddot{\mathbf{q}}^i$ are the acceleration components in the Cartesian coordinate system and torsional rotational acceleration of the i -th control point.

5.5 Kinematic relations

Components of the strain tensor of an arbitrary beam point in the convective coordinate system are given as:

$$\hat{\varepsilon}_{ij} = \frac{1}{2} (\hat{g}_{ij}^* - \hat{g}_{ij}) \quad (5.51)$$

Applying the rigid cross-section assumption, the terms $\hat{\varepsilon}_{22}$, $\hat{\varepsilon}_{33}$ and $\hat{\varepsilon}_{23}$ for an arbitrary beam point vanishes.

The axial strain component can be obtained from the corresponding components of the metric tensors for the undeformed and deformed beam configurations:

$$\hat{\varepsilon}_{11} = \frac{1}{2} (\hat{g}_{11}^* - \hat{g}_{11}) \quad (5.52)$$

Substituting \hat{g}_{11} given in Equation 4.15 for the deformed and undeformed beam configuration, the axial strain component becomes:

$$\begin{aligned} \hat{\varepsilon}_{11} = & \frac{1}{2} (g_{11}^* - g_{11}) - \eta (\overline{K}_3^* - \overline{K}_3) + \zeta (\overline{K}_2^* - \overline{K}_2) - \eta\zeta (\overline{K}_3^*K_2^* - \overline{K}_3K_2) + \\ & \frac{1}{2} \left[\eta^2 (\overline{K}_3^*K_3^* - \overline{K}_3K_3) + \zeta^2 (\overline{K}_2^*K_2^* - \overline{K}_2K_2) \right] + \\ & \frac{1}{2} (\eta^2 + \zeta^2) (K_1^*K_1^* - K_1K_1) \end{aligned} \quad (5.53)$$

In the IGA - based formulation of the Bernoulli-Euler beam element, the following reference deformation terms are chosen:

$$\varepsilon_{11} = \frac{1}{2}(g_{11}^* - g_{11}), \quad \varkappa_1 = K_1^* - K_1, \quad \varkappa_2 = \bar{K}_2^* - \bar{K}_2, \quad \varkappa_3 = \bar{K}_3^* - \bar{K}_3 \quad (5.54)$$

If the nonlinear terms with respect to the reference deformation are neglected, Equation 5.53 can be written as:

$$\hat{\varepsilon}_{11} = g_0 [(1 + \eta K_3 - \zeta K_2) \varepsilon_{11} - \eta \varkappa_3 + \zeta \varkappa_2] + (\eta^2 + \zeta^2) K_1 \varkappa_1 \quad (5.55)$$

Using Equations 5.7, 5.8, 5.12 and Equation 4.11 for the case of the undeformed and deformed beam configuration, reference deformation terms for the Bernoulli-Euler beam in the linear formulation are:

$$\varepsilon_{11} = \mathbf{g}_1 \cdot \mathbf{u}_1 \quad (5.56)$$

$$\varkappa_1 = \mathbf{g}_{2,1}^* \cdot \mathbf{g}_3^* - \mathbf{g}_{2,1} \cdot \mathbf{g}_3 = \mathbf{u}_1 \cdot (K_3 \mathbf{g}_3 + K_2 \mathbf{g}_2) + \varphi_{,1} \quad (5.57)$$

$$\varkappa_2 = -\mathbf{g}_{1,1}^* \cdot \mathbf{g}_3^* + \mathbf{g}_{1,1} \cdot \mathbf{g}_3 = -\mathbf{g}_3 \cdot \left(\mathbf{u}_{1,1} - \frac{1}{2} \frac{g_{,1}}{g} \mathbf{u}_1 \right) + \bar{K}_3 \varphi \quad (5.58)$$

$$\varkappa_3 = \mathbf{g}_{1,1}^* \cdot \mathbf{g}_2^* - \mathbf{g}_{1,1} \cdot \mathbf{g}_2 = \mathbf{g}_2 \cdot \left(\mathbf{u}_{1,1} - \frac{1}{2} \frac{g_{,1}}{g} \mathbf{u}_1 \right) - \bar{K}_2 \varphi \quad (5.59)$$

Matrix formulation of the reference deformation terms is given as:

$$\underbrace{\begin{bmatrix} \varepsilon_{11} \\ \varkappa_1 \\ \varkappa_2 \\ \varkappa_3 \end{bmatrix}}_{\boldsymbol{\varepsilon}} = \underbrace{\begin{bmatrix} x_1^m & 0 & 0 & 0 \\ K_3 x_3^m + K_2 x_2^m & 0 & 0 & 1 \\ \Gamma_{11}^1 x_3^m & -x_3^m & \bar{K}_3 & 0 \\ -\Gamma_{11}^1 x_2^m & x_2^m & \bar{K}_2 & 0 \end{bmatrix}}_{\mathbf{L}} \underbrace{\begin{bmatrix} u_{m,1} \\ u_{m,11} \\ \varphi \\ \varphi_{,1} \end{bmatrix}}_{\mathbf{u}_\xi} \quad (5.60)$$

Components of the vector \mathbf{u}_ξ can be parametrized using NURBS parametrization as:

$$\mathbf{u}_\xi = \sum_{i=0}^N \mathbf{B}_i \mathbf{q}^i = \mathbf{B} \mathbf{q} \quad (5.61)$$

where:

$$\mathbf{B} = [\mathbf{B}_0 \quad \cdots \quad \mathbf{B}_i \quad \cdots \quad \mathbf{B}_N] \quad (5.62)$$

$$\mathbf{B}_i^T = \begin{bmatrix} R_{i,1}(\xi) & 0 & 0 & R_{i,11}(\xi) & 0 & 0 & 0 & 0 \\ 0 & R_{i,1}(\xi) & 0 & 0 & R_{i,11}(\xi) & 0 & 0 & 0 \\ 0 & 0 & R_{i,1}(\xi) & 0 & 0 & R_{i,11}(\xi) & 0 & 0 \\ 0 & 0 & 0 & 0 & 0 & 0 & R_i(\xi) & R_{i,1}(\xi) \end{bmatrix} \quad (5.63)$$

and:

$$\mathbf{q}^T = [\mathbf{q}^1 \quad \cdots \quad \mathbf{q}^i \quad \cdots \quad \mathbf{q}^n], \quad \mathbf{q}^i = \begin{bmatrix} u_1^i \\ u_2^i \\ u_3^i \\ \varphi^i \end{bmatrix} \quad (5.64)$$

Due to the Bernoulli-Euler assumption, the shear deformation at the beam's centerline vanishes. However, deformation for an arbitrary beam point using Equation 5.51 and 4.15 for undeformed and deformed beam configuration is given as:

$$\hat{\varepsilon}_{12} = \frac{1}{2} (\hat{g}_{12}^* - \hat{g}_{12}) = -\frac{1}{2} \zeta \varkappa_1 \quad (5.65)$$

$$\hat{\varepsilon}_{13} = \frac{1}{2} (\hat{g}_{13}^* - \hat{g}_{13}) = -\frac{1}{2} \eta \varkappa_1 \quad (5.66)$$

As can be noticed in Equation 5.55, the axial strain component couples the axial, flexural and torsional deformations. Following the relations given in Equation 4.17, the axial strain component in ξ_λ frame of reference is defined as:

$$\hat{\varepsilon}_{11}(\xi_\lambda) = \frac{1}{g_0} [(1 + \eta K_3 - \zeta K_2) \varepsilon_{11} - \eta \varkappa_3 + \zeta \varkappa_2] \quad (5.67)$$

where only axial and flexural deformation are coupled. In the ξ_λ frame of reference the shear strain components for the Bernoulli-Euler beam are:

$$\hat{\varepsilon}_{12}(\xi_\lambda) = -\frac{1}{2g_0} \zeta \varkappa_1 \quad (5.68)$$

$$\hat{\varepsilon}_{13}(\xi_\lambda) = -\frac{1}{2g_0} \eta \varkappa_1 \quad (5.69)$$

5.6 Constitutive relations

Assuming linear elastic material behavior, the constitutive relations can be written as:

$$\hat{S}_j^i = 2\mu \hat{\varepsilon}_j^i + \lambda \delta_j^i \hat{\varepsilon}_m^m \quad (5.70)$$

where \hat{S}_j^i and $\hat{\varepsilon}_j^i$ respectively represents the mix component of the second Piola - Kirchhoff stress tensor and Green - Lagrangian strain tensor of an arbitrary point, while μ and λ are Lamé's constants:

$$\mu = \frac{E}{2(1+\nu)}, \quad \lambda = \frac{E\nu}{(1+\nu)(1-2\nu)} \quad (5.71)$$

In previous relations, E represents the Young's modulus and ν denotes the Poisson's ratio. Using this formulation the deformation is small but in general strain can be finite.

Condition of zero values of the stress components \hat{S}_2^2 and \hat{S}_3^3 , yields a new relation between the stress and strain components:

$$\hat{S}_j^i = 2\mu \left(\hat{\varepsilon}_j^i + \nu \delta_j^i \hat{\varepsilon}_1^1 \right) \quad (5.72)$$

Equation 5.72 can be written in the direct notation as:

$$\hat{\mathbf{S}} = \mathbf{D} : \hat{\boldsymbol{\varepsilon}} \quad (5.73)$$

where \mathbf{D} is the constitutive tensor. The contravariant components of the stress tensor of an arbitrary point given with respect to the covariant components of the strain tensor are:

$$\hat{S}^{ij} = 2\mu \hat{g}^{ip} \hat{g}^{jm} \hat{\varepsilon}_{pm} + \lambda \delta_m^i \hat{g}^{jm} \hat{g}^{rn} \hat{\varepsilon}_{rn} \quad (5.74)$$

The contravariant components of the stress tensor formulated in the NURBS moving frame of reference are non-zero, which is the main motivation for the introduction of the ξ_λ frame of reference, making the formulation more efficient. Using the ξ_λ frame of reference, components of the stress tensor are obtained as:

$$\hat{S}^{11} = Eg^{11}g^{11}\hat{\varepsilon}_{11} \quad (5.75)$$

$$\hat{S}^{1\bar{\alpha}} = 2\mu g^{11}\hat{\varepsilon}_{1\bar{\alpha}} \quad (\bar{\alpha} = 2, 3) \quad (5.76)$$

5.7 Strong formulation

Using Cauchy equilibrium equation for dynamic formulation:

$$\rho \mathbf{a} = \nabla \cdot \mathbf{t} + \mathbf{f} \quad (5.77)$$

with the corresponding boundary conditions, the strong form is obtained [49]. In this equation ρ is the mass density, \mathbf{a} is the acceleration vector, \mathbf{t} is the Cauchy stress tensor, \mathbf{f} is external force vector per volume, while $\nabla \cdot$ is the divergence operator.

The previous equation can be presented in a component formulation as:

$$\rho a^i = t^{ij}|_j + f^i \quad (5.78)$$

5.8 Weak formulation

Multiplying Equation 5.77 with an arbitrary vector \mathbf{h} and applying the integration over the deformed volume domain, a new relation is obtained:

$$\int_V \rho \mathbf{a} \cdot \mathbf{h} dV = \int_V (\nabla \cdot \mathbf{t}) \cdot \mathbf{h} dV + \int_V \mathbf{f} \cdot \mathbf{h} dV \quad (5.79)$$

The first term on the right side of Equation 5.79 can be modified using the following relation:

$$\nabla \cdot (\mathbf{t} \cdot \mathbf{h}) = (\nabla \cdot \mathbf{t}) \cdot \mathbf{h} + \mathbf{t} : \nabla \mathbf{h} \quad (5.80)$$

as:

$$\int_V \rho \mathbf{a} \cdot \mathbf{h} dV = \int_V \nabla \cdot (\mathbf{t} \cdot \mathbf{h}) dV - \int_V \mathbf{t} : \nabla \mathbf{h} dV + \int_V \mathbf{f} \cdot \mathbf{h} dV \quad (5.81)$$

Using the divergence theorem for transforming the volume to surface integral and applying the Neumann boundary conditions, the weak formulation of the corresponding initial value problem is obtained:

$$\int_V \mathbf{t} : \nabla \mathbf{h} dV = \int_V \mathbf{f} \cdot \mathbf{h} dV - \int_V \rho \mathbf{a} \cdot \mathbf{h} dV + \int_S \mathbf{p} \cdot \mathbf{h} dS \quad (5.82)$$

Equation 5.82 can be written in component form as:

$$\int_V t^{ij} h_{i|j} dV = \int_V f^i h_i dV - \int_V \rho a^i h_i dV + \int_S p^i h_i dS \quad (5.83)$$

Weak formulation given by Equations 5.81 and 5.82 presents a starting point for formulation of numerical methods in the computational mechanics.

Choosing the virtual displacement $\delta \hat{\mathbf{u}}$ for the test function, the principle of the virtual work is given as:

$$\int_V \mathbf{t} : \nabla \delta \hat{\mathbf{u}} dV = \int_V \mathbf{f} \cdot \delta \hat{\mathbf{u}} dV - \int_V \rho \hat{\mathbf{a}} \cdot \delta \hat{\mathbf{u}} dV + \int_S \mathbf{p} \cdot \delta \hat{\mathbf{u}} dS \quad (5.84)$$

The above relation in the undeformed configuration can be expressed as:

$$\int_{V_o} \mathbf{S} : \delta \boldsymbol{\varepsilon} dV_o = \int_{V_o} \mathbf{f} \cdot \delta \hat{\mathbf{u}} dV_o - \int_{V_o} \rho_o \hat{\mathbf{a}} \cdot \delta \hat{\mathbf{u}} dV_o + \int_{S_o} \mathbf{p} \cdot \delta \hat{\mathbf{u}} dS_o \quad (5.85)$$

where V_o and S_o represents volume and area elements on the undeformed configuration. In the previous relation the contribution of the internal forces (δW_{int}), the inertial forces (δW_{iner}) and the external forces (δW_{ext}) in virtual work are:

$$\delta W_{int} = \int_{V_o} \mathbf{S} : \delta \boldsymbol{\varepsilon} dV_o \quad (5.86)$$

$$\delta W_{iner} = \int_{V_o} \rho_o \hat{\mathbf{a}} \cdot \delta \hat{\mathbf{u}} dV_o \quad (5.87)$$

$$\delta W_{ext} = \int_{V_o} \mathbf{f} \cdot \delta \hat{\mathbf{u}} dV_o + \int_{S_o} \mathbf{p} \cdot \delta \hat{\mathbf{u}} dS_o \quad (5.88)$$

5.9 Governing equation of motion of the Bernoulli-Euler beam

Using ξ_λ frame of reference, the virtual work of the internal beam forces is defined as:

$$\delta W_{int}(\xi_\lambda) = \int_{V_o} \left(\hat{S}^{11} \delta \hat{\varepsilon}_{11} + 2\hat{S}^{12} \delta \hat{\varepsilon}_{12} + 2\hat{S}^{13} \delta \hat{\varepsilon}_{13} \right) dV_o \quad (5.89)$$

In the linear formulation, the beam configuration is assumed to be known quantity. Consequently, the variation of the Bernoulli-Euler strain components is obtained directly from Equations 5.67 - 5.69 as:

$$\delta \hat{\varepsilon}_{11}(\xi_\lambda) = \frac{1}{g_0} [(1 + \eta K_3 - \zeta K_2) \delta \varepsilon_{11} - \eta \delta \varkappa_3 + \zeta \delta \varkappa_2] \quad (5.90)$$

$$\delta \hat{\varepsilon}_{12}(\xi_\lambda) = -\frac{1}{2g_0} \zeta \delta \varkappa_1 \quad (5.91)$$

$$\delta \hat{\varepsilon}_{13}(\xi_\lambda) = -\frac{1}{2g_0} \eta \delta \varkappa_1 \quad (5.92)$$

In addition, the variation of the reference deformation terms is obtained from Equations 5.60 and 5.61 as:

$$\delta \boldsymbol{\varepsilon} = \mathbf{LB} \delta \mathbf{q} \quad (5.93)$$

where $\delta \mathbf{q}$ represents vector whose components are the variation of the control point displacements and the torsional rotation.

Substituting Equations 5.75 and 5.76 and Equation 5.90 - 5.92 into Equation 5.89, the contribution of the internal forces for the Bernoulli-Euler beam can be written as:

$$\delta W_{int}(\xi_\lambda) = \int_{V_o} (N\delta\varepsilon_{11} + M_1\delta\kappa_1 + M_2\delta\kappa_2 + M_3\delta\kappa_3) dV_o \quad (5.94)$$

where N , M_1 , M_2 , M_3 are the energy conjugate cross-section forces:

$$N = \int (1 + \eta K_3 - \zeta K_2) S^{11} d\eta d\zeta \quad (5.95)$$

$$M_1 = \int (\eta S^{12} - \zeta S^{13}) d\eta d\zeta \quad (5.96)$$

$$M_2 = \int \eta S^{11} d\eta d\zeta \quad (5.97)$$

$$M_3 = - \int \zeta S^{11} d\eta d\zeta \quad (5.98)$$

Equations 5.95 - 5.98 can be written in the matrix form as:

$$\underbrace{\begin{bmatrix} N \\ M_1 \\ M_2 \\ M_3 \end{bmatrix}}_{\mathbf{R}_k} = \frac{1}{g^2} \underbrace{\begin{bmatrix} EA & 0 & EI_2 & -EI_3 \\ 0 & \mu g I_{11} & 0 & 0 \\ EI_2 & 0 & EI_{22} & -EI_{23} \\ -EI_3 & 0 & -EI_{32} & EI_{33} \end{bmatrix}}_{\mathbf{D}_k} \underbrace{\begin{bmatrix} \varepsilon_{11} \\ \kappa_1 \\ \kappa_2 \\ \kappa_3 \end{bmatrix}}_{\varepsilon_k} \quad (5.99)$$

where:

$$A = \int \frac{(1 + \eta K_3 - \zeta K_2)}{g_0} d\eta d\zeta \quad (5.100)$$

$$I_{11} = \int \frac{\eta^2 + \zeta^2}{g_0} d\eta d\zeta \quad (5.101)$$

$$I_{22} = \int \frac{\eta^2}{g_0} d\eta d\zeta \quad (5.102)$$

$$I_{33} = \int \frac{\zeta^2}{g_0} d\eta d\zeta \quad (5.103)$$

$$I_{23} = I_{32} = - \int \frac{\eta\zeta}{g_0} d\eta d\zeta \quad (5.104)$$

Substituting Equations 5.60, 5.61, 5.93 and 5.99 into Equation 5.94:

$$\delta W_{int}(\xi_\lambda) = \int_{V_o} \mathbf{R}_k \delta \boldsymbol{\varepsilon}_k dV_o = \int_{V_o} \boldsymbol{\varepsilon}_k^T \mathbf{D}_k \delta \boldsymbol{\varepsilon}_k dV_o = \mathbf{q}^T \int_{\xi} \mathbf{B}^T \mathbf{L}^T \mathbf{D}_k \mathbf{L} \mathbf{B} \sqrt{g} d\xi \delta \mathbf{q} \quad (5.105)$$

stiffness matrix is obtained:

$$\mathbf{K} = \int_{\xi} \mathbf{B}^T \mathbf{L}^T \mathbf{D}_k \mathbf{L} \mathbf{B} \sqrt{g} d\xi \quad (5.106)$$

Implementation of the internal part of the virtual work requires a variation of the displacement field ($\delta\hat{\mathbf{u}}$). As the configuration of the beam is known during deformation, the variation of the displacement vectors is obtained from Equation 5.33 as:

$$\delta\hat{\mathbf{u}} = \mathbf{C}\mathbf{G}_u\mathbf{R}\delta\mathbf{q} \quad (5.107)$$

Substituting Equations 5.50 and 5.107 in the inertial part of the virtual work given in Equation 5.87:

$$\delta W_{iner} = \ddot{\mathbf{q}}^T \int_{V_o} \rho_o \mathbf{R}^T \mathbf{G}_u^T \mathbf{C}^T \mathbf{C} \mathbf{G}_u \mathbf{R} dV_o \delta\mathbf{q} \quad (5.108)$$

mass matrix is obtained:

$$\mathbf{M} = \int_{\xi} \rho_o \mathbf{R}^T \mathbf{G}_u^T \mathbf{D}_m \mathbf{G}_u \mathbf{R} \sqrt{g} d\xi \quad (5.109)$$

where:

$$\mathbf{D}_m = \int \mathbf{C}^T \mathbf{C} d\eta d\zeta = \int \begin{bmatrix} 1 & \eta & \zeta \\ \eta & \eta^2 & \eta\zeta \\ \zeta & \eta\zeta & \zeta^2 \end{bmatrix} d\eta d\zeta \quad (5.110)$$

External load on the beam element can only be defined on the beam's centerline, thus the contribution of the external forces of the virtual work is defined as:

$$\delta W_{ext} = \int_{\xi} \mathbf{f} \cdot \delta\mathbf{u} d\xi \quad (5.111)$$

where $\delta\mathbf{u}$ represents the virtual displacement of the beam's centerline:

$$\delta\mathbf{u} = \sum_{i=0}^N \mathbf{R}_{ui} \delta\mathbf{q}^i = \mathbf{R}_u \delta\mathbf{q} \quad (5.112)$$

In the previous relation \mathbf{R}_u is defined as:

$$\mathbf{R}_u = \begin{bmatrix} \mathbf{R}_{u0} & \mathbf{R}_{u1} & \cdots & \mathbf{R}_{ui} & \cdots & \mathbf{R}_{uN} \end{bmatrix}, \quad \mathbf{R}_{ui} = \begin{bmatrix} R_i(\xi) & 0 & 0 & 0 \\ 0 & R_i(\xi) & 0 & 0 \\ 0 & 0 & R_i(\xi) & 0 \end{bmatrix} \quad (5.113)$$

Substituting the expression of the virtual displacement of the beam's centerline in Equation 5.111:

$$\delta W_{ext} = \int_{\xi} \mathbf{f} \cdot \mathbf{R}_u d\xi \delta\mathbf{q} \quad (5.114)$$

external load vector is defined:

$$\mathbf{Q} = \int_{\xi} \mathbf{f} \cdot \mathbf{R}_u d\xi \quad (5.115)$$

Substituting Equations 5.105, 5.108 and 5.114 into Equation 5.85 and dividing by $\delta\mathbf{q}$, the governing equation of the motion of the Bernoulli-Euler curved spatial beam using isogeometric approach in linear analysis is defined as:

$$\mathbf{M}\ddot{\mathbf{q}} + \mathbf{K}\mathbf{q} = \mathbf{Q} \quad (5.116)$$

5.10 Free vibration analysis

For the purpose of the free vibration analysis, the external load vector vanishes, thus the Equation 5.116 is defined as:

$$\mathbf{M}\ddot{\mathbf{q}} + \mathbf{K}\mathbf{q} = 0 \quad (5.117)$$

A solution of the previous equation can be assumed as:

$$\ddot{\mathbf{q}} = \mathbf{q}_k e^{i\omega_k t} \quad (5.118)$$

where i is the imaginary number, ω_k is the natural frequency, while \mathbf{q}_k is its corresponding modal vector.

Substituting Equation 5.118 into Equation 5.117 yields:

$$\left(\mathbf{K} - \omega_k^2 \mathbf{M}\right) \mathbf{q}_k = 0 \quad (5.119)$$

The natural frequencies are obtained from:

$$\det\left(\mathbf{K} - \omega_k^2 \mathbf{M}\right) = 0 \quad (5.120)$$

while the corresponding modal vectors are obtained from Equation 5.119 using well-known procedure.

5.11 Transient analysis

Equation 5.116 is an ordinary differential equation and for the requirement of the transient analysis the time discretization has to be applied by dividing the continuous time t into time intervals Δt_n . Direct time integration can be conducted using implicit or explicit integration schemes [50]. In this study, the explicit time integration scheme is employed, which calculates the equilibrium of the system at time (t_{i+n}) from the equilibrium of the system at the current time (t_n) . In order to employ the explicit time integration scheme, Equation 5.116 is set for the current time:

$$\mathbf{M}\ddot{\mathbf{q}}_n + \mathbf{K}\mathbf{q}_n = \mathbf{Q}_n \quad (5.121)$$

where $\ddot{\mathbf{q}}_n$ and \mathbf{q}_n are acceleration and displacement components in the control points, while \mathbf{Q}_n is the external load vector at current time t_n .

At current time point t_n , the configuration of the system is known in terms of displacement vector of the control points, while the acceleration vector is unknown. This equation can be solved using Newmark- β method [51]. Applying Newmark- β method with $\beta = 0$ [26], explicit dynamic integration is used, also known as a central difference method by relations:

$$\dot{\mathbf{q}}_n = \frac{\mathbf{q}_{n+1} - \mathbf{q}_{n-1}}{\Delta t_{n-1/2} + \Delta t_{n+1/2}} \quad (5.122)$$

$$\ddot{\mathbf{q}}_n = \frac{1}{\Delta t_n} \left(\dot{\mathbf{q}}_{n+1/2} - \dot{\mathbf{q}}_{n-1/2} \right) = \frac{1}{\Delta t_n} \left(\frac{\mathbf{q}_{n+1} - \mathbf{q}_n}{\Delta t_{n+1/2}} - \frac{\mathbf{q}_n - \mathbf{q}_{n-1}}{\Delta t_{n-1/2}} \right) \quad (5.123)$$

Substituting Equation 5.123 into Equation 5.121 the configuration at the later time is calculated:

$$\mathbf{q}_{n+1} = \mathbf{q}_n + \Delta t_{n+1/2} \left(\Delta t_n \mathbf{M}^{-1} (\mathbf{Q}_n - \mathbf{K} \mathbf{q}_n) + \frac{\mathbf{q}_n - \mathbf{q}_{n-1}}{\Delta t_{n-1/2}} \right) \quad (5.124)$$

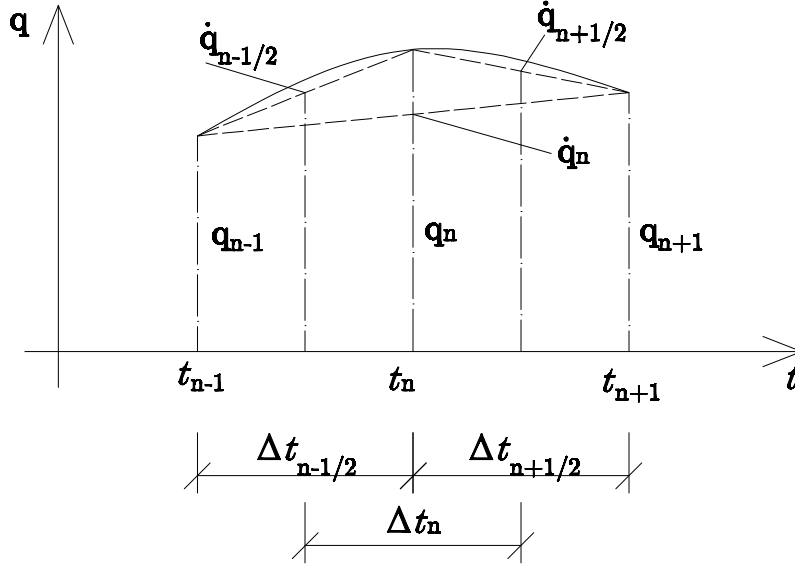


Figure 5.2: Schematic representation of the central difference method

In the linear analysis, the time intervals are equal (Δt), therefore the configuration at the later time is:

$$\mathbf{q}_{n+1} = 2\mathbf{q}_n - \mathbf{q}_{n-1} + \Delta t^2 \mathbf{M}^{-1} (\mathbf{Q}_n - \mathbf{K} \mathbf{q}_n) \quad (5.125)$$

The main problem regarding the central difference method is its conditional stability [52], as the time step in the linear analysis is bounded by:

$$\Delta t_{max} = \frac{2}{\omega_{max}} \quad (5.126)$$

where ω_{max} is the maximum natural frequency of the system.

5.12 Moving load and moving mass model

Mass moving along the structure generates a dynamic response, significant for structures such as bridges and cranes. Therefore, the accurate model of this load has to be defined. Most of the research on this topic describes the influence of the moving mass using moving load model [53], [54], where the inertial part of the moving mass is neglected, and only the influence of the gravitational acceleration is taken into account:

$$\mathbf{f}_m = m \mathbf{g}_m \quad (5.127)$$

where m is the mass, while \mathbf{g}_m is the gravitational acceleration. As can be noticed from the previous equation, the moving load model defines the moving force with constant magnitude and direction.

However, effects of the inertial term of the moving mass on the dynamic response can be significant in some cases (for curved beams [40]). Consequently, moving mass model is formulated, taking into account the inertial term of the moving mass, given by the following expression:

$$\mathbf{f}_m = m (\mathbf{g}_m - \mathbf{a}_m) \quad (5.128)$$

where \mathbf{a}_m is the acceleration of the moving mass. The acceleration is obtained from the trajectory of the moving mass as its double material derivative. The trajectory of the mass represents the spatial curved line and can be given in the Frenet - Serret reference frame using tangent, normal and binormal vectors denoted as \mathbf{t}_m , \mathbf{n}_m and \mathbf{b}_m . Using this frame of reference, the acceleration of the mass is obtained as [55]:

$$\mathbf{a}_m(s) = KV^2\mathbf{n}_m + a\mathbf{t}_m \quad (5.129)$$

where K is the trajectory curvature, V is the velocity magnitude, while a is the acceleration magnitude given in the arc - length coordinate. The trajectory of the moving mass is directly related to the beam geometry, thus the acceleration in the NURBS moving frame of reference is given as:

$$\mathbf{a}_m(\xi) = \left(\Gamma_{11}^1 V_\xi^2 + a_\xi \right) \mathbf{g}_1 + KgV_\xi^2 \mathbf{g}_2 \quad (5.130)$$

where

$$V_\xi = \frac{V}{\sqrt{g}}, \quad a_\xi = -\frac{\Gamma_{11}^1 V^2}{g} + \frac{a}{\sqrt{g}} \quad (5.131)$$

In the moving mass model, both the direction and magnitude of the moving mass vary with respect to time and space. This can be observed from Equation 5.129 as in general the curvature K is variable for the curved beam as well as the velocity V and the acceleration a .

5.13 Boundary conditions

Particular attention should be paid to the Dirichlet boundary conditions due to the presented formulation of the Bernoulli-Euler spatial beam element using the isogeometric approach where degrees of freedom (DOF) are three displacements in the direction to the Cartesian coordinate system ($u_i, i = 1, 2, 3$) and torsional rotation of beam's cross-section (φ_1). Rotations about principle axes (φ_2, φ_3) do not represent DOFs of the Bernoulli-Euler spatial beam element. However, their application is essential in the formulation of boundary conditions. The following boundary conditions can be assigned to the ends of spatial beam element:

1. Free (F)
 $u_i \neq 0 \quad (i = 1, 2, 3), \quad \varphi_j \neq 0 \quad (j = 1, 2, 3)$
2. Simply supported (SS)
 $u_i = 0 \quad (i = 1, 2, 3), \quad \varphi_j \neq 0 \quad (j = 1, 2, 3)$
3. Clamped (C1)
 $u_i = 0 \quad (i = 1, 2, 3), \quad \varphi_1 \neq 0 \quad \varphi_k = 0 \quad (k = 2, 3)$
4. Fully clamped (C2)
 $u_i = 0 \quad (i = 1, 2, 3), \quad \varphi_j = 0 \quad (j = 1, 2, 3)$

Application of F and SS boundary conditions is accomplished by removing the corresponding rows and columns in the stiffness and mass matrices. Before applying C1 and C2 boundary

conditions, modifications due to constrains of the principle axis rotations are necessary. Rotation about the principle axes are obtained from Equation 5.12 as:

$$\varphi^2 = \frac{1}{2\sqrt{g}} \left(-\tilde{u}_{3|1} + \tilde{u}_{1|3} \right), \quad \varphi^3 = \frac{1}{2\sqrt{g}} \left(u_{2|1} - u_{1|2} \right) \quad (5.132)$$

Previous equation can be further modified applying Bernoulli-Euler assumption and Equation 5.22, hence the rotations can be written as:

$$\varphi^2 = -\frac{1}{\sqrt{g}} \mathbf{g}_3 \cdot \mathbf{u}_{,1}, \quad \varphi^3 = \frac{1}{\sqrt{g}} \mathbf{g}_2 \cdot \mathbf{u}_{,1} \quad (5.133)$$

Introducing NURBS parameterization in previous equations with clamped constrains, the displacement components are coupled as:

$$\varphi^2 = 0 \quad \rightarrow \quad \mathbf{g}_3 \cdot \mathbf{u}_{,1} = \mathbf{g}_3 \cdot \sum_{i=0}^n R_{i,1}(\xi) \mathbf{u}_i = x_3^m \sum_{i=0}^n R_{i,1}(\xi) u_i^m = 0 \quad (5.134)$$

$$\varphi^3 = 0 \quad \rightarrow \quad \mathbf{g}_2 \cdot \mathbf{u}_{,1} = \mathbf{g}_2 \cdot \sum_{i=0}^n R_{i,1}(\xi) \mathbf{u}_i = x_2^m \sum_{i=0}^n R_{i,1}(\xi) u_i^m = 0 \quad (5.135)$$

It is important to notice that nonzero derivatives at the beginning of the beam are only defined for the first two basis functions, which can be concluded from Equations 3.1, 3.2 and 3.3. Hence, the clamped constrain at the beginning of the beam entails:

$$x_3^1 u_1^1 + x_3^2 u_1^2 + x_3^3 u_1^3 = 0 \quad (5.136)$$

$$x_2^1 u_1^1 + x_2^2 u_1^2 + x_2^3 u_1^3 = 0 \quad (5.137)$$

where x_3^m are Cartesian components of the basis vector \mathbf{g}_3 at the beginning of the beam. These relations allow displacement of the second control point only in direction with tangent vector at the beginning of the beam thus the number of degrees of freedom is reduced by two. The same conclusion can be derived for the clamped endpoint of the beam element where only the last two basis functions have non-zero derivatives.

6 Geometrically nonlinear dynamic formulation of plane Bernoulli - Euler beam

Theoretical considerations of the dynamic behaviour of plane Bernoulli-Euler beam concerning the geometrically nonlinear formulation are presented in this chapter. Bernoulli-Euler and beam hypothesis are taken into consideration using strain-rate tensor, while acceleration field is derived neglecting the product of the velocity quantities. Product of the velocity gradient components, and the product of the angular velocity vector components are neglected. Implementation of the explicit integration scheme has simplified the variation of the axial component of the strain tensor, which is defined for the geometrically nonlinear formulation.

Plane beams are constrained with two conditions. The first condition is related to the beam geometry, as beam's centerline with the corresponding vectors \mathbf{g}_1 and \mathbf{g}_2 lies in the plane defined with the basis vector \mathbf{g}_3 , denoted as a beam plane, Figure 6.1. In addition, the displacements of the beam occur only in the beam plane. As a consequence of this constrains, the direction of the basis vector \mathbf{g}_3 during the deformation process is unchanged.

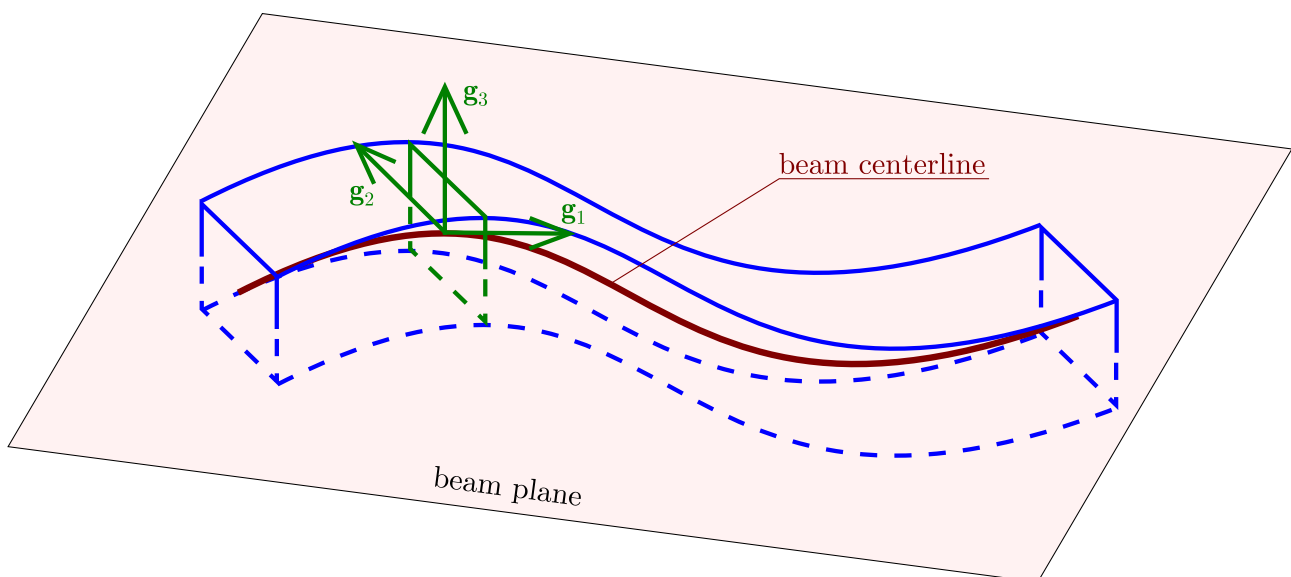


Figure 6.1: Arbitrary curved plane beam

The position vector of an arbitrary point of the plane beam in the undeformed configuration is defined as:

$$\hat{\mathbf{r}} = \mathbf{r} + \eta \mathbf{g}_2 \quad (6.1)$$

with corresponding basis vector:

$$\hat{\mathbf{g}}_1 = \frac{d\hat{\mathbf{r}}}{d\xi} = (1 - \eta K) \mathbf{g}_1 = g_0 \mathbf{g}_1 \quad (6.2)$$

Orthogonality between the arbitrary point basis vectors $\hat{\mathbf{g}}_1$ and \mathbf{g}_2 is preserved, which can be concluded from the previous equation, thus the application of the ξ_λ frame of reference is avoided.

Geometrically nonlinear formulation of the Bernoulli-Euler beam becomes more efficient in terms of number DOFs and procedure of the beam derivation, if material derivatives of the deformation components are used instead of strain components [23]. Consequently,

$$d_{22} = 0, \quad d_{12} = 0 \quad (6.3)$$

where d_{ij} are the components of the strain - rate tensor. Applying beam and Bernoulli - Euler hypotheses on the strain - rate tensor yields:

$$\tilde{v}_{2|2} = 0, \quad \tilde{v}_{1|2} = -\tilde{v}_{2|1} \quad (6.4)$$

which will be used in the forthcoming derivations.

6.1 Deformed configuration of beam

Due to the external plane load acting on the beam, the position of arbitrary point of beam is given as:

$$\hat{\mathbf{r}}^* = \hat{\mathbf{r}} + \hat{\mathbf{u}} \quad (6.5)$$

where $\hat{\mathbf{u}}$ represents the displacement vector of an arbitrary point. The position vector of an arbitrary point in the deformed configuration of the beam can also be defined as:

$$\hat{\mathbf{r}}^* = \mathbf{r}^* + \eta \mathbf{g}_2^* \quad (6.6)$$

Due to the rigid cross-section assumption, the basis vector \mathbf{g}_2^* in the geometrically nonlinear formulation is defined using the rotation tensor \mathbf{R}_g :

$$\mathbf{g}_2^* = \mathbf{R}_g \cdot \mathbf{g}_2 \quad (6.7)$$

It is important to point out that the description of the rotation in the geometrically nonlinear formulation requires the application of the rotation tensor [23]. Different rotation parameterization can be found in [56]. However, the exponential parametrization has been found to be the most convenient, given as:

$$\mathbf{R}_g = e^{\Phi} \quad (6.8)$$

where Φ represents the skew-symmetric tensor. The skew-symmetric tensor can be written as:

$$\Phi \cdot \mathbf{a} = \phi \times \mathbf{a} \quad (6.9)$$

where \mathbf{a} is an arbitrary vector, while ϕ is the axial (dual) vector of the skew - symmetric tensor Φ .

Advantage of the exponential parameterization of the rotation tensor can be found in the material derivative of the rotation tensor:

$$\dot{\mathbf{R}}_g = \dot{\Phi} \cdot e^{\Phi} = \dot{\Phi} \cdot \mathbf{R}_g \quad (6.10)$$

with corresponding relation:

$$\dot{\Phi} \cdot \mathbf{a} = \dot{\phi} \times \mathbf{a} = \boldsymbol{\omega} \times \mathbf{a} \quad (6.11)$$

where $\boldsymbol{\omega}$ is the angular velocity vector [23]:

$$\boldsymbol{\omega} = \frac{1}{2\sqrt{g^*}} e^{klm} \tilde{v}_{m|l} \mathbf{g}_k^* \quad (6.12)$$

Plane formulation of the curved beam implies only rotation about the basis vector \mathbf{g}_3 . Applying Bernoulli - Euler assumption, given by Equation 6.4, the angular rotation vector is defined as:

$$\boldsymbol{\omega} = \frac{1}{\sqrt{g^*}} \tilde{v}_{2|1} \mathbf{g}_3^* = \tilde{\omega}^3 \mathbf{g}_3^* \quad (6.13)$$

Using exponential parameterization of the rotation tensor, its variation is obtained as:

$$\delta \mathbf{R}_g = \delta \Phi \cdot e^{\Phi} = \delta \Phi \cdot \mathbf{R}_g \quad (6.14)$$

with corresponding relation:

$$\delta \Phi \cdot \mathbf{a} = \delta \phi \times \mathbf{a} = \delta \phi \times \mathbf{a} \quad (6.15)$$

where $\delta \phi$ is variation of axial vector:

$$\delta \phi = \frac{1}{2\sqrt{g^*}} e^{klm} \delta \tilde{u}_{m|l} \mathbf{g}_k^* \quad (6.16)$$

For the case of a plane beam, the variation of the axial vector is:

$$\delta \phi = \frac{1}{\sqrt{g^*}} \delta \tilde{u}_{2|1} \mathbf{g}_3^* \quad (6.17)$$

6.2 Displacement field

Displacement field of the plane curved beam is obtained by substituting Equations 6.1, 6.6 into Equation 6.5:

$$\hat{\mathbf{u}} = \mathbf{u} + \eta \mathbf{u}_2 = \underbrace{\begin{bmatrix} 1 & \eta \end{bmatrix}}_{\mathbf{C}_N} \underbrace{\begin{bmatrix} \mathbf{u} \\ \mathbf{u}_2 \end{bmatrix}}_{\mathbf{u}_{nc}} \quad (6.18)$$

In order to employ the principle of virtual work, the variation of the displacement field is found as:

$$\delta \hat{\mathbf{u}} = \delta \mathbf{u} + \eta \delta \mathbf{u}_2 = \mathbf{C}_N \underbrace{\begin{bmatrix} \delta \mathbf{u} \\ \delta \mathbf{u}_2 \end{bmatrix}}_{\delta \mathbf{u}_{nc}} \quad (6.19)$$

where the variation of beam's centerline displacement is:

$$\delta \mathbf{u} = \underbrace{\begin{bmatrix} \mathbf{i}_1 & \mathbf{i}_2 \\ & \end{bmatrix}}_{\mathbf{i}_N} \begin{bmatrix} \delta u_1 \\ \delta u_2 \end{bmatrix} \quad (6.20)$$

Using Equations 6.7, 6.14 - 6.17, the variation of the displacement field second term (\mathbf{u}_2) is:

$$\delta \mathbf{u}_2 = \delta \mathbf{g}_2^* = -\frac{1}{g^*} \delta \tilde{u}_{2|1} \mathbf{g}_1^* = -\left(\delta \mathbf{u}_{,1} \cdot \mathbf{g}_2^* \right) \frac{\mathbf{g}_1^*}{g^*} \quad (6.21)$$

Term $\delta \tilde{u}_{2|1}$ is obtained from the following relation:

$$\delta \mathbf{u}_{,m} = \delta \left(\tilde{u}_{k|m} \mathbf{g}^{*k} \right) = \delta \tilde{u}_{k|m} \mathbf{g}^{*k} + \tilde{u}_{k|m} \delta \mathbf{g}^{*k} \quad (6.22)$$

Matrix representation of Equation 6.21 is given as:

$$\delta \mathbf{u}_2 = -\frac{1}{g^*} \begin{bmatrix} x_2^{1*} \mathbf{g}_1^* & x_2^{2*} \mathbf{g}_1^* \end{bmatrix} \begin{bmatrix} \delta u_{1,1} \\ \delta u_{2,1} \end{bmatrix} = -\frac{1}{g^*} \underbrace{\begin{bmatrix} x_2^{1*} x_1^{1*} & x_2^{1*} x_1^{2*} \\ x_2^{2*} x_1^{1*} & x_2^{2*} x_1^{2*} \end{bmatrix}}_{\mathbf{B}_N} \underbrace{\begin{bmatrix} \mathbf{i}_1 \\ \mathbf{i}_2 \end{bmatrix}}_{\mathbf{i}_N^T} \begin{bmatrix} \delta u_{1,1} \\ \delta u_{2,1} \end{bmatrix} \quad (6.23)$$

Combining Equations 6.20 and 6.23, vector $\delta \mathbf{u}_{nc}$ can be represented as:

$$\delta \mathbf{u}_{nc} = \underbrace{\begin{bmatrix} \mathbf{i} & 0 \\ 0 & \mathbf{i} \end{bmatrix}}_{\mathbf{G}_N} \underbrace{\begin{bmatrix} \mathbf{I} & 0 \\ 0 & \mathbf{B}^T \end{bmatrix}}_{\mathbf{u}_{ncc}} \begin{bmatrix} \delta u_1 \\ \delta u_2 \\ \delta u_{1,1} \\ \delta u_{2,1} \end{bmatrix}, \quad \mathbf{I} = \begin{bmatrix} 1 & 0 \\ 0 & 1 \end{bmatrix} \quad (6.24)$$

NURBS parameterization of the vector \mathbf{u}_{ncc} is obtained as:

$$\mathbf{u}_{ncc} = \sum_{i=0}^N \mathbf{R}_i \delta \mathbf{q}_i = \mathbf{R} \mathbf{q} \quad (6.25)$$

where:

$$\mathbf{R}^T = \begin{bmatrix} \mathbf{R}_0 \\ \vdots \\ \mathbf{R}_i \\ \vdots \\ \mathbf{R}_N \end{bmatrix}, \quad \mathbf{R}_i = \begin{bmatrix} R_i(\xi) & 0 \\ 0 & R_i(\xi) \\ R_{i,1}(\xi) & 0 \\ 0 & R_{i,1}(\xi) \end{bmatrix} \quad (6.26)$$

$$\delta \mathbf{q}^T = \left[\mathbf{q}^0 \quad \dots \quad \mathbf{q}^i \quad \dots \quad \mathbf{q}^N \right], \quad \delta \mathbf{q}^i = \begin{bmatrix} \delta u_1^i \\ \delta u_2^i \end{bmatrix} \quad (6.27)$$

Finally, the variation field of the displacement is obtained as:

$$\delta \hat{\mathbf{u}} = \mathbf{C}_N \mathbf{G}_N \mathbf{R} \delta \mathbf{q} \quad (6.28)$$

6.3 Velocity field

The velocity field is obtained as a material derivative of the displacement field:

$$\hat{\mathbf{v}} = \frac{D}{Dt}(\hat{\mathbf{u}}) = \dot{\hat{\mathbf{u}}} = \dot{\mathbf{u}} + \eta \dot{\mathbf{u}}_2 = \mathbf{v} + \eta \mathbf{v}_2 = \mathbf{C}_N \begin{bmatrix} \mathbf{v} \\ \mathbf{v}_2 \end{bmatrix} \quad (6.29)$$

where the velocity of the beam's centerline is:

$$\mathbf{v} = \underbrace{\begin{bmatrix} \mathbf{i}_1 & \mathbf{i}_2 \end{bmatrix}}_{\mathbf{i}_N} \begin{bmatrix} \dot{u}_1 \\ \dot{u}_2 \end{bmatrix} \quad (6.30)$$

Using Equation 6.9, the term \mathbf{v}_2 is:

$$\mathbf{v}_2 = \dot{\mathbf{g}}_2^* = \overline{\mathbf{R}_g \cdot \mathbf{g}_2} = \dot{\Phi} \cdot \mathbf{g}_2^* \quad (6.31)$$

By substituting Equations 6.10 - 6.13 and relation $\tilde{v}_{ij} = \mathbf{v}_{,j} \cdot \mathbf{g}_i$ into Equation 6.31, term \mathbf{v}_2 is:

$$\mathbf{v}_2 = \frac{1}{\sqrt{g^*}} \tilde{v}_{2|1} \mathbf{g}_3^* \times \mathbf{g}_2^* = -\frac{1}{g^*} (\mathbf{v}_{,1} \cdot \mathbf{g}_2^*) \mathbf{g}_1^* \quad (6.32)$$

Following the derivation procedures from the previous section, the velocity field of the plane curved beam is:

$$\hat{\mathbf{v}} = \mathbf{C}_N \mathbf{G}_N \mathbf{R} \dot{\mathbf{q}}, \quad \dot{\mathbf{q}}^T = [\dot{q}^0 \quad \dots \quad \dot{q}^i \quad \dots \quad \dot{q}^N], \quad \dot{q}^i = \begin{bmatrix} \dot{u}_1^i \\ \dot{u}_2^i \end{bmatrix} \quad (6.33)$$

6.4 Acceleration field

By definition, the acceleration field represents the material derivative of the velocity field:

$$\hat{\mathbf{a}} = \frac{D}{Dt}(\hat{\mathbf{v}}) = \dot{\hat{\mathbf{v}}} = \dot{\mathbf{v}} + \eta \dot{\mathbf{v}}_2 = \mathbf{a} + \eta \mathbf{a}_2 = \mathbf{C}_N \begin{bmatrix} \mathbf{a} \\ \mathbf{a}_2 \end{bmatrix} \quad (6.34)$$

where the acceleration of the beam's centerline is:

$$\mathbf{a} = \underbrace{\begin{bmatrix} \mathbf{i}_1 & \mathbf{i}_2 \end{bmatrix}}_{\mathbf{i}_N} \begin{bmatrix} \ddot{u}_1 \\ \ddot{u}_2 \end{bmatrix} \quad (6.35)$$

The material derivative of Equation 6.31 represents:

$$\mathbf{a}_2 = \overline{\boldsymbol{\omega} \times \mathbf{g}_2^*} = \dot{\boldsymbol{\omega}} \times \mathbf{g}_2^* + \boldsymbol{\omega} \times (\boldsymbol{\omega} \times \mathbf{g}_2^*) \quad (6.36)$$

Using Equation 6.13, the material derivative of angular velocity vector for the plane curved beam is:

$$\dot{\boldsymbol{\omega}} = \dot{\tilde{\omega}}^3 \mathbf{g}_3^* \quad (6.37)$$

where

$$\dot{\omega}^3 = \frac{\dot{v}_{2|1}\sqrt{g^*} - \sqrt{g^*}\dot{v}_{2|1}}{g^*} = \frac{\mathbf{a}_{,1} \cdot \mathbf{g}_2^*}{\sqrt{g^*}} - \frac{\mathbf{g}_1^* \cdot \mathbf{i}_\alpha \tilde{v}_{\alpha,1} \tilde{\omega}^3 \sqrt{g^*}}{(g^*)^{3/2}} - \frac{\mathbf{v}_{1|1} \cdot \mathbf{v}_{2|1}}{(g^*)^{3/2}} \quad (6.38)$$

The product of the velocity gradient components, as well as the product between the velocity gradient components and the angular velocity vector component, is assumed to be negligible in comparison to the velocity gradient and the angular velocity vector components. Consequently, only the first term in Equation 6.38.

In the second part of Equation 6.36 the vector triple product, can be written as:

$$\boldsymbol{\omega} \times (\boldsymbol{\omega} \times \mathbf{g}_2^*) = (\boldsymbol{\omega} \cdot \mathbf{g}_2^*) \boldsymbol{\omega} - (\boldsymbol{\omega} \cdot \boldsymbol{\omega}) \mathbf{g}_2^* = (\tilde{\omega}^3 \tilde{\omega}^3 \mathbf{g}_3^* \cdot \mathbf{g}_2^*) \mathbf{g}_3^* - (\tilde{\omega}^3 \tilde{\omega}^3) \mathbf{g}_2^* \quad (6.39)$$

Assuming the product of the angular velocity vector components small in comparison to the angular velocity vector components, the vector triple product vanishes.

By substituting Equations 6.37 - 6.39 into Equation 6.36, the second term of the acceleration field is:

$$\mathbf{a}_2 = -\frac{1}{g^*} (\mathbf{a}_{,1} \cdot \mathbf{g}_2^*) \mathbf{g}_1^* \quad (6.40)$$

As in the previous section, the acceleration field is obtained as:

$$\hat{\mathbf{a}} = \mathbf{C}_N \mathbf{G}_N \mathbf{R} \ddot{\mathbf{q}}, \quad \ddot{\mathbf{q}}^T = [\ddot{\mathbf{q}}^0 \quad \dots \quad \ddot{\mathbf{q}}^i \quad \dots \quad \ddot{\mathbf{q}}^N], \quad \ddot{\mathbf{q}}^i = \begin{bmatrix} \ddot{u}_1^i \\ \ddot{u}_2^i \end{bmatrix} \quad (6.41)$$

6.5 Kinematic relations

For the case of a plane Bernoulli-Euler beam, only axial component in the strain tensor exists, which can be defined in the convective coordinate system as:

$$\hat{\varepsilon}_{11} = \frac{1}{2} (\hat{g}_{11}^* - \hat{g}_{11}) = \frac{1}{2} (\hat{\mathbf{g}}_1^* \cdot \hat{\mathbf{g}}_1^* - \hat{\mathbf{g}}_1 \cdot \hat{\mathbf{g}}_1) \quad (6.42)$$

Substituting Equation 6.2 for deformed and undeformed configuration in previous relation yields:

$$\hat{\varepsilon}_{11} = \frac{1}{2} (g^* - g) - \eta (K^* g^* - K g) + \frac{1}{2} \eta^2 (g^* K^{*2} - g K^2) = \varepsilon_{11} - \eta \varkappa + \eta^2 \kappa \quad (6.43)$$

where $g = g_{11}$ and $g^* = g_{11}^*$. In the previous equation the reference deformation terms are selected as:

$$\varepsilon_{11} = \frac{1}{2} (g^* - g), \quad \varkappa = K^* g^* - K g, \quad \kappa = g^* K^{*2} - g K^2 \quad (6.44)$$

Matrix representation of Equation 6.43 is given as:

$$\hat{\varepsilon}_{11} = \varepsilon_{11} - \eta \varkappa + \eta^2 \kappa = \underbrace{\begin{bmatrix} 1 & -\eta & \eta^2 \end{bmatrix}}_{\mathbf{C}_{\xi_n}} \underbrace{\begin{bmatrix} \varepsilon_{11} \\ \varkappa \\ \kappa \end{bmatrix}}_{\boldsymbol{\varepsilon}_n} \quad (6.45)$$

The variation of the axial strain component is:

$$\delta\hat{\varepsilon}_{11} = \delta\varepsilon_{11} - \eta\delta\mathcal{K} - \eta^2\delta\kappa = \underbrace{\begin{bmatrix} 1 & -\eta & \eta^2 \end{bmatrix}}_{\mathbf{C}_{\xi n}} \underbrace{\begin{bmatrix} \delta\varepsilon_{11} \\ \delta\mathcal{K} \\ \delta\kappa \end{bmatrix}}_{\delta\varepsilon_n} \quad (6.46)$$

Applying variation to the reference deformation terms given in Equation 6.44 yields:

$$\delta\varepsilon_{11} = \mathbf{g}_1^* \cdot \delta\mathbf{u}_{,1} \quad (6.47)$$

$$\delta\mathcal{K} = \left(\delta\mathbf{u}_{1,1} - \frac{1}{2} \frac{g_{,1}^*}{g^*} \delta\mathbf{u}_{,1} \right) \cdot \mathbf{g}_2^* \quad (6.48)$$

$$\delta\kappa = -2 \frac{\overline{K}^*}{g^{*2}} \delta\mathbf{u}_{,1} \cdot \mathbf{g}_1^* + \left(\frac{1}{g^*} \delta\mathbf{u}_{1,1} - \frac{1}{2} \frac{g_{,1}^*}{g^{*2}} \delta\mathbf{u}_{,1} \right) \cdot \mathbf{g}_2^* \quad (6.49)$$

Matrix representation of the variation of the reference deformation terms is:

$$\underbrace{\begin{bmatrix} \delta\varepsilon_{11} \\ \delta\mathcal{K} \\ \delta\kappa \end{bmatrix}}_{\delta\varepsilon_n} = \underbrace{\begin{bmatrix} x_1^{m*} & 0 \\ -\Gamma_{11}^{1*} x_2^{m*} & x_2^{m*} \\ -\Gamma_{11}^{1*} x_2^{m*} - 2 \frac{K^*}{g^*} x_1^{m*} & \frac{x_2^{m*}}{g^*} \end{bmatrix}}_{\mathbf{L}_n} \underbrace{\begin{bmatrix} \delta u_{m,1} \\ \delta u_{m,11} \end{bmatrix}}_{\delta\mathbf{u}_{\xi n}} \quad (6.50)$$

Components of the vector $\delta\mathbf{u}_{\xi n}$ can be parameterized using NURBS parameterization:

$$\mathbf{u}_{\xi n} = \sum_{i=0}^N \mathbf{B}_{ni} \delta\mathbf{q}_n^i = \mathbf{B}_n \delta\mathbf{q}_n \quad (6.51)$$

where

$$\mathbf{B} = [\mathbf{B}_{n0} \quad \dots \quad \mathbf{B}_{ni} \quad \dots \quad \mathbf{B}_{nN}], \quad \mathbf{B}_{ni} = \begin{bmatrix} R_{i,1} & 0 \\ 0 & R_{i,1} \\ R_{i,11} & 0 \\ 0 & R_{i,11} \end{bmatrix} \quad (6.52)$$

$$\delta\mathbf{q}_n = [\delta\mathbf{q}_n^1 \quad \dots \quad \delta\mathbf{q}_n^i \quad \dots \quad \delta\mathbf{q}_n^N], \quad \delta\mathbf{q}_n^i = \begin{bmatrix} \delta u_{1n}^i \\ \delta u_{2n}^i \end{bmatrix} \quad (6.53)$$

Finally, the reference variation of the axial strain is given as:

$$\delta\hat{\varepsilon}_{11} = \mathbf{C}_{\xi n} \mathbf{L}_n \mathbf{B}_n \delta\mathbf{q}_n \quad (6.54)$$

6.6 Constitutive relations

Beam formulation is conducted in small strain conditions in order to apply constitutive Hook's law [30]:

$$\hat{S}^{kl} = 2\mu \left(\hat{g}^{*1k} \hat{g}^{*1k} \hat{\varepsilon}_{kl} + \nu \hat{g}^{*11} \hat{g}^{*11} \hat{\varepsilon}_{11} \right) \quad (6.55)$$

In the case of plane curved beam only the first term of the stress tensor is defined:

$$\hat{S}^{11} = E\hat{\varepsilon}_{11} \frac{1}{g_0^{*4}} \frac{1}{g^{*2}} \quad (6.56)$$

6.7 Weak formulation

The principle of virtual work defined by Equation 5.85 can also be applied for the case of the geometrically nonlinear dynamic formulation of the plane Bernoulli-Euler beam. Substituting Equation 6.56, 6.45 and 6.54 into the internal forces contribution of the virtual work given by Equation 5.86, yields:

$$\delta W_{int} = \int_{V_o} \hat{\mathbf{S}} \delta \hat{\boldsymbol{\varepsilon}} dV_o = \int_{V_o} \hat{S}^{11} \delta \hat{\varepsilon}_{11} dV_o = \int_{\xi} \boldsymbol{\varepsilon}_n^T \mathbf{D}_n \mathbf{L}_n \mathbf{B}_n \sqrt{g} d\xi \delta \mathbf{q}_n = \mathbf{F}_{int} \delta \mathbf{q}_n \quad (6.57)$$

where

$$\mathbf{D}_n = \frac{E}{g^{*2}} \int \mathbf{C}_{\xi n}^T \mathbf{C}_{\xi n} d\eta d\zeta \quad (6.58)$$

Internal forces of the plane curved Bernoulli-Euler beam (\mathbf{F}_{int}) represents the point forces at the control points, which can be defined as:

$$\mathbf{F}_{int} = \int_{\xi} \boldsymbol{\varepsilon}_n^T \mathbf{D}_n \mathbf{L}_n \mathbf{B}_n \sqrt{g} d\xi \quad (6.59)$$

By substituting Equations 6.41 and 6.28 into the inertial forces contribution of the virtual work, given by Equation 5.87, the mass matrix (\mathbf{M}) is derived as follows:

$$\delta W_{ine} = \int_{V_o} \rho_o \hat{\mathbf{a}} \cdot \delta \hat{\mathbf{u}} dV = \ddot{\mathbf{q}} \int_{\xi} \rho_o \mathbf{R}^T \mathbf{G}_n^T \mathbf{D}_{mn} \mathbf{G}_n \mathbf{R} \sqrt{g} d\xi \delta \mathbf{q} = \ddot{\mathbf{q}}^T \mathbf{M} \delta \mathbf{q}_n \quad (6.60)$$

where

$$\mathbf{D}_{mn} = \int \mathbf{C}_n^T \mathbf{C}_n d\eta d\zeta \quad (6.61)$$

In order to determine the influence of the external forces in the virtual work, the variation of the beam's centerline displacement should be defined:

$$\delta \mathbf{u} = \sum_{i=0}^N \mathbf{R}_{ui} \delta \mathbf{q}^i = \mathbf{R}_u \delta \mathbf{q} \quad (6.62)$$

where

$$\mathbf{R}_u = [\mathbf{R}_{u0} \quad \mathbf{R}_{u1} \quad \dots \quad \mathbf{R}_{ui} \quad \dots \quad \mathbf{R}_{uN}], \quad \mathbf{R}_{ui} = \begin{bmatrix} R_i(\xi) & 0 \\ 0 & R_i(\xi) \end{bmatrix} \quad (6.63)$$

Substituting the previous relation in the contribution of the external forces, given by Equation 5.88, yields:

$$\delta W_{ext} = \int_{\xi} \mathbf{f} \cdot \delta \mathbf{u} d\xi = \int_{\xi} \mathbf{f} \cdot \mathbf{R}_u d\xi \delta \mathbf{q}_n = \mathbf{F}_{ext} \delta \mathbf{q}_n \quad (6.64)$$

In the previous relation, the external point forces at the control points are defined as:

$$\mathbf{F}_{ext} = \int_{\xi} \mathbf{f} \cdot \mathbf{R}_u d\xi \quad (6.65)$$

Finally, the governing equation of motion for the curved Bernoulli-Euler beam element for geometrically nonlinear formulation defined using isogeometric approach is obtained by substituting Equations 6.57, 6.60 and 6.64 into Equation 5.85 as:

$$\mathbf{M}\ddot{\mathbf{q}} = \mathbf{F}_{ext} - \mathbf{F}_{int} \quad (6.66)$$

6.8 Transient analysis

Using explicit time integration schemes, internal and external forces at the control points are known, while the acceleration vector is an unknown quantity. Consequently, Equation 6.66 should be modified as:

$$\ddot{\mathbf{q}} = \mathbf{M}^{-1} (\mathbf{F}_{ext} - \mathbf{F}_{int}) \quad (6.67)$$

When the accelerations of the control points are computed from Equation 6.67, the velocity and displacements can be calculated using relations 5.122 and 5.123.

The explicit time integration scheme is conditionally stable. In the linear formulation, the time step is bounded by the system's maximum natural frequency. However, in the nonlinear analysis, a reduction factor γ should be included [57]:

$$\Delta t_n < \Delta t_{n,max} = \gamma \frac{2}{\omega_{n,max}} \quad (6.68)$$

In the scope of this study, the influence of the factor γ has not been analyzed. The numerical verification of the dynamic response of the plane curved Bernoulli-Euler isogeometric beam, has been carried out assuming $\gamma = 0.9$, ensuring convergence of the numerical calculations.

7 Object-Oriented Computer Program

The algorithms presented in the previous chapters are implemented in Matlab using Object - Oriented Programming (OOP). In comparison to the Procedural - Programming, OOP has shown significant advantages such as reliability, reusability and extendibility [58]. Adding a new feature in OOP or fixing an old one takes less time and effort. In addition, OOP has achieved significant decrease in program size and complexity. OOP is based on the concept of objects which can contain properties and methods. Objects represent the instances of the classes, which can be connected using different relationships. The graphical representation of the classes and their relationships can be presented using the Unified Modeling Language (UML). Simplified UML class model of the isogeometric formulation of the presented problems is shown in Figure 7.1, where classes and their relationships are given without the arguments and return value types of a method. In the following, the short explanation of the given classes is given with the adequate properties and methods.

Input represents the class which encapsulates the information regarding the analysis problem, with the following properties: MaterialProperties, CrossSection, FunctionDegree, KnotVector, WeightVector, BoundaryConditions. Presented class does not contain methods.

BSplineBasis is the class representing the B - Spine basis functions. Consequently, the properties are knot vector (KnotVector) and degree of basis function (FunctionDegree). Necessary methods contained in the class are NumberOfFunction(), SpanOfParametricPoint(), FunctionValue(), FunctionDerivative(), PlotFunction(), PlotFunctionDerivative().

NURBS_Basis is a subclass of the **BSplineBasis** class and for its construction weight vector is required which represents the property of the class (WeightVector). The class methods are: NURBS_function(), NURBS_derivative(), PlotNURBS() and PlotNURBS_derivative(). The methods of the **BSplineBasis** and **NURBS_Basis** classes implements the procedures regarding the basis functions as given in [9] and [8].

Refinement represents the class in which the properties are DegreeElevation and FunctionContinuity while the methods are three types of refinement procedures for the IGA based analysis: P_ref(), H_ref() and K_ref() which are presented in [9], [8] and [1].

Composition of the **Refinement** class objects creates the **Geometry** class where control points (ControlPoints) are additional property. In addition, **Geometry** class uses **Integration** class in which only QuadNode() method is contained [10].

BernoulliEuler class encapsulates the element formulation of Bernoulli - Euler beam. The class properties are Material and Section, while the class methods are: L_Matrix(), B_Matrix(), Deformation(), SectionProp(), Force(), Material(), StiffnessMatrix() and MassMatrix(). In

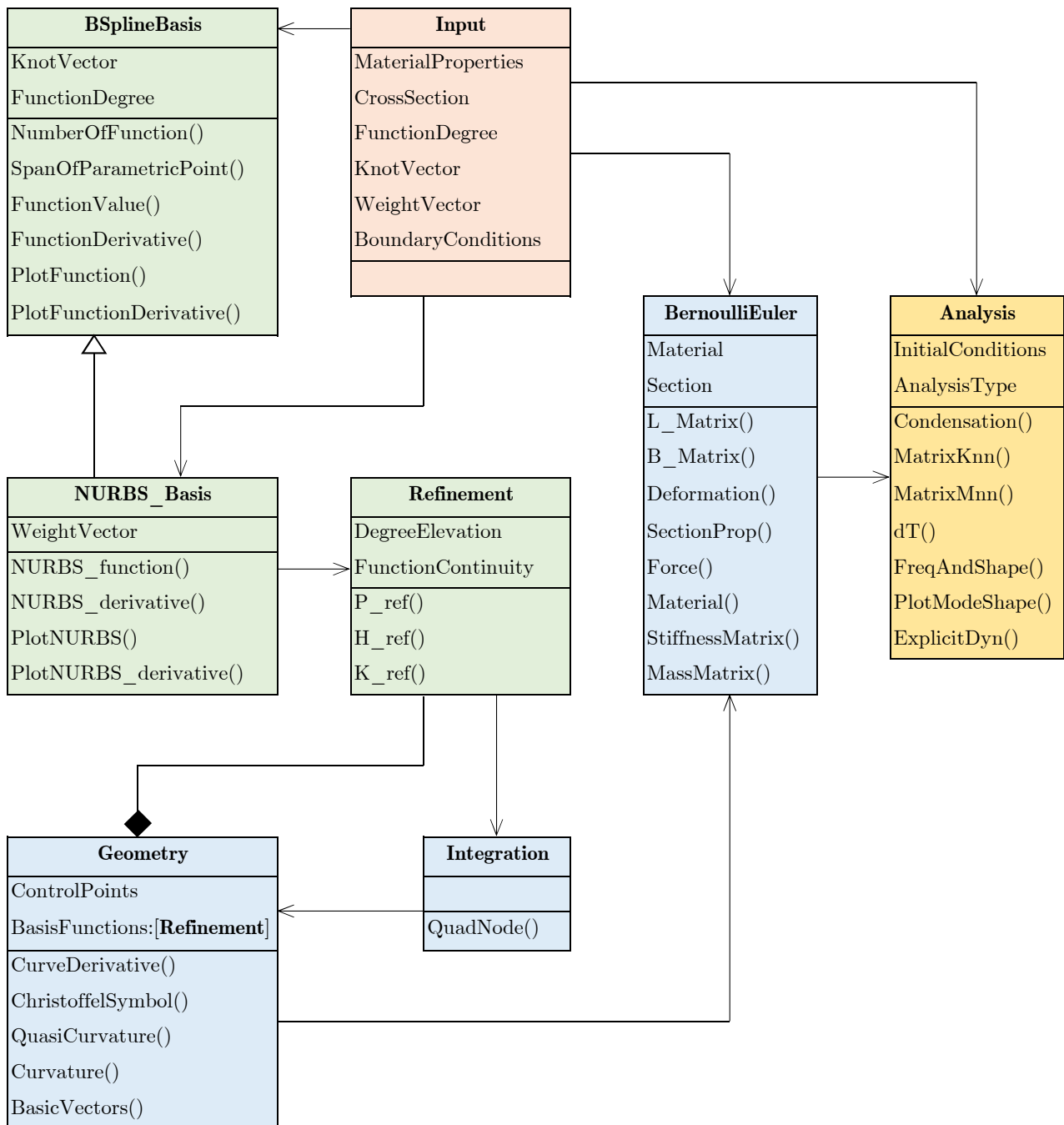


Figure 7.1: Simplified UML class diagram of the dynamic analysis of the isogeometric Bernoulli - Euler beam

this class the plane and spatial beam can be formulated for the linear and nonlinear dynamic analysis, depending on the analysis type.

Analysis class is a class containing all procedures regarding the linear and geometrically nonlinear dynamic analysis. Boundary conditions are taken into account and the stiffness and mass matrix of the system are formulated, which are used for the free vibration or transient analysis in the linear and geometrical nonlinear case. The class properties are InitialConditions and AnalysisType, while its methods are: Condensation(), MatrixKnn(), MatrixMnn(), dT(), FreqAndShape(), PlotModeShape() and ExplicitDyn().

In the UML class diagram of the IGA procedure three relationships can be found: inheritance (line with an unfilled arrowhead), association (arrow line) and composition (line with the filled diamond shape).

8 Numerical examples

8.1 Free vibration analysis

8.1.1 Validation study

In this section, the validation study of the proposed method for free vibration analysis will be conducted. The natural frequencies of the fully clamped - fully clamped conical helix obtained using the Bernoulli-Euler isogeometric beam element are compared with available results from the literature [59], and the results from the commercial finite element (FE) software package Abaqus [60]. The base and top radius of the conical helix are $R_1 = 25mm$ and $R_2 = 5mm$, with constant pitch angle $\alpha = 4.8^\circ$ and 6.5 coils, Figure 8.1(a). The cross-section of the conical helix is circular with diameter $d = 2mm$, while the beam material is defined using the Young's modulus $E = 210GPa$, the Poisson's ratio $\nu = 0.3$ and the mass density $\rho = 7850kg/m^3$.

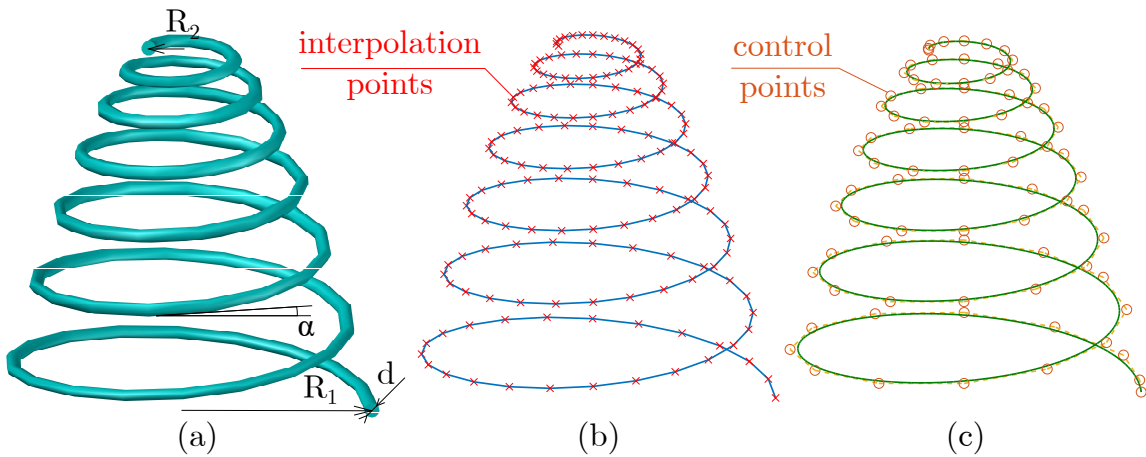


Figure 8.1: (a) conical helix geometry; (b) interpolation points of the conical helix; (c) NURBS based parameterization control points of the conical helix

Geometry of the conical helix is defined based on 78 interpolation points (Figure 8.1(b)), which are imported in the Rhinoceros NURBS modeling software [61] and used to construct a free-form NURBS based curve with 81 control points and the degree of B-spline basis functions $p = 3$, Figure 8.1(c). For the FE analysis, the Rhinoceros geometry model of the free-form curve is converted into a polyline with 256 line segments of the average length of $0.0025m$. The conical helix in Abaqus is modeled using the B33 beam element based on the Bernoulli - Euler hypothesis. The results of the first ten natural frequencies obtained using the presented approach, Abaqus,

and results given in [59] are given in Table 8.1. An excellent agreement is achieved between the results obtained using isogeometric formulation (I), and the results obtained using the FE software Abaqus (A), which is confirmed with the relative error less than 1.0 % (Δ_{I-F}). The higher relative error is observed between the results obtained using the presented approach and the results from the literature (Y) based on the Timoshenko beam formulation [59]. In addition, the first three mode shapes of the conical helix are obtained using the presented isogeometric approach and compared with the mode shapes from Abaqus, Figure 8.2.

Table 8.1: First ten natural frequencies [Hz] obtained using the present study (IGA) compared with the literature results (Yildirim) and the results from the Abaqus (Abaqus) presented with the relative error [%] between corresponding frequencies ($\Delta_{X-Y} = \frac{X-Y}{X} * 100$)

Mode	IGA (I) 312 DOFs	Abaqus (A) 2054 DOFs	Yildirim (Y) [59]	Δ_{I-A}	Δ_{I-Y}
1	108.39	108.27	110.64	0.11	-2.03
2	112.76	112.51	115.19	0.22	-2.11
3	134.20	133.16	135.91	0.78	-1.26
4	141.88	140.83	143.77	0.74	-1.31
5	193.39	192.67	196.92	0.36	-1.80
6	200.65	200.07	204.3	0.29	-1.79
7	218.07	217.43	-	0.29	-
8	229.11	228.4	-	0.31	-
9	265.74	265.16	-	0.22	-
10	281.55	280.02	-	0.54	-

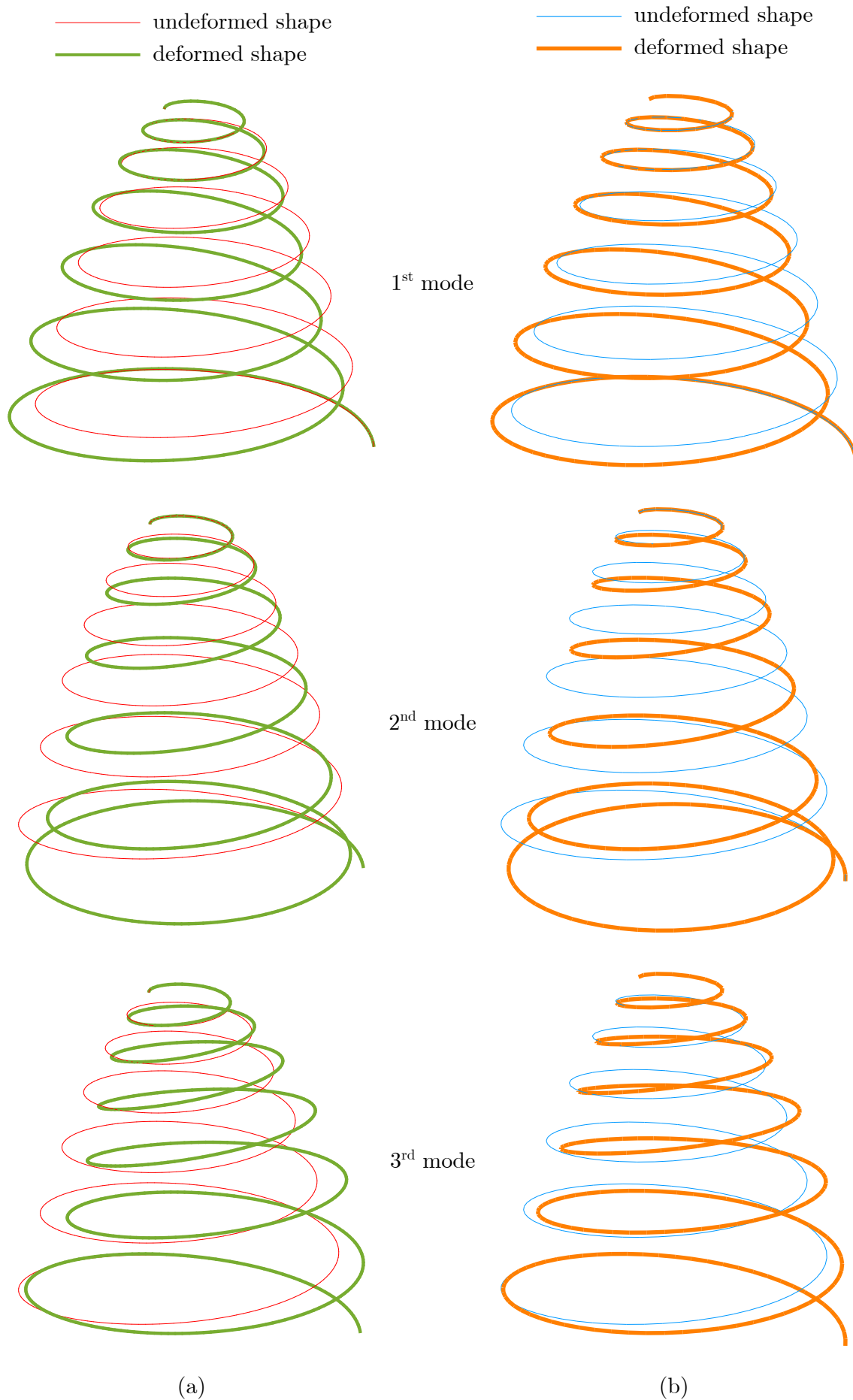


Figure 8.2: First three mode shapes of the conical helix obtained using: (a) presented isogeometric approach, (b) FEM based software Abaqus

8.1.2 Convergence study

The convergence study of the presented isogeometric approach is demonstrated on the example of an spatial curved beam. The geometry of the fully clamped - simply supported curve, Figure 8.3, is defined using the following control points:

$$\mathbf{CP}^T = \begin{bmatrix} 3 & 3 & -3 & -5 & 3 & 3 & -3 & -3 & 3 & 3 & 6 & 6 & 9 & 12 \\ 0 & 3 & 3 & -5 & -3 & 3 & 3 & -3 & -3 & 0 & 0 & 0 & 0 & 0 \\ 8 & 7.5 & 6.5 & 5.5 & 4.5 & 3.5 & 2.5 & 1.5 & 0.5 & 0 & 1 & 0 & 0 & 0 \end{bmatrix} \quad (8.1)$$

and the 3rd - order basis functions defined over the knot vector and weight vector::

$$\boldsymbol{\xi}^T = [0 \ 0 \ 0 \ 0 \ 1/7 \ 2/7 \ 3/7 \ 4/7 \ 5/7 \ 6/7 \ 1 \ 1 \ 1 \ 1] \quad (8.2)$$

$$\mathbf{w}^T = [1 \ 1 \ 1 \ 10 \ 1 \ 1 \ 1 \ 1 \ 1 \ 1 \ 1 \ 1 \ 1 \ 1] \quad (8.3)$$

The beam material is defined using the Young's modulus $E = 31.5GPa$, the Poisson's ratio $\nu = 0.2$, and the mass density $\rho = 2500kg/m^3$. The cross-section is circular with a diameter $d = 0.1m$.

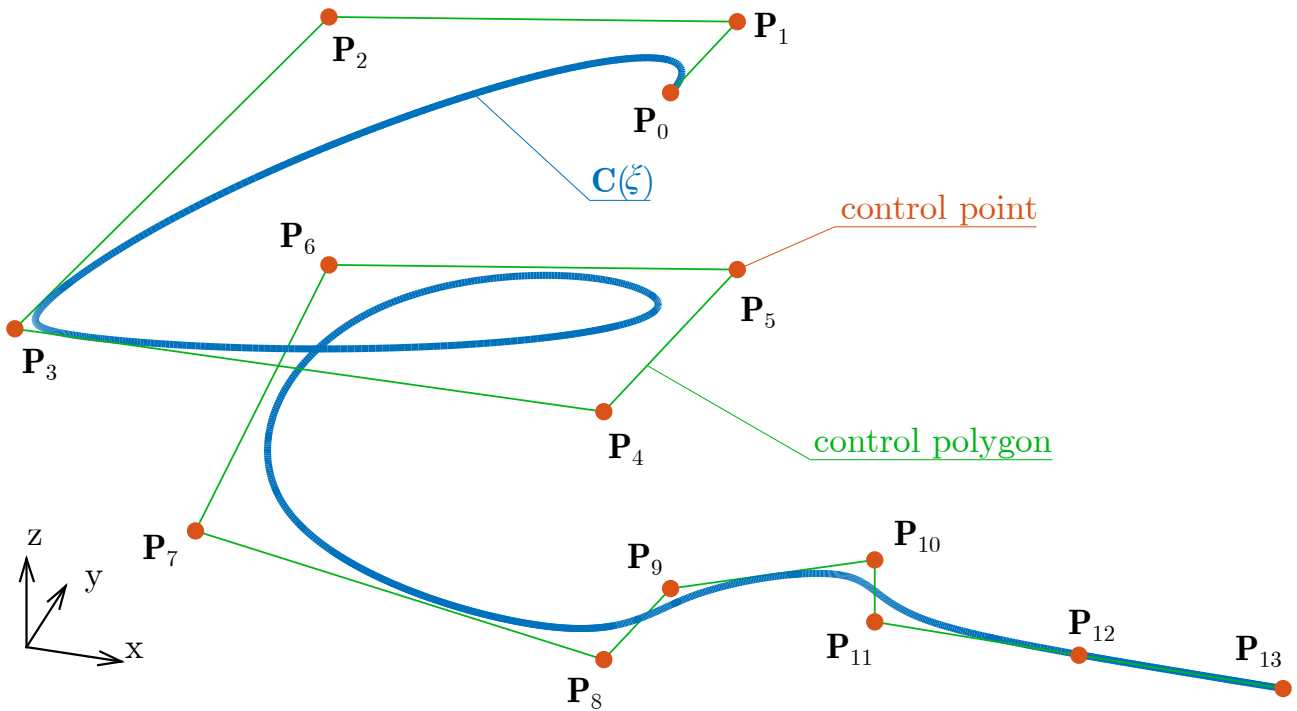


Figure 8.3: An arbitrary curve $\mathbf{C}(\xi)$ with corresponding control points \mathbf{P}_i

First, the H - refinement procedure is applied to demonstrate the convergence property of the presented isogeometric approach. This procedure is conducted by knot insertion, hence the number of control points and the number of DOFs increase. In Table 8.2, the first ten natural frequencies of the structure with respect to the number of DOFs are presented. As can be noticed, the H - refinement convergence property of the isogeometric approach is satisfactory. Differences between the natural frequencies of the spatial beam with 224 DOFs and 280 DOFs is negligible as demonstrated with the relative error (Δ). Aforementioned leads to the conclusion that the spatial beam model with 224 DOFs gives the accurate results of the considered natural frequencies.

Table 8.2: Convergence of the first ten natural frequencies of the presented approach with variable numbers of DOFs obtained applying H - refinement procedure

Mode	44 DOFs	92 DOFs	144 DOFs	176 DOFs	224 DOFs	280 DOFs	Δ [%]
1	0.7564	0.4553	0.4261	0.4206	0.4034	0.3995	-0.98
2	1.0679	0.5722	0.4604	0.4532	0.4433	0.4363	-1.60
3	1.3222	0.6862	0.6270	0.6168	0.6082	0.6039	-0.71
4	2.5097	0.8432	0.7450	0.7199	0.7129	0.7091	-0.54
5	3.3681	1.0349	0.9396	0.9144	0.8980	0.8923	-0.64
6	4.3789	1.8702	1.5117	1.4070	1.3427	1.3182	-1.86
7	5.3475	2.0596	1.5512	1.5980	1.4548	1.4376	-1.20
8	8.2056	2.6546	2.3032	2.1660	2.0878	2.0638	-1.16
9	9.6639	2.8893	2.3649	2.3600	2.3046	2.2982	-0.29
10	11.869	4.2264	3.1792	2.9852	2.8662	2.8353	-1.10

The same conclusion can be drawn from Figure 8.4, which presents the convergence rate of the beam's natural frequencies computed using the H - refinement.

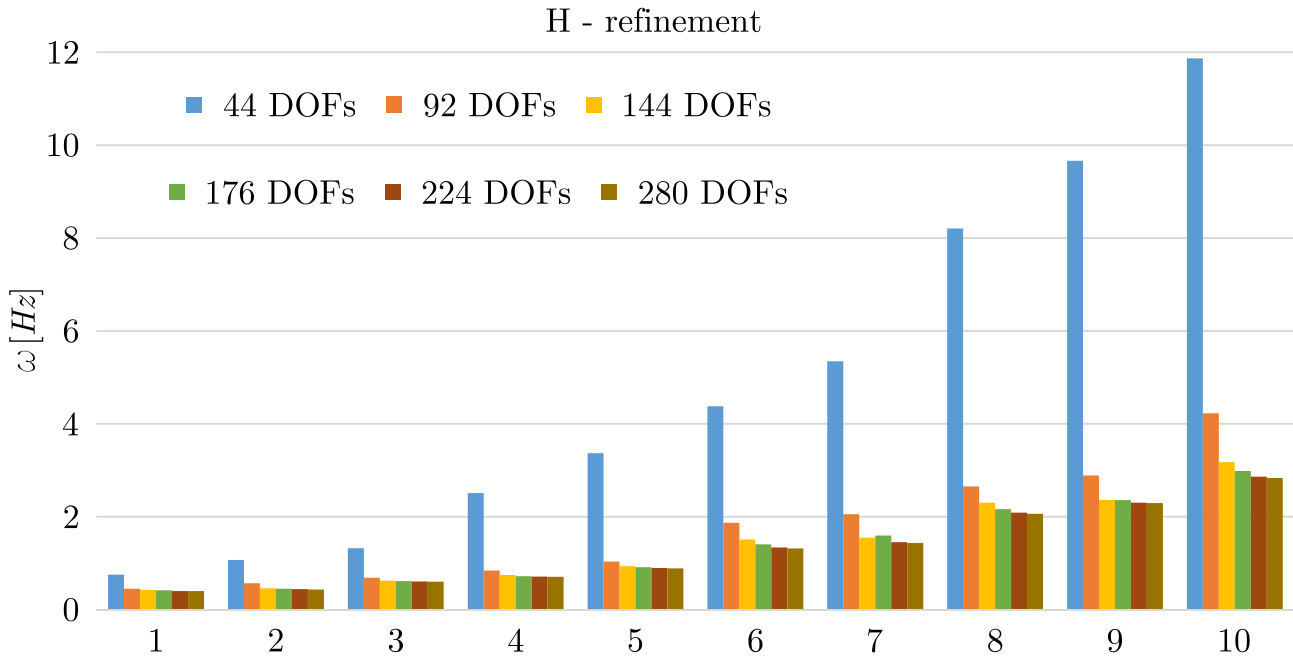


Figure 8.4: Convergence of the first ten natural frequencies computed using the H - refinement for isogeometric beam element

An additional convergence study has been conducted applying the P - refinement, where the number of DOFs is increased by order elevation of the basis functions. The results of the first ten natural frequencies of the spatial beam have been calculated and presented in Table 8.3. Convergence has been achieved with the beam model with 220 DOFs, verified by the relative error Δ between the beam model with 264 DOFs and 220 DOFs.

In Figure 8.5 the convergence rate of the given refinement procedure is presented.

Table 8.3: Convergence of the first ten natural frequencies of the presented study using the P - refinement procedure

Mode	p = 3	p = 4	p = 5	p = 6	p = 7	p = 8	Δ [%]
	44 DOFs	88 DOFs	132 DOFs	176 DOFs	220 DOFs	264 DOFs	
1	0.7564	0.4605	0.4195	0.4106	0.4007	0.3970	-0.93
2	1.0679	0.5276	0.4643	0.4410	0.4370	0.4338	-0.74
3	1.3222	0.6812	0.6103	0.6094	0.6026	0.6017	-0.15
4	2.5097	0.7944	0.7223	0.7148	0.7107	0.7087	-0.28
5	3.3681	1.0158	0.9086	0.9005	0.8920	0.8896	-0.27
6	4.3789	1.7677	1.3755	1.3253	1.3145	1.3054	-0.70
7	5.3475	1.8876	1.6269	1.5496	1.4709	1.4395	-2.18
8	8.2056	2.4605	2.1175	2.0518	2.0584	2.0352	-1.14
9	9.6639	2.5991	2.3718	2.2793	2.3077	2.2423	-2.92
10	11.869	3.7272	2.9055	2.8272	2.8300	2.7961	-1.21

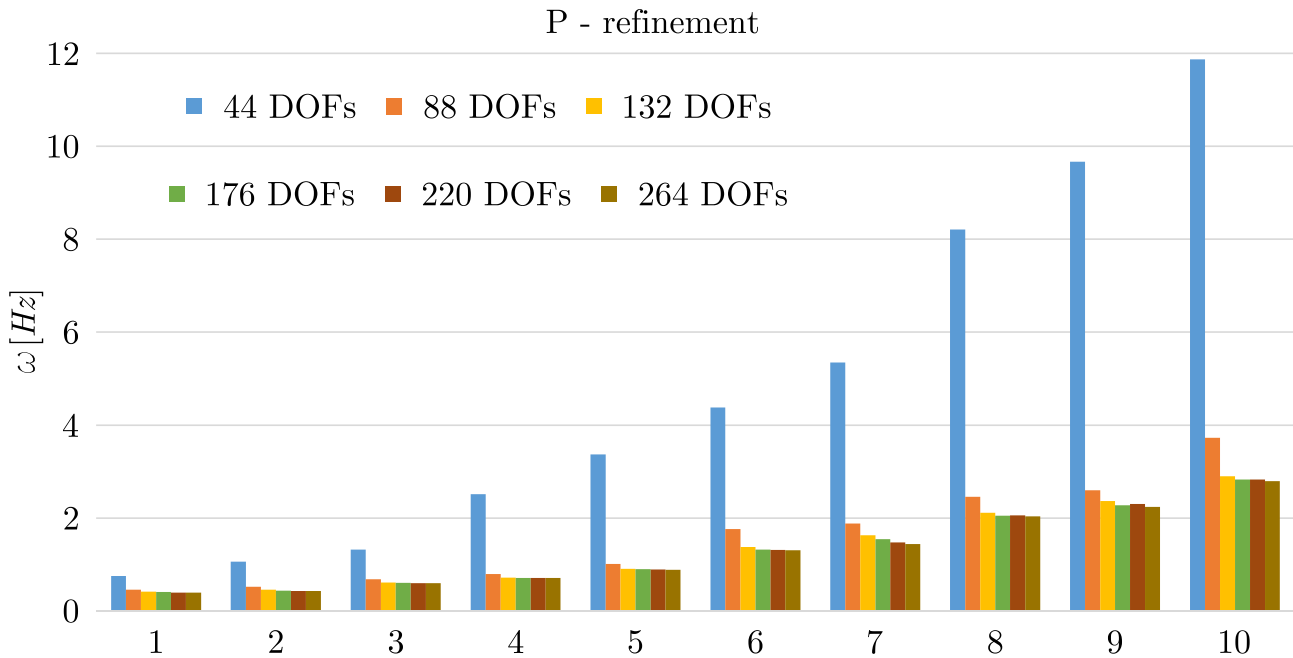


Figure 8.5: Convergence of the first ten natural frequencies computed using the P - refinement for isogeometric beam element

In order to demonstrate the advantage of the presented approach, the convergence of the natural frequencies obtained using the FEM is given. A physical discretization is applied using the interpolation points to define the geometry of the FE model, forming six different FE models with respect to the length of finite elements, Figure 8.6. The results of the natural frequencies are presented in Table 8.4 with respect to the number of DOFs. The last column of the table shows the relative error (Δ) between the sixth FE model with 762 DOFs and the isogeometric beam model obtained using the H - refinement procedure with 280 DOFs. As can be noticed, the adequate results of the natural frequencies are obtained with a considerably less number of DOFs using isogeometric beam model compared to the FE model.

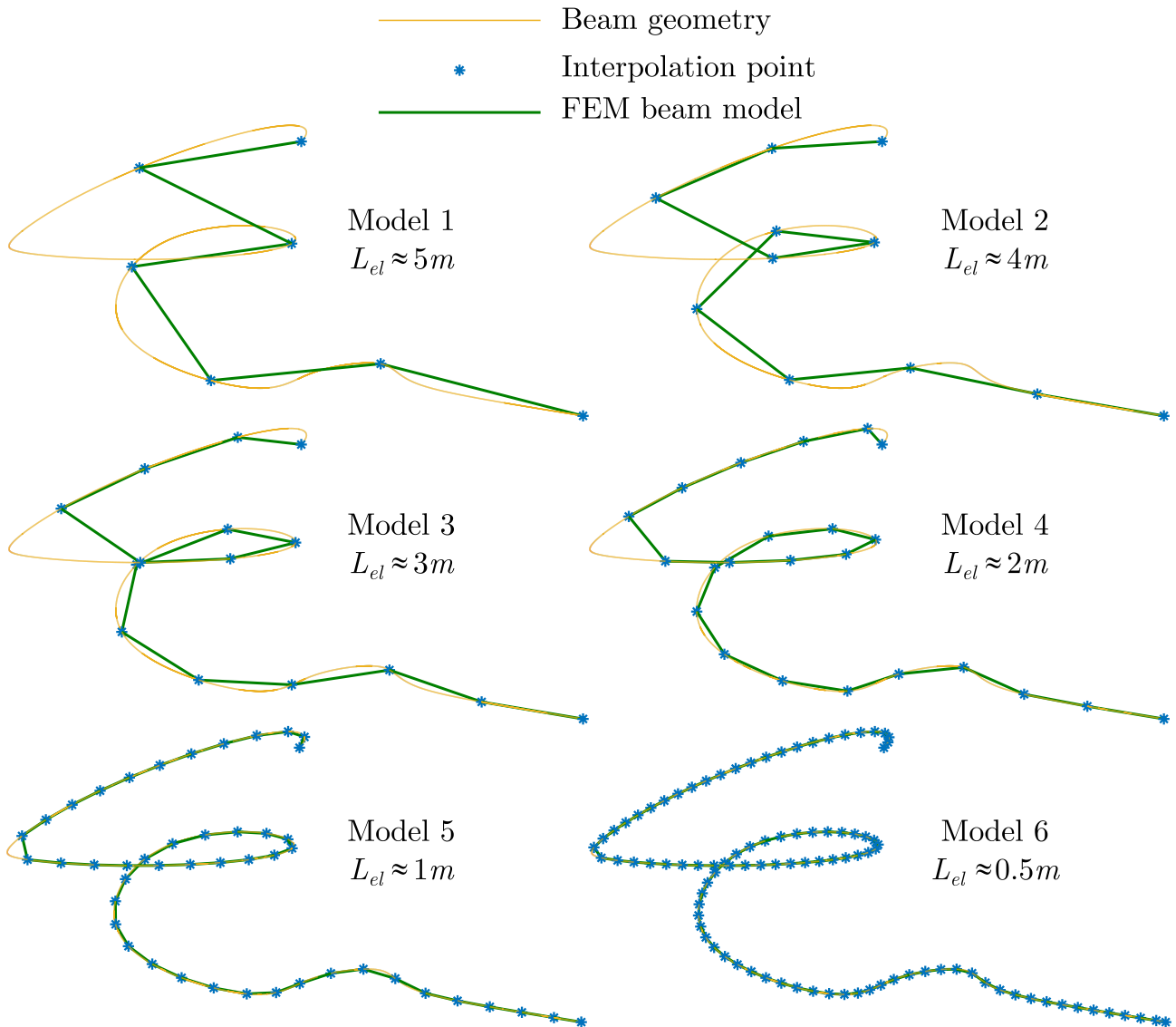


Figure 8.6: Finite element models of the spatial beam

In addition, the first five mode shapes are obtained using the isogeometric approach, and a good agreement has been achieved with the mode shapes obtained using Abaqus, Figure 8.7.

8.1.3 Influence of boundary conditions

In this section, the influence of boundary conditions on the natural frequencies of the curved spatial beam is investigated. The beam geometry and the mechanical properties are taken from the previous example. Analysis has been conducted on the beam model with 224 DOFs obtained using the H - refinement procedure. The following boundary conditions have been considered: fully clamped (C), simply supported (SS) and free (F). The results of the first ten natural frequencies for different types of boundary conditions have been calculated using the isogeometric approach and presented in Table 8.5. As expected, the boundary conditions significantly affect the natural frequencies of the curved spatial beam. A stiffer beam has a higher value of the natural frequency, which is demonstrated for the case of the fully clamped - fully clamped boundary conditions.

Table 8.4: Convergence of the first ten natural frequencies obtained using FEM - based software Abaqus

	Model 1	Model 2	Model 3	Model 4	Model 5	Model 6	
Mode	42 DOFs	74 DOFs	106 DOFs	170 DOFs	362 DOFs	762 DOFs	Δ [%]
1	0.6472	0.5364	0.4943	0.4488	0.4102	0.4002	0.18
2	1.2036	0.6964	0.5794	0.4996	0.4474	0.4372	0.21
3	1.6235	1.0378	0.8928	0.7581	0.6345	0.6086	0.78
4	2.0611	1.2421	0.9828	0.8188	0.7314	0.7127	0.51
5	2.6692	1.3111	1.1402	1.0063	0.9136	0.8933	0.11
6	2.7452	2.0272	1.7250	1.4968	1.3426	1.3140	-0.32
7	3.0944	2.1783	1.8986	1.6470	1.4712	1.4374	-0.01
8	3.4226	2.6949	2.4952	2.2386	2.0928	2.0581	-0.28
9	4.0822	2.9734	2.7006	2.4195	2.3369	2.3001	0.08
10	12.8930	4.0433	3.5451	3.1491	2.8927	2.8326	-0.10

Table 8.5: Influence of boundary conditions on the spatial curved beam

	C-C	SS-C	C-SS	F-C	C-F
Mode	280 DOFs	283 DOFs	283 DOFs	286 DOFs	286 DOFs
1	0.3995	0.1660	0.2599	0.1355	0.1288
2	0.4363	0.3416	0.3394	0.1376	0.1370
3	0.6039	0.4447	0.5888	0.2704	0.2669
4	0.7091	0.6639	0.6617	0.2969	0.2932
5	0.8923	0.8016	0.7335	0.4248	0.4047
6	1.3182	1.1031	1.2238	0.6142	0.6220
7	1.4376	1.1202	1.3336	0.7542	0.7454
8	2.0638	1.5951	1.5594	0.8446	0.8438
9	2.2982	1.6576	1.7163	1.2451	1.2499
10	2.8353	2.3401	2.3195	1.5278	1.5202

8.2 Linear dynamic analysis of a curved spatial beam

8.2.1 Moving load problem

8.2.1.1 Validation and convergence study

In this example, the validation study of the presented theoretical considerations is conducted. The horizontally curved arch beam with length $L = 24m$ and subtended angle $\alpha = 30^\circ$ is subjected to the out-of-plane and in-plane moving load with constant magnitude and constant velocity. Displacements, as well as torsional rotations at points P1 and P4 are restrained. The beam geometry has been modeled with one isogeometric element using four control points with

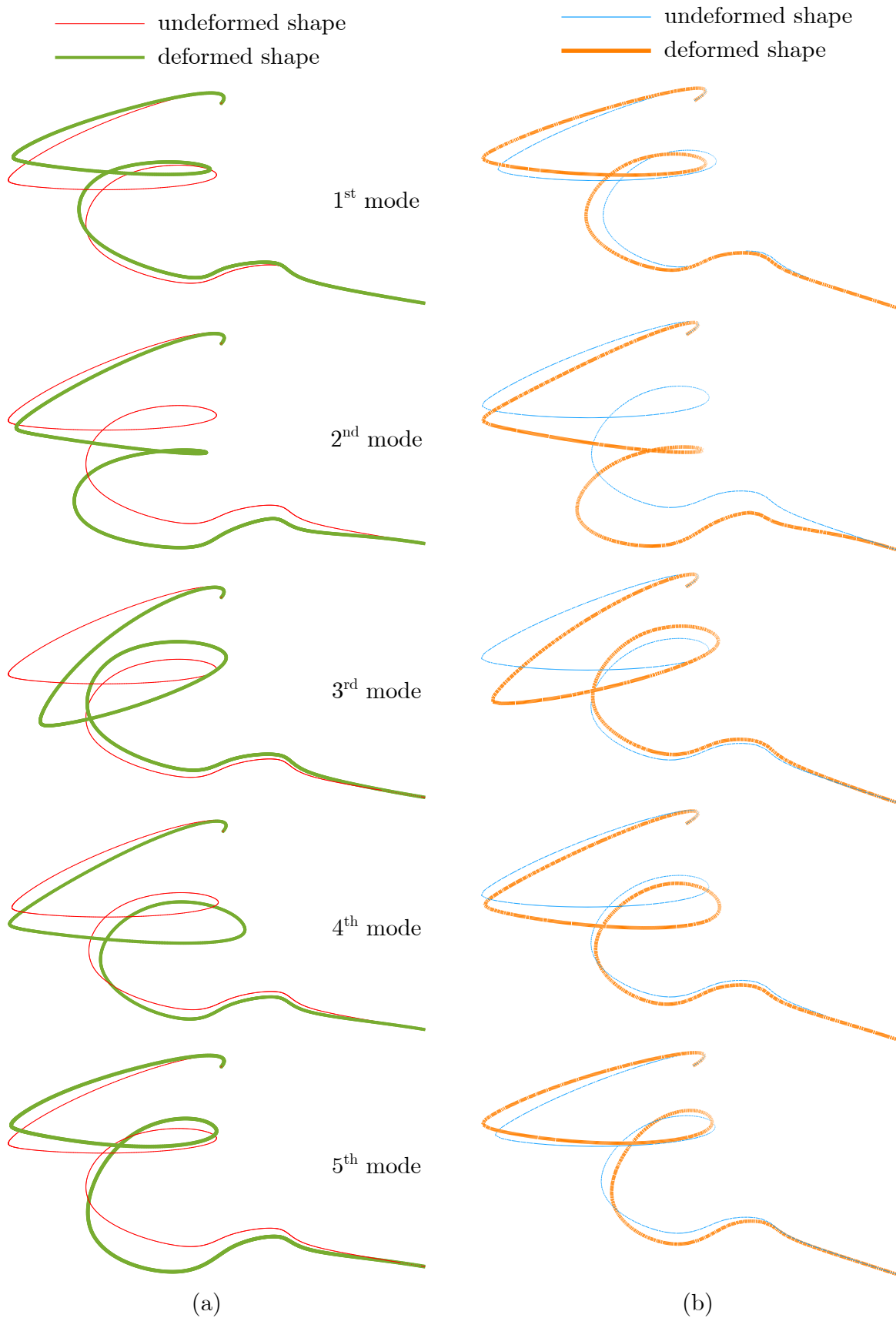


Figure 8.7: First five mode shapes of the spatial beam obtained using: (a) presented isogeometric approach, (b) FEM based software Abaqus

corresponding weights, as given in Figure 8.8, and 3rd-degree NURBS basis functions. The beam material is homogeneous defined using the Young's modulus $E = 32.2GPa$, the Poisson's

ratio $\nu = 0.2$ and the mass density $\rho = 2400 \text{ kg/m}^3$, while the cross-section is rectangular with the dimensions $b/h = 5/1.8 \text{ m}$. The mass m moving along the curved beam with constant velocity $V = 40 \text{ m/s}$ has generated the gravitational out-of-plane load $f_w = -m \cdot g$, as well as inertial in-plane moving load $f_u = m \cdot V^2/R$ directed toward the arch center. In previous relations, g is the gravitational acceleration, while R represents the arch radius. Displacements of the beam's midpoint obtained using the isogeometric approach have been compared with the semi-analytical results from the literature [39] applicable only for the simply supported arches. It is important to point out that the beam model presented in [39] is based on the Timoshenko beam theory. Besides the validation study, the same beam is used for the convergence study of the presented approach using H -, P - and K - refinement.

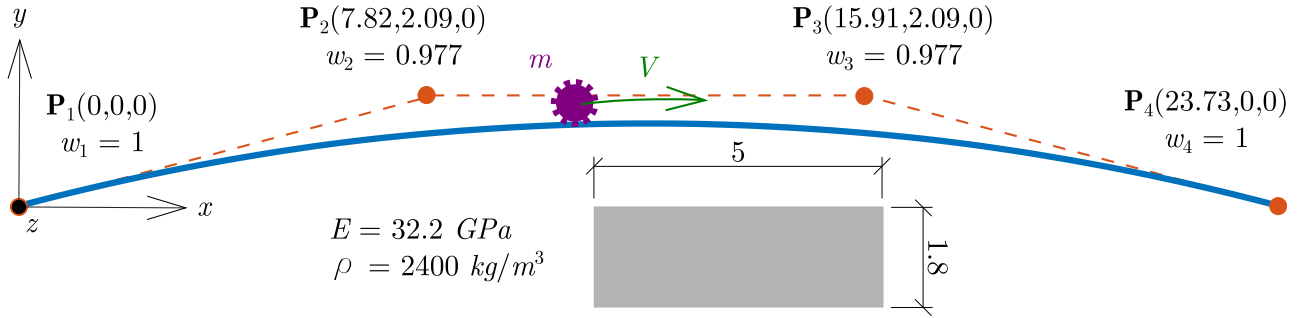


Figure 8.8: Geometry of the beam subjected to the moving load

First, the convergence study of the proposed method has been conducted by applying the P - refinement procedure. The beam's midpoint in-plane (u) and out-of-plane (w) displacements obtained using P - refinement procedure are presented respectively in Figure 8.9 and Figure 8.10.

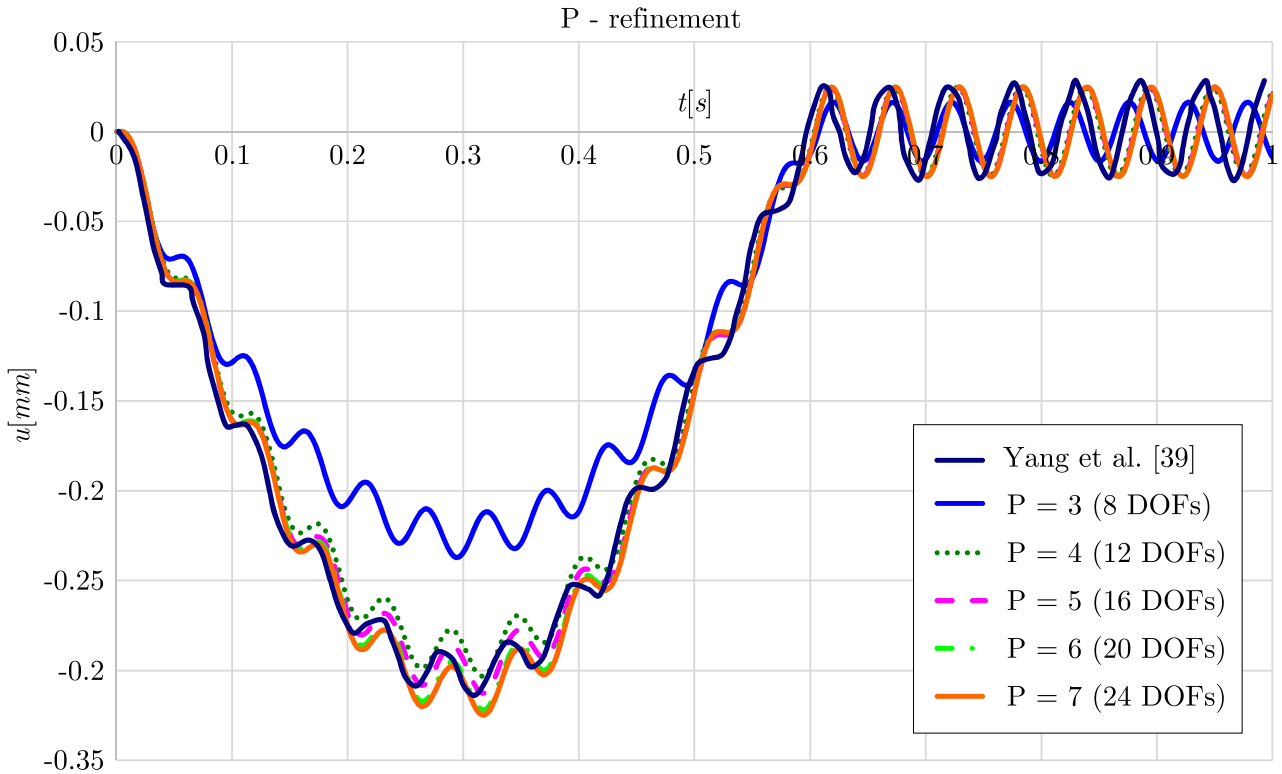


Figure 8.9: In-plane displacement (u) of the beam's midpoint obtained using the P - refinement procedure

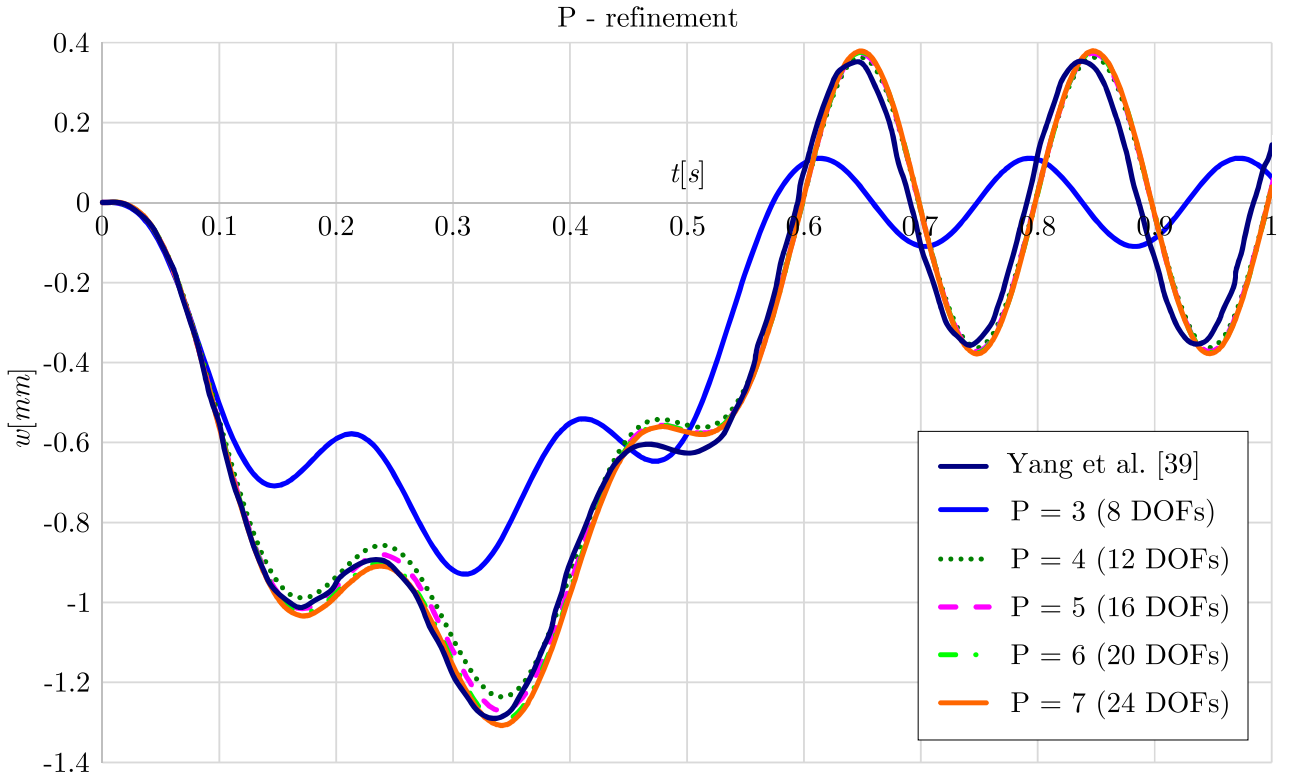


Figure 8.10: Out-of-plane displacement (w) of the beam's midpoint obtained using the P - refinement procedure

As can be noticed, the converged results for both displacements have been achieved with the 6th - order NURBS basis function model (20 DOFs). The converged results are in good agreement with the results from the literature. However, the displacements obtained using the presented isogeometric method are slightly greater than the displacements from the literature, which indicates that the isogeometric model is more flexible than the literature model. This observation is contradictory with respect to the applied beam theories in the presented isogeometric approach and in the literature. Therefore, additional free vibration analysis has been carried out using the FE commercial software Abaqus. The natural frequencies for two directions calculated using the presented approach, Abaqus and the results from the literature are presented in Table 8.6. The natural frequencies obtained from FE commercial software Abaqus are calculated using the B33 beam element based on the Bernoulli-Euler beam theory and the B31 beam element based on the Timoshenko beam theory.

Table 8.6: In-plane (Ω_u) and out-of-plane (Ω_w) natural frequencies [rad/s] obtained using isogeometric approach, FEM software Abaqus and the results from the literature

	IGA	Abaqus (B33)	Abaqus (B31)	Yang et al. [39]
Ω_u	31.15	31.31	31.05	32.1
Ω_w	112.21	115.18	110.29	115.4

As can be observed from the previous table, the beam's natural frequencies obtained using the isogeometric approach and the FE software package Abaqus (B33 and B31) are slightly lower than the literature results. Aforementioned also indicates that the literature model is stiffer than the isogeometric model. The reason for this can be found in reference [39]. The displacements are represented as the sum of a series of sine functions, and only the first mode is taken into consideration, which can lead to the stiffer beam formulation [39].

In addition, the H - refinement procedure is applied in the convergence study by knot insertion, while conserving C^2 continuity. Figure 8.11 and Figure 8.12 show the beam's midpoint in-plane (u) and out-of-plane (w) displacements, respectively. As can be noticed, the results have converged for the case of model 4 with 20 DOFs.

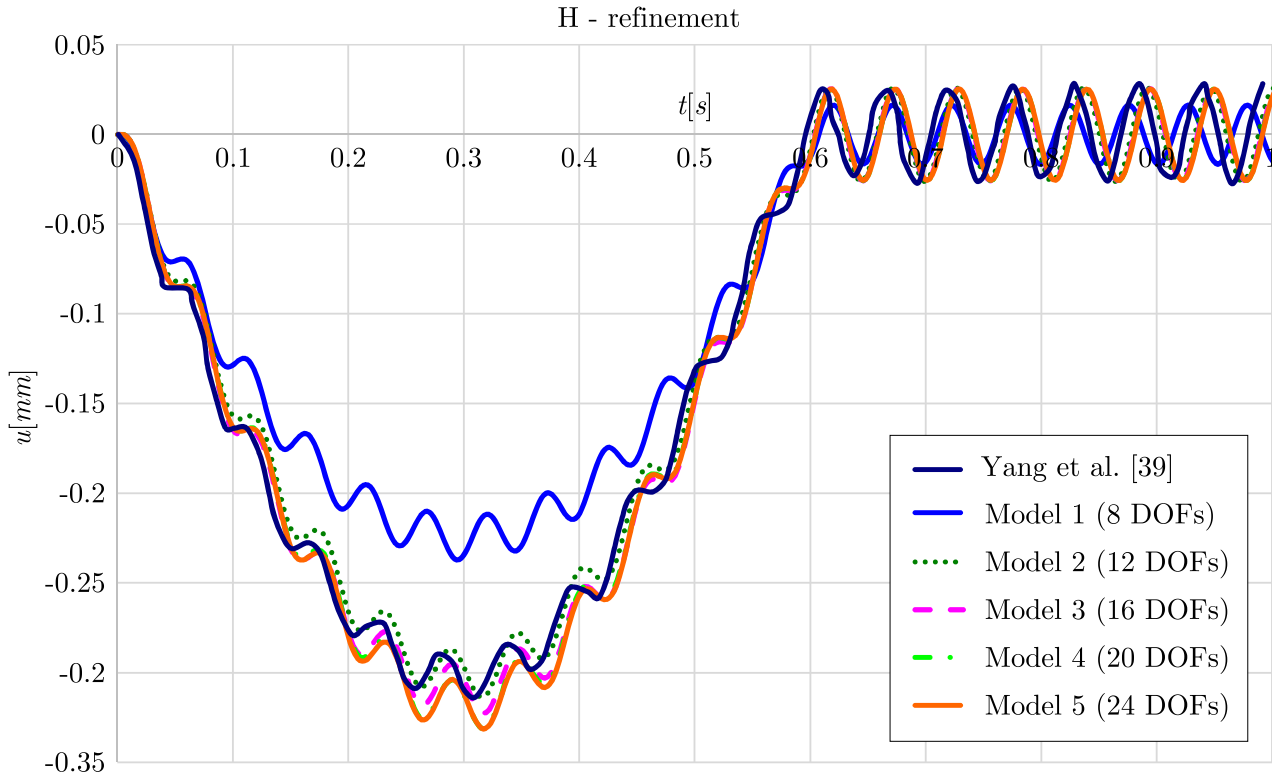


Figure 8.11: In-plane displacement (u) of the beam's midpoint obtained using the H - refinement procedure

At the end of the convergence study, K - refinement procedure is applied. Displacements of the beam's midpoint are obtained using isogeometric models applying different degree and continuity of NURBS basis functions, Figure 8.13 and Figure 8.14. As can be noticed, in the case of K - refinement procedure, the number of DOFs is not directly related to the accuracy of the results, which is shown for the case of the 3rd - order NURBS basis functions and C^1 continuity with 16 DOFs.

8.2.1.2 Parametric study

The effect of the moving load magnitude and velocity are investigated for the simply supported spatial curved beam. The geometry of the beam is defined using four control points with unit weight vector and 3rd - order B-spline basis functions, Figure 8.15. The beam material is defined with the Young's modulus $E = 210GPa$, the Poisson's ratio $\nu = 0.2$ and the mass density $\rho = 7850kg/m^3$, while the beam cross-section is rectangular with the dimensions $b/h = 0.1/0.1m$. The moving mass m is modeled as a gravitational force with constant magnitude $F = -m \cdot g$ and direction, forming the moving load model. The load is moving along the beam with a constant velocity V . In order to investigate the influence of the moving load magnitude and velocity on the response of the curved beam, the displacements of the beam at the load position are analyzed. The calculations have been conducted using the isogeometric beam model with 7th - order B-spline basis functions (24 DOFs) obtained using the P - refinement procedure.

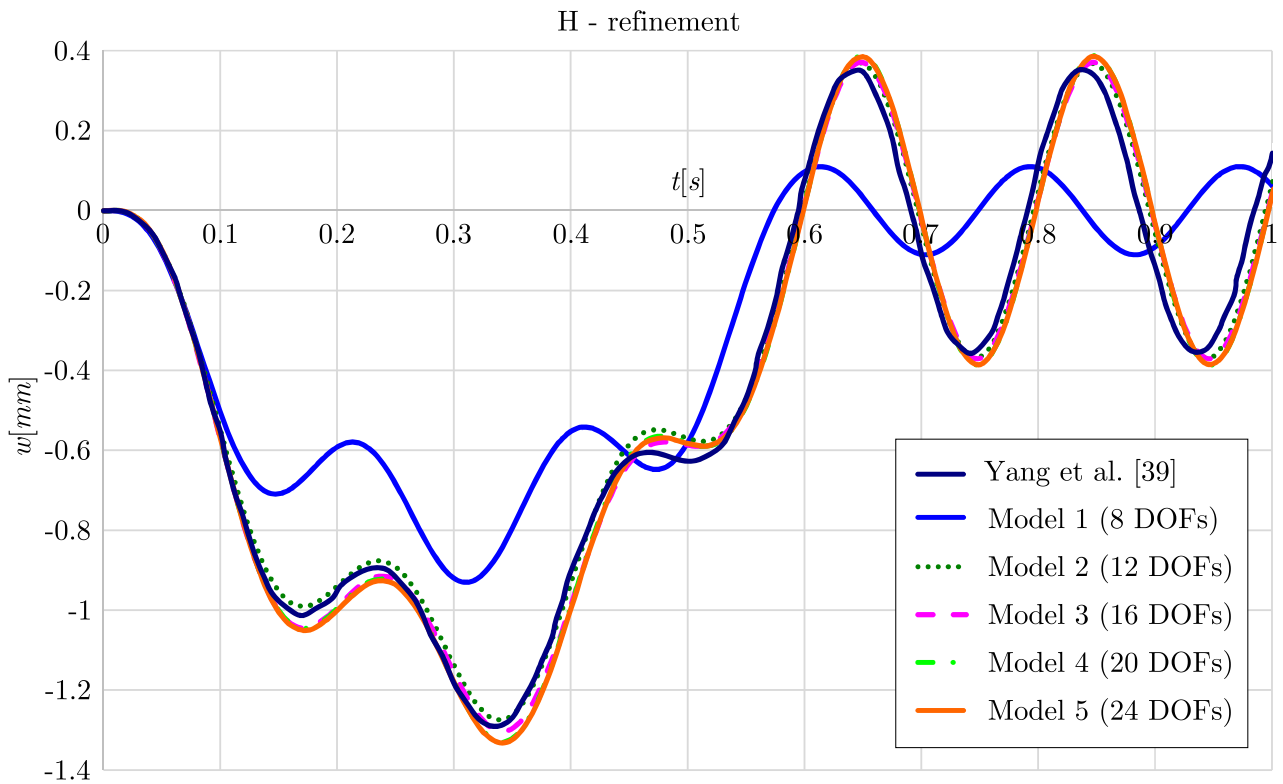


Figure 8.12: Out-of-plane displacement (w) of the beam's midpoint obtained using the H - refinement procedure

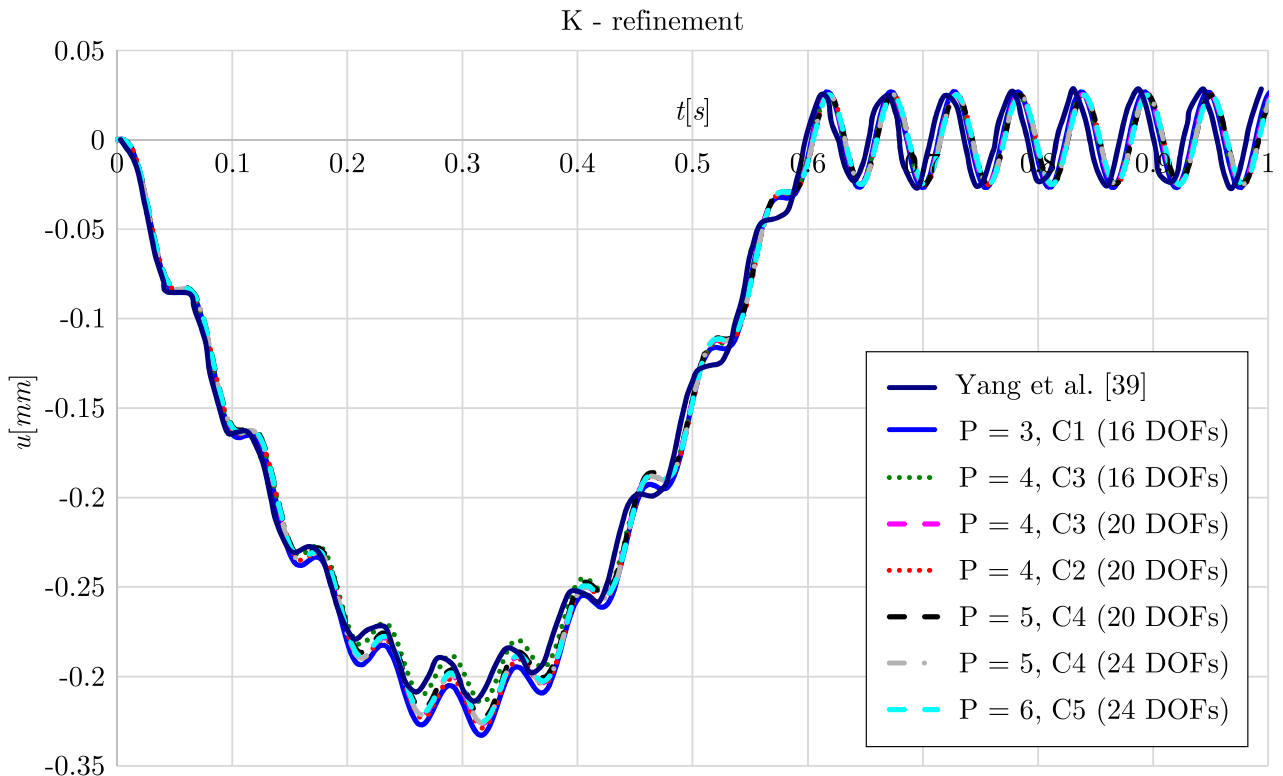


Figure 8.13: In-plane displacement (u) of the beam's midpoint obtained using the K - refinement procedure

First, the effect of the moving load magnitude on the spatial beam response is investigated. Three cases of moving load magnitude are analyzed, $F = 1kN$, $F = 50kN$, $F = 100kN$ with constant velocity of $V = 40m/s$. In order to compare the results, the displacements of the

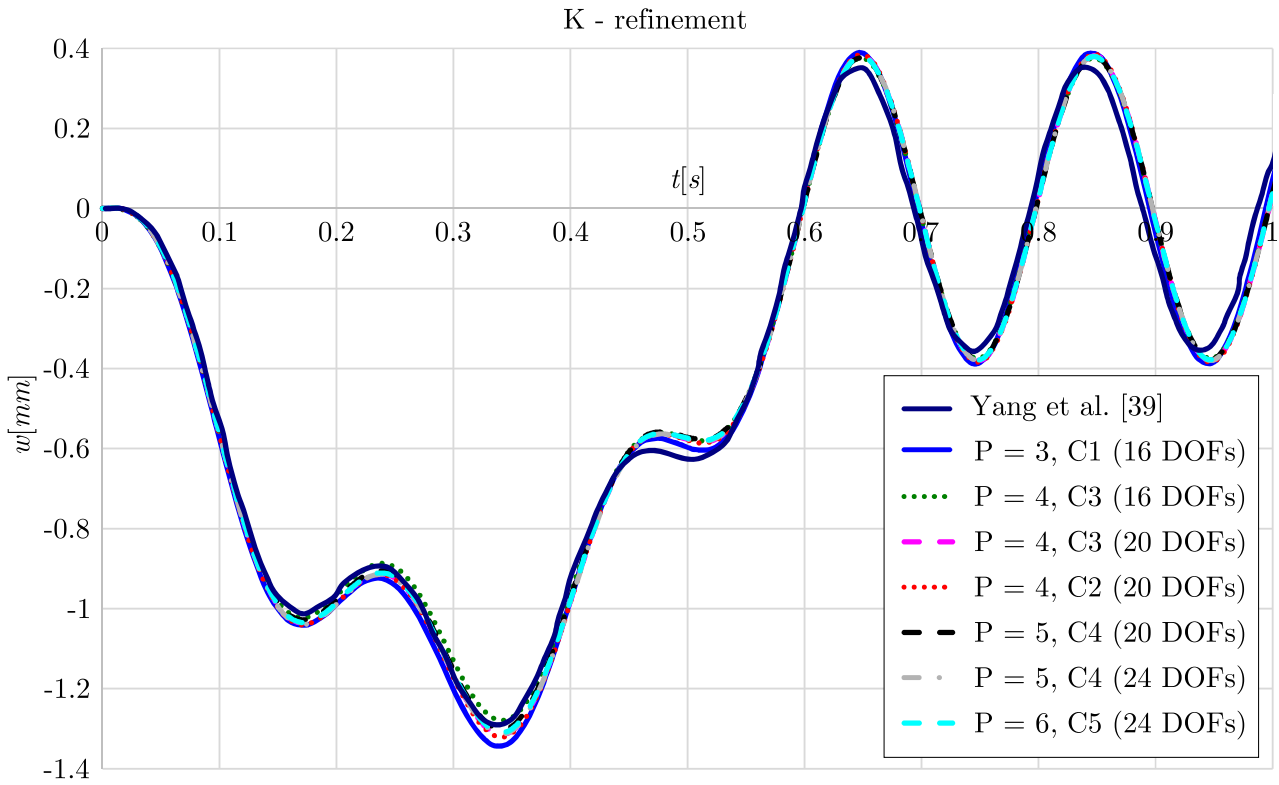


Figure 8.14: Out-of-plane displacement (w) of the beam’s midpoint obtained using the K - refinement procedure

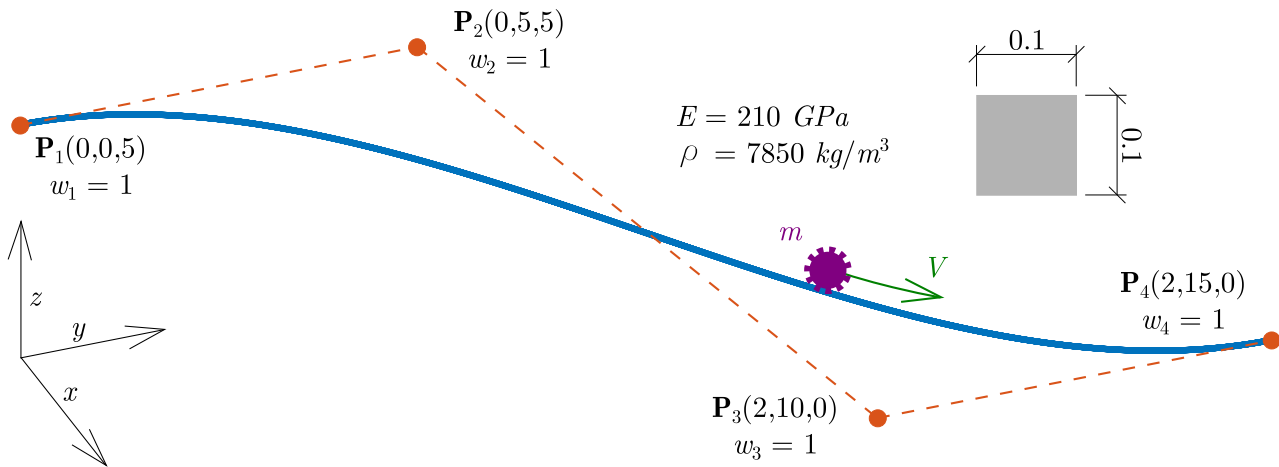


Figure 8.15: Simply supported curved spatial beam subjected to moving mass

beam at the moving load position have been divided by the moving load magnitude, forming normalized displacements. The normalized components of the beam displacement in Cartesian coordinates denoted as u , v and w are presented in Figures 8.16 - 8.18, respectively. As can be seen, the normalized displacement components are equal for all calculated moving load magnitude cases. As expected, the linear relation between the load magnitude and beam response holds for the linear dynamic formulation of the curved spatial beam subjected to the moving load.

Next, the effect of the moving load velocity on the beam response is investigated. In order to compare the displacement components of the beam at the position of the moving load, moving load traveling time has been divided by the total traveling time, forming normalized dimensionless time coordinate. Components of the beam displacements at the moving load

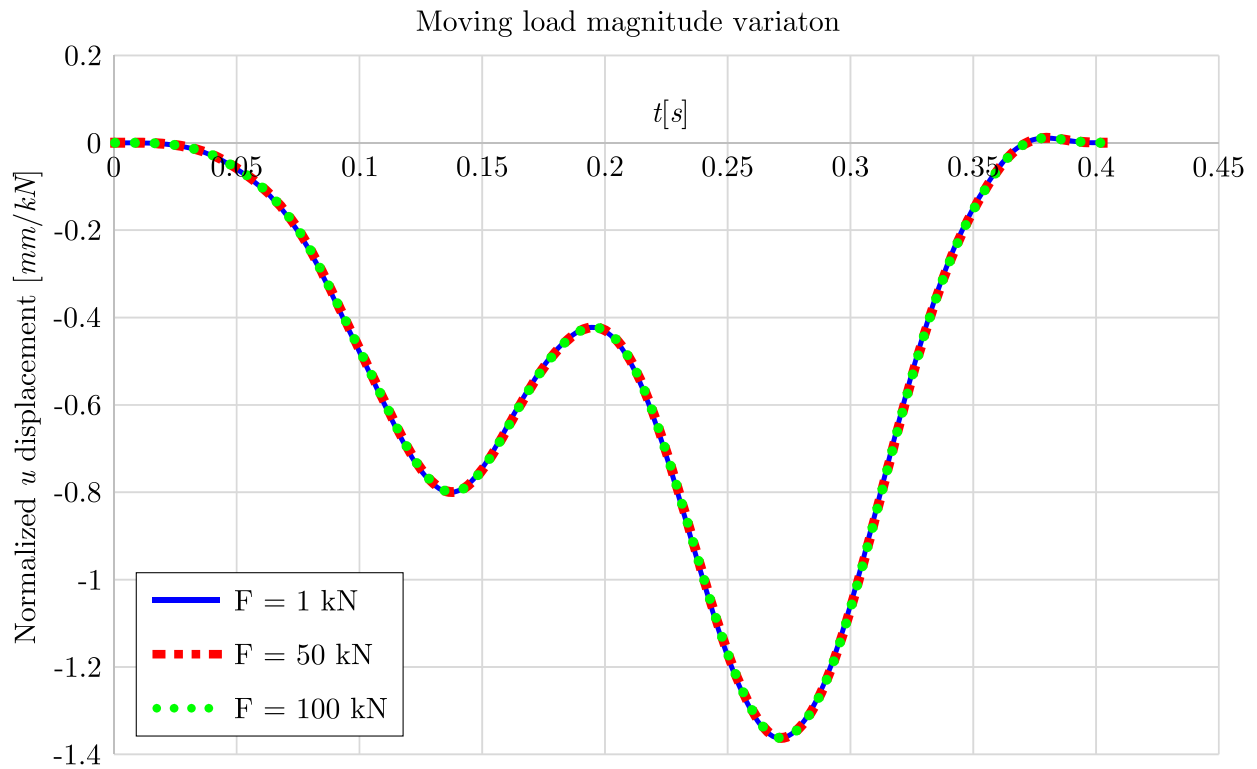


Figure 8.16: Normalized u displacement with respect to the moving load magnitude variation

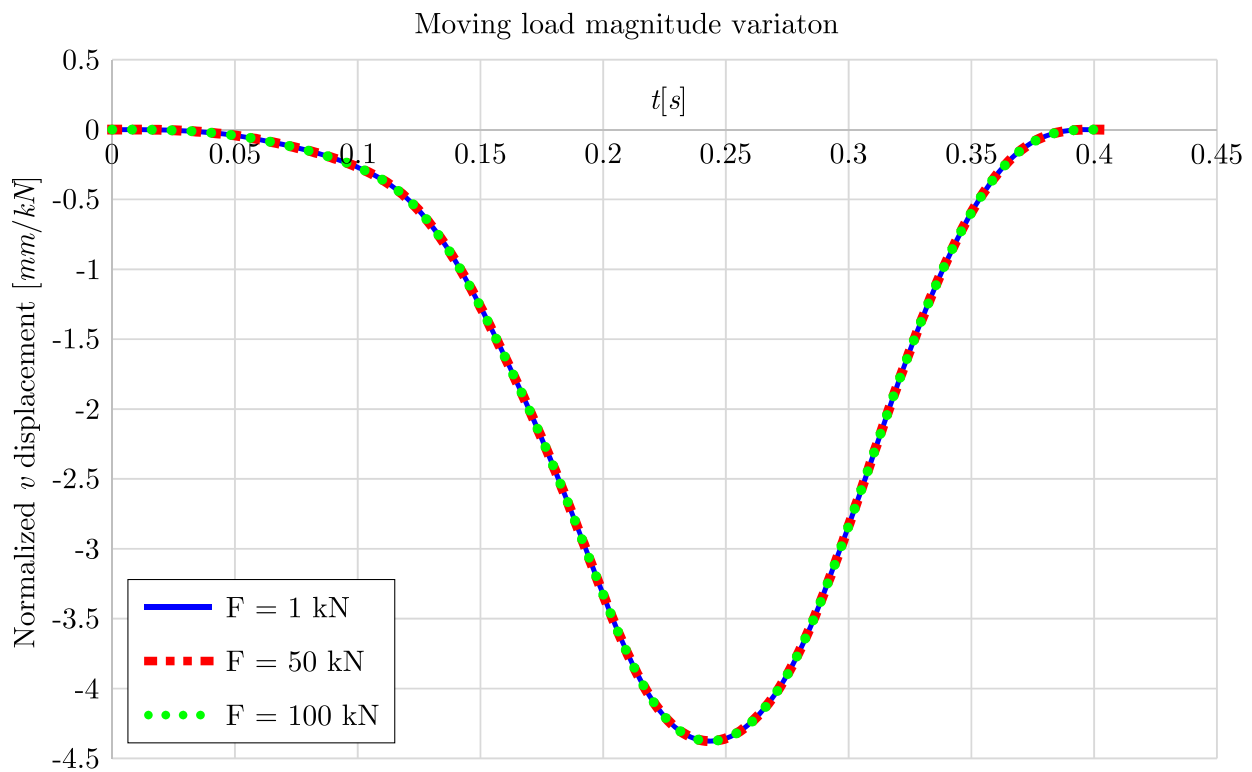


Figure 8.17: Normalized v displacement with respect to the moving load magnitude variation

position have been presented in Figures 8.19 - 8.21. Maximum displacement for u component of the beam displacement appears for moving load velocity of $V = 50m/s$, while maximum displacement of other two displacement components v and w occur for velocity of $V = 20m/s$. Beside the magnitude, moving load velocity can affect the sign of the displacement component,

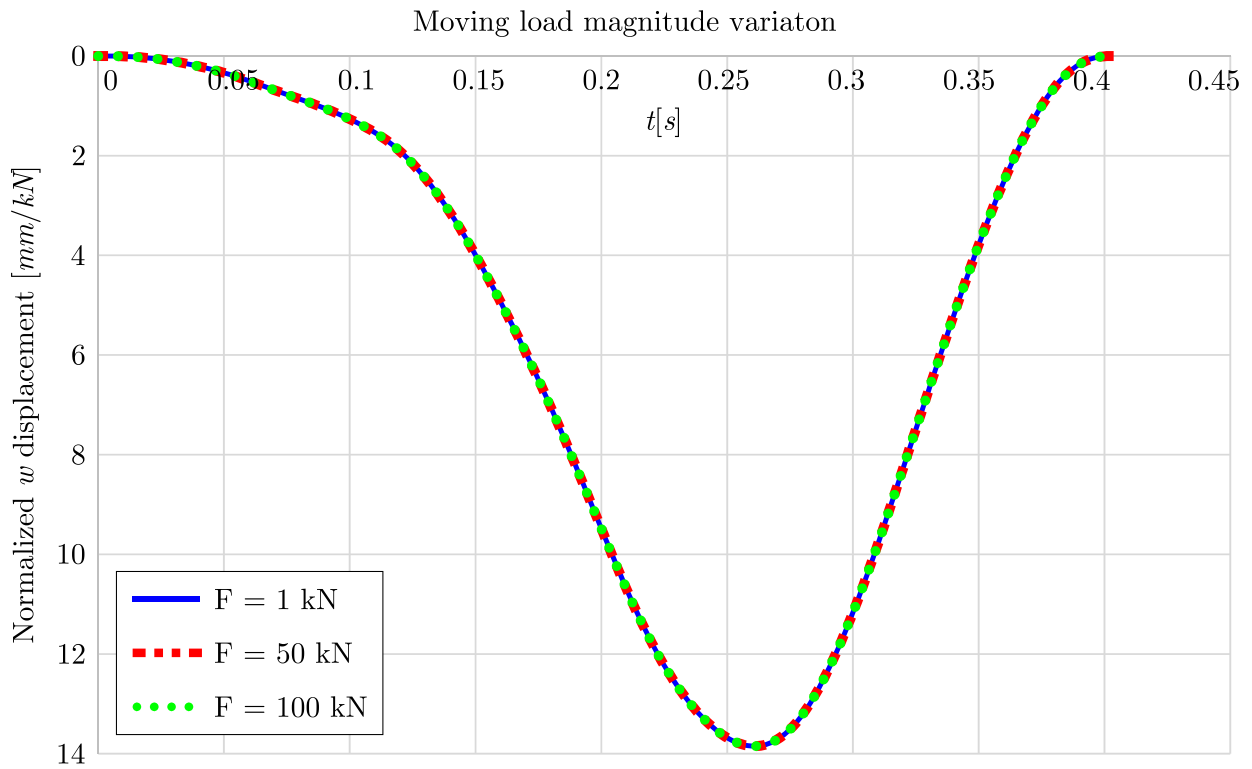


Figure 8.18: Normalized w displacement with respect to the moving load magnitude variation

which can be observed for the displacement component u for the velocity of approximately $V = 70\text{m/s}$.

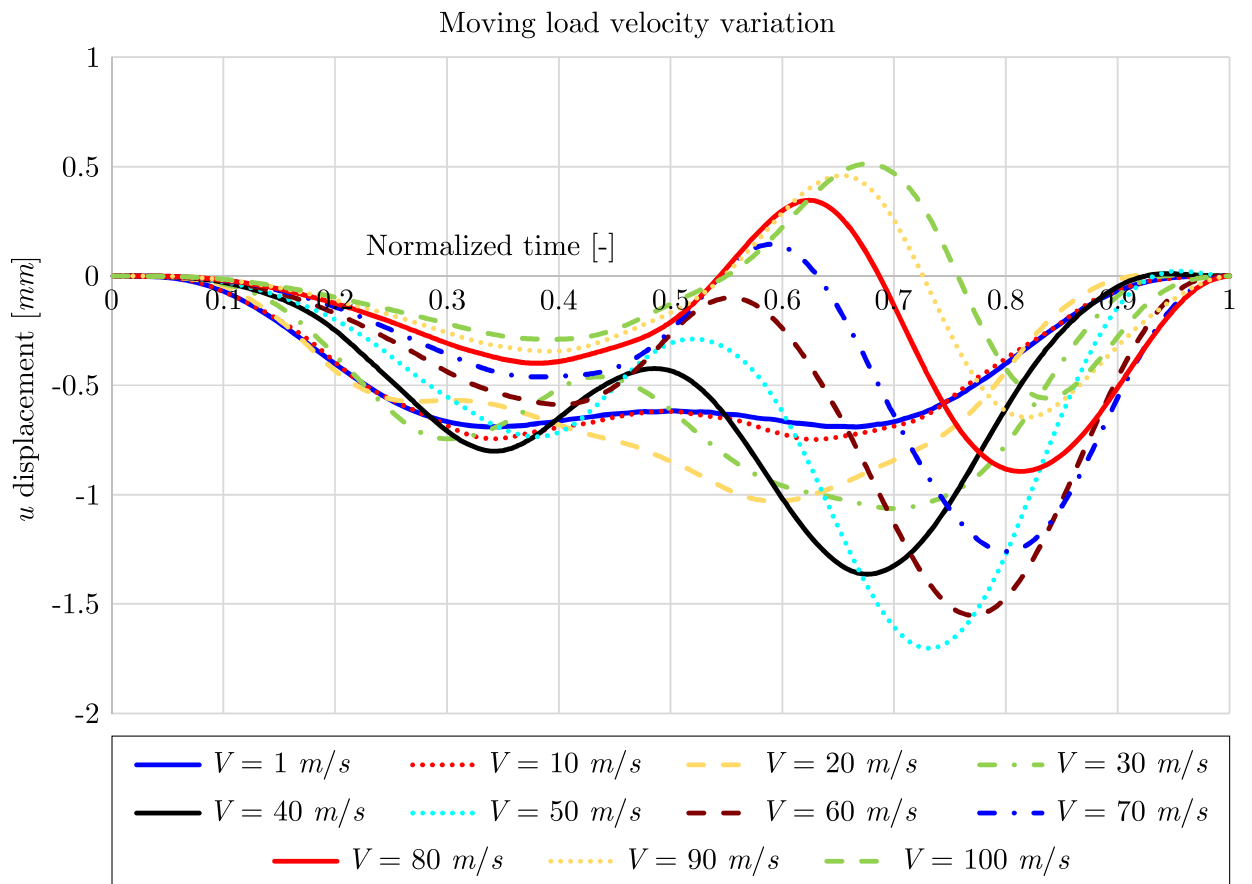


Figure 8.19: u displacement with respect to the moving load velocity

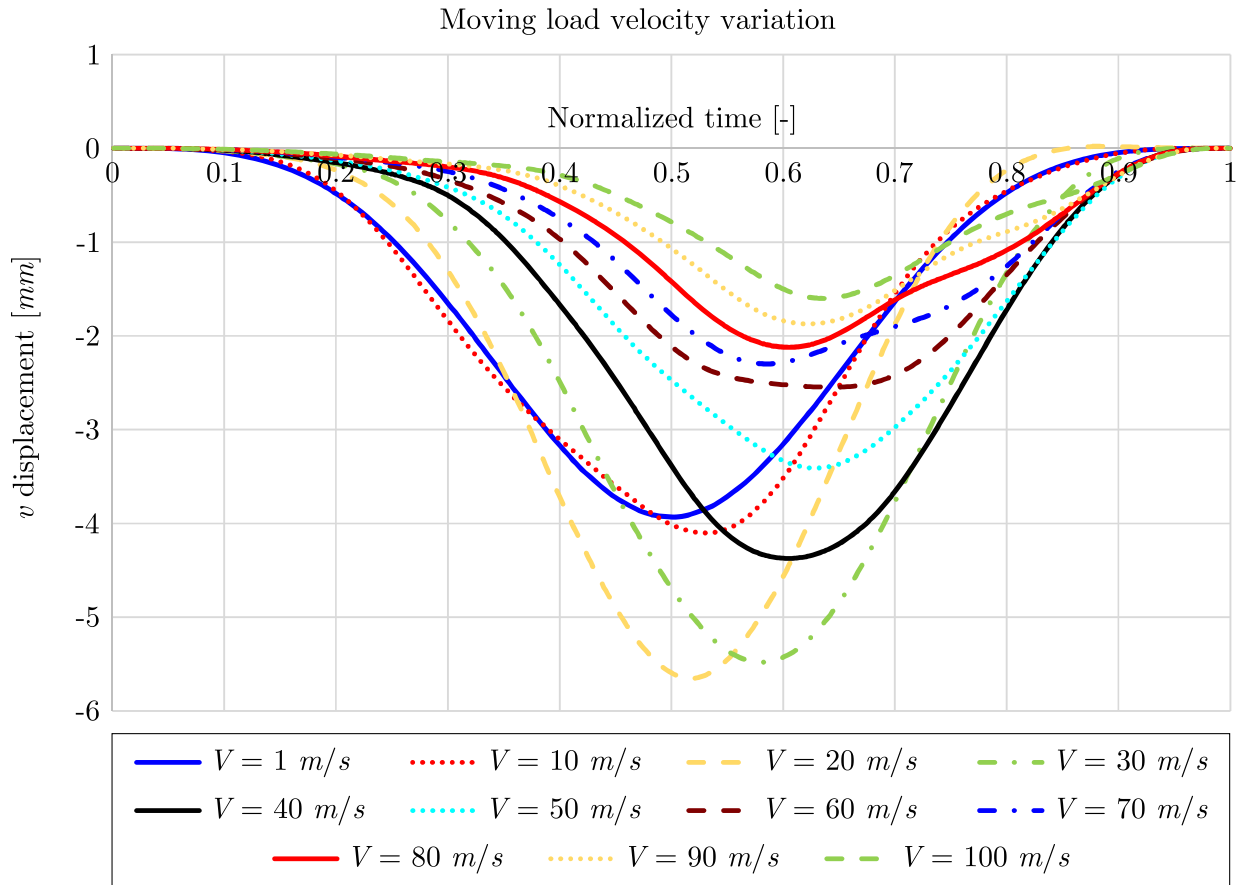


Figure 8.20: v displacement with respect to the moving load velocity

8.2.2 Moving mass problem

8.2.2.1 Validation and convergence study

In Section 8.2.1.1, validation and convergence study of the moving load model has been presented for the load with constant magnitude. This load has been generated by the mass m moving with constant velocity $V = 40 \text{ m/s}$ along the curved beam with constant curvature. Therefore, the same example has been chosen to validate the moving mass model of the curved spatial beam formulated using the isogeometric approach. During the validation and convergence study of the moving mass model, the results of the beam's midpoint displacement obtained using the moving mass model are identical to the result obtained using the moving load model. This is demonstrated in Figure 8.22 for the case of the beam model with 24 DOFs obtained using the P - refinement procedure with 7th - order NURBS basis functions. Consequently, the moving mass model provides accurate results with satisfactory convergence property, indicated by the identical results between the moving load and the moving mass model. The identical results are obtained due to the beam's constant curvature, which generates the force with constant magnitude. In the next section, the beam with variable curvature will be analyzed, and the differences between the results obtained using the moving load and the moving mass model will be presented.

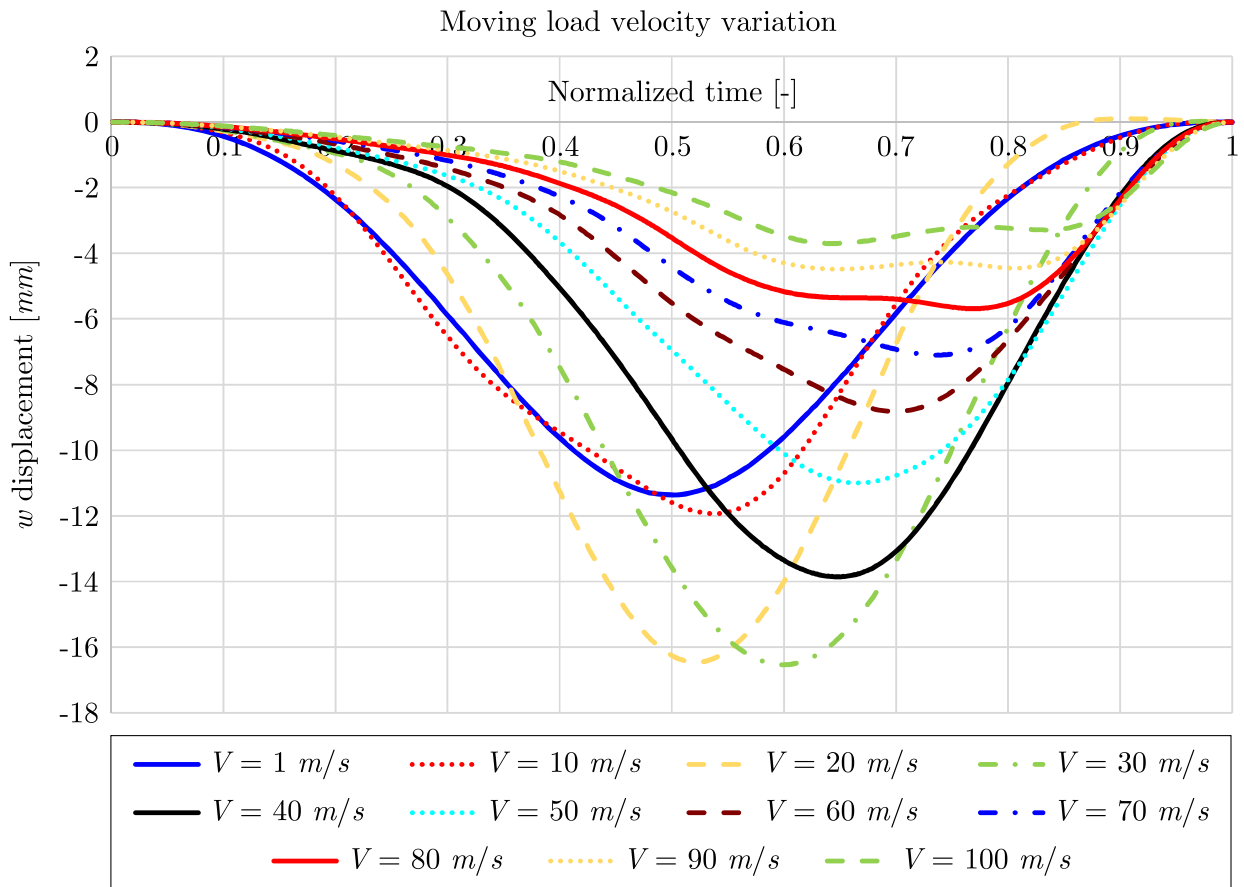


Figure 8.21: w displacement with respect to the moving load velocity

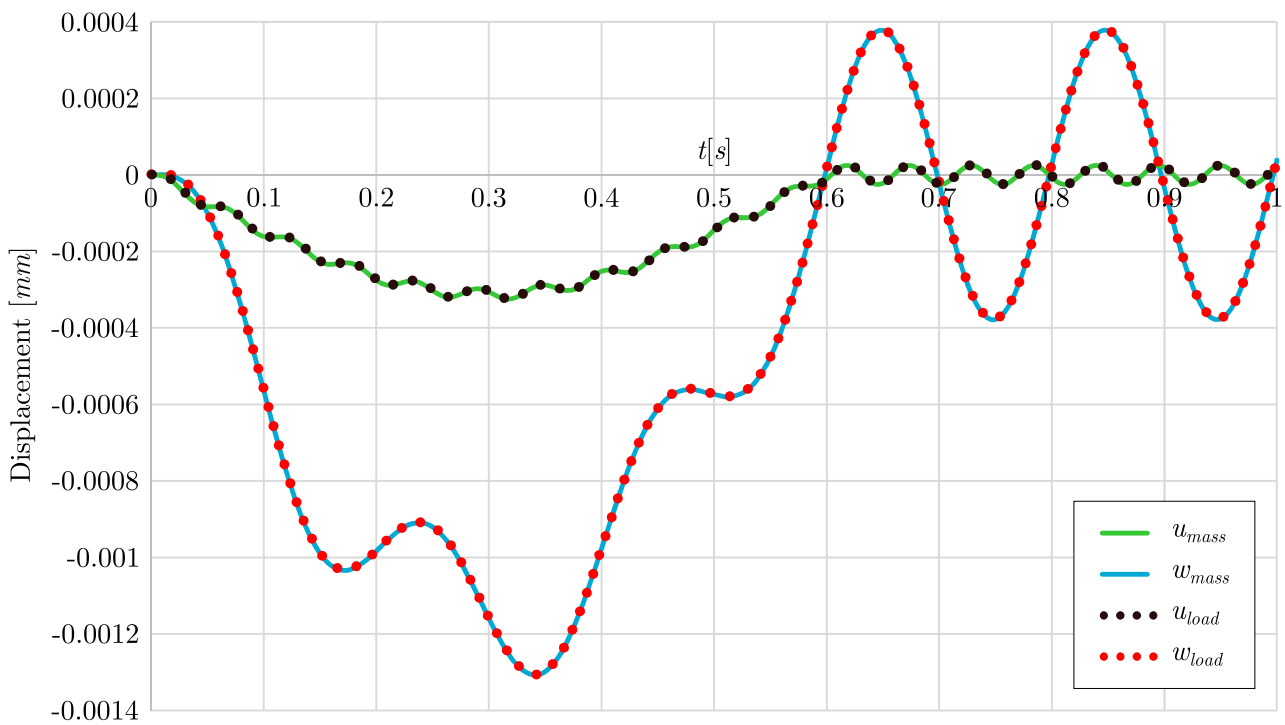


Figure 8.22: In-plane (u) and out-of-plane (w) beam's midpoint displacement obtained using moving mass model ($mass$) and moving load model ($load$)

8.2.2.2 Parametric study

To investigate the influence of the moving mass magnitude and velocity on the response of the curved spatial beam, beam described in Section 8.2.1.2 is analyzed. As demonstrated in theoretical considerations, mass moving along the beam generates the inertial force, which will be included in the dynamic response analysis in line with the gravitational force.

Beam displacement at the position of the moving mass is observed for the three cases of mass magnitudes: $m = 0.01t$, $m = 1t$ and $m = 100t$. In Figures 8.23 - 8.25 Cartesian components of the normalized displacement are presented. As can be noticed from the presented figures, mass magnitude does not influence the normalized displacement. Consequently, linear relation holds for the case of moving mass model of the curved spatial beam in the linear dynamic formulation.

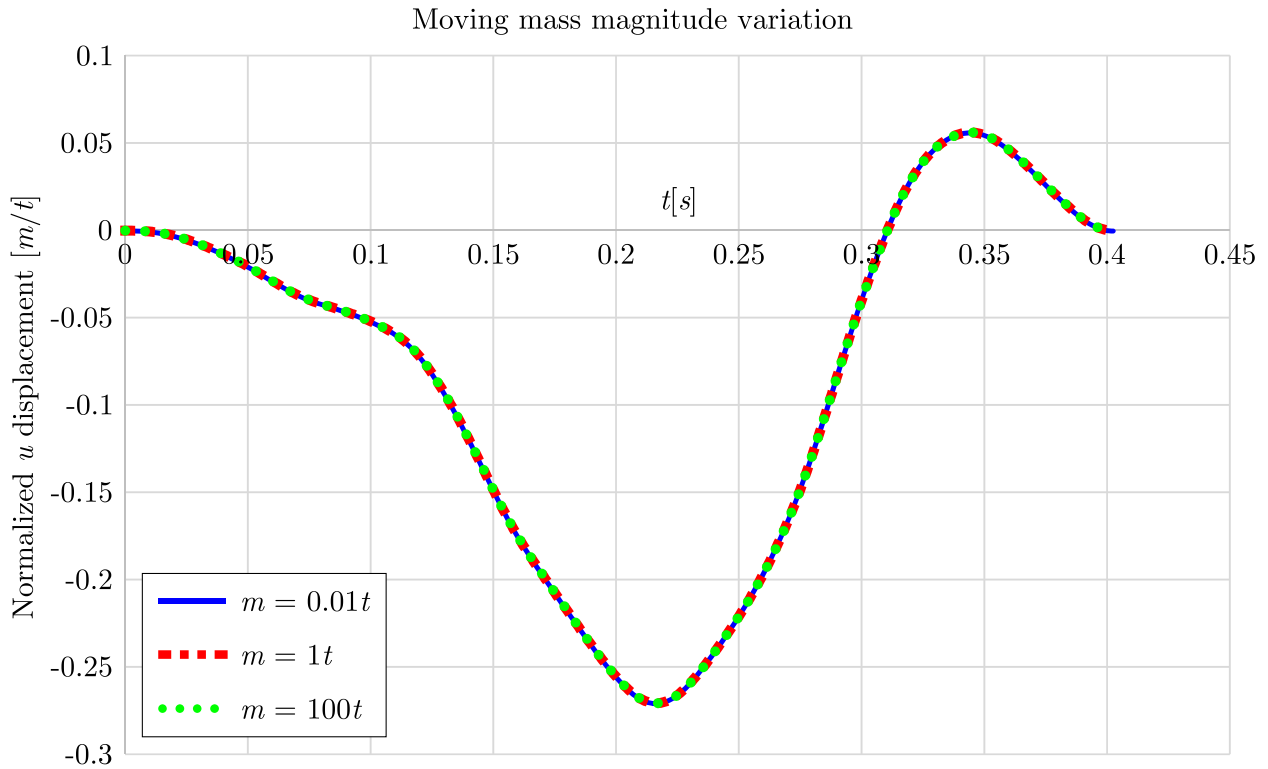
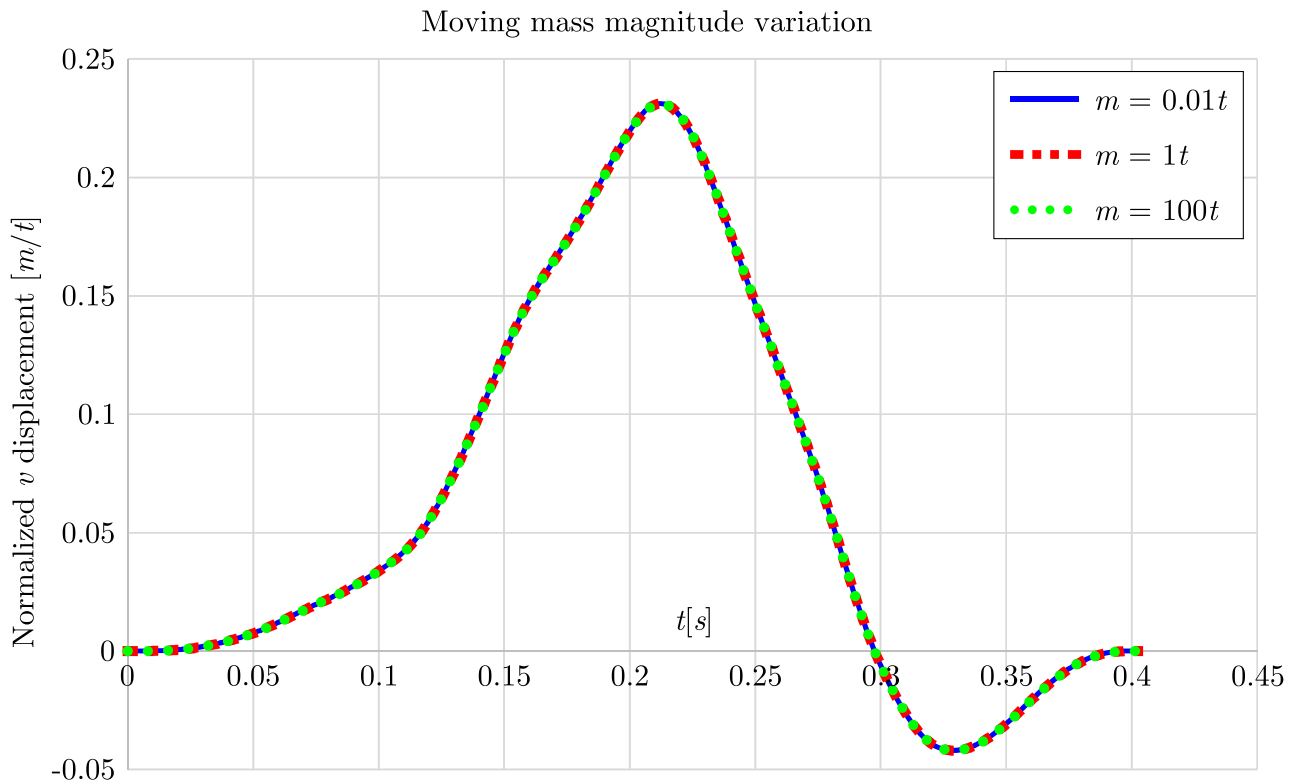
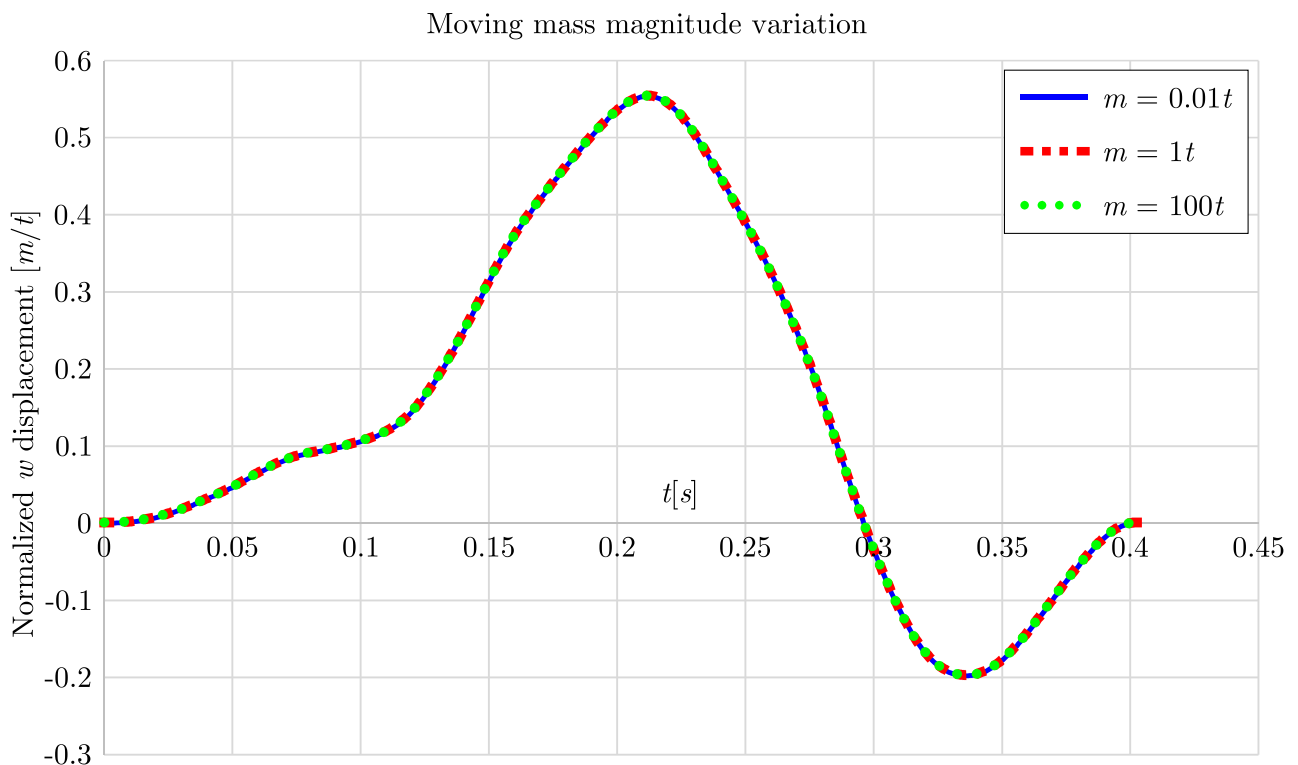


Figure 8.23: Normalized u displacement with respect to the moving mass magnitude variation

In addition, the influence of the moving mass velocity on the response of the curved spatial beam is analyzed. In Figures 8.26 - 8.28 beam displacement components at the moving mass position are presented. As can be observed from the figures, the maximum displacement of the curved spatial beam at the position of the moving mass increases as the moving mass velocity increases. It is also important to note that the sign of the displacement components changes with respect to the moving mass velocity, which can be observed for all displacement components. Therefore, the moving mass velocity has a significant impact on the response of the curved spatial beam. As can be observed from the figures, the higher mass velocities have shown to produce large beam displacements, hence the linear analysis is no longer applicable.

Finally, the beam displacement components obtained using the moving load and the moving mass model are compared. In Figures 8.29 - 8.32 displacement components of the beam at the position of the moving mass are given for the following moving mass velocities: $V = 1m/s$, $V = 10m/s$, $V = 30m/s$ and $V = 50m/s$. In case of the moving mass velocity of $V = 1m/s$, the inertial load of the moving mass model are negligible. Consequently, the displacement

Figure 8.24: Normalized v displacement with respect to the moving mass magnitude variationFigure 8.25: Normalized w displacement with respect to the moving mass magnitude variation

components obtained using the moving load and the moving mass model are the same. The displacement obtained using moving load and moving mass formulations diverges as a moving mass velocity increases, due to the increased inertial load in the moving mass model.

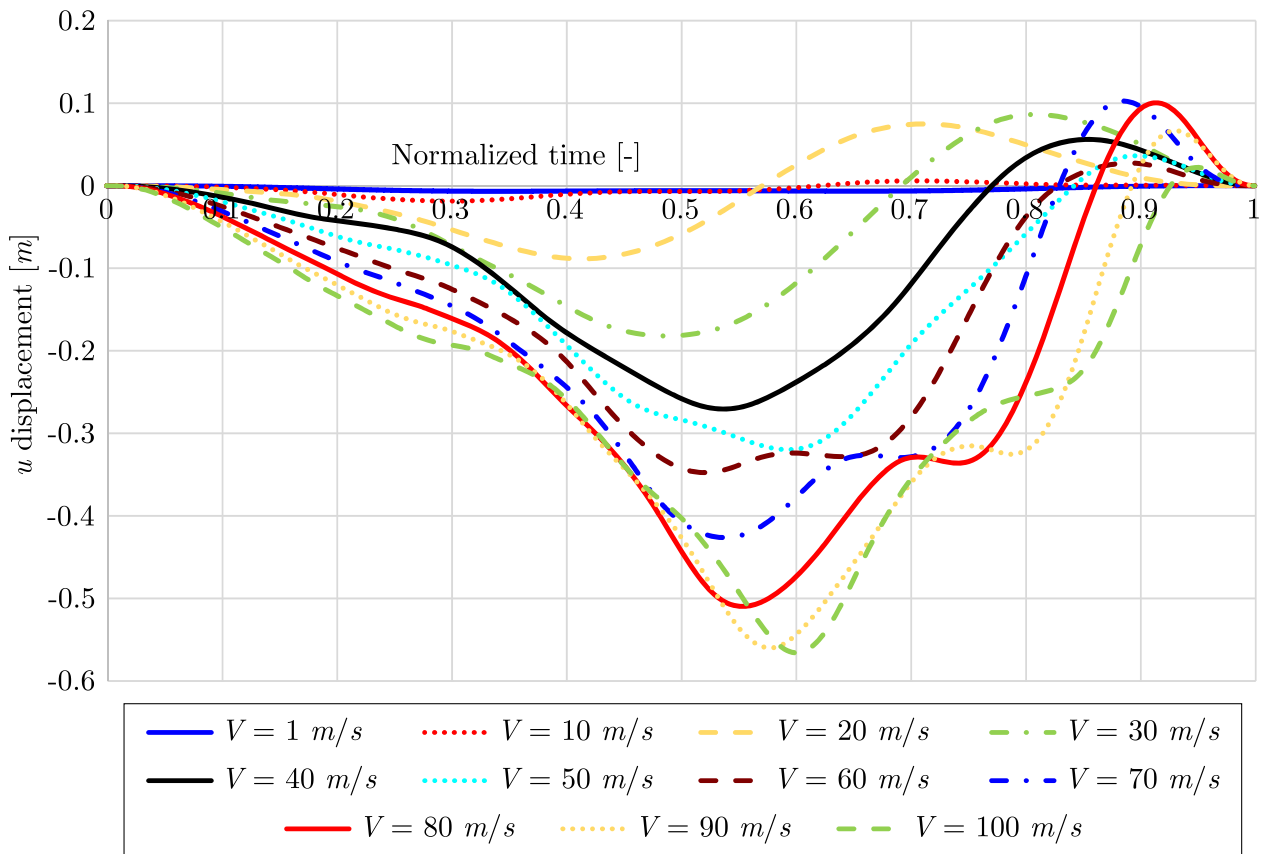


Figure 8.26: u displacement with respect to the moving mass velocity

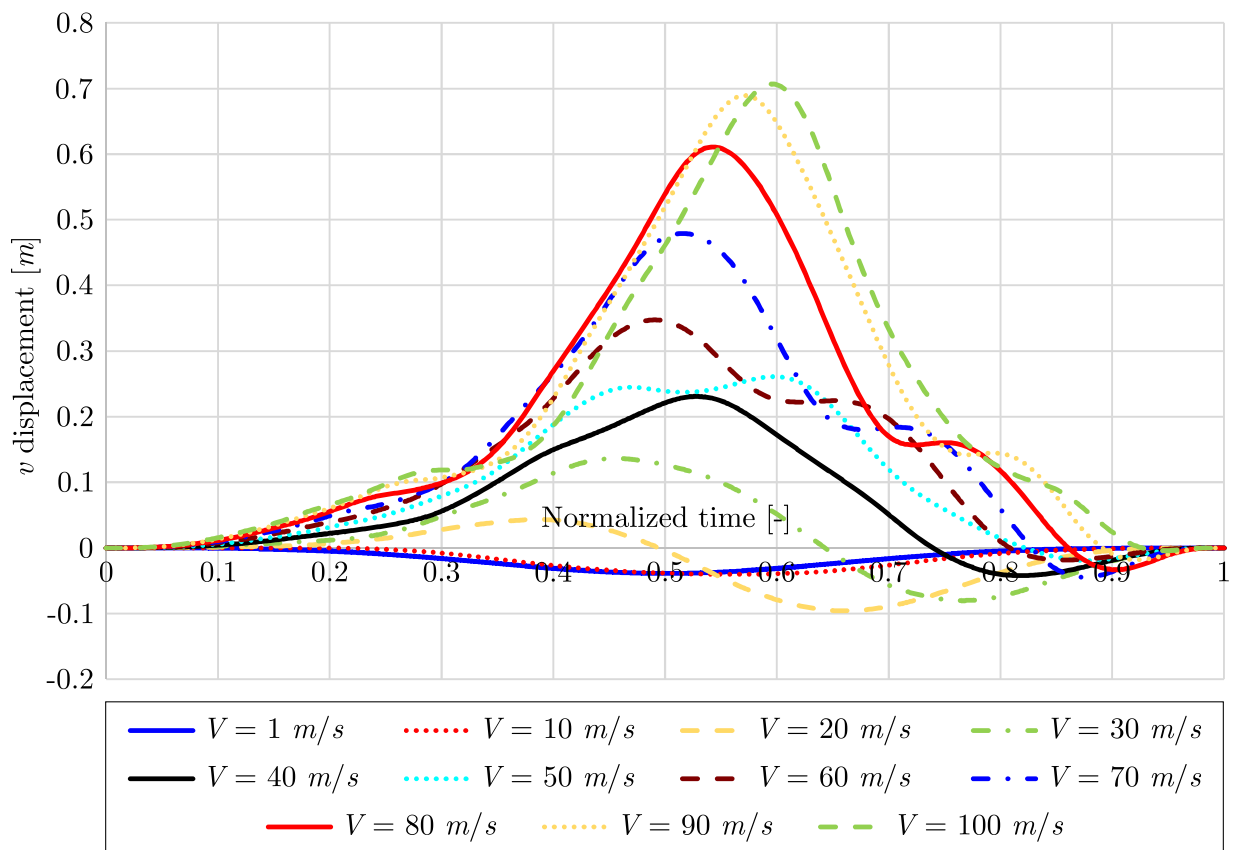


Figure 8.27: v displacement with respect to the moving mass velocity

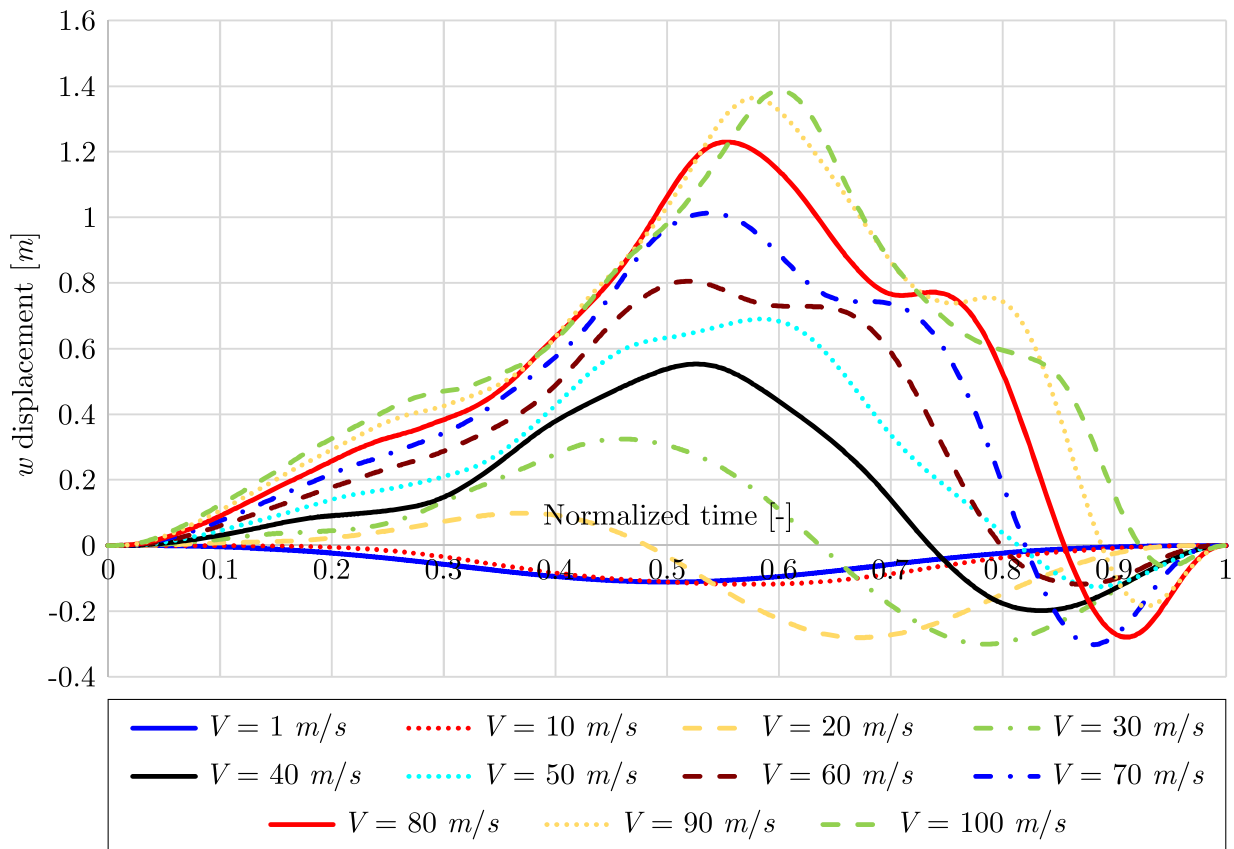


Figure 8.28: w displacement with respect to the moving mass velocity

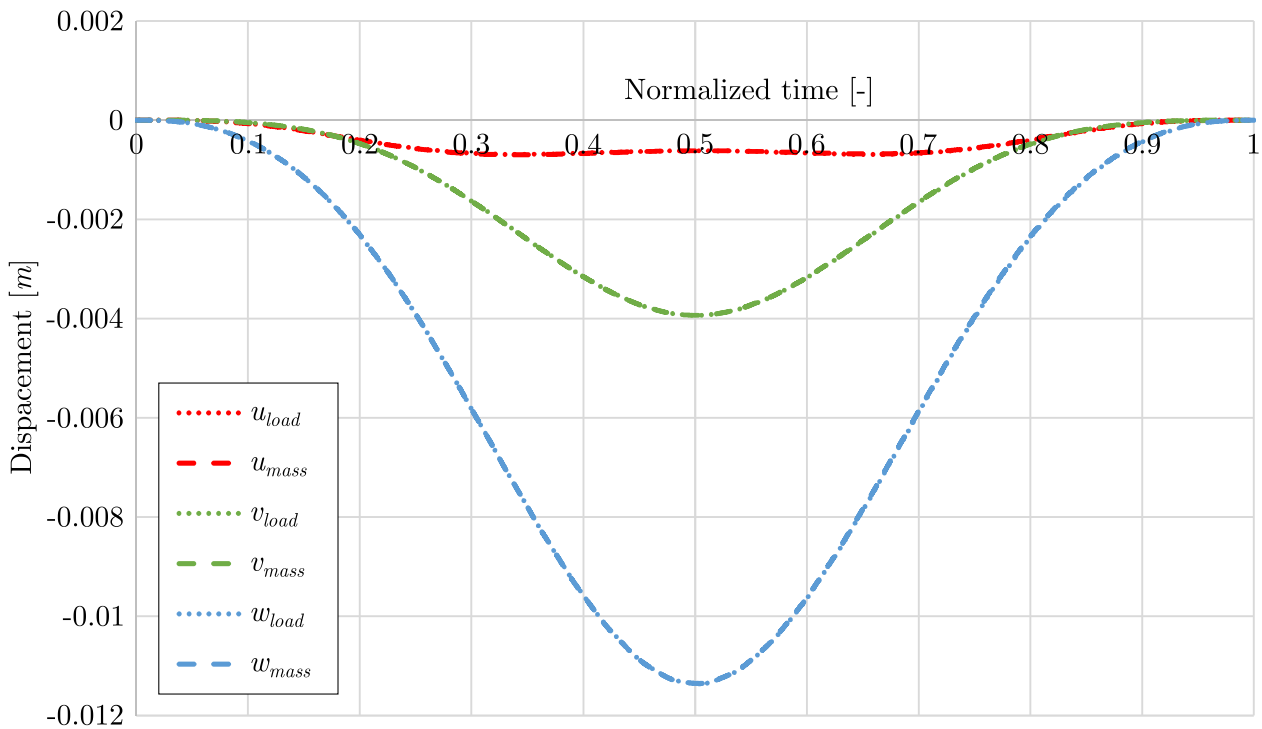


Figure 8.29: Displacements of the beam at the position of the moving mass of velocity $V = 1$ m/s obtained from moving load and moving mass model

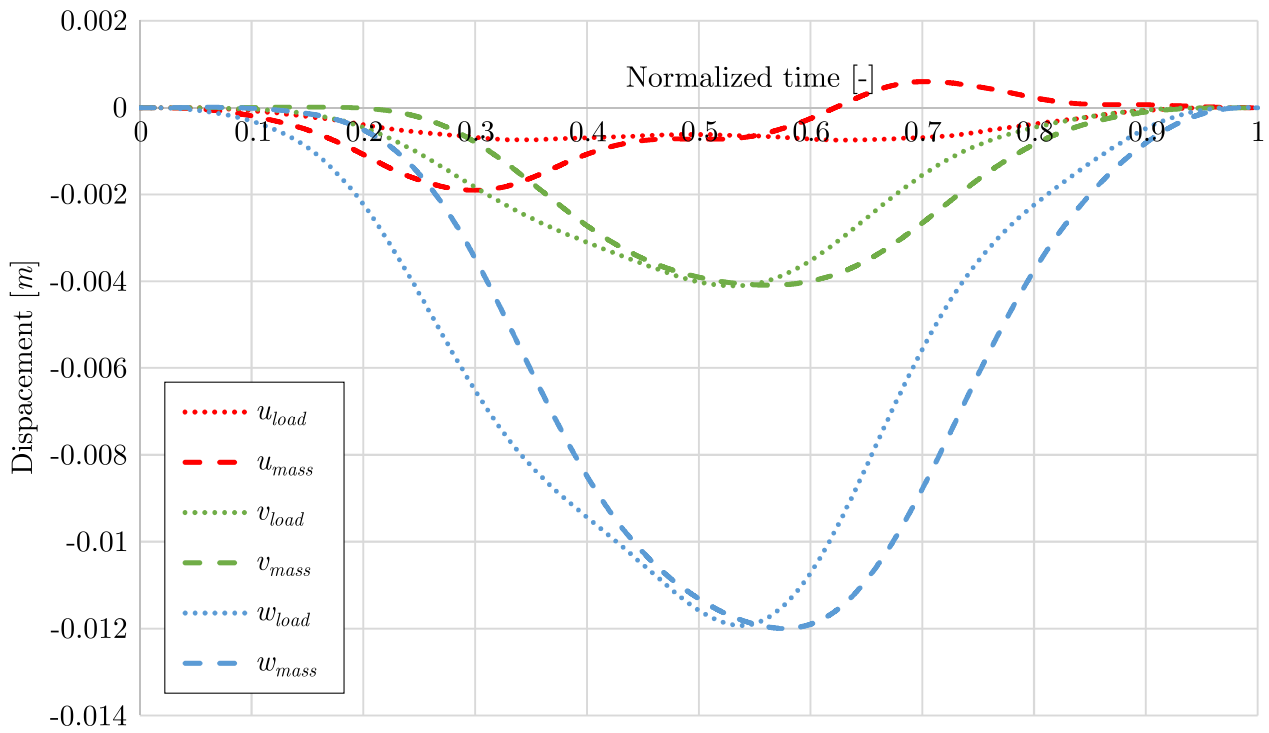


Figure 8.30: Displacements of the beam at the position of the moving mass of velocity $V = 10$ m/s obtained from moving load and moving mass model

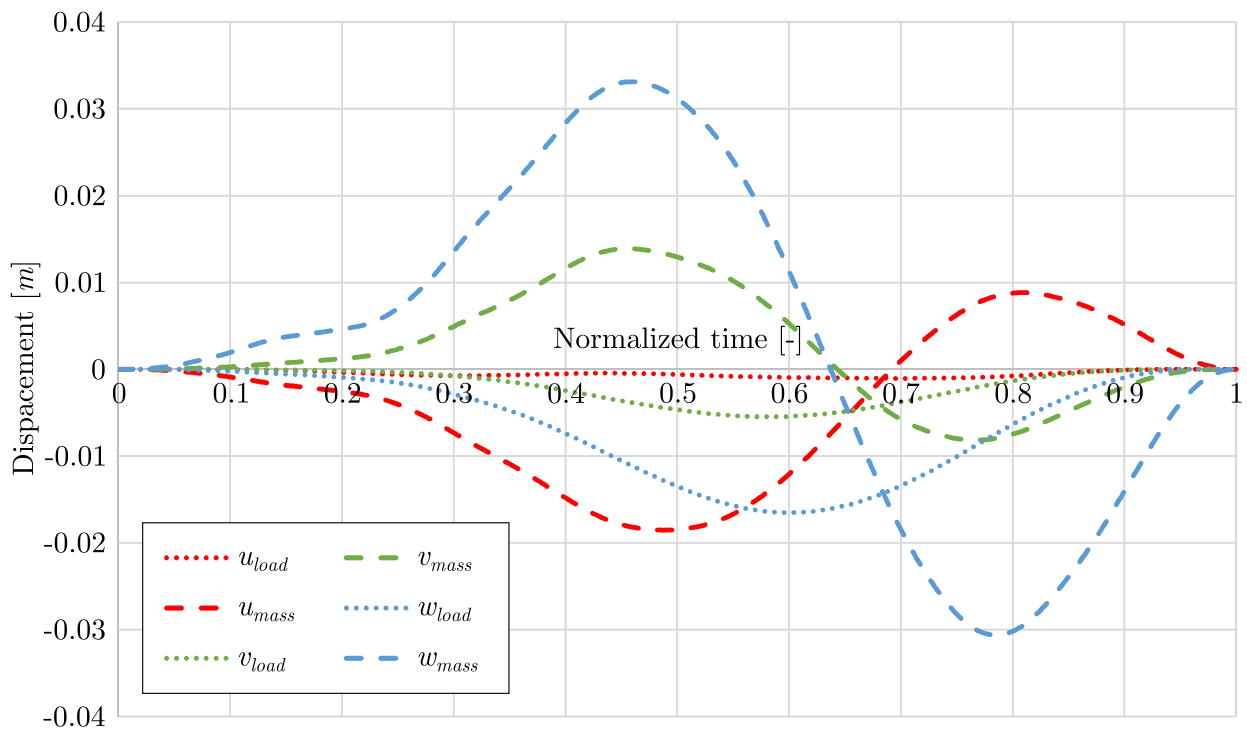


Figure 8.31: Displacements of the beam at the position of the moving mass of velocity $V = 30$ m/s obtained from moving load and moving mass model

8.3 Nonlinear dynamic analysis of curved plane beam

In this section, the property of the geometrically nonlinear dynamic formulation for a plane curved Bernoulli - Euler beam defined using isogeometric approach will be given. After analyzing

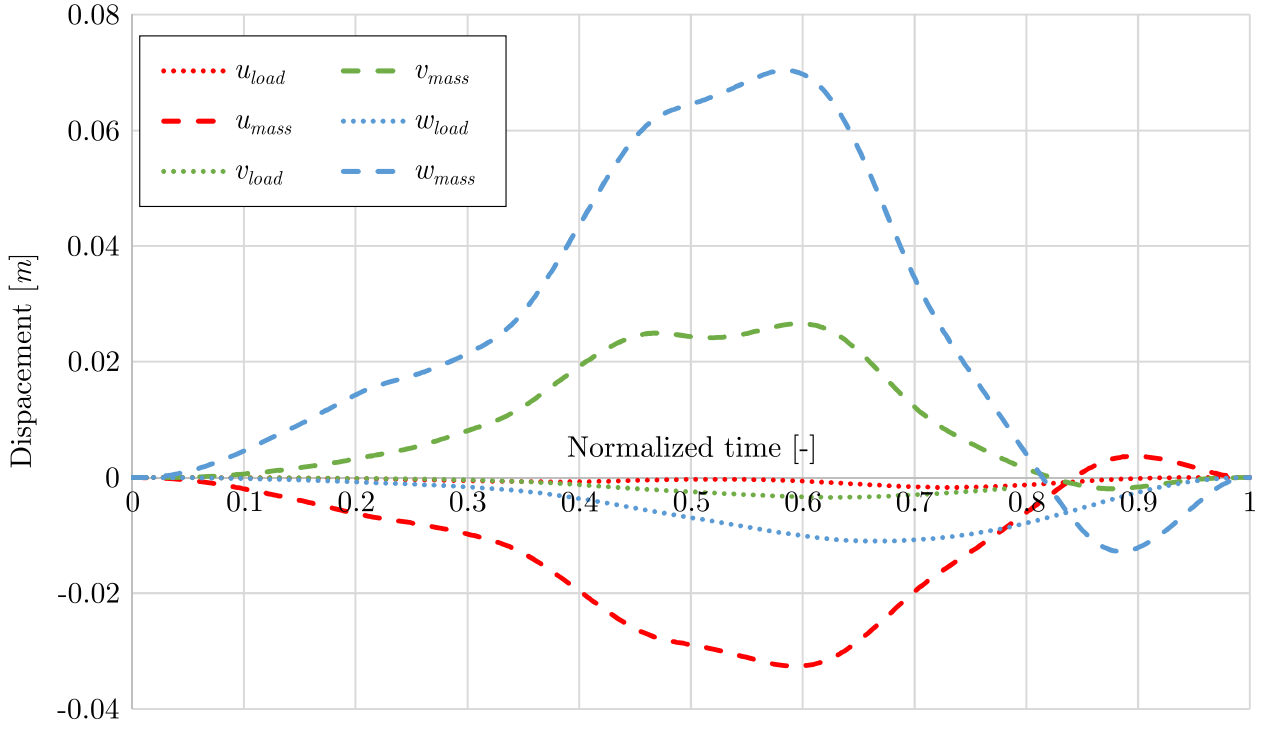


Figure 8.32: Displacements of the beam at the position of the moving mass of velocity $V = 50$ m/s obtained from moving load and moving mass model

the time-varying load, the moving load and the moving mass effects on the curved plane beam in the geometrically nonlinear formulation will be presented.

8.3.1 Harmonic load

8.3.1.1 Validation and convergence study

The numerical example has been conducted to illustrate the convergence property of the geometrically nonlinear dynamic formulation of a curved plane beam obtained using the isogeometric approach. Also, this example is used to show the accuracy of the proposed formulation.

Geometry of the cantilever beam is defined as the circular arc of radius $R = 10m$ and subtended angle of 60° , Figure 8.33, discretized using the control points:

$$\mathbf{CP}^T = \begin{bmatrix} 0 & 3.17 & 6.83 & 10 \\ 0 & 1.83 & 1.83 & 0 \end{bmatrix} \quad (8.4)$$

and corresponding 3rd - order NURBS base functions constructed over knot vector:

$$\boldsymbol{\xi}^T = [0 \ 0 \ 0 \ 0 \ 1 \ 1 \ 1 \ 1] \quad (8.5)$$

and weight vector:

$$\mathbf{w}^T = [1 \ 0.911 \ 0.911 \ 1] \quad (8.6)$$

The beam cross-section is rectangular with the dimensions $b/h = 0.1/0.1m$, while the beam material is defined using the Young's modulus $E = 210GPa$ and the mass density $\rho = 7850kg/m^3$.

Cantilever curved beam is subjected to the harmonic load at the free end:

$$F(t) = 30 * \sin(10t) \tag{8.7}$$

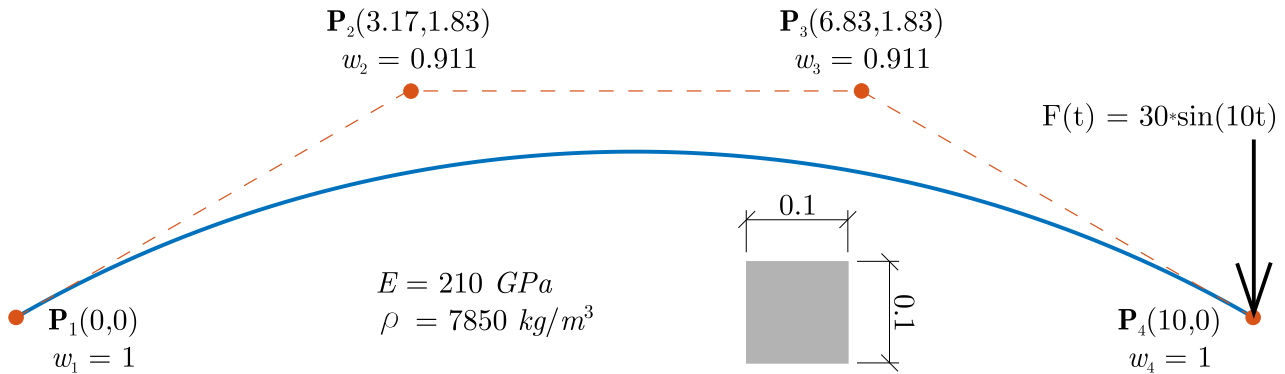


Figure 8.33: Circular arch subjected to the time varying load

Horizontal and vertical displacements of the beam free end obtained using the isogeometric approach are compared with the results from Abaqus with 630 DOFs. Beam structure is modeled in Abaqus using 209 B21 beam elements, based on the Timoshenko beam theory, which are only available for the explicit geometrically nonlinear dynamic analysis.

In Figures 8.34 and 8.35 the convergence of the beam free end obtained using the P - refinement procedure has been presented. As can be noticed, the results have converged for the model with 6th - order NURBS basis functions (11 DOFs). The converged results are in excellent agreement with the results obtained using the FE commercial software Abaqus.

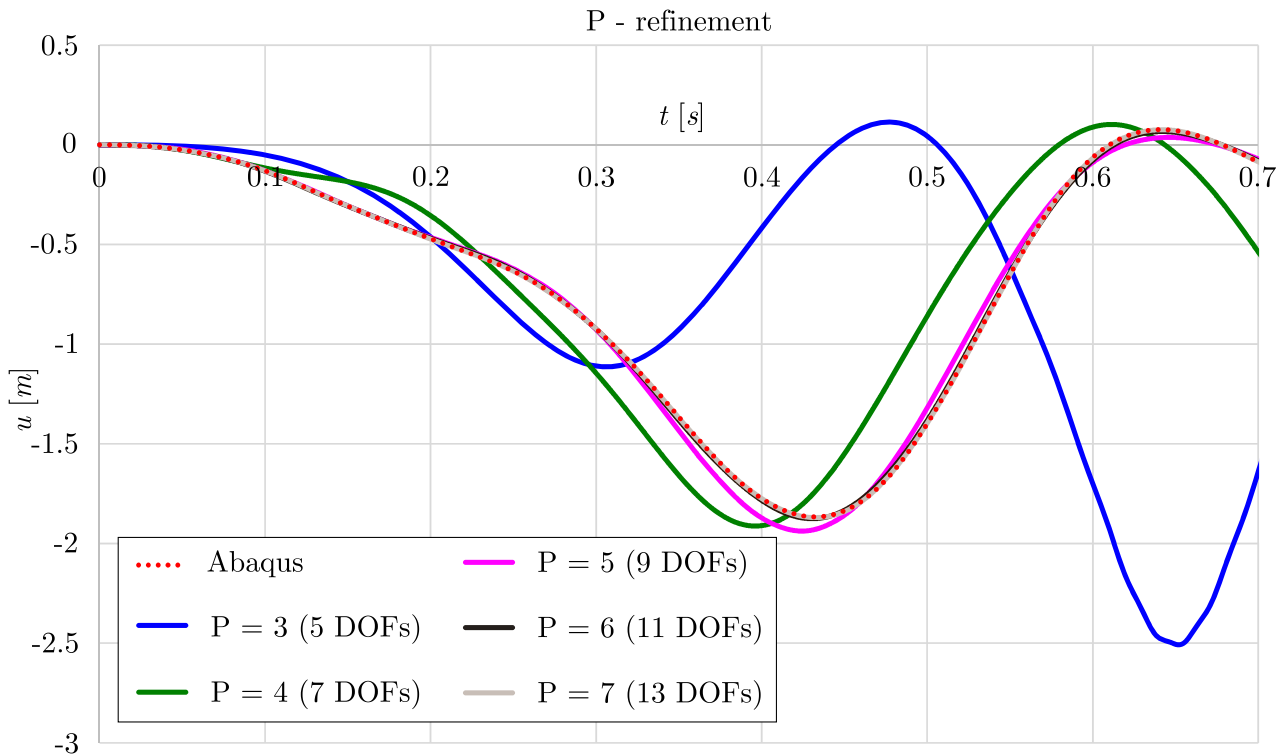


Figure 8.34: Convergence of the horizontal displacement of the beam free end obtained using the P - refinement isogeometric procedure

By inserting additional knots uniformly in the model with the 3rd - order NURBS basis functions, H - refinement procedure is applied. In Figures 8.36 and 8.37 the results of horizontal (u) and

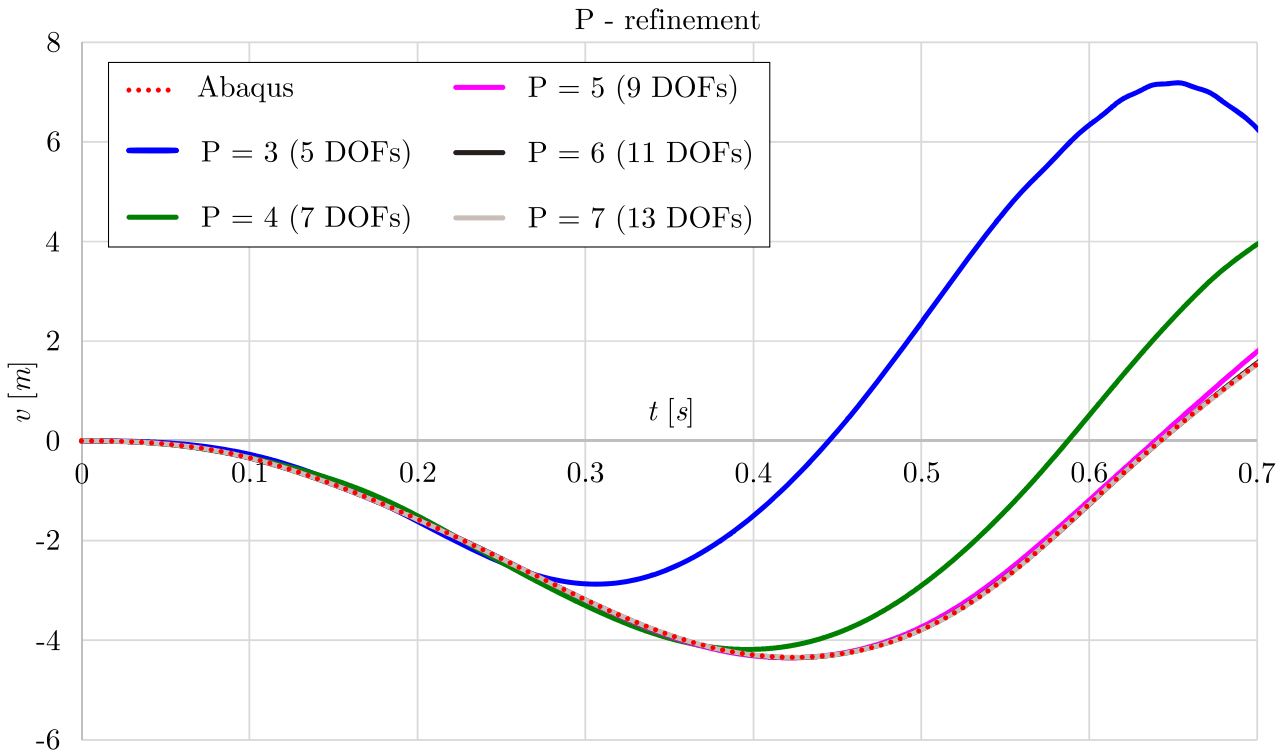


Figure 8.35: Convergence of the vertical displacement of the beam free end obtained using the P - refinement isogeometric procedure

vertical (v) displacements of beam free end are shown for various models obtained using the H - refinement procedure. As can be noticed, the results are in excellent agreement with the reference results and have converged for the model with 15 DOFs.

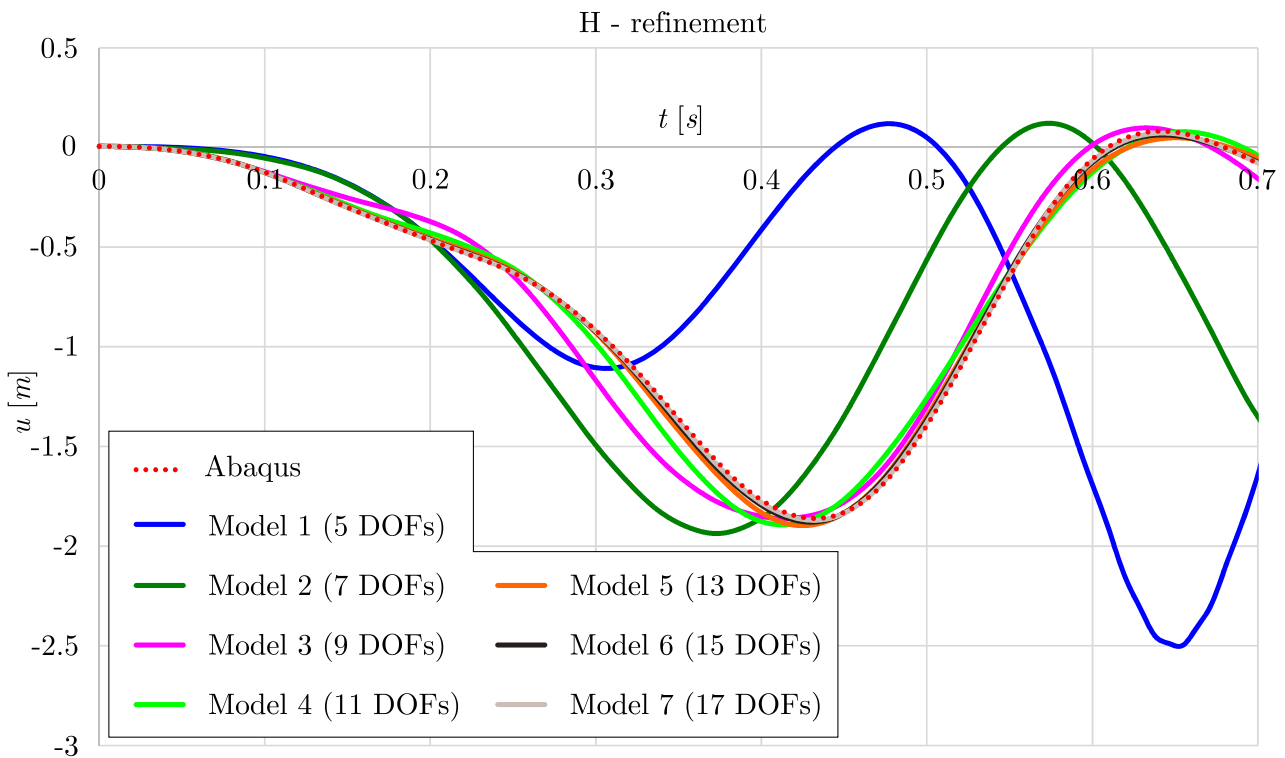


Figure 8.36: Convergence of the horizontal displacement of the beam free end obtained using the H - refinement isogeometric procedure

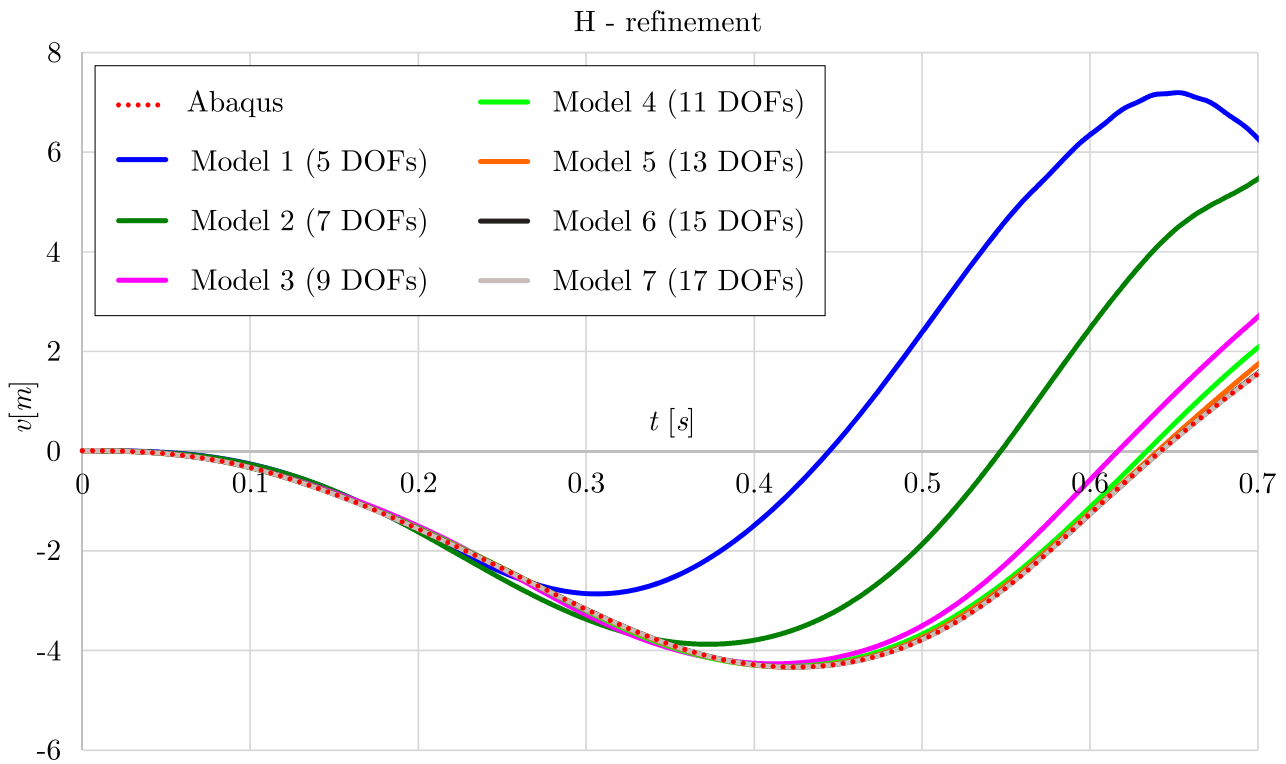


Figure 8.37: Convergence of the vertical displacement of the beam free end obtained using the H - refinement isogeometric procedure

Figures 8.38 and 8.39 represents the horizontal displacement of the beam free end, while Figures 8.40 and 8.41 represents its vertical displacement obtained using the K - refinement procedure. As can be noticed, for higher order of NURBS basis functions and lower continuity, the results converge faster and become more accurate.

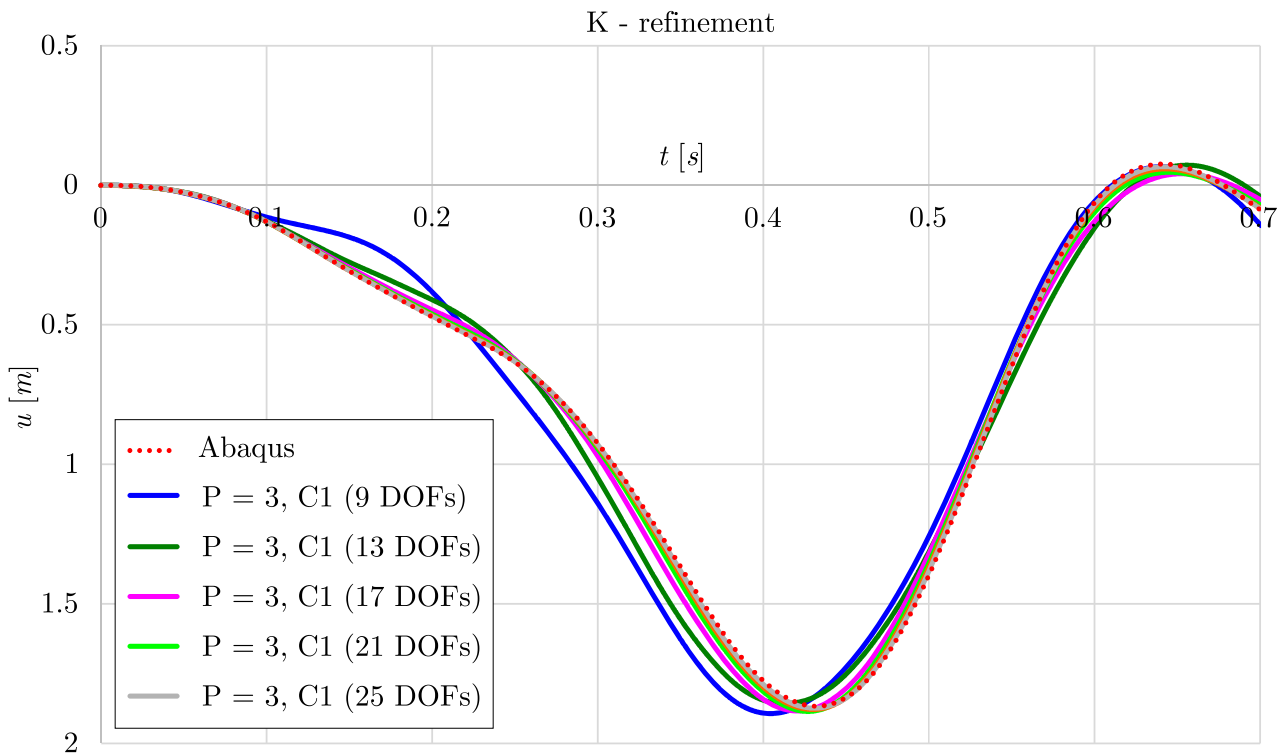


Figure 8.38: Convergence of the horizontal displacement of the beam free end obtained using the K - refinement isogeometric procedure - Part 1

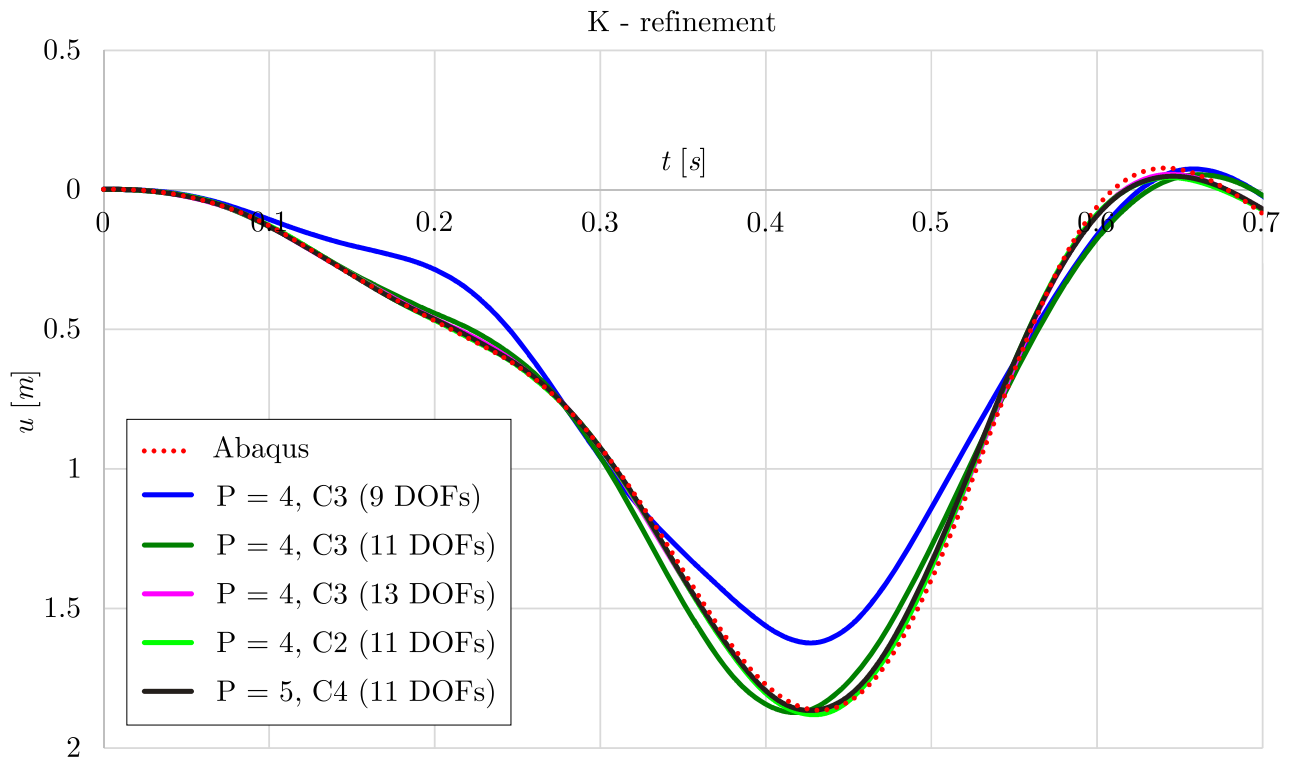


Figure 8.39: Convergence of the horizontal displacement of the beam free end obtained using the K - refinement isogeometric procedure - Part 2

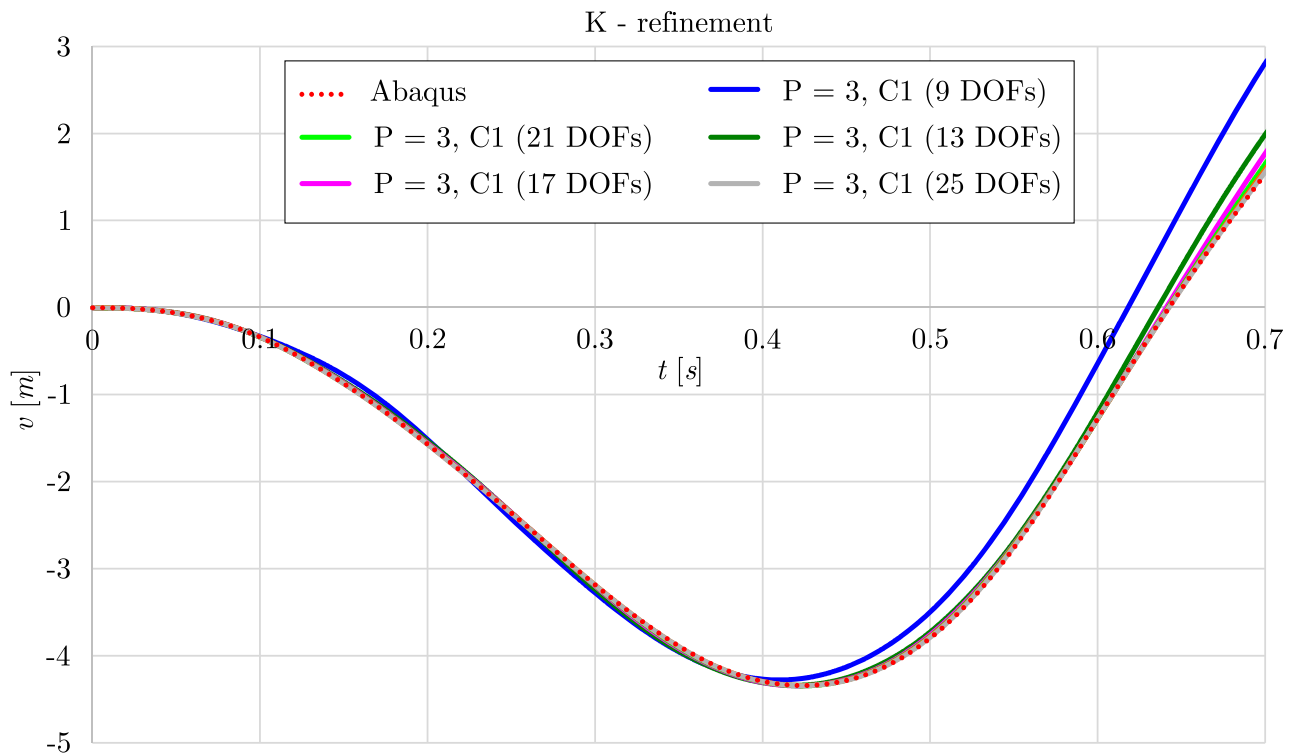


Figure 8.40: Convergence of the vertical displacement of the beam free end obtained using the K - refinement isogeometric procedure - Part 1

8.3.1.2 Parametric study

Effects of geometrical nonlinearity on the dynamic response of curved plane beam are demonstrated on the example of cantilever beam described in the previous section. The displacements

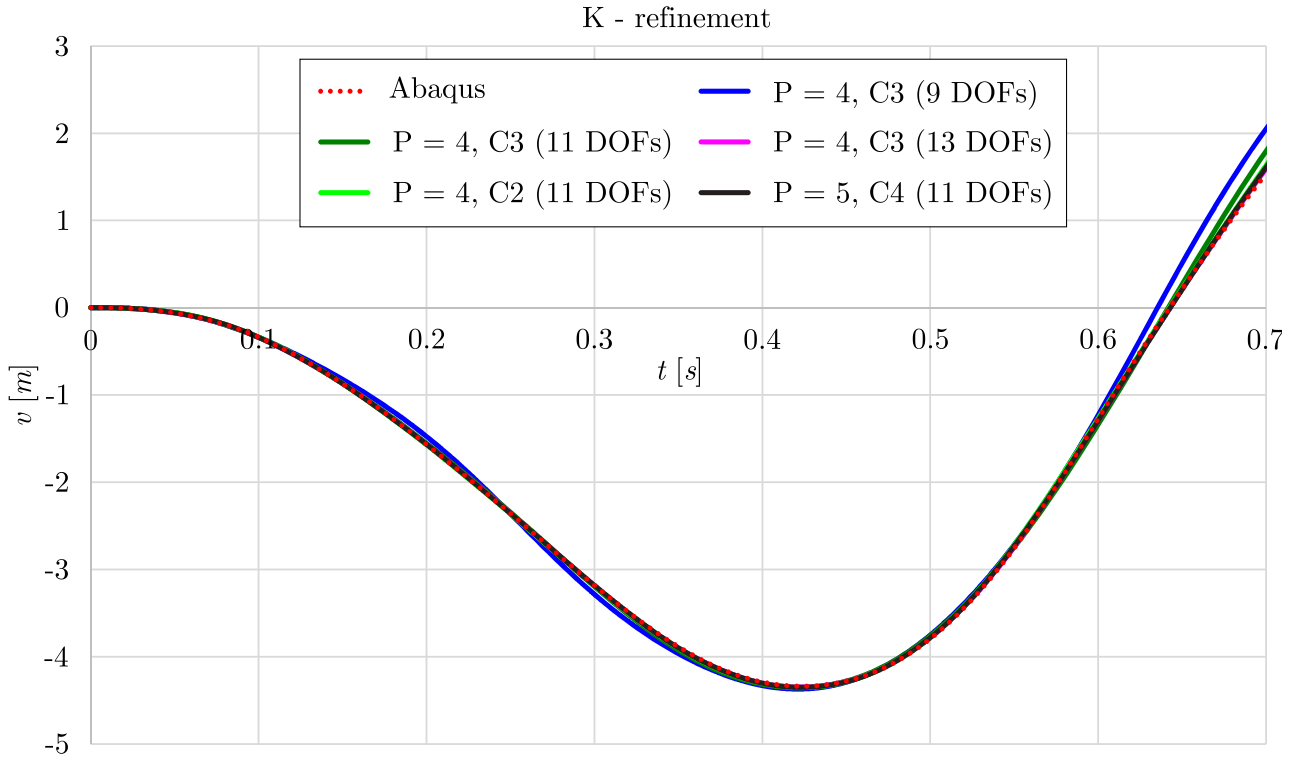


Figure 8.41: Convergence of the vertical displacement of the beam free end obtained using the K - refinement isogeometric procedure - Part 2

of the beam free end are obtained using the model with 6th - order NURBS basis functions (11 DOFs) for variable dynamic load amplitudes. In order to compare the results, displacements have been divided by the load amplitude, forming normalized displacements. In Figures 8.42 and 8.43 normalized horizontal and vertical displacement of the beam free end have been presented respectively. As can be seen, the normalized displacements increase as the load amplitude increases. Moreover, for the load amplitude of $F = 0.1kN$, the normalized displacements have the same values as normalized displacements obtained in the linear dynamic analysis.

8.3.2 Moving load problem

8.3.2.1 Validation and convergence study

Simply supported plane curved beam is subjected to the moving load, Figure 8.44. The beam geometry is defined using four control points with corresponding weight vector and 3rd - order NURBS basis functions constructed over the knot vector:

$$\mathbf{w}^T = [0 \ 0 \ 0 \ 0 \ 1 \ 1 \ 1 \ 1] \quad (8.8)$$

The Young's modulus $E = 210GPa$ and the mass density $\rho = 7850kg/m^3$ constitute the beam homogeneous material. For the purpose of convergence and accuracy study, the load magnitude is constant $F = 200kN$, as well as the load velocity $V = 10m/s$. In order to study the behaviour of the proposed method, displacements of the beam midpoint have been calculated. The same beam has been modeled using the FEM commercial software Abaqus with 1181 B21 elements and 3543 DOFs. The moving mass in Abaqus has been defined as a reference point with adequate mass magnitude, connected to the plane beam using spring. Surface-to-surface contact (Explicit)

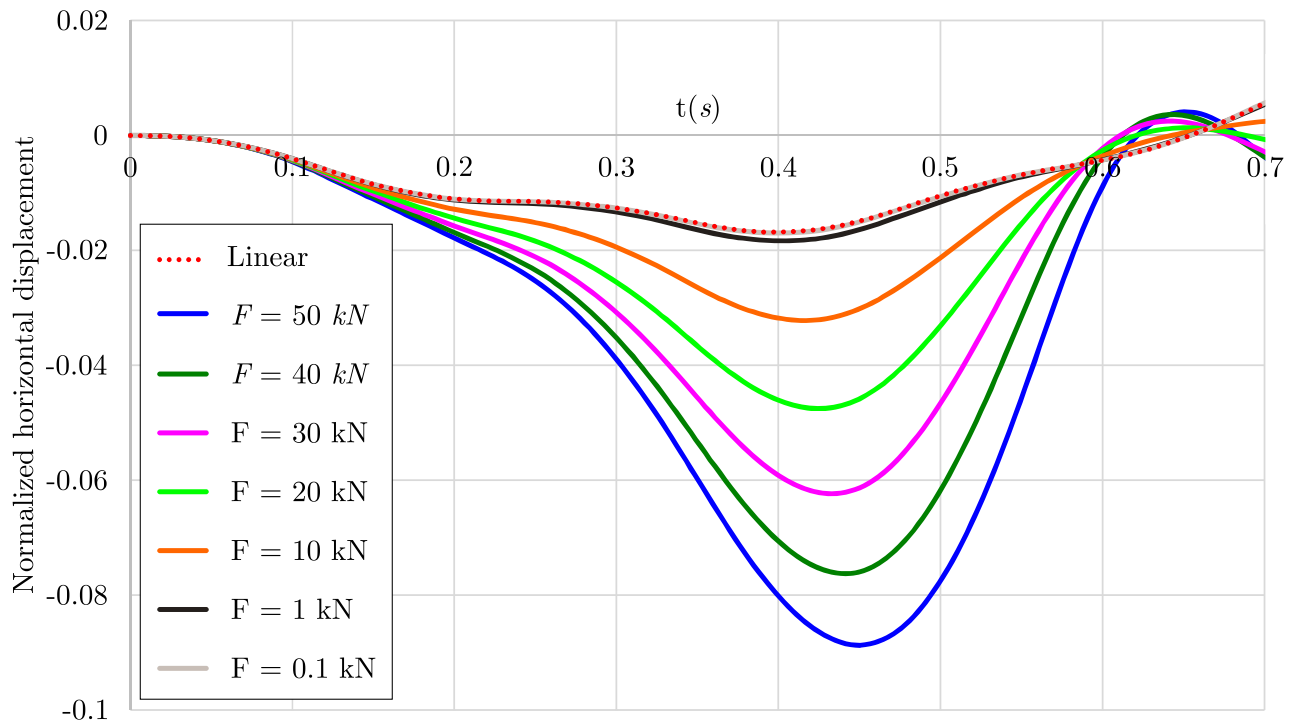


Figure 8.42: Normalized tip horizontal displacement with the variable amplitude of the load

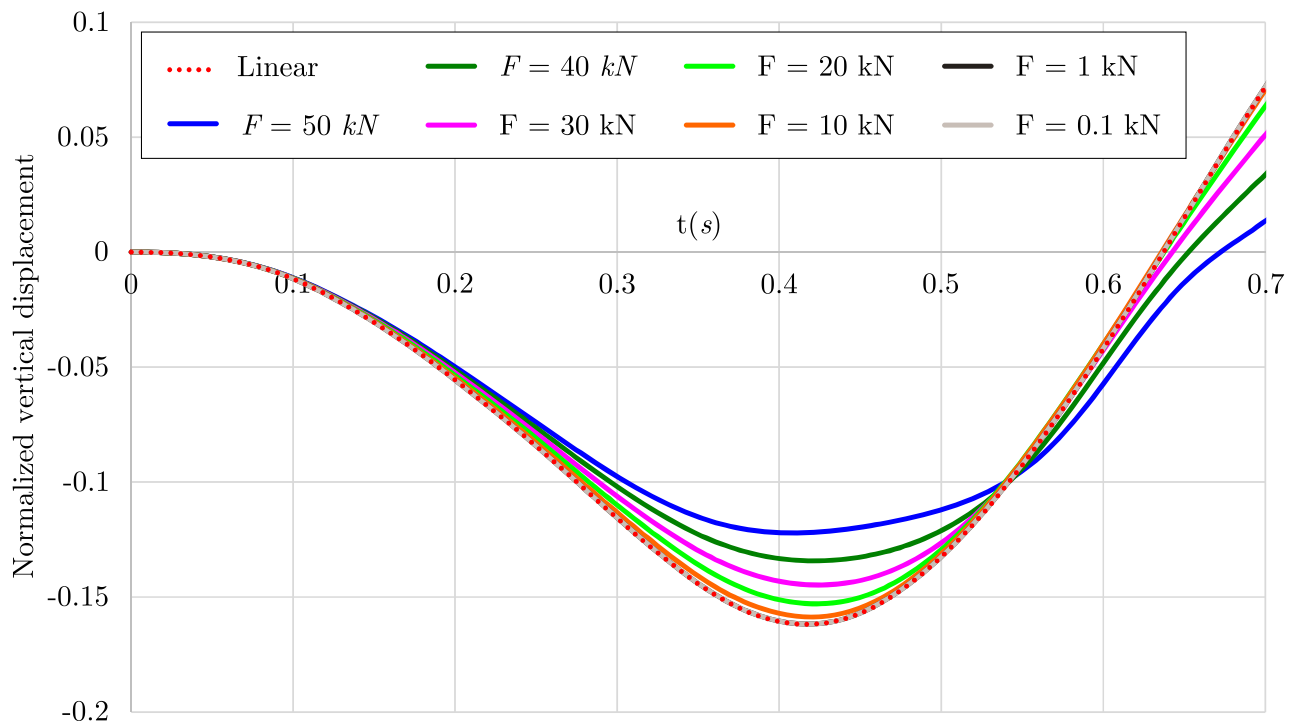


Figure 8.43: Normalized tip vertical displacement with the variable amplitude of the load

feature of Abaqus has been used to simulate the motion of the moving mass on the beam with a kinematic contact method and finite sliding. Contact interaction property has been defined in the tangent direction as a rough, and in normal direction as a hard contact.

First, the P - refinement procedure has been conducted. In Figure 8.45 and Figure 8.46, horizontal and vertical displacements of the beam midpoint have been presented applying P - refinement procedure. As can be noticed, the horizontal displacement has converged for the model with 11th-order NURBS basis functions, while the vertical displacement has converged

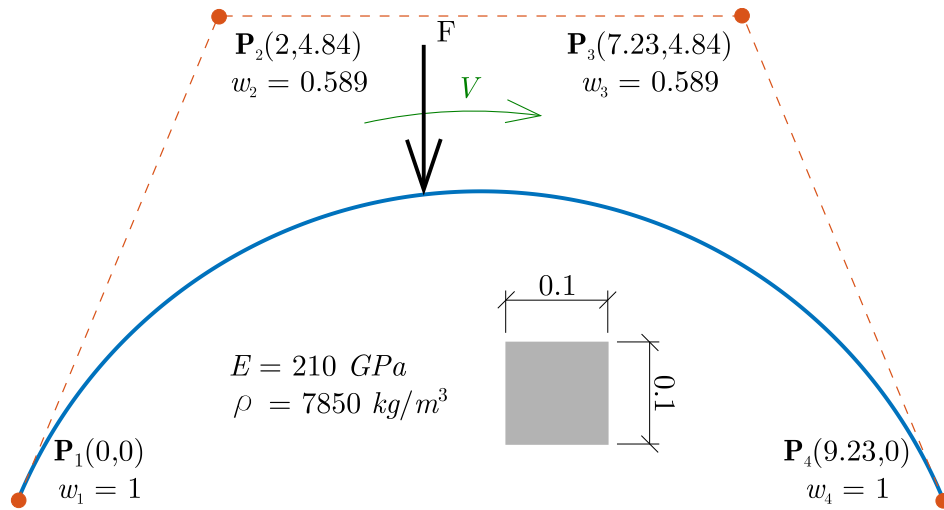


Figure 8.44: Circular arch subjected to moving load

for the model with 12th-order NURBS basis functions. The converged results are in good agreement with the results obtained using Abaqus. Also, the displacements are smaller than the displacements obtained using Abaqus, which is caused by the difference in the applied beam theory.

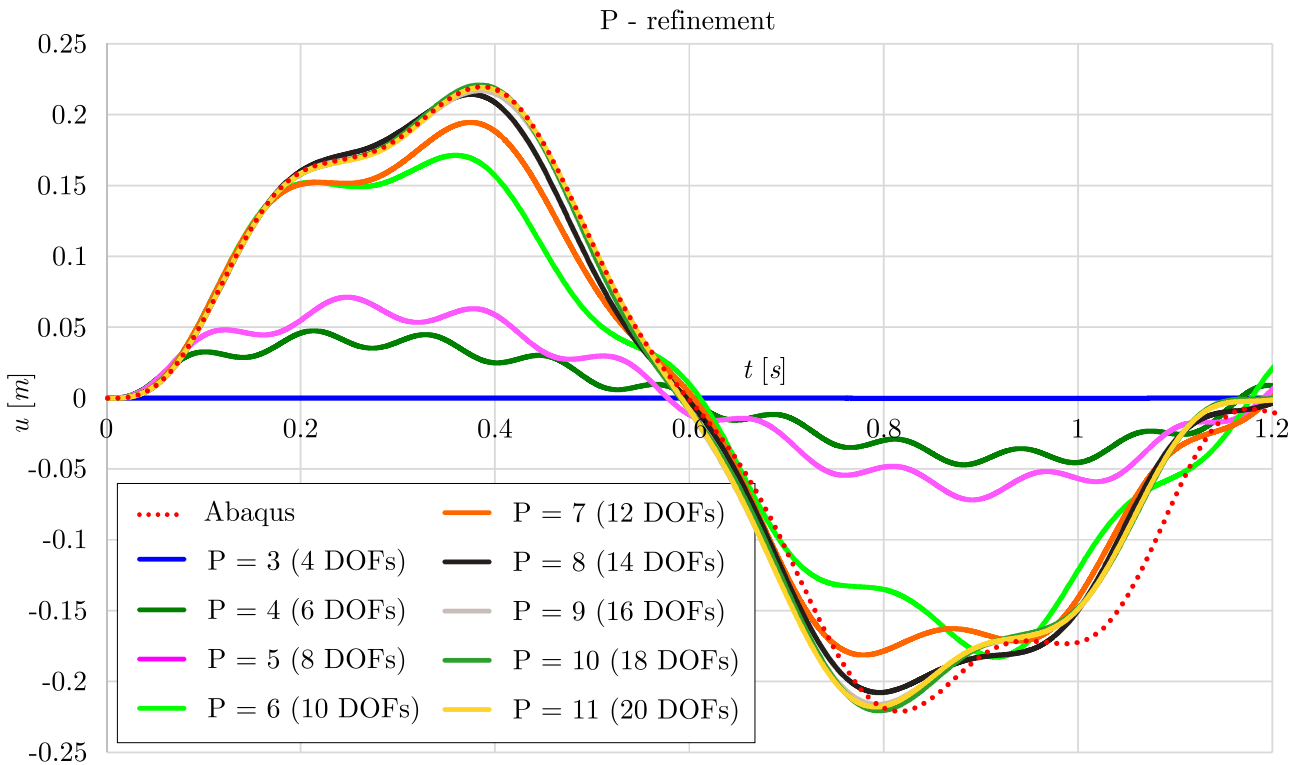


Figure 8.45: Convergence of the horizontal displacement of the beam’s midpoint obtained using P - refinement

Furthermore, the H - refinement procedure has been conducted to analyze the convergence property of the proposed method, Figure 8.47 and Figure 8.48. As can be noticed, the model with 24 DOFs gives converged results the horizontal displacement of the beam’s midpoint, while 26 DOFs are needed for the converged results of its vertical displacement.

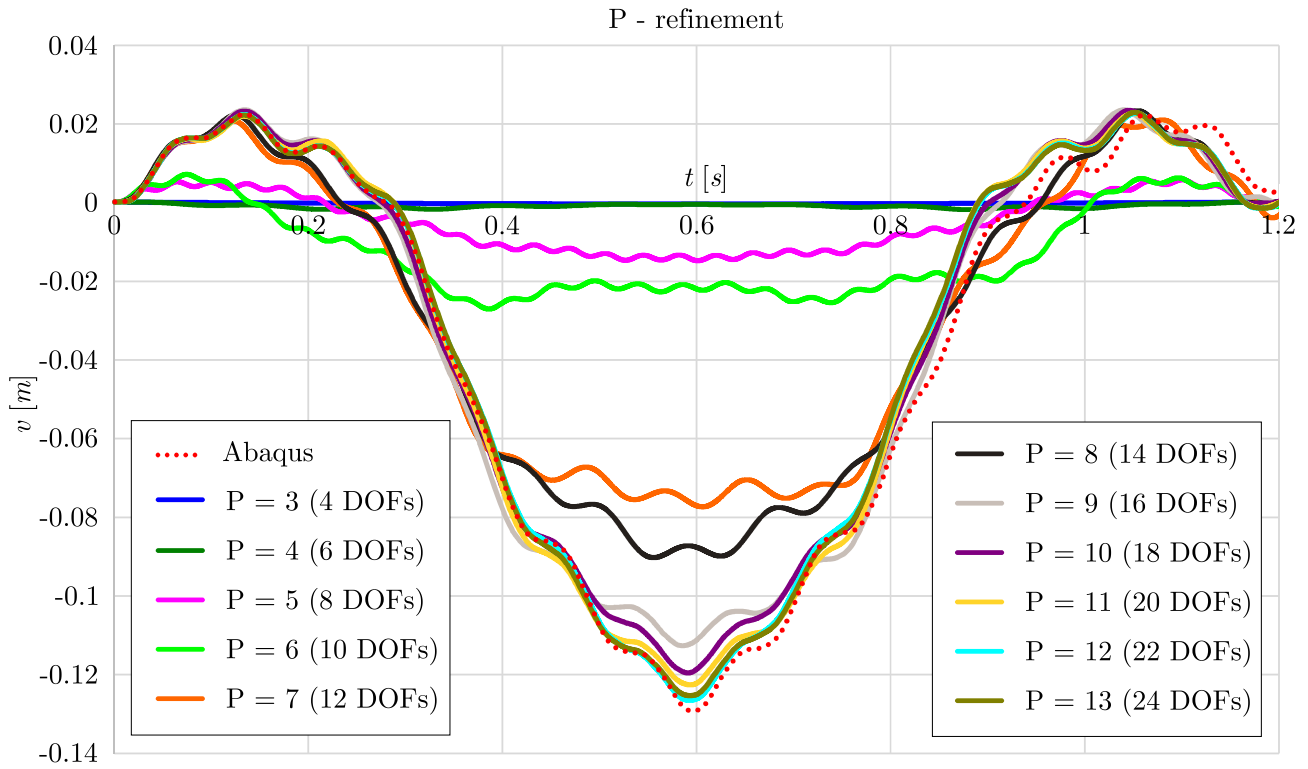


Figure 8.46: Convergence of the vertical displacement of the beam's midpoint obtained using P - refinement

In the end, the K - refinement procedure has been applied. The results of the horizontal and the vertical displacements of the beam's midpoint for the different function degree and continuity are presented in Figures 8.49 - 8.60.

In Table 8.7, minimal time step Δt , the number of required time steps n_t , and the number of the integration points n_{int} are presented for the converged results for the case of P -, H - and K - refinement. As the continuity of the basis function decreases, the number of the time steps and the integration points decreases as well. Aforementioned is important, as the time step represents the main drawback in the explicit geometrically nonlinear dynamic analysis.

8.3.2.2 Parametric study

In this section, the influence of the moving load magnitude and velocity on the beam displacement is presented on the example of the beam from the previous example. The results are obtained using the model with 6th-order NURBS basis function, and C^2 continuity.

First, the influence of the moving load magnitude (F) has been analyzed. The beam's midpoint horizontal and vertical displacements for the different load magnitude cases have been calculated. In order to compare the results, the displacements have been divided by the load magnitude, forming the normalized displacements, Figures 8.61 and 8.62. As can be noticed, the normalized displacements change with the load magnitude, which does not occur in the linear analysis. Increase of the load magnitude produces the increase of the normalized displacements.

The moving load velocity effect on the beam's midpoint displacements has been investigated, Figures 8.63 and 8.64. Normalized time for the different load velocity cases has been achieved by dividing the load traveling time with the total load traveling time. Horizontal and vertical

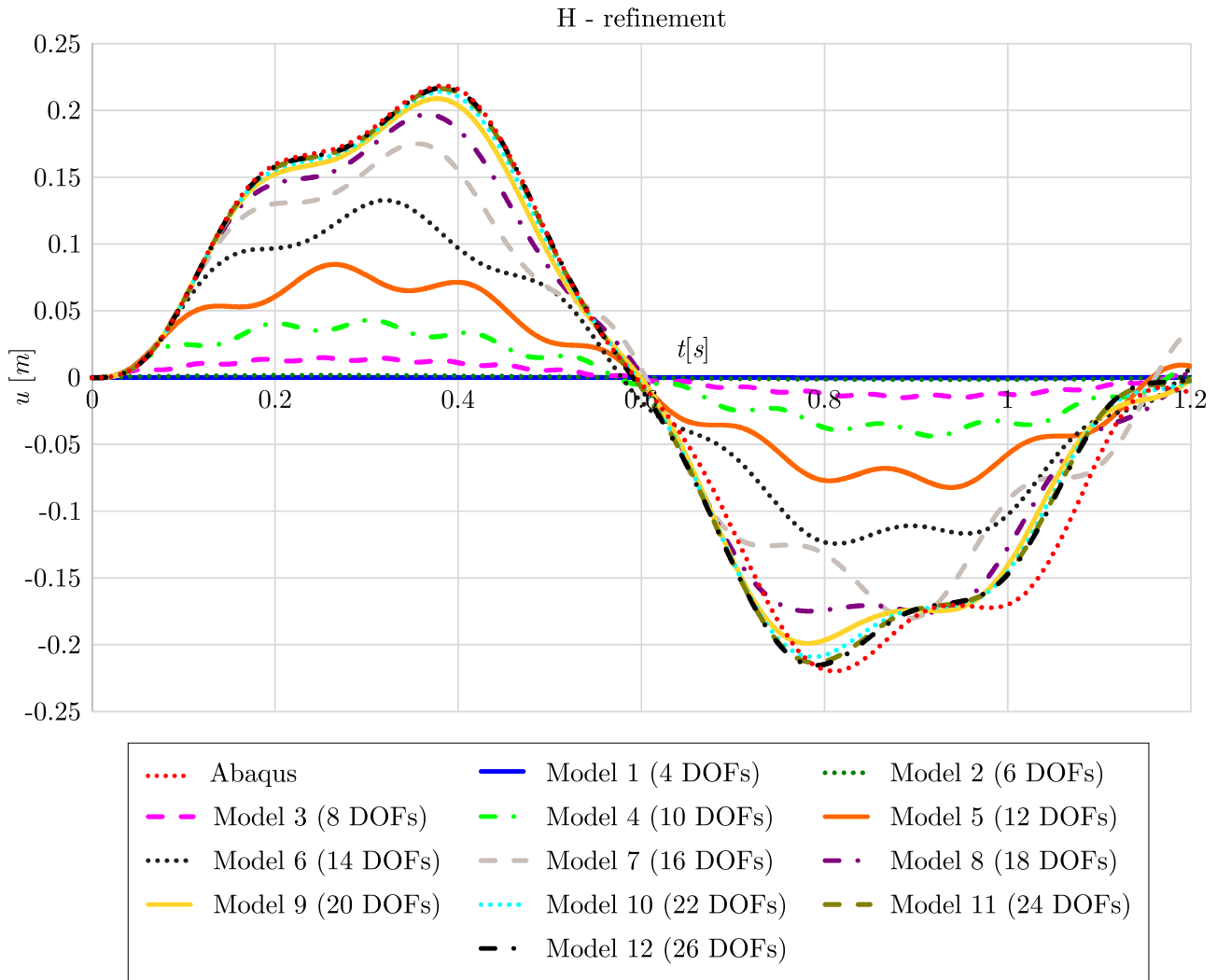


Figure 8.47: Convergence of the horizontal displacement of the beam's midpoint obtained using H - refinement

displacements of the beam's midpoint vary for the different load velocities. The maximum displacement does not have to be achieved for the biggest load velocity, which can be observed for the case of the horizontal displacement, where the maximum is obtained for the load velocity of approximately $V = 40m/s$.

In addition, the horizontal projection of the moving load velocity (\mathbf{V}_x) is presented in Figure 8.65 for the case of two load magnitudes, $F = 1kN$ and $F = 200kN$. For the case of load magnitude $F = 1kN$, the results of the geometrically linear and nonlinear analysis coincide. In this example, the horizontal projection of the moving load velocity corresponds to the case of the load movement on the undeformed beam. For the load magnitude $F = 200kN$, the horizontal projection of the moving load velocity differs from the previous example, as beam displacement is significant for the larger load magnitude.

8.3.3 Moving mass problem

In this section, the difference between the moving load and moving mass model in the geometrically nonlinear formulation of the plane beam is investigated. Beam model presented in the previous section has been used in the analysis. The mass moving along the beam with the

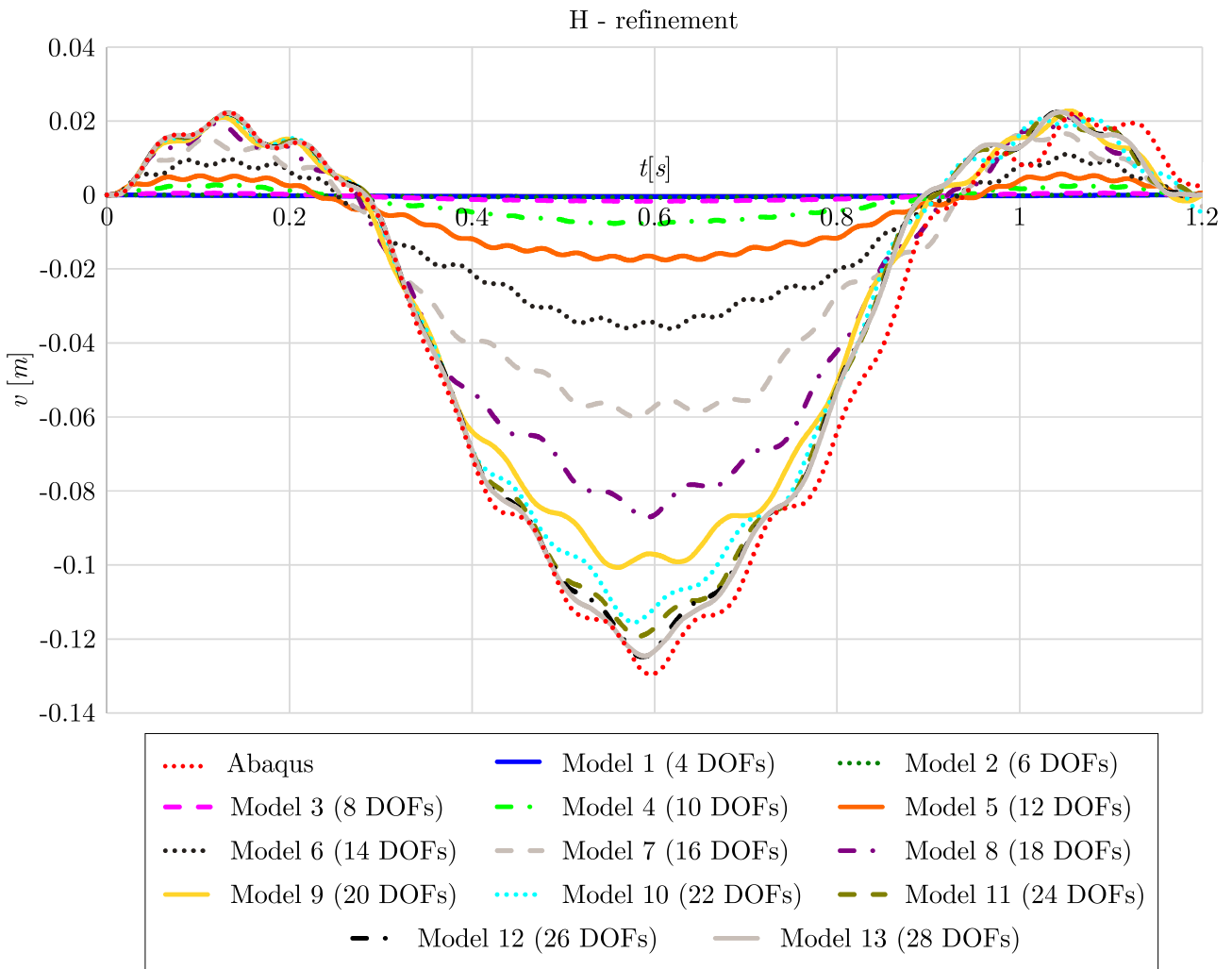


Figure 8.48: Convergence of the horizontal displacement of the beam's midpoint obtained using H - refinement

constant velocity $V = 10m/s$ is obtained by dividing the load magnitude $F = 200kN$ with the gravitational acceleration $g = 9.81m/s^2$. In Figures 8.66 and 8.67 horizontal and vertical displacements of the beam's midpoint obtained using moving load and moving mass models are presented. As can be noticed, a significant difference between the results can be observed in both the magnitude and sign of the displacements.

Table 8.7: Number of degrees of freedom (DOF), time step (Δt), number of required time steps (n_t) and number of integration points (n_{int}) for the converged models obtained using P -, H - and K - refinement procedures

		DOF	Δt	n_t	n_{int}
P - ref	P12	22	2.86e-5	41983	13
H - ref	P3	26	3.47e-5	34565	48
	P3, C1	40	2.57e-5	46633	40
	P4, C3	26	2.87e-5	41822	55
	P4, C2	26	3.61e-5	33252	30
	P4, C1	24	4.50e-5	26695	20
	P5, C4	26	2.47e-5	48611	60
	P5, C3	24	3.43e-5	35006	30
	P5, C2	32	3.60e-5	33372	24
	P5, C1	34	4.35e-5	27575	18
	P6, C5	26	2.21e-5	54245	63
	P6, C4	22	3.45e-5	34779	28
	P6, C3	28	2.86e-5	41961	28
	P6, C2	18	5.40e-5	22211	14
K - ref	P7, C6	26	2.05e-5	58403	64
	P7, C5	28	2.23e-05	53742	40
	P7, C4	30	2.33e-05	51586	32
	P8, C7	26	1.97e-05	60976	63
	P8, C6	26	2.33E-05	51412	36
	P8, C5	26	2.59E-05	46255	27
	P8, C4	22	3.48E-05	34459	18
	P9, C8	24	2.27E-05	52966	50
	P9, C7	28	1.98E-05	60677	40
	P9, C6	22	3.15E-05	38122	20
	P10, C9	24	2.30E-05	52183	44
	P10, C8	24	2.19E-05	54747	33
	P10, C7	24	2.66E-05	45165	22
	P11, C10	22	2.82E-05	42543	24

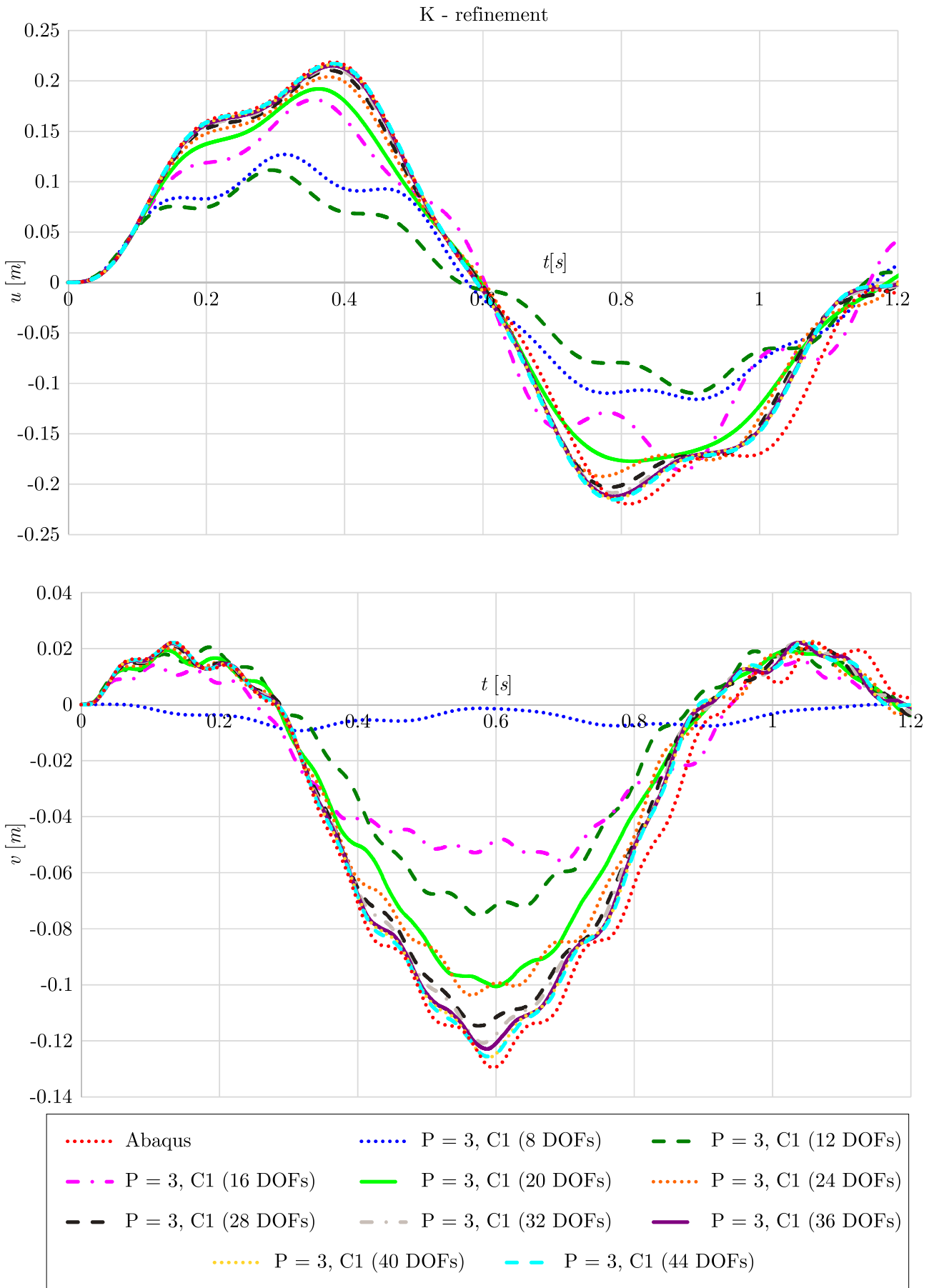


Figure 8.49: Convergence of the horizontal and vertical displacement of the beam's midpoint obtained using K - refinement, part 1

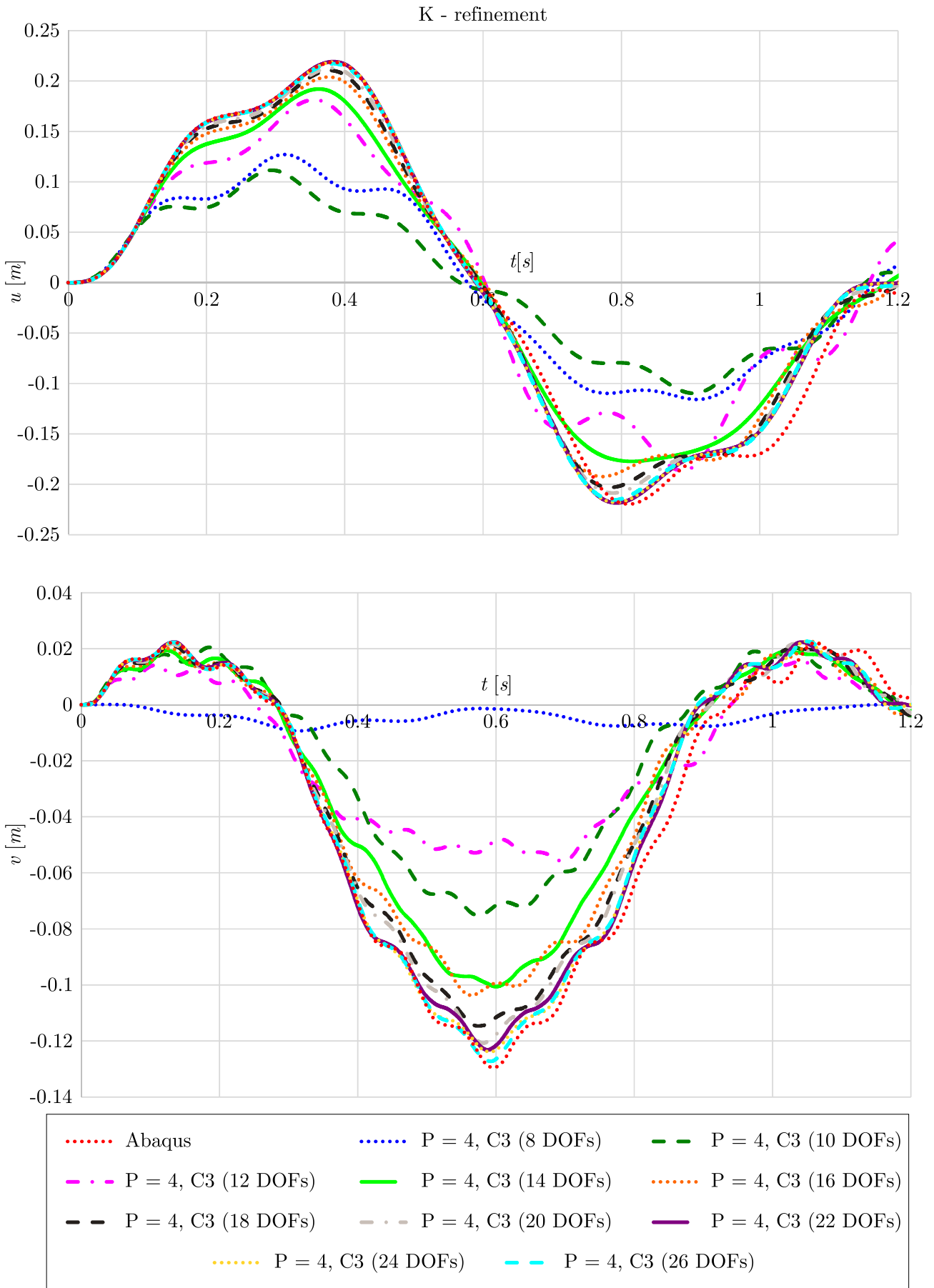


Figure 8.50: Convergence of the horizontal and vertical displacement of the beam's midpoint obtained using K - refinement, part 2

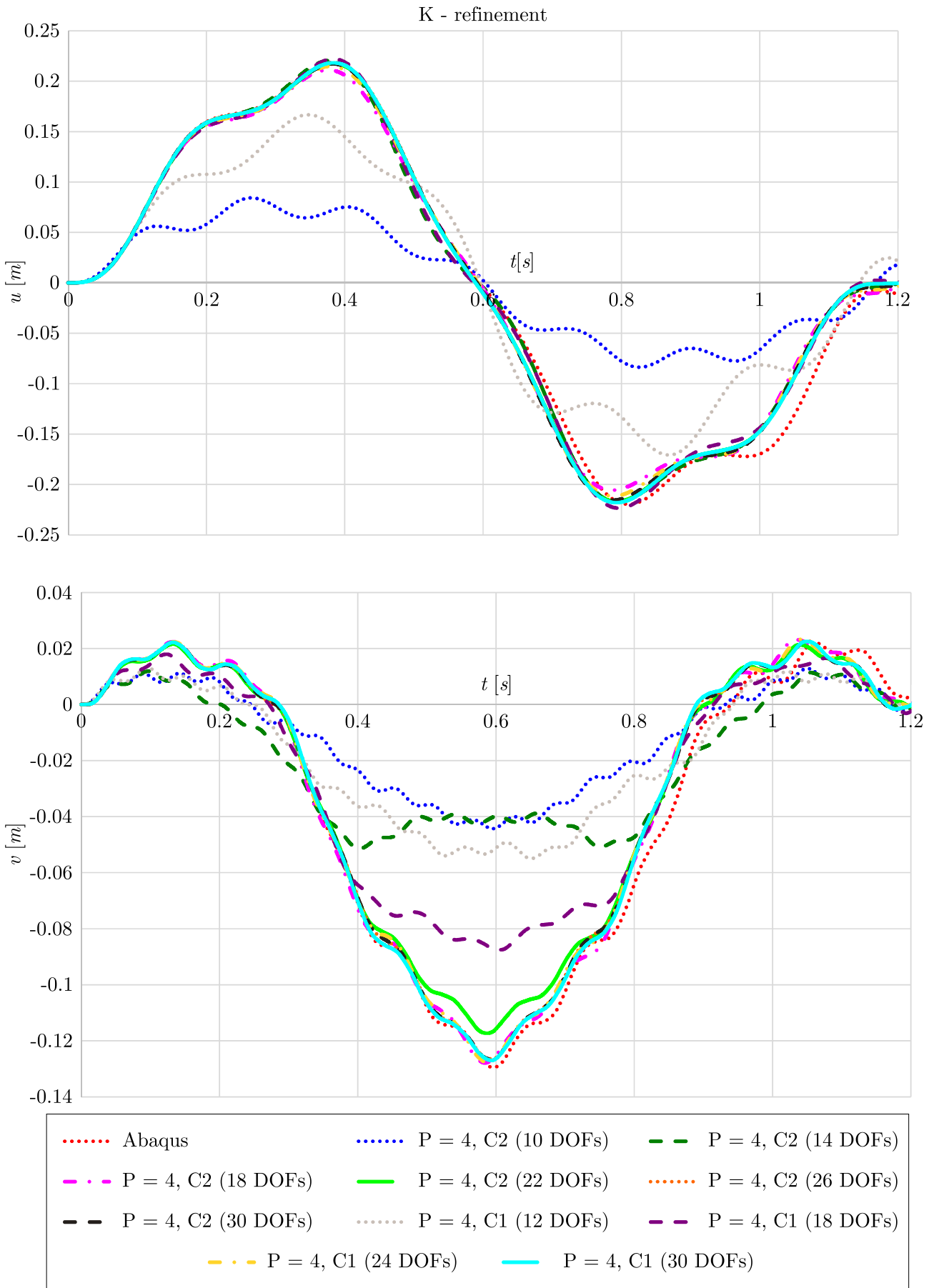


Figure 8.51: Convergence of the horizontal and vertical displacement of the beam's midpoint obtained using K - refinement, part 3

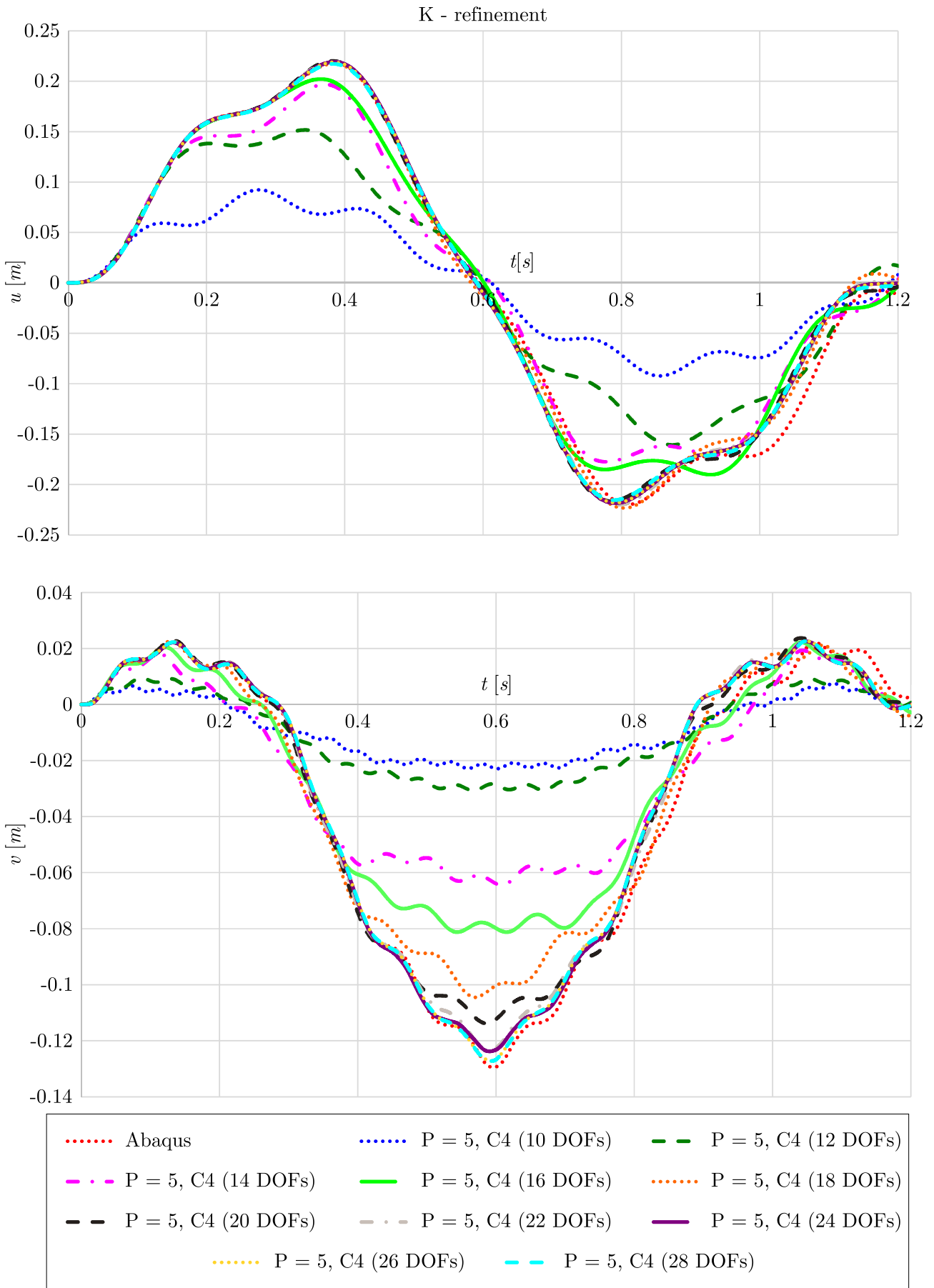


Figure 8.52: Convergence of the horizontal and vertical displacement of the beam's midpoint obtained using K - refinement, part 4

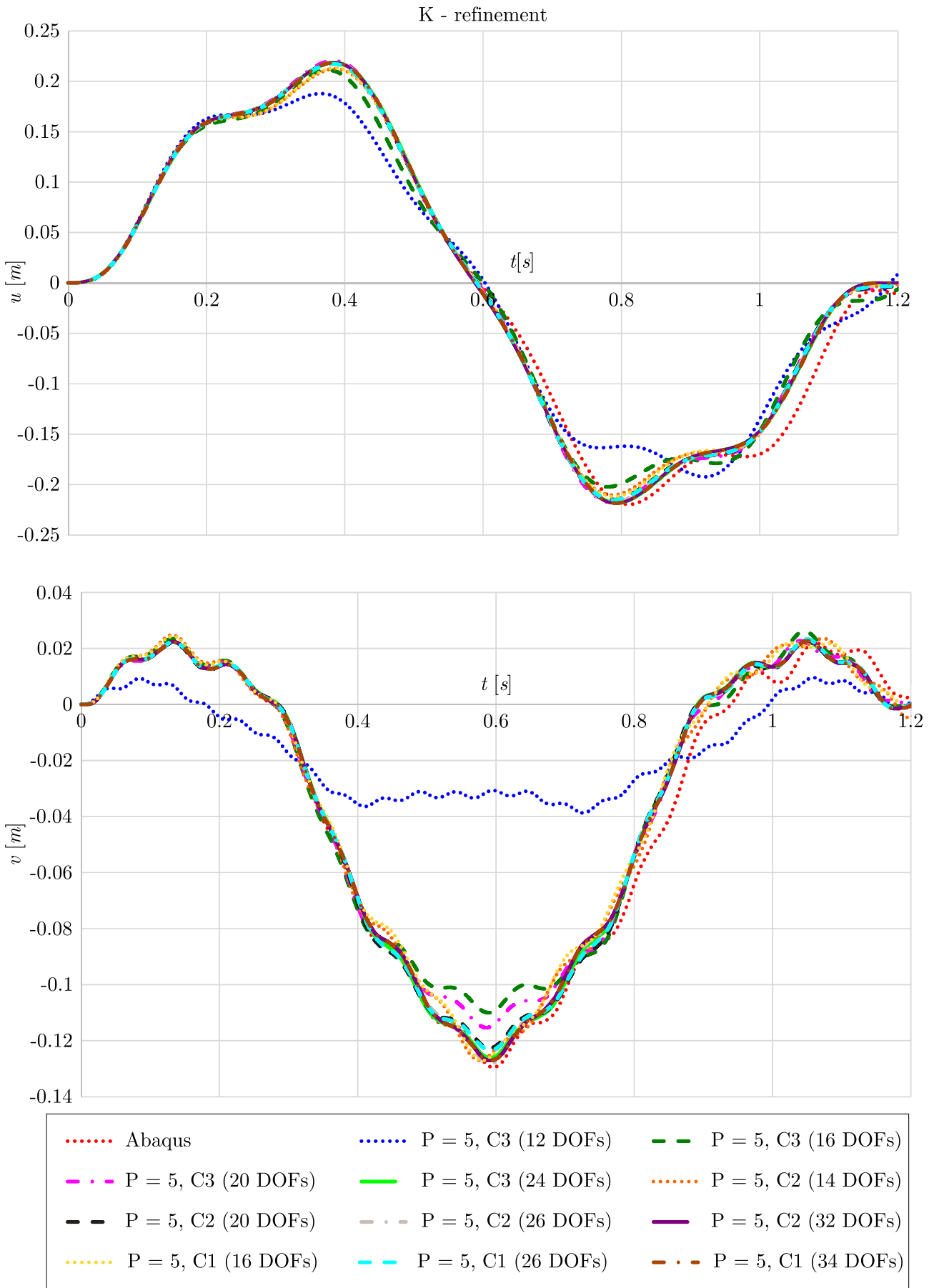


Figure 8.53: Convergence of the horizontal and vertical displacement of the beam's midpoint obtained using K - refinement, part 5

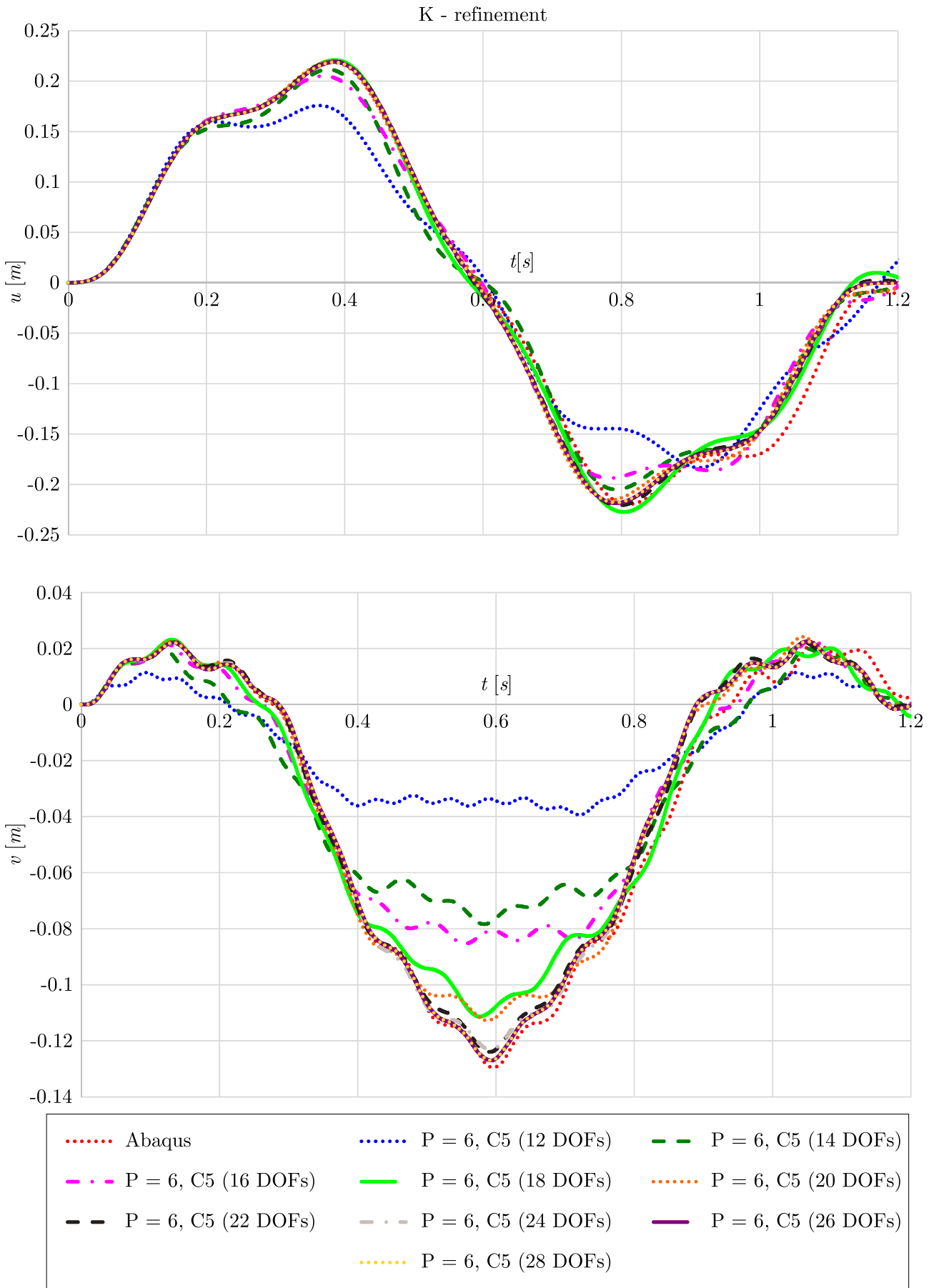


Figure 8.54: Convergence of the horizontal and vertical displacement of the beam's midpoint obtained using K - refinement, part 6

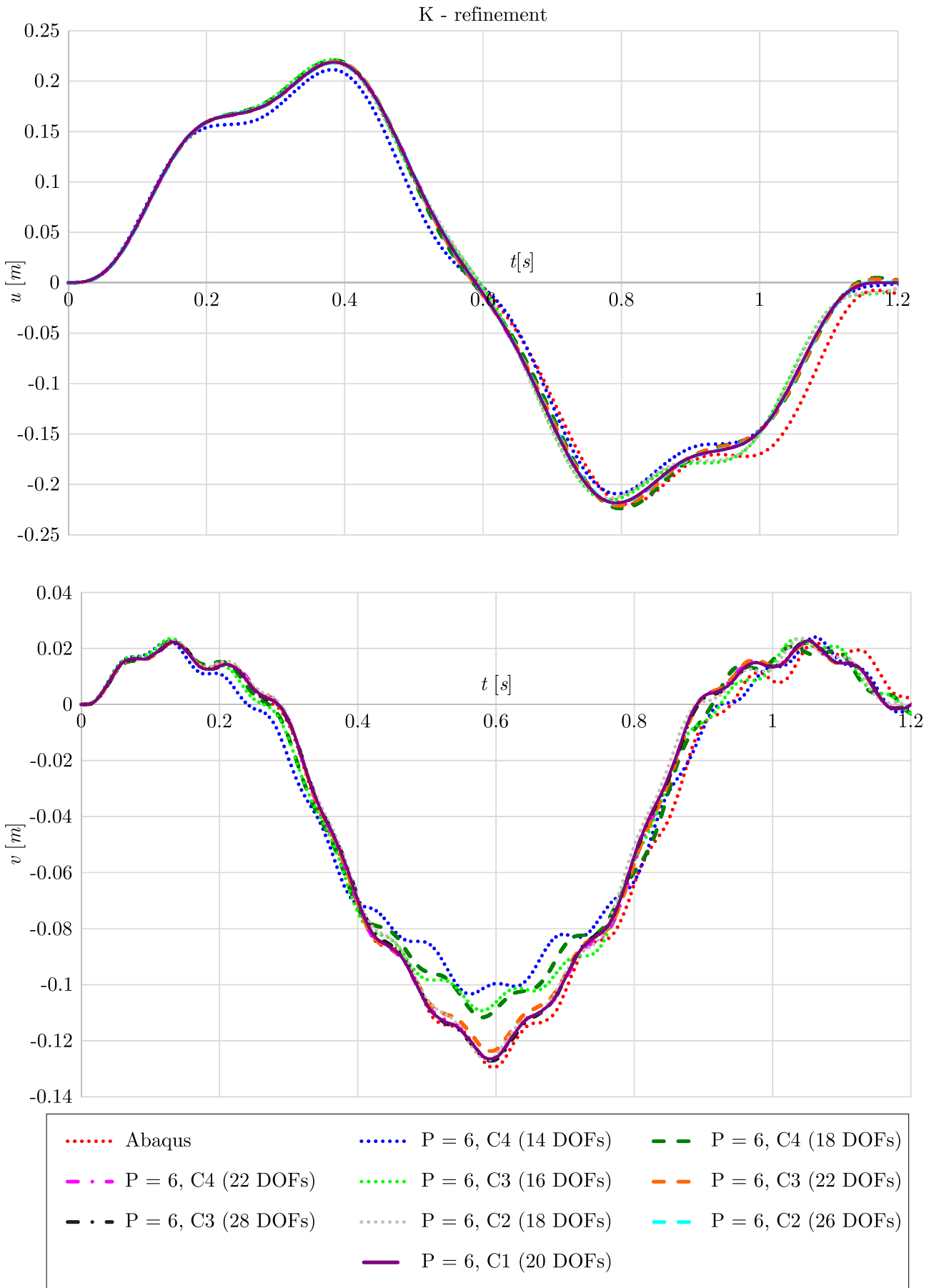


Figure 8.55: Convergence of the horizontal and vertical displacement of the beam's midpoint obtained using K - refinement, part 7

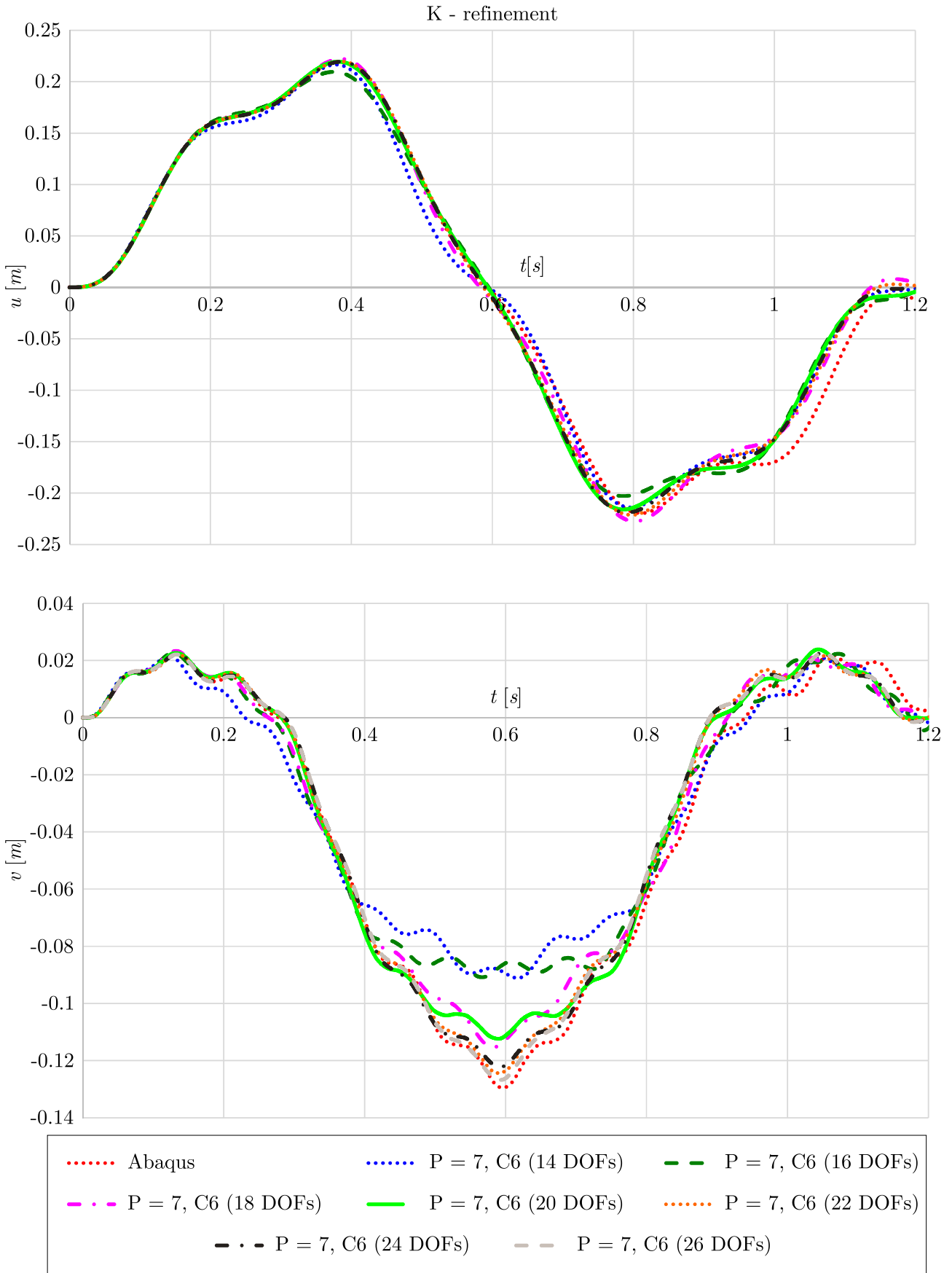


Figure 8.56: Convergence of the horizontal and vertical displacement of the beam's midpoint obtained using K - refinement, part 8

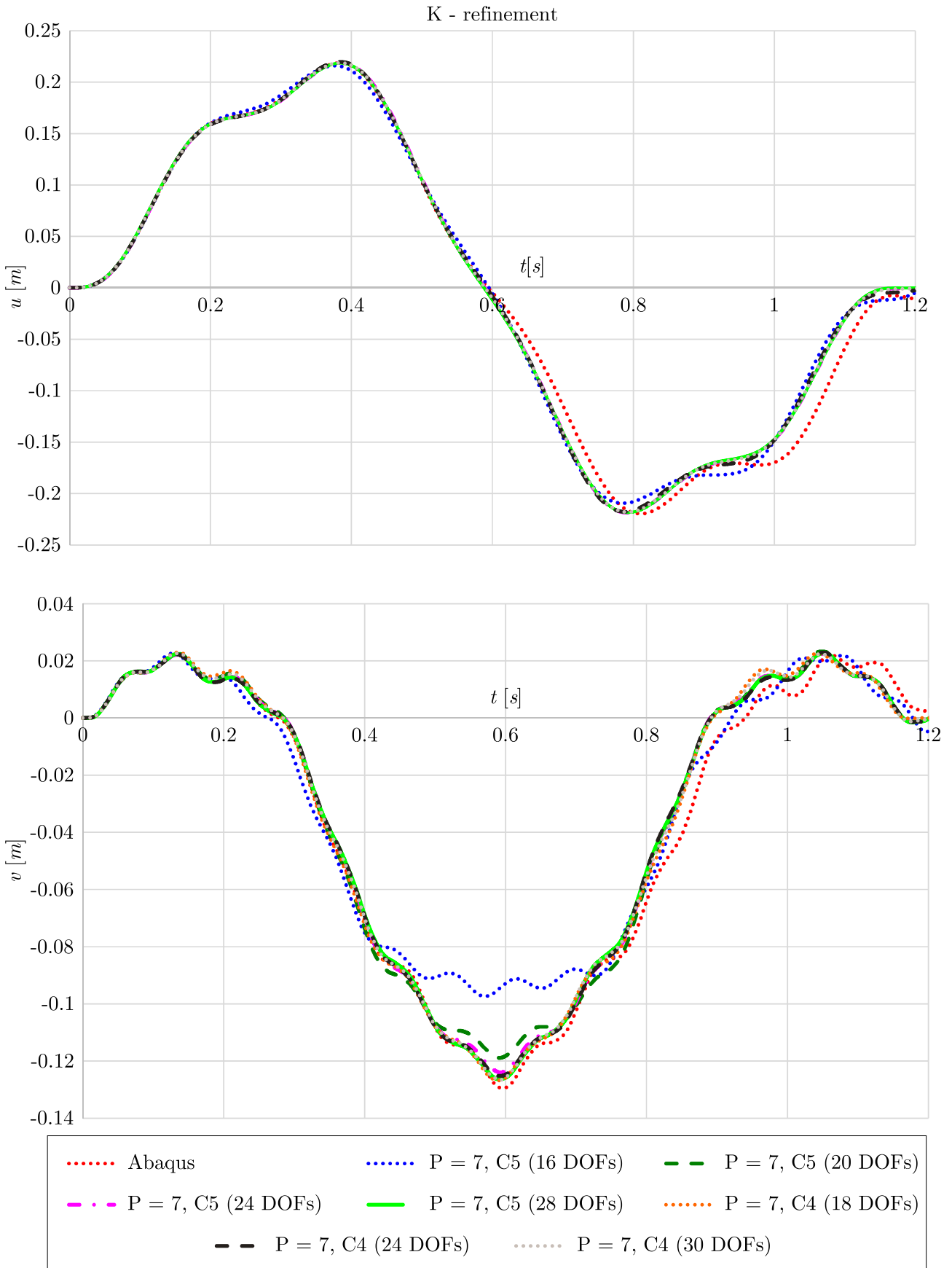


Figure 8.57: Convergence of the horizontal and vertical displacement of the beam's midpoint obtained using K - refinement, part 9

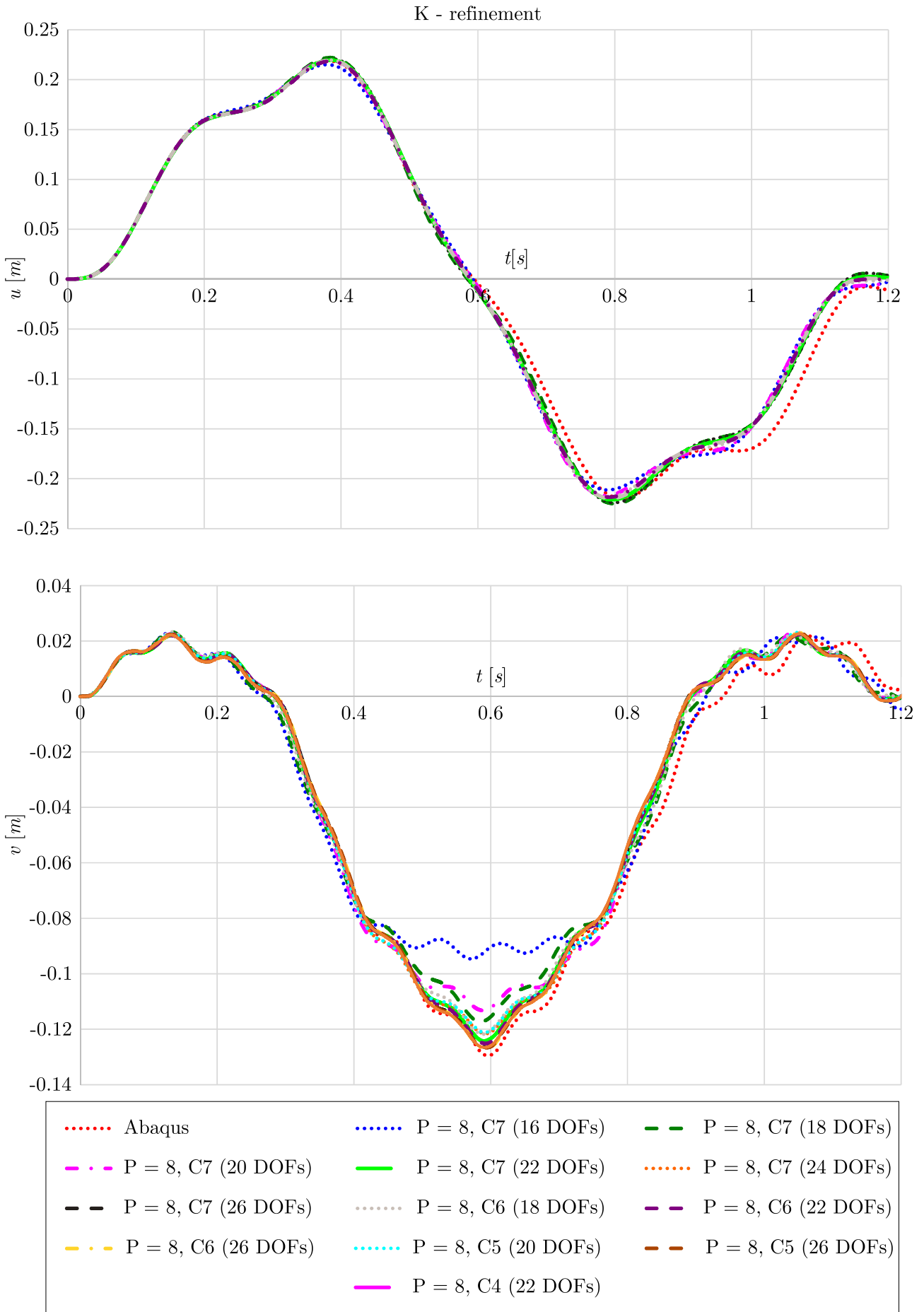


Figure 8.58: Convergence of the horizontal and vertical displacement of the beam’s midpoint obtained using K - refinement, part 10

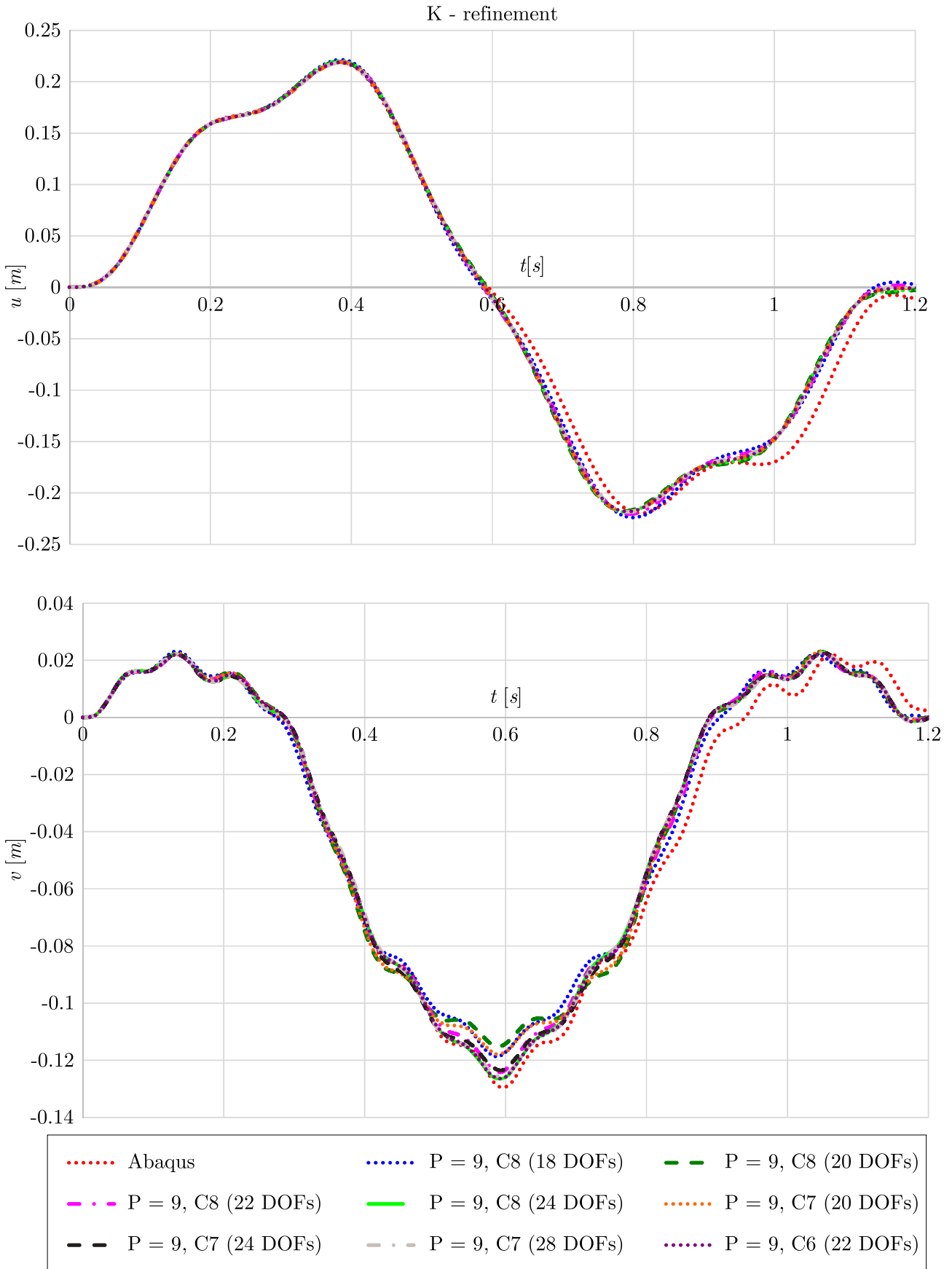


Figure 8.59: Convergence of the horizontal and vertical displacement of the beam’s midpoint obtained using K - refinement, part 11

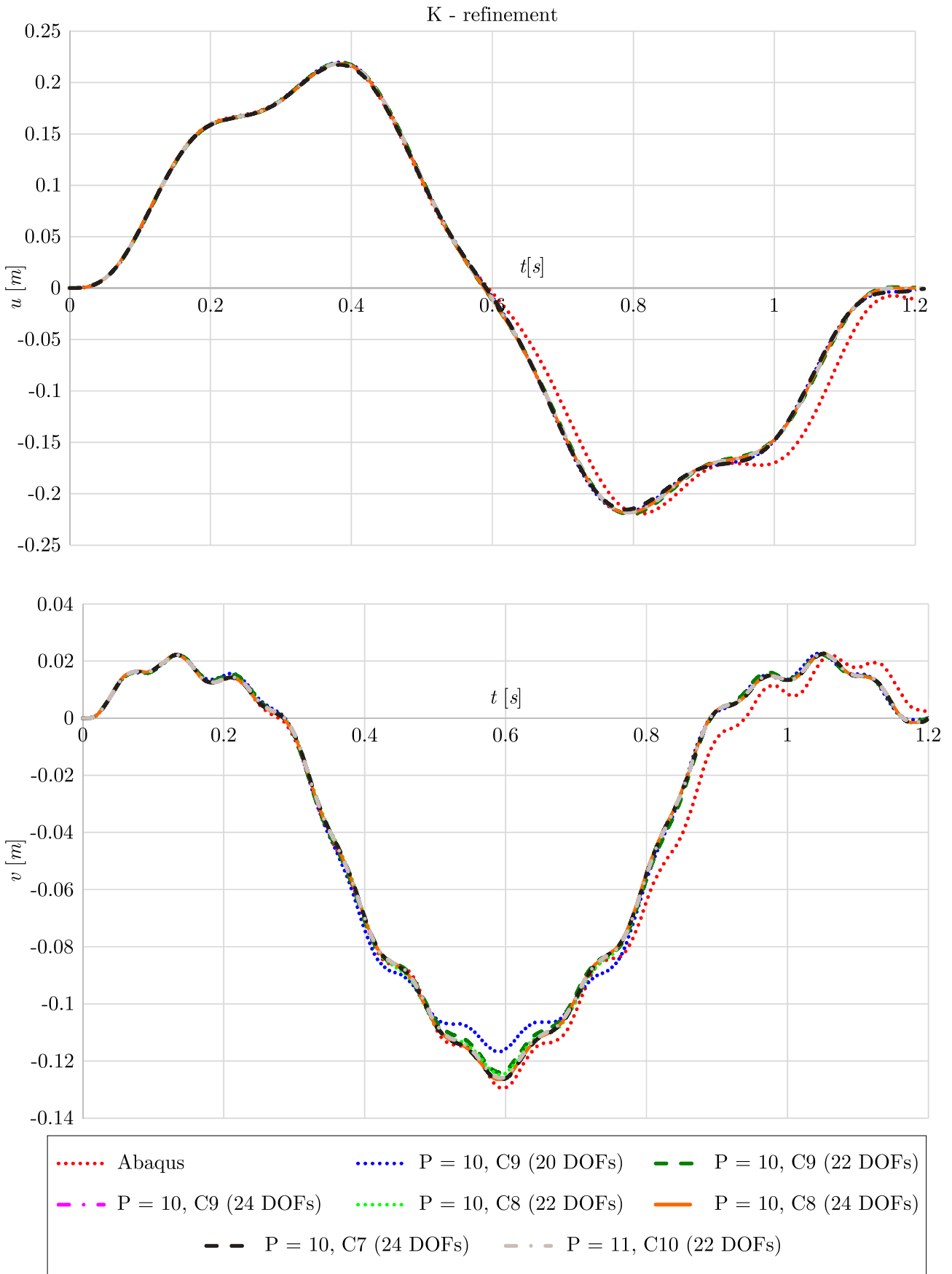


Figure 8.60: Convergence of the horizontal and vertical displacement of the beam's midpoint obtained using K - refinement, part 12

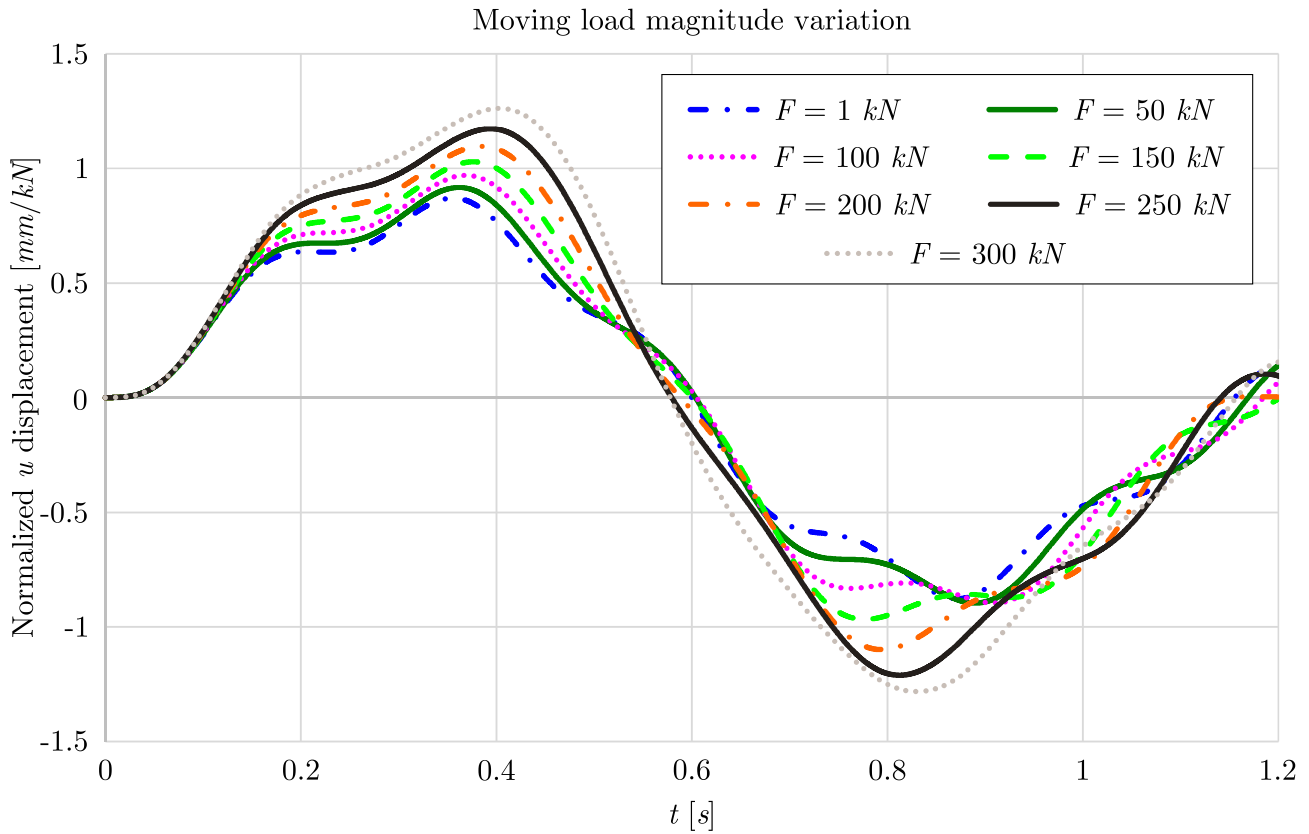


Figure 8.61: Normalized horizontal displacement of the beam's midpoint for different moving load magnitude

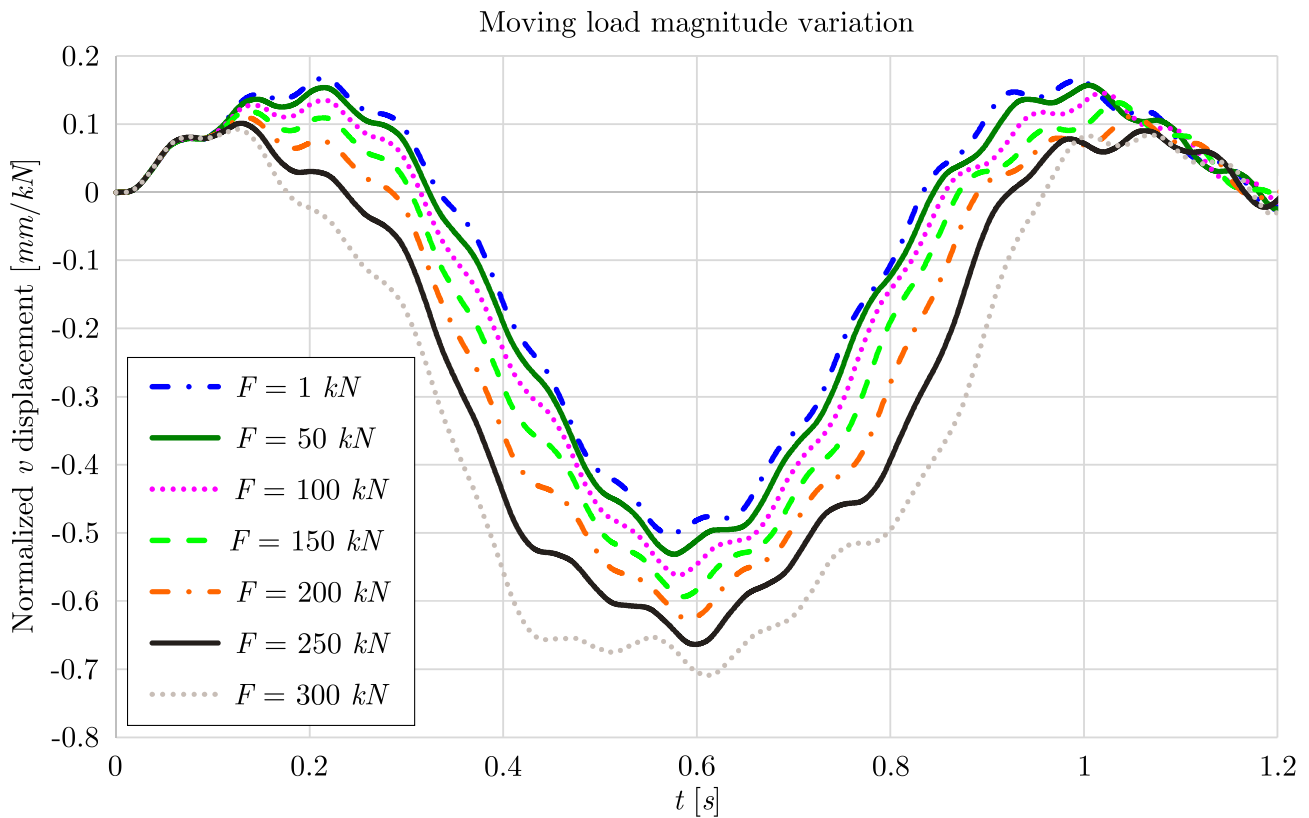


Figure 8.62: Normalized vertical displacement of the beam's midpoint for different moving load magnitude

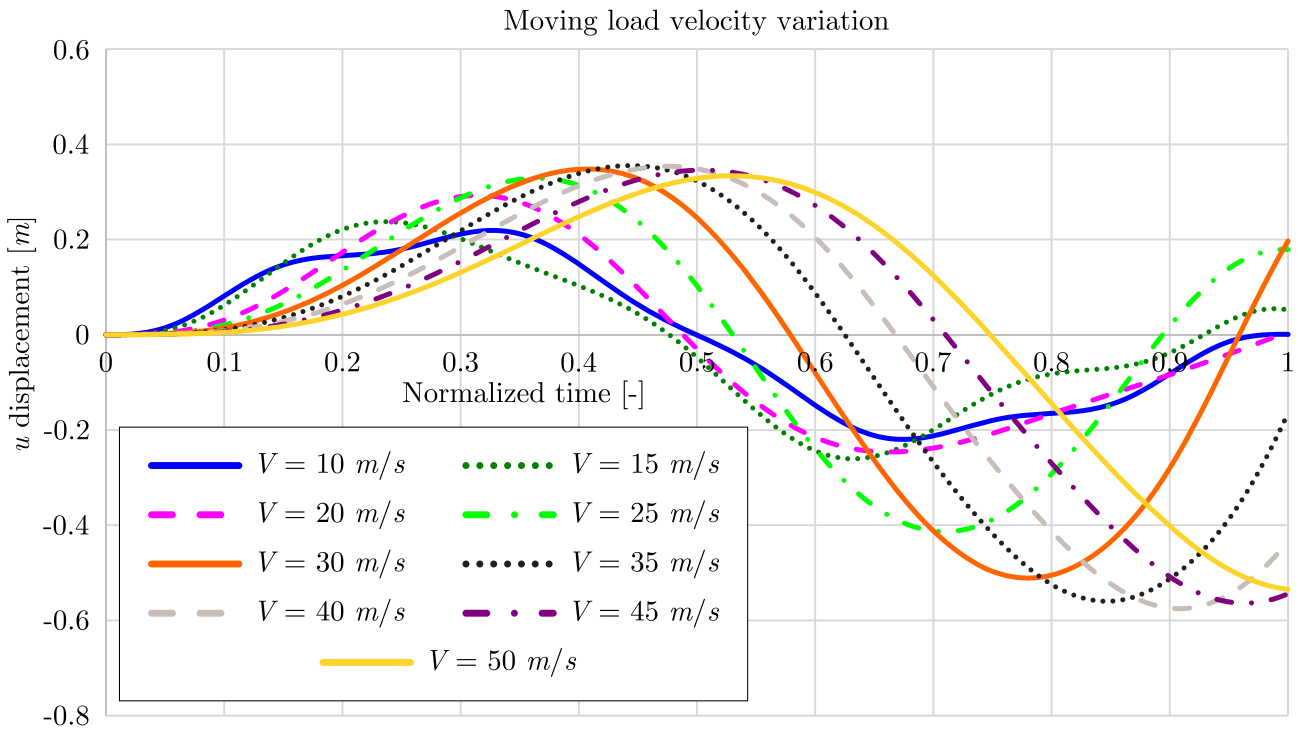


Figure 8.63: Horizontal displacement of the beam’s midpoint for different moving load velocities

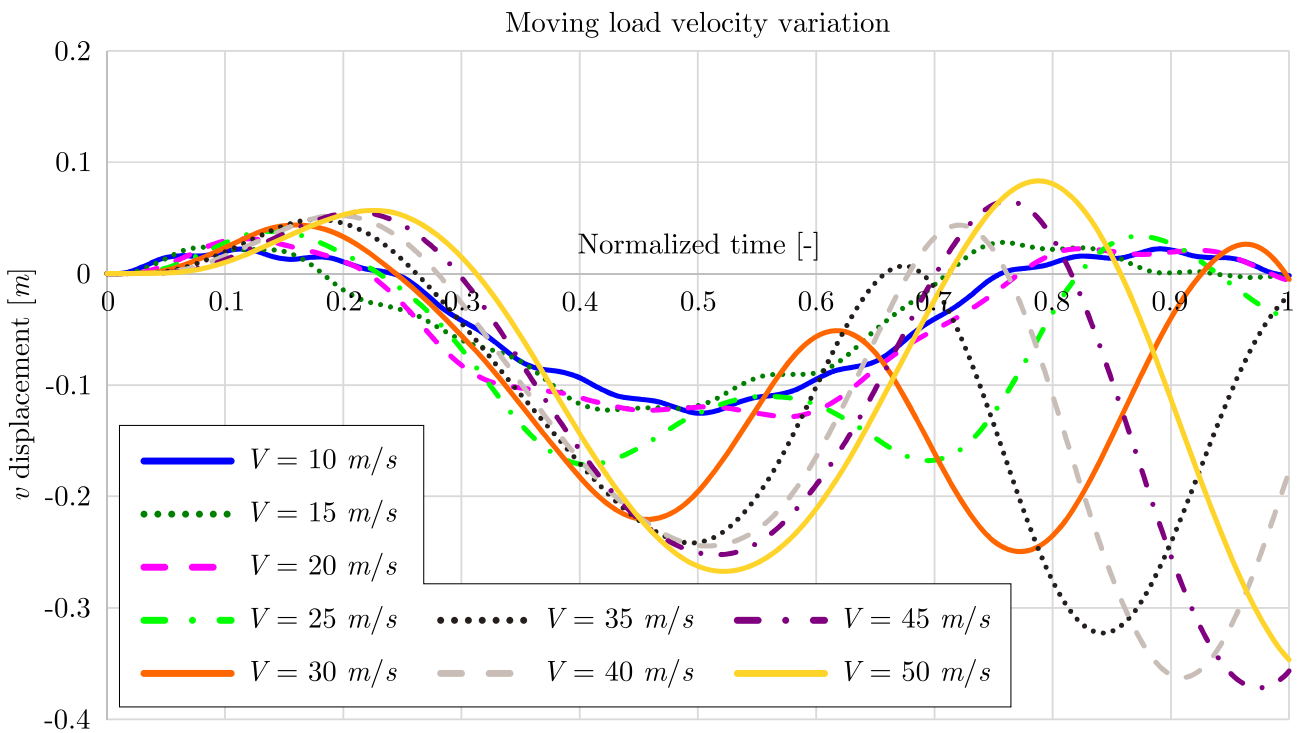


Figure 8.64: Vertical displacement of the beam’s midpoint for different moving load velocities

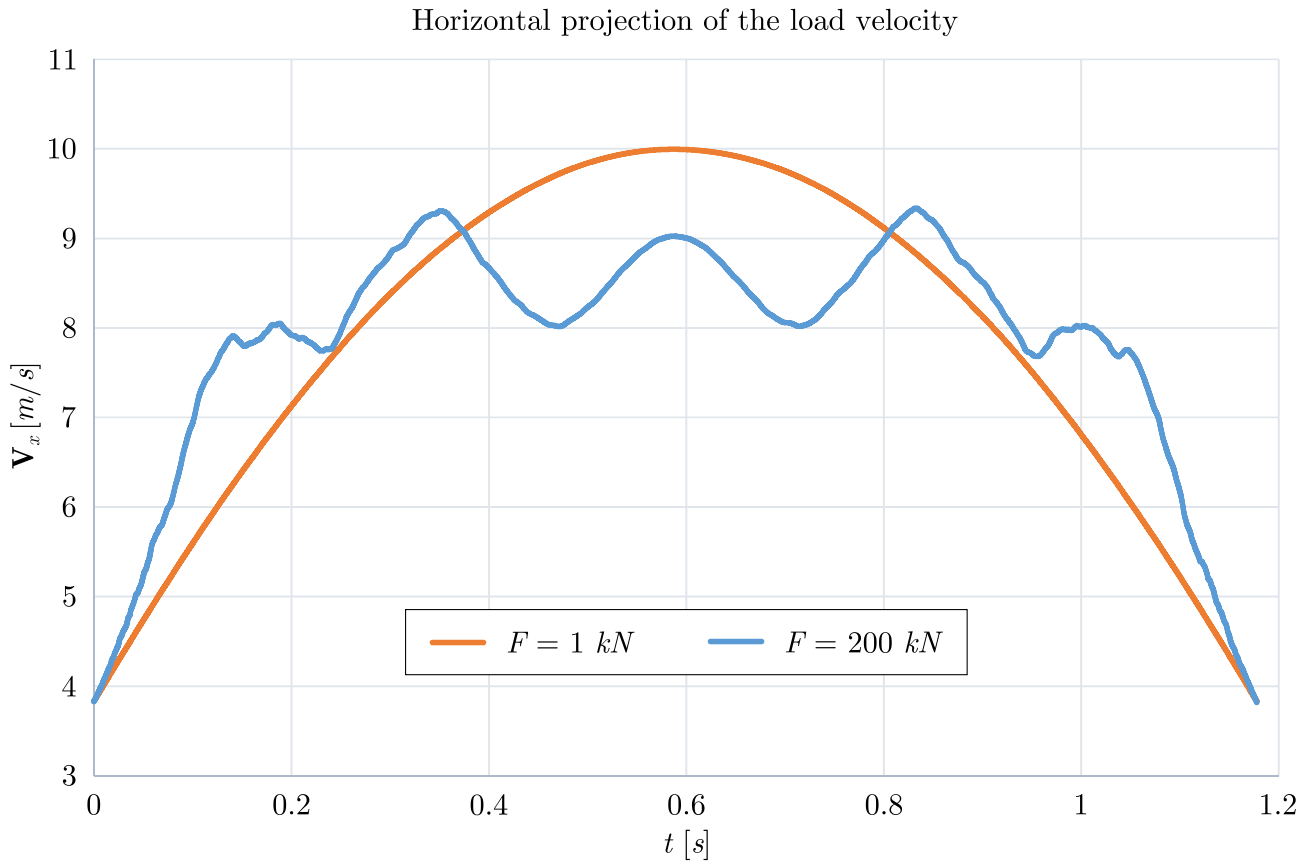


Figure 8.65: Load velocity horizontal projection for two cases of load magnitude, $F = 1 \text{ kN}$ and $F = 200 \text{ kN}$

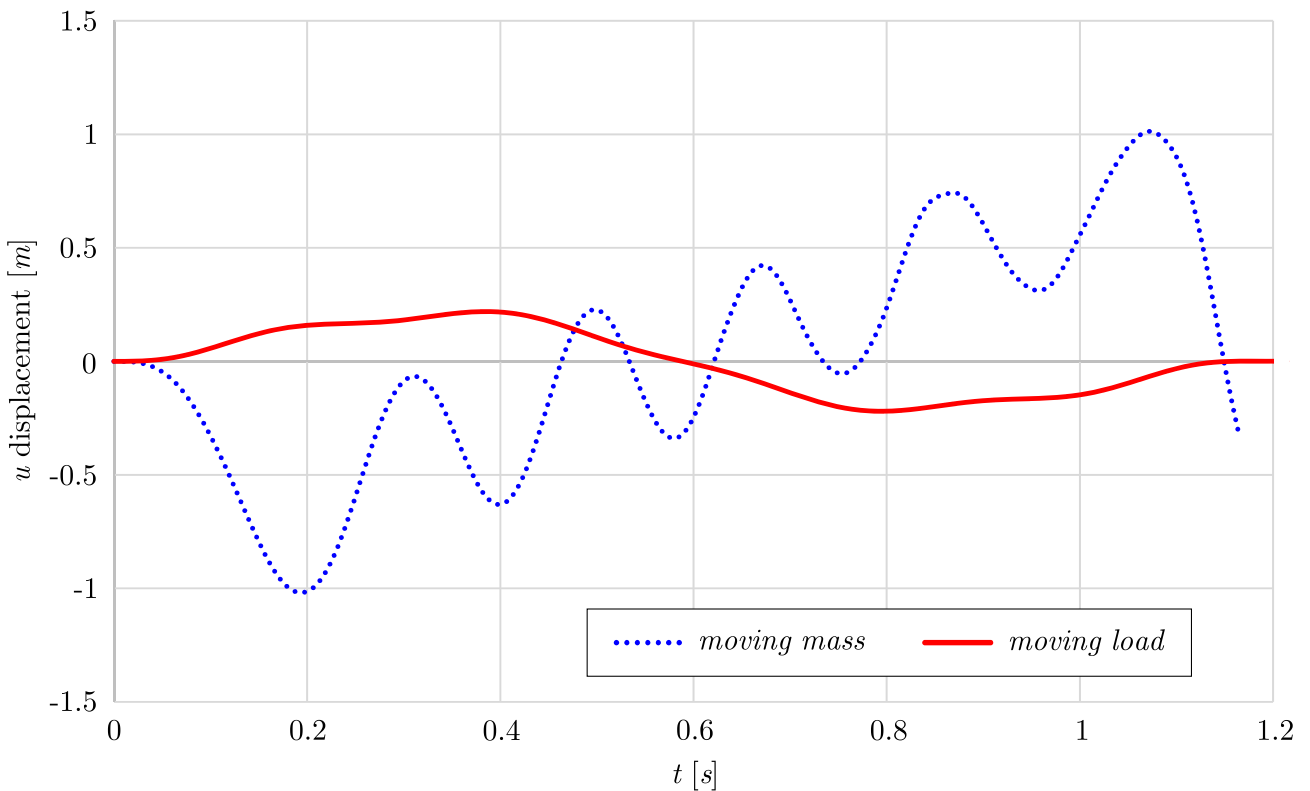


Figure 8.66: Moving load/mass study - horizontal displacement

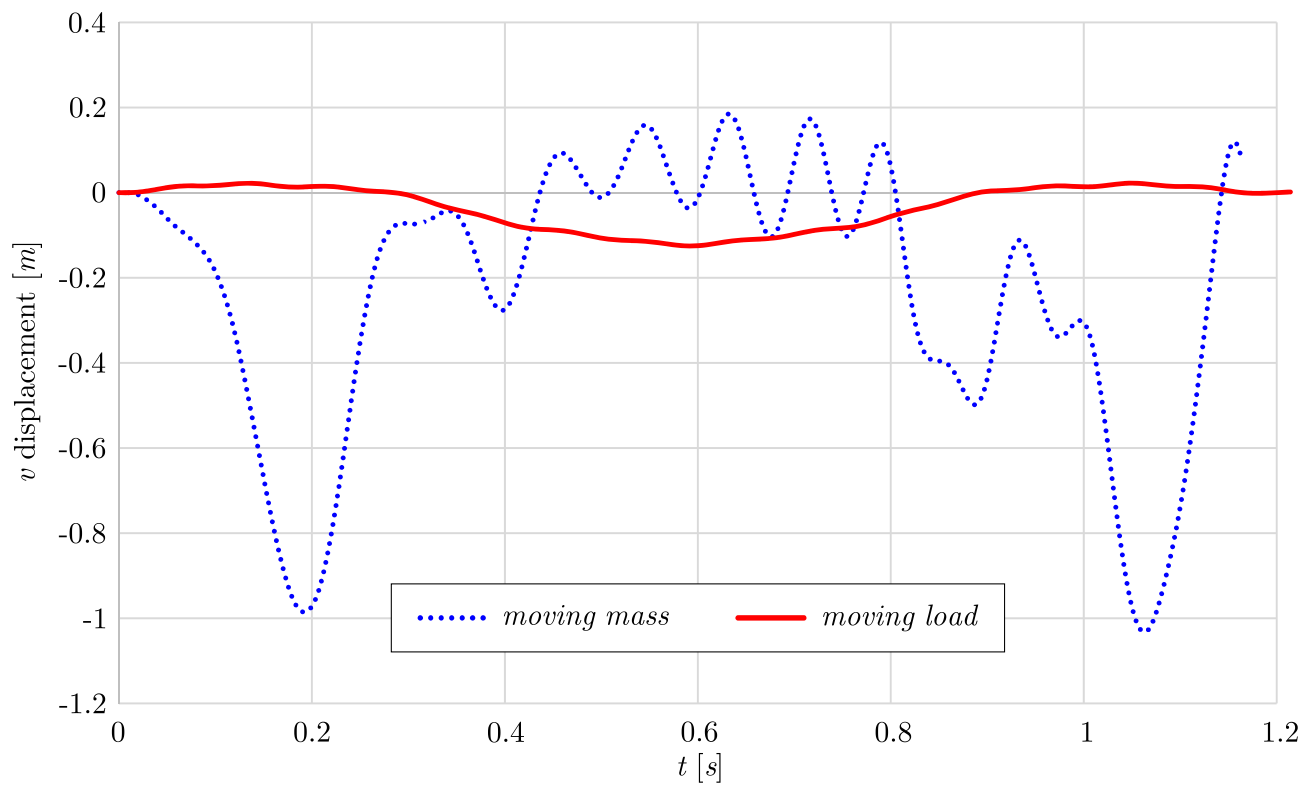


Figure 8.67: Moving load/mass study - vertical displacement

9 Conclusions and recommendations for future work

A novel approach based on the fundamental relations of the differential geometry and Cauchy continuum beam model is presented and applied to derive the stiffness and consistent mass matrices of the corresponding spatial curved beam element. The proposed formulation has been validated and its accuracy and convergence have been demonstrated using numerical examples for free vibration and transient linear and geometrically nonlinear analysis of Bernoulli-Euler curved beams. The isogeometric approach was used to analyze the influence of the moving mass on the curved beam in linear and geometrically nonlinear formulations. The moving mass was formulated as a moving load and moving mass model, where the effects of the mass inertia are taken into account.

From the number of numerical analyses, the following conclusions have been drawn:

- The isogeometric method has shown the capability to provide accurate results for the free vibration analysis of the spatial curved beams. The natural frequencies obtained using the presented approach are in excellent agreement with the results obtained using commercial FE software Abaqus and the literature results. The available results from the literature are obtained using Timoshenko beam theory which gives a more flexible beam than the Bernoulli - Euler beam theory. Consequently, the natural frequencies obtained using the presented approach are slightly higher than the results from the literature. Although the results from the Abaqus are obtained using B33 beam element, based on the Bernoulli - Euler beam theory, it can be noticed that its results are slightly lower than the results obtained using the presented approach. The cause for that can be found in the formulation of the B33 beam element as the rotary inertia for twist around the beam axis is the same as for Timoshenko beams [62]. The convergence study of the free vibration analysis has shown that the relatively small number of DOFs is required to obtain the converged results of the natural frequencies. The same spatial beam has been modeled using Abaqus, which shows that in order to obtain converged results, in comparison to the isogeometric approach, larger number of DOFs are required. Based on the results it can be concluded that the isogeometric approach has an advantage over the FEM, which is particularly useful in the dynamic analysis, as the time necessary for the analysis is directly related to the number of DOFs.
- The analysis of the boundary conditions influence on the curved spatial beam was shown that the various types of boundary conditions (clamped, simply supported and free) can be applied to the presented isogeometric Bernoulli - Euler beam element. In addition, the analysis has shown that the stiffer beam has a higher value of the natural frequencies.

- The proposed method has demonstrated excellent performance in the linear dynamic analysis of the curved spatial beam subjected to the moving load. The results obtained using the isogeometric approach have fast convergence rate and satisfactory accuracy in comparison to the available results from the literature. As shown in the examples, the moving load velocity has a significant impact on the beam response. It can be observed that the maximum displacement has occurred for the specific moving load velocity (critical velocity) and is not the same for the vertical and two horizontal displacements. The magnitude of the moving load velocity can also change the sign of the beam displacement component, as shown in the numerical examples.
- The same model has been used to validate the moving load and moving mass model in the dynamic linear analysis. The magnitude of the moving mass velocity has a significant impact on the beam displacement, and the sign of all beam displacements can be changed as a consequence of the mass velocity. The beam displacements obtained using a moving load and moving mass model are compared for the different velocity magnitude. As the velocity magnitude decreases, the differences between the models become negligible.
- The example of the curved plane beam formulated using geometric nonlinearity has shown that the proposed method gives accurate results compared to the results obtained using commercial FE software Abaqus. Abaqus beam element library does not include Bernoulli - Euler beam element in the explicit geometrically nonlinear dynamic analysis. Consequently, the Timoshenko B21 beam element was used in order to model curved plane beam in the examples of the geometrically nonlinear dynamic analysis. As can be seen, the results obtained using the proposed method converges fast in the geometrically nonlinear formulation of the curved plane beam. The same beam has been used for the parametric study in which the influence of the load magnitude on the beam response was analyzed. As can be observed, the beam displacement and the magnitude of the load are not proportional, which is demonstrated with the normalized beam displacement. As load magnitude decreases, the beam response obtained using geometrically nonlinear formulation approaches to the response obtained using the linear formulation.
- The proposed method provided accurate results in comparison to the results obtained using software Abaqus in the analysis of the moving mass influence on the curved plane beam formulated using geometric nonlinearity. From the converged models obtained using P -, H - and K - refinement procedures, the required number of time steps and the number of integration points were extracted. As can be observed, lower continuity of the NURBS basis functions decreased the number of time steps and integration points, which significantly decreased the time necessary for the analysis. Moving load parametric study has shown that the direct relationship between the beam displacement and the moving load magnitude cannot be established, while the moving load velocity has a significant impact on the beam response. Same as in the linear formulation, the magnitude of the moving load velocity is not proportional to the beam displacements, introducing the phenomenon of the critical velocity, which was not analyzed in this study. Finally, the comparison between the moving load and moving mass model in the geometrically nonlinear formulation is given. As in the linear formulation of the beam, the significant difference in the results can be observed between the moving load and moving mass model.

Several future directions are possible to continue and enhance the work presented in this thesis:

- Special attention should be focused on the geometrically nonlinear formulation of the spatial curved Bernoulli - Euler beam using isogeometric approach. Main problem in this formulation is related to the torsional rotation of the beam's cross section, which represents

the tensor quantity. One of the possible solution of the torsional parametrization can be obtained using exponential parameterization, as presented in this study.

- The presented Object - Oriented computer program is developed only for the Bernoulli - Euler isogeometric beam. However, the upgrade is possible considering the Timoshenko beam theory and the corresponding isogeometric beam element. This approach will extend the range of possible structural applications to the beam elements with larger section heights, such as deep beams. Thereafter, the limitations of Bernoulli - Euler and Timoshenko isogeometric beam elements could be identified for the plane and spatial curved beams.
- Explicit dynamic geometrically nonlinear formulation has limitations regarding the buckling analysis, which can be overcome using the implicit dynamic formulation. Aforementioned formulation can be applied for the static and dynamic buckling analysis of the curved plane and spatial beams.
- The phenomenon of the moving mass critical velocity has been observed, both for the linear and geometrically nonlinear formulation. Further investigation of this phenomenon is of great importance for the curved beams.
- Influence of the friction between the curved beam and moving mass is not accounted in the presented study. It is assumed that its influence can be significant in the dynamic analysis, thus additional investigation should be conducted in the future research.

Bibliography

- [1] J. A. Cottrell, T. J. R. Hughes, Y. Bazilevs, “Isogeometric Analysis”, *Isogeometric Analysis: Toward Integration of CAD and FEA* (2009), pp. 1–335, DOI: 10.1002/9780470749081.
- [2] G. Radenković, *Isogeometric Structural Analysis (in Serbian)*, University of Belgrade, Faculty of Architecture, 2014.
- [3] T. J. R. Hughes, J. A. Cottrell, Y. Bazilevs, “Isogeometric analysis: CAD, finite elements, NURBS, exact geometry and mesh refinement”, *Computer Methods in Applied Mechanics and Engineering* 194.39-41 (2005), pp. 4135–4195, ISSN: 00457825, DOI: 10.1016/j.cma.2004.10.008.
- [4] J. A. Cottrell, T. J. R. Hughes, A. Reali, “Studies of refinement and continuity in isogeometric structural analysis”, *Computer Methods in Applied Mechanics and Engineering* 196.41-44 (2007), pp. 4160–4183, ISSN: 00457825, DOI: 10.1016/j.cma.2007.04.007.
- [5] L. Beirão da Veiga et al., “Some estimates for h-p-k-refinement in Isogeometric Analysis”, *Numerische Mathematik* 118.2 (2011), pp. 271–305, ISSN: 0029599X, DOI: 10.1007/s00211-010-0338-z.
- [6] T. J. R. Hughes, A. Reali, G. Sangalli, “Duality and unified analysis of discrete approximations in structural dynamics and wave propagation: Comparison of p-method finite elements with k-method NURBS”, *Computer Methods in Applied Mechanics and Engineering* 197.49-50 (2008), pp. 4104–4124, ISSN: 00457825, DOI: 10.1016/j.cma.2008.04.006.
- [7] J. Cottrell et al., “Isogeometric analysis of structural vibrations”, *Computer Methods in Applied Mechanics and Engineering* 195.41-43 (2006), pp. 5257–5296, ISSN: 00457825, DOI: 10.1016/j.cma.2005.09.027.
- [8] L. Piegl, W. Tiller, *The Nurbs Book*, Springer, 1995, pp. 1–646, ISBN: 3540615458.
- [9] D. F. Rogers, *An introduction to NURBS: with historical perspective*, 2001, p. 324, ISBN: 1558606696, DOI: 10.1016/B978-155860737-8/50008-9, arXiv: arXiv:1011.1669v3.
- [10] T. J. R. Hughes, A. Reali, G. Sangalli, “Efficient quadrature for NURBS-based isogeometric analysis”, *Computer Methods in Applied Mechanics and Engineering* 199.5-8 (2010), pp. 301–313, ISSN: 00457825, DOI: 10.1016/j.cma.2008.12.004.
- [11] M. H. Seon, H. Benaroya, T. Wei, “Dynamics of transversely vibrating beams using four engineering theories”, *Journal of Sound and Vibration* 225 (1999), pp. 935–988, DOI: jsvi.1999.225.
- [12] L. Beirão da Veiga, C. Lovadina, A. Reali, “Avoiding shear locking for the Timoshenko beam problem via isogeometric collocation methods”, *Computer Methods in Applied Mechanics and Engineering* 241-244 (2012), pp. 38–51, ISSN: 00457825, DOI: 10.1016/j.cma.2012.05.020.

- [13] F. Auricchio et al., “Locking-free isogeometric collocation methods for spatial Timoshenko rods”, *Computer Methods in Applied Mechanics and Engineering* 263 (2013), pp. 113–126, ISSN: 00457825, DOI: 10.1016/j.cma.2013.03.009.
- [14] R. Bouclier, T. Elguedj, A. Combescure, “Locking free isogeometric formulations of curved thick beams”, *Computer Methods in Applied Mechanics and Engineering* 245-246 (2012), pp. 144–162, ISSN: 00457825, DOI: 10.1016/j.cma.2012.06.008.
- [15] X. Li, J. Zhang, Y. Zheng, “NURBS-based isogeometric analysis of beams and plates using high order shear deformation theory”, *Mathematical Problems in Engineering* 2013 (2013), ISSN: 1024123X, DOI: 10.1155/2013/159027.
- [16] L. Greco, M. Cuomo, “B-Spline interpolation of Kirchhoff-Love space rods”, *Computer Methods in Applied Mechanics and Engineering* 256 (2013), pp. 251–269, ISSN: 00457825, DOI: 10.1016/j.cma.2012.11.017.
- [17] L. Greco, M. Cuomo, “An implicit G1 multi patch B-spline interpolation for Kirchhoff-Love space rod”, *Computer Methods in Applied Mechanics and Engineering* 269 (2014), pp. 173–197, ISSN: 00457825, DOI: 10.1016/j.cma.2013.09.018.
- [18] S. B. Raknes et al., “Isogeometric rotation-free bending-stabilized cables: Statics, dynamics, bending strips and coupling with shells”, *Computer Methods in Applied Mechanics and Engineering* 263 (2013), pp. 127–143, ISSN: 00457825, DOI: 10.1016/j.cma.2013.05.005.
- [19] A. Borković et al., “Rotation-free isogeometric analysis of an arbitrarily curved plane Bernoulli–Euler beam”, *Computer Methods in Applied Mechanics and Engineering* 334 (2018), pp. 238–267, ISSN: 00457825, DOI: 10.1016/j.cma.2018.02.002.
- [20] A. Borković et al., “Rotation-free isogeometric dynamic analysis of an arbitrarily curved plane Bernoulli-Euler beam”, *Engineering Structures* 181 (2019), pp. 192–215, ISSN: 01410296, DOI: 10.1016/j.engstruct.2018.12.003.
- [21] G. Radenković, A. Borković, “Linear static isogeometric analysis of an arbitrarily curved spatial Bernoulli–Euler beam”, *Computer Methods in Applied Mechanics and Engineering* 341 (2018), pp. 360–396, ISSN: 00457825, DOI: 10.1016/j.cma.2018.07.010.
- [22] D. Wang, W. Liu, H. Zhang, “Superconvergent isogeometric free vibration analysis of Euler-Bernoulli beams and Kirchhoff plates with new higher order mass matrices”, *Computer Methods in Applied Mechanics and Engineering* 286 (2015), pp. 230–267, ISSN: 00457825, DOI: 10.1016/j.cma.2014.12.026.
- [23] G. Radenković, *Finite rotation and finite defirmation isogeometric structural analysis (in Serbian)*, University of Belgrade, Faculty of Architecture, 2017.
- [24] K. J. Bathe, S. Bolourchi, “Large displacement analysis of three-dimensional beam structures”, *International Journal for Numerical Methods in Engineering* 14 (1979), pp. 961–986, ISSN: 0029-5981, DOI: 10.1002/nme.1620140703.
- [25] K.-J. Bathe, *Finite Element Procedures*, K.J. Bathe, Watertown, MA, 2016, ISBN: 978-0-9790049-5-7.
- [26] T. Belytschko, “A survey of numerical methods and computer programs for dynamic structural analysis”, *Nuclear engineering and design* 37 (1976), pp. 23–34.
- [27] S. H. Lo, “Geometrically nonlinear formulation of 3D finite strain beam element with large rotations”, *Computers and Structures* 44.1-2 (1992), pp. 147–157, ISSN: 00457949, DOI: 10.1016/0045-7949(92)90234-Q.
- [28] K. M. Hsiao, R. T. Yang, “A co-rotational formulation for nonlinear dynamic analysis of curved euler beam”, *Computers and Structures* 54.6 (1995), pp. 1091–1097, ISSN: 00457949, DOI: 10.1016/0045-7949(94)00399-N.

- [29] S. L. Chan, “Large deflection dynamic analysis of space frames”, *Computers and Structures* 58.2 (1996), pp. 381–387, ISSN: 00457949, DOI: 10.1016/0045-7949(95)00145-7.
- [30] C. M. Saravia, “A large deformation-small strain formulation for the mechanics of geometrically exact thin-walled composite beams”, *Thin-Walled Structures* 84 (2014), pp. 443–451, ISSN: 02638231, DOI: 10.1016/j.tws.2014.05.014.
- [31] P. F. Pai, “Three kinematic representations for modeling of highly flexible beams and their applications”, *International Journal of Solids and Structures* 48.19 (2011), pp. 2764–2777, ISSN: 00207683, DOI: 10.1016/j.ijsolstr.2011.06.001.
- [32] A. M. Bauer et al., “Nonlinear isogeometric spatial Bernoulli beam”, *Computer Methods in Applied Mechanics and Engineering* 303 (2016), pp. 101–127, ISSN: 00457825, DOI: 10.1016/j.cma.2015.12.027.
- [33] G. G. Stokes, “Discussion of a Differential Equation relating to the Breaking of Railway Bridges”, *Mathematical and Physical Papers vol.2*, vol. vi, Cambridge: Cambridge University Press, 1849, pp. 178–220, ISBN: 9780511702259, DOI: 10.1017/CB09780511702259.013.
- [34] H. H. Jeffcott, “On the vibration of beams under the action of moving loads”, *Philosophical Magazine* 7 (1929), pp. 66–97, DOI: <http://dx.doi.org/10.1080/14786440708564857>.
- [35] M. Skeer, J. Hribar, “Dynamic response of systems subject to moving mass excitations”, *Journal of the Franklin Institute* 287.4 (1969), pp. 319–331, ISSN: 00160032, DOI: 10.1016/0016-0032(69)90004-0.
- [36] M. M. Stanisic, J. C. Hardin, “On the response of beams to an arbitrary number of concentrated moving masses”, *Journal of the Franklin Institute* 287.2 (1969), pp. 115–123, ISSN: 00160032, DOI: 10.1016/0016-0032(69)90120-3.
- [37] J. E. Akin, M. Mofid, “Numerical Solution for Response of Beams with Moving Mass”, *Journal of Structural Engineering* 115.1 (1989), pp. 120–131, ISSN: 0733-9445, DOI: 10.1061/(ASCE)0733-9445(1989)115:1(120).
- [38] J. Genin, E. Ting, Z. Vafa, “Curved bridge response to a moving vehicle”, *Journal of Sound and Vibration* 81.4 (1982), pp. 469–475, ISSN: 0022460X, DOI: 10.1016/0022-460X(82)90290-5.
- [39] Y.-B. Yang, C.-M. Wu, J.-D. Yau, “Dynamic Response of a Horizontally Curved Beam Subjected To Vertical and Horizontal Moving Loads”, *Journal of Sound and Vibration* 242.3 (2001), pp. 519–537, ISSN: 0022460X, DOI: 10.1006/jsvi.2000.3355.
- [40] S. M. Lin, K. W. Lee, “Instability and vibration of a vehicle moving on curved beams with different boundary conditions”, *Mechanics of Advanced Materials and Structures* 23.4 (2016), pp. 375–384, ISSN: 15376532, DOI: 10.1080/15376494.2014.981618.
- [41] G. Sheng, X. Wang, “The geometrically nonlinear dynamic responses of simply supported beams under moving loads”, *Applied Mathematical Modelling* 48 (2017), pp. 183–195, ISSN: 0307904X, DOI: 10.1016/j.apm.2017.03.064.
- [42] E. Zupan, D. Zupan, “Dynamic analysis of geometrically non-linear three-dimensional beams under moving mass”, *Journal of Sound and Vibration* 413 (2018), pp. 354–367, ISSN: 10958568, DOI: 10.1016/j.jsv.2017.10.013.
- [43] S. H. Li, J. Y. Ren, “Analytical study on dynamic responses of a curved beam subjected to three-directional moving loads”, *Applied Mathematical Modelling* 58 (2018), pp. 365–387, ISSN: 0307904X, DOI: 10.1016/j.apm.2018.02.006.

- [44] V. N. Van Do, T. H. Ong, C. H. Thai, “Dynamic responses of Euler–Bernoulli beam subjected to moving vehicles using isogeometric approach”, *Applied Mathematical Modelling* 51 (2017), pp. 405–428, ISSN: 0307904X, DOI: 10.1016/j.apm.2017.06.037.
- [45] L. Beirão da Veiga et al., “Some estimates for h-p-k-refinement in Isogeometric Analysis”, *Numerische Mathematik* 118.2 (2011), pp. 271–305, ISSN: 0029599X, DOI: 10.1007/s00211-010-0338-z.
- [46] M. P. do Carmo, *Differential Geometry of Curves and Surfaces*, Prentice-Hall, 1976, p. 511, ISBN: 0132125897.
- [47] M. Spivak, *A Comprehensive Introduction to Differential Geometry, Vol. II*, Publish or Perish, Inc., 1999, p. 361, ISBN: 978-0914098713.
- [48] M. Jočković et al., “Free vibration analysis of spatial Bernoulli–Euler and Rayleigh curved beams using isogeometric approach”, *Applied Mathematical Modelling* 71 (2019), pp. 152–172, ISSN: 0307904X, DOI: 10.1016/j.apm.2019.02.002.
- [49] J. Jaric, *Continuum mechanics (in Serbian)*, Gradjevinska knjiga, Beograd, 1988.
- [50] P. Wriggers, *Nonlinear Finite Element Methods*, Springer-Verlag Berlin Heidelberg, 2008, ISBN: 978-3-540-71000-4.
- [51] N. M. Newmark, “A method of computation for structural dynamics”, *Journal of the Engineering Mechanics Division - ASCE* 85 (1959), pp. 67–94.
- [52] C. Adam et al., “Stable time step estimates for NURBS-based explicit dynamics”, *Computer Methods in Applied Mechanics and Engineering* 295 (2015), pp. 581–605, ISSN: 00457825, DOI: 10.1016/j.cma.2015.03.017.
- [53] J. S. Wu, L. K. Chiang, “Dynamic analysis of an arch due to a moving load”, *Journal of Sound and Vibration* 269.3-5 (2004), pp. 511–534, ISSN: 0022460X, DOI: 10.1016/S0022-460X(03)00020-8.
- [54] M. R. Rostam et al., “Vibration suppression of curved beams traversed by off-center moving loads”, *Journal of Sound and Vibration* 352 (2015), pp. 1–15, ISSN: 10958568, DOI: 10.1016/j.jsv.2015.04.038.
- [55] M. F. Beatty, *Principles of Engineering Mechanics: Dynamics - The Analysis of Motion*, Springer, 2005, ISBN: 9780387237046.
- [56] A. Ibrahimbegovic, “On the choice of finite rotation parameters”, *Computer Methods in Applied Mechanics and Engineering* 149.1-4 (1997), pp. 49–71, ISSN: 00457825, DOI: 10.1016/S0045-7825(97)00059-5.
- [57] A. Bartezzaghi et al., “An explicit dynamics GPU structural solver for thin shell finite elements”, *Computers and Structures* 154 (2015), pp. 29–40, ISSN: 00457949, DOI: 10.1016/j.compstruc.2015.03.005.
- [58] A. H. Register, *A guide to MATLAB object-oriented programming*, 2007, p. 354, ISBN: 978-1-58488-911-3.
- [59] V. Yildirim, N. Ince, “Natural frequencies of helical springs of arbitrary shape”, *Journal of Sound and Vibration* 204.2 (1997), pp. 311–329, ISSN: 0022460X, DOI: 10.1006/jsvi.1997.0940.
- [60] Simulia, FEA Abaqus, *Dassault Systemes Simulia Corporation*, 2014.
- [61] Rhinoceros, *Rhinoceros version 6*, 2018.
- [62] Simulia, Abaqus, *User Manual. Version 6.13. Providence, RI, USA: DS SIMULIA Corp.* 2013.

Biography

Miloš Jočković was born on April 06, 1988 in Sremska Mitrovica, Republic of Serbia. He finished elementary school and gymnasium in Šid as a holder of the diploma “Vuk Karadžić“.

He enrolled the BSc studies at the Faculty of Civil Engineering in Belgrade in 2007 and graduated in 2011 (Module Structures) with the average grade of 9.54/10. He defended his thesis “Reinforced concrete structure of a commercial building” with the highest grade thus acquire the title Bachelor of Science. He enrolled the MSc studies at the Faculty of Civil Engineering in Belgrade in 2011 and graduated in 2013 (Module Structures) with the average grade of 9.57/10. He defended his thesis “Free vibration of plate assemblies using spectral element method” on the Chair of engineering mechanics and theory of structures with the highest grade thus acquire the title Master of Science. He enrolled the PhD studies at the Faculty of Civil Engineering in Belgrade in 2013/2014. He has passed all the exams from the curriculum with the average grade of 9.88/10.

In 2011 the foundation “Prof. Milan Đurić” awarded him for his achieved results in the theory of structures courses during the studies. In addition, during the period from 2007 until 2011 the Faculty of Civil Engineering in Belgrade awarded him for the achieved accomplishment during the studies. He was scholarship holder from Republic of Serbia for the period from 2008 until 2010, and the foundation “Dositeja” for the years 2010 and 2011.

During 2012, Miloš Jočković was working for the National oil company NIS, and the Serbia and Montenegro air traffic services SMATSA LLC. Since November 2013 he has been working as a researcher on the Project “Towards Development of Sustainable Cities: Influence of traffic induced vibrations on buildings and humans” (TR36046 lead by Prof. Dr Mira Petronijević). From June 2013 until December 2013 he participated in Project "Implementing MATLAB tool for analysing flutter instability" financed by the DAAD foundation – Germany. Since November 2014 he has been working at the Faculty of Civil Engineering, University of Belgrade as a Teaching Assistant - PhD Student for the scientific filed Engineering mechanics and theory of structures. Since the election, he has been teaching exercises in the subjects Matrix structural analysis, Finite element method and Computer aided numerical structural analysis and design. Since 2015, Miloš has been participated as the Scholarship Holder in the international PhD program SEEFORM (South Eastern European Graduate School for Master and PhD), financed by DAAD, Germany. As a SEEFORM scholar he spent five-months-long research stays at Hochschule Bochum (Bochum University of Applied Sciences). He is a member of Serbian Society of Mechanics. He speaks and writes English. He is married with one child.

As an author or coauthor, Miloš Jočković has published 1 article in the international journal (M21), 2 articles in the international journal (M24), 8 papers in the proceedings of international

conferences (M33), 2 papers in the proceedings of national conferences (M63) and 4 papers in the national monograph.

Изјава о ауторству

Име и презиме аутора Милош Јочковић

Број индекса 904/13

Изјављујем

да је докторска дисертација под насловом

Isogeometric approach in dynamic analysis of spatial curved beams

(Изогеометријски приступ у динамичкој анализи просторних криволинијских гредних носача)

- резултат сопственог истраживачког рада;
- да дисертација у целини ни у деловима није била предложена за стицање друге дипломе према студијским програмима других високошколских установа;
- да су резултати коректно наведени и
- да нисам кршио/ла ауторска права и користио/ла интелектуалну својину других лица.

Потпис аутора

У Београду, април 2021.

Изјава о истоветности штампане и електронске верзије докторског рада

Име и презиме аутора	Милош Јочковић
Број индекса	904/13
Студијски програм	Грађевинарство
Наслов рада	Isogeometric approach in dynamic analysis of spatial curved beams
Ментор	Ванр. проф. Др. Марија Нефовска – Даниловић Универзитет у Београду, Грађевински факултет Prof. Dr.-Ing. Matthias Baitsch Hochschule Bochum, Bochum University of Applied Science

Изјављујем да је штампана верзија мог докторског рада истоветна електронској верзији коју сам предао/ла ради похрањена у **Дигиталном репозиторијуму Универзитета у Београду**.

Дозвољавам да се објаве моји лични подаци везани за добијање академског назива доктора наука, као што су име и презиме, година и место рођења и датум одбране рада.

Ови лични подаци могу се објавити на мрежним страницама дигиталне библиотеке, у електронском каталогу и у публикацијама Универзитета у Београду.

Потпис аутора

У Београду, април 2021.

Изјава о коришћењу

Овлашћујем Универзитетску библиотеку „Светозар Марковић“ да у Дигитални репозиторијум Универзитета у Београду унесе моју докторску дисертацију под насловом:

Isogeometric approach in dynamic analysis of spatial curved beams

(Изогеометријски приступ у динамичкој анализи просторних криволинијских гредних носача)

која је моје ауторско дело.

Дисертацију са свим прилозима предао/ла сам у електронском формату погодном за трајно архивирање.

Моју докторску дисертацију похрањену у Дигиталном репозиторијуму Универзитета у Београду и доступну у отвореном приступу могу да користе сви који поштују одредбе садржане у одабраном типу лиценце Креативне заједнице (Creative Commons) за коју сам се одлучио/ла.

1. Ауторство (CC BY)
2. Ауторство – некомерцијално (CC BY-NC)
3. Ауторство – некомерцијално – без прерада (CC BY-NC-ND)
4. Ауторство – некомерцијално – делити под истим условима (CC BY-NC-SA)
5. Ауторство – без прерада (CC BY-ND)
6. Ауторство – делити под истим условима (CC BY-SA)

(Молимо да заокружите само једну од шест понуђених лиценци.
Кратак опис лиценци је саставни део ове изјаве).

Потпис аутора

У Београду, април 2021.

1. **Ауторство.** Дозвољаваате умножавање, дистрибуцију и јавно саопштавање дела, и прераде, ако се наведе име аутора на начин одређен од стране аутора или даваоца лиценце, чак и у комерцијалне сврхе. Ово је најслободнија од свих лиценци.

2. **Ауторство – некомерцијално.** Дозвољаваате умножавање, дистрибуцију и јавно саопштавање дела, и прераде, ако се наведе име аутора на начин одређен од стране аутора или даваоца лиценце. Ова лиценца не дозвољава комерцијалну употребу дела.

3. **Ауторство – некомерцијално – без прерада.** Дозвољаваате умножавање, дистрибуцију и јавно саопштавање дела, без промена, преобликовања или употребе дела у свом делу, ако се наведе име аутора на начин одређен од стране аутора или даваоца лиценце. Ова лиценца не дозвољава комерцијалну употребу дела. У односу на све остале лиценце, овом лиценцом се ограничава највећи обим права коришћења дела.

4. **Ауторство – некомерцијално – делити под истим условима.** Дозвољаваате умножавање, дистрибуцију и јавно саопштавање дела, и прераде, ако се наведе име аутора на начин одређен од стране аутора или даваоца лиценце и ако се прерада дистрибуира под истом или сличном лиценцом. Ова лиценца не дозвољава комерцијалну употребу дела и прерада.

5. **Ауторство – без прерада.** Дозвољаваате умножавање, дистрибуцију и јавно саопштавање дела, без промена, преобликовања или употребе дела у свом делу, ако се наведе име аутора на начин одређен од стране аутора или даваоца лиценце. Ова лиценца дозвољава комерцијалну употребу дела.

6. **Ауторство – делити под истим условима.** Дозвољаваате умножавање, дистрибуцију и јавно саопштавање дела, и прераде, ако се наведе име аутора на начин одређен од стране аутора или даваоца лиценце и ако се прерада дистрибуира под истом или сличном лиценцом. Ова лиценца дозвољава комерцијалну употребу дела и прерада. Слична је софтверским лиценцама, односно лиценцама отвореног кода.